UNIVERSITY
OF MICHIGAN

MAY 6 1959

ENGINEERING
LIBRARY

JOURNAL OF FLUID MECHANICS

VOLUME 5 PART 3

APRIL 1959

PUBLISHED BY

CAMBRIDGE UNIVERSITY PRESS

BENTLEY HOUSE, 200 EUSTON ROAD, LONDON, N.W. 1

AMERICAN BRANCH: 32 EAST 57TH STREET, NEW YORK 22, N.Y.

Price 30*s.* (*U.S.A.* $5.00)

The JOURNAL OF FLUID MECHANICS exists for the publication of theoretical and experimental investigations of all aspects of the mechanics of fluids, and is issued in four parts per volume.

EDITOR

DR G. K. BATCHELOR

Cavendish Laboratory, University of Cambridge, Cambridge, England

ASSISTANT EDITORS

DR T. B. BENJAMIN, DR I. PROUDMAN, DR P. G. SAFFMAN

Cavendish Laboratory, University of Cambridge, Cambridge, England

ASSOCIATE EDITORS

PROF. G. F. CARRIER

Pierce Hall, Harvard University, Cambridge 38, *Massachusetts, U.S.A.*

DR W. C. GRIFFITH

Research and Development Laboratory, Missile Systems Division, Lockheed Aircraft Corporation, Palo Alto, California, U.S.A.

PROF. M. J. LIGHTHILL

Department of Mathematics, The University, Manchester, England

PROF. R. R. LONG

School of Engineering, The Johns Hopkins University, Baltimore 18, *Maryland, U.S.A.*

Authors wishing to have papers published in the JOURNAL should communicate them to any one of the persons named above, choosing one in their own country where possible.

Authors are urged to ensure that their papers are written clearly and attractively, in order that their work will be readily accessible to readers.

Manuscripts should be typed in double spacing on one side of the paper only, with references listed at the end in alphabetical order of authors. Drawings should be done on a large scale in Indian ink on tracing cloth or drawing paper, the lettering being shown clearly in pencil for reproduction by the printer; the list of captions should be typed at the end of the manuscript. Proofs of papers from overseas will usually be despatched to authors by airmail. There is no charge for publication. Authors are entitled to receive 50 offprints of a paper in the JOURNAL free of charge, and additional offprints can be purchased if ordered in advance.

SUBSCRIPTIONS

The subscription price for a volume of four parts is £5. 10*s*. net, post free, payable in advance; separate parts 30*s*. net, plus postage. Subscriptions may be sent to any bookseller, or to the Cambridge University Press, Bentley House, 200 Euston Road, London, N.W.1.

Subscribers in the United States should send their orders to the Cambridge University Press, American Branch, 32 East 57th Street, New York 22. The subscription price per volume is $18.50, post free, payable in advance; separate parts $5.00, plus postage.

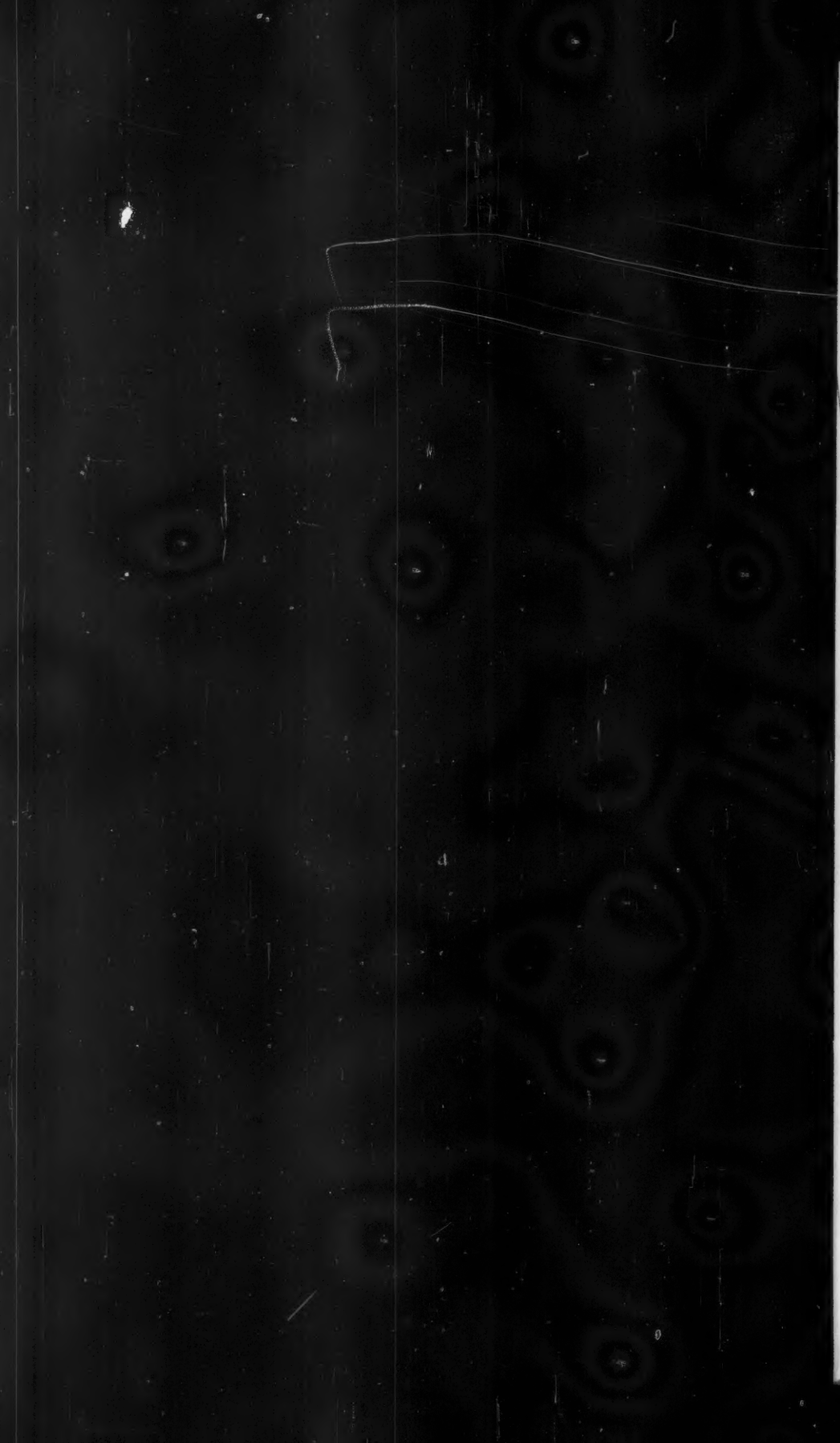

Experimental studies of supercavitating flow about simple two-dimensional bodies in a jet

By EDWARD SILBERMAN
St Anthony Falls Hydraulic Laboratory, University of Minnesota

(Received 8 August 1958)

A two-dimensional free-jet water tunnel developed at the St Anthony Falls Hydraulic Laboratory of the University of Minnesota is described briefly. Results of experimental measurements on a two-dimensional cup, symmetrical wedges, inclined flat plates, and a circular cylinder in the tunnel are given.

Measured force coefficients at zero cavitation number are in good agreement with theory. Shapes of the cavities were computed for one of the wedges and for one of the plates at zero cavitation number; the observed shapes are also in good agreement with the theory.

For non-zero cavitation numbers, theoretical results for force coefficients were available for comparison in only two cases. For one of these, the cup, agreement between theory and experiment was good up to a cavitation number of about 0·5. For the other, a symmetrical wedge, experimental results were compared with a linear theory with good agreement for cavitation numbers between about 0·1 and 0·3. In the case of the wedge, measured cavity lengths were somewhat shorter than predicted by the linear theory. All other comparisons with theory at non-zero cavitation number had to be made with the theory as developed for infinite fluid. The experimental force coefficients were less than predicted by infinite-fluid theory, but tended to approach the theoretical values as the cavitation number increased. A similar tendency marked the comparison between the experimental data and data taken by others in closed tunnels.

1. Introduction

In modern technology, it has become desirable to operate hydrofoils at such speeds that steady-state (or quasi-steady-state) cavities are formed of lengths equal to or many times greater than the chord length of the foil. Conventional water tunnels are limited in their usefulness for studying such supercavitating flows by blockage at small cavitation numbers (cavitation number is defined by equation (1) below). The blockage problem has been fully discussed by Birkhoff, Plesset & Simmons (1950). There is no blockage problem in a free jet, however, and experimental studies of supercavitating flows can be conducted at extremely small cavitation numbers—even zero—in a suitably designed free-jet tunnel.

A brief description of a two-dimensional, free-jet water tunnel developed at the St Anthony Falls Hydraulic Laboratory of the University of Minnesota is contained herein, together with the results of some experimental measurements on

simple, two-dimensional bodies (the cup, symmetrical wedge, inclined flat plate, and circular cylinder). The experimental results are compared with theoretical predictions and with measurements by others in closed tunnels, when available.

The usefulness of experimental measurements of supercavitating flows obtained in a water tunnel is limited by the problem of converting data from tunnel boundary conditions to infinite fluid. Some discussion of this problem for a free-jet tunnel has appeared in the literature (e.g. Birkhoff, Plesset & Simmons (1952) and Cohen & Tu (1956)); and it is known that, in general, cavity lengths will be shorter and drag coefficients will be less in a free jet than in infinite fluid. A better quantitative idea of these wall corrections than previously available may be obtained by comparing the present experimental results and related theory with the theory for infinite fluid and experimental results for closed tunnels. In fact, the purpose of the experimental programme described herein was to investigate the utility of the two-dimensional free-jet tunnel for studying supercavitating flows in infinite fluid.

2. The free-jet tunnel

Figure 1 illustrates the free-jet tunnel and figure 2 (plate 1) shows the two-dimensional test section. The entire test section is enclosed by a sealed housing when the tunnel is in operation. The housing creates an evacuated chamber through which the jet passes. The tunnel was originally designed as an axially symmetric jet of 10 in. diameter. A detailed description of the basic tunnel was given by Christopherson (1953). The tunnel is not recirculating but draws water directly from a river supply and wastes it to the river at a lower level.

As may be seen in figure 1, the axis of the jet is vertical, and the test section has been placed at such a height that the region surrounding the jet at the test section may be maintained at vapour pressure by the weight of the suspended water column in the vertical conduit. Pressures intermediate between vapour pressure and atmospheric pressure may be obtained by admitting atmospheric air to the test section, thereby lowering the water column. The maximum velocity available in the tunnel is 50 ft./sec, but this maximum is reduced as the operating pressure is increased by admitting air.

The tunnel is made two-dimensional by inserting two parallel, flat plates into the jet as shown in figure 2 (plate 1). Each plate is $\frac{3}{8}$ in. thick by 7 in. wide and the plates are 5 in. apart, fixing the span of test bodies at 5 in. The jet varies in width between the 10 in. width of the original axially symmetric tunnel at the plane of symmetry and about 8·7 in. at the side plates. (The side plates are completely surrounded by the jet; only the support structure penetrates the jet walls.) The nominal width of the jet is taken as 10 in.

The plates extend 3·5 ft. downstream from the test-body location; this length brings the ends of the plates to the top of the water column when the tunnel is operated at minimum pressure. When the cavity length produced by a given test body exceeds about 3·5 ft. or when the cavity width exceeds about 7 in., the cavity breaks out or vents to the surrounding chamber, splitting the cavity and producing a cavitation number which is effectively zero. There is, therefore, a gap

in the cavitation numbers obtainable in the tunnel between zero and the cavitation number corresponding to a 3·5 ft. long or 7 in. wide cavity. The plates extend about 6 in. upstream from the test body, and their leading edges are shaped so as to produce minimum cavitation. (The final shape was determined by trial and error in the tunnel.)

Each plate is made from a single sheet of brass, but one of the plates contains a plane Plexiglas window fitted smoothly into the brass. The upper edge of the

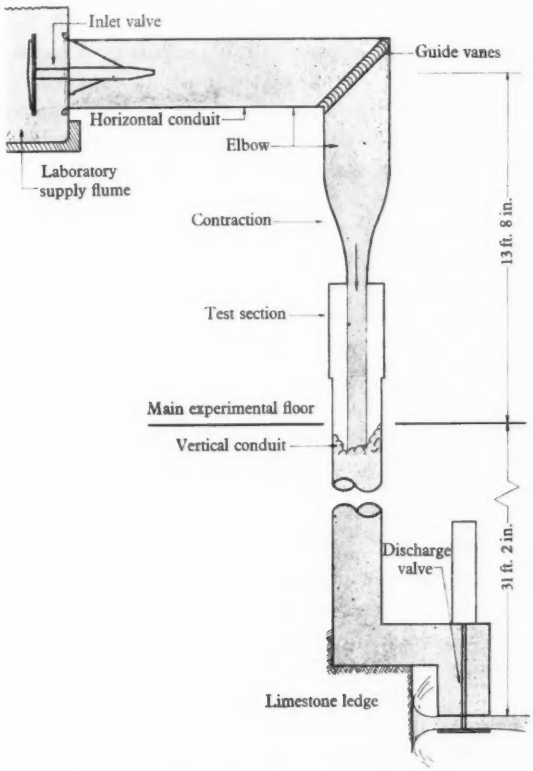

FIGURE 1. General scheme of water tunnel.

window is about 1·5 in. downstream from the centre of the test-body location. In line with this window, there is another window in the chamber housing; this second window is curved on the inside so as to come just into contact with the 10 in. axially symmetric jet, and is flat on the outside. Profiles of two-dimensional cavities may be inspected and photographed through these windows. One difficulty inherent in the window arrangement is that frequently the water between the two windows cavitates before the minimum cavitation number for the test body is reached, thus precluding observation at the lowest cavitation numbers. (It has been determined by photographing a grid in the tunnel that distortion through the windows is negligible.)

The brass wall opposite the window wall is provided with two pressure taps located about 1·5 in. downstream from the centre of the test-body location. One or both of these can be used to measure cavity pressure or to admit air to a cavity.

Each side plate houses a removable dynamometer, drag being measured on one side and lift on the other. (Because the jet is symmetrical, it is assumed that half the drag and half the lift are supported on each side.) Strain gauges are used as the sensing elements in the dynamometers. Each dynamometer is wafer-like, being $\frac{3}{16}$ in. thick and of $2\frac{1}{2}$ in. diameter, and is fitted into a 2·56 in. diameter recess in the corresponding side plate. As used in the experiments to be described, the drag dynamometer measures up to 20 lb., and the lift dynamometer up to 80 lb. within the linear calibration range. The dynamometer readings are repeatable in static calibration within about 1 % of full scale; in use, however, fluctuation of the load makes it necessary to read average forces, and accuracy to 1 % cannot be claimed. Interactions between lift, drag, and moment are very small and are eliminated by dead-weight calibration. The moment is not measured.

Each dynamometer recess is covered on the test-body side by disks 2·54 in. in diameter which are an integral part of the test body. Bodies and disks are made from stainless steel and oven-brazed to each other. The disks are 5·00 in. apart and, when in place, form a smooth continuation of the two-dimensional plates with a 0·01 in. annular gap. Load is transferred from a test body to the dynamometers through circular hubs on the disks which fit snugly into holes in the dynamometer. Set screws keep the hubs from turning or moving endwise, once angle of attack has been established. Application of load produces a small displacement in part of the dynamometer and in the covering disks. The annular gap thus becomes asymmetrical. There is some leakage through the annular gap, and this leakage sometimes interferes with cavity observation; but the leakage does not appear to influence force measurements.

Water velocity is determined by measuring the pressure drop in the nozzle leading to the jet. The pressure drop was previously calibrated against velocity by weighing the discharge up to velocities of about 30 ft./sec; the calibration curve was linear up to this velocity, and the straight line was extended to the highest velocities. The calibration curve was verified by measurements in the jet with a Pitot-static tube up to the highest velocities. These measurements also demonstrated that the velocity between the side plates at the test-body location, at 40 ft./sec. mean velocity, was uniform within 1 %; any boundary layer was confined to a region $\frac{1}{4}$ in. thick near each wall which could not be reached by the Pitot-static tube. This uniform velocity profile makes it possible, for computational purposes, to consider the flow to be that of an ideal, infinite, two-dimensional jet rather than a jet from a nozzle.

The calibrated velocity occurs at the end of the nozzle. The actual velocity head at the test body is composed of the velocity head at the nozzle exit plus the vertical distance from nozzle exit to centre of test body—7 in. in this tunnel. That this is the case was verified by measurements with a total-head tube with no body in the tunnel.

3. Experimental results

Some observed force coefficients are shown in figures 3 to 6. Cavity lengths, measured from photographs, are given in figure 7. Typical photographs are shown in figure 8 (plate 2). The shapes investigated were a two-dimensional cup (figure 3), two symmetrical wedges (figure 4), flat plates at four angles of attack (figure 5), and a circular cylinder (figure 6).

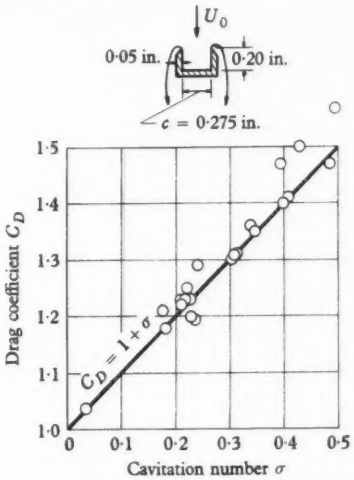

FIGURE 3. Drag coefficient for two-dimensional cup.

In presenting the data, the following parameters are used:

cavitation number	$\sigma = (p_0 - p_k)/q,$	(1)
or	$\sigma_v = (p_0 - p_v)/q,$	(1*a*)
lift coefficient	$C_L = L/lcq,$	(2)
drag coefficient	$C_D = D/lcq,$	(3)
Reynolds number	$\mathrm{Re} = U_0 c/\nu.$	(4)

Here p_0 is the measured pressure in the chamber surrounding the jet, p_k is the measured cavity pressure, p_v is the vapour pressure of water at the operating temperature, $q = \frac{1}{2}\rho U_0^2$ is the reference dynamic pressure, U_0 is the velocity which would exist in the undisturbed jet at the position of the centre of the test body, L is the lift or net force on the body normal to U_0, D is the drag or net force on the body parallel to U_0, c is the chord length or other characteristic dimension of the body, l is the span (5 in. in this tunnel), ρ is the density of the water, and ν is the coefficient of kinematic viscosity of the water.

In the case of one of the wedges (figure 4*b*) and for the circular cylinder (figures 6*b* and 6*c*), the experiments were carried into the non-cavitating range. In these two cases the cavitation number is defined by (1*a*) because it was impossible to measure cavity pressure directly. All other experiments were limited

to the very small cavitation numbers associated with supercavitating flows; cavity pressure was measured directly and cavitation number is defined by (1). Almost all the data were obtained in a range of velocities U_0 from about 38 to 45 ft./sec. Some data were obtained at velocities as low as 20 ft./sec: these data are appropriately indicated where they occur.

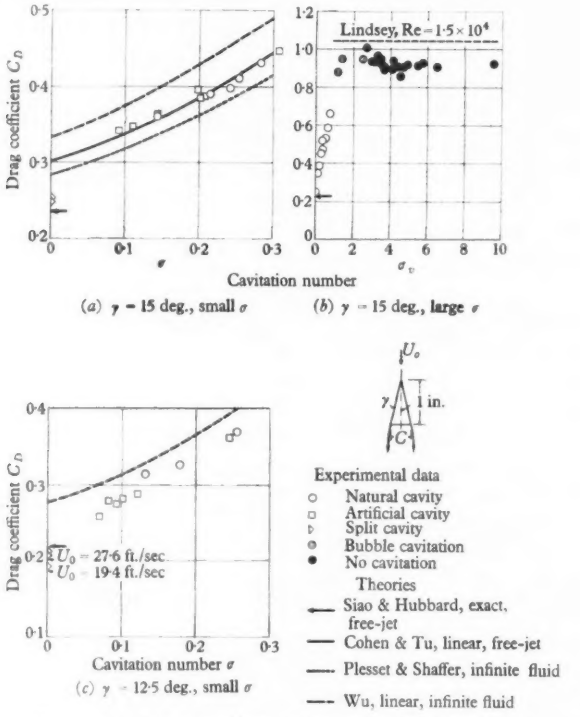

FIGURE 4. Drag coefficients for symmetrical wedges.

The lift L was taken directly from measured data for use in (2). The drag coefficient according to (3) was corrected, before plotting the data, by subtracting the calculated skin-friction drag coefficient for the end disks and the calculated skin-friction coefficient for the test body. The corrections are described in Appendix A. Therefore, the plotted drag coefficients relate to form or cavitation drag of the test bodies.

For the flat plates at small angles of attack, it was found that the drag coefficient, especially, was very sensitive to the sharpness of the leading edge. These edges were kept honed, and the tunnel was stopped and the edges were cleaned after each measurement was obtained. (Bits of grass from the river water accumulated on the leading edges.) Nevertheless, the drag data were difficult to reproduce, as may be seen in figures 5*a* and 5*c*.

Three different classes of cavities were generated. Naturally occurring, closed cavities are indicated by circles in the force-coefficient graphs. These cavities are

produced by controlling the parameters p_0 and q in equation (1). Closed cavities obtained by extending control to p_k by feeding air to the wakes of the bodies are indicated by square symbols and are called 'artificial'. Split cavities, illustrated

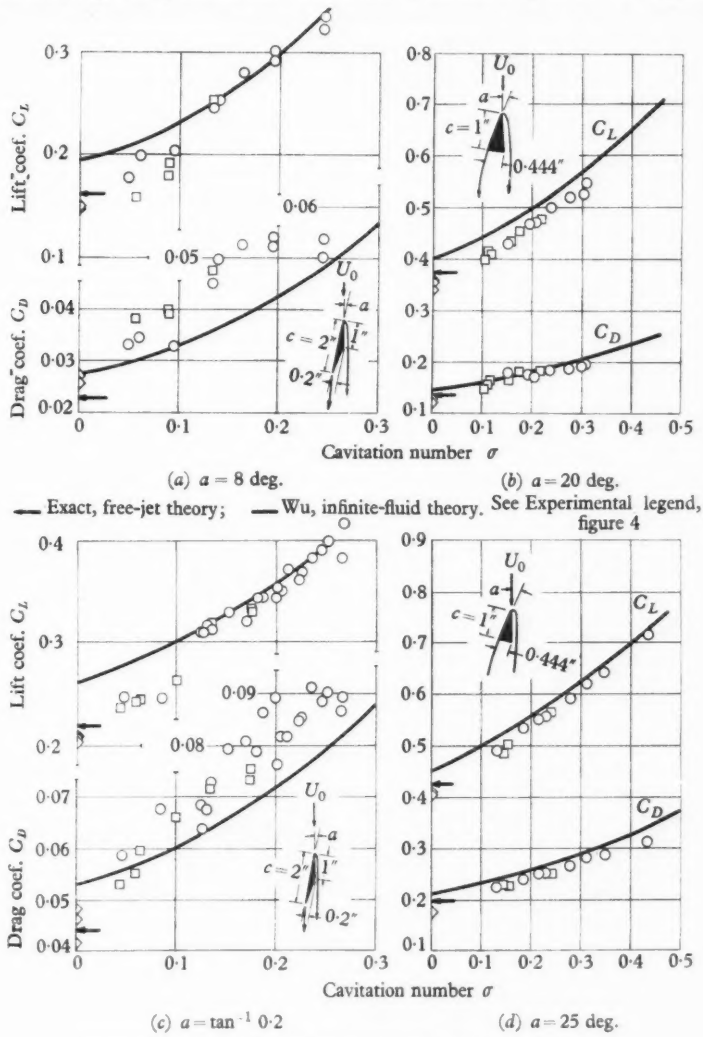

FIGURE 5. Lift and drag coefficients for inclined flat plates.

by photographs in figures 8*a* and 8*b* (plate 2), occur when a cavity is vented to the surrounding chamber; they are indicated by half-diamond-shaped symbols. There is an advantage in operating with an artificial cavity because, for the same cavitation number, q can be smaller and p_0 larger than for a natural cavity. With small q and large p_0, secondary cavitation of the leading edges of the side plates and of the space between the observation windows can be reduced or eliminated.

The experimental data indicate that there is no significant difference between natural and artificial cavities.

Visual observation showed that the cavity walls were generally laminar as they left the test bodies, except in the case of the 2 in. chord flat plates. The laminar

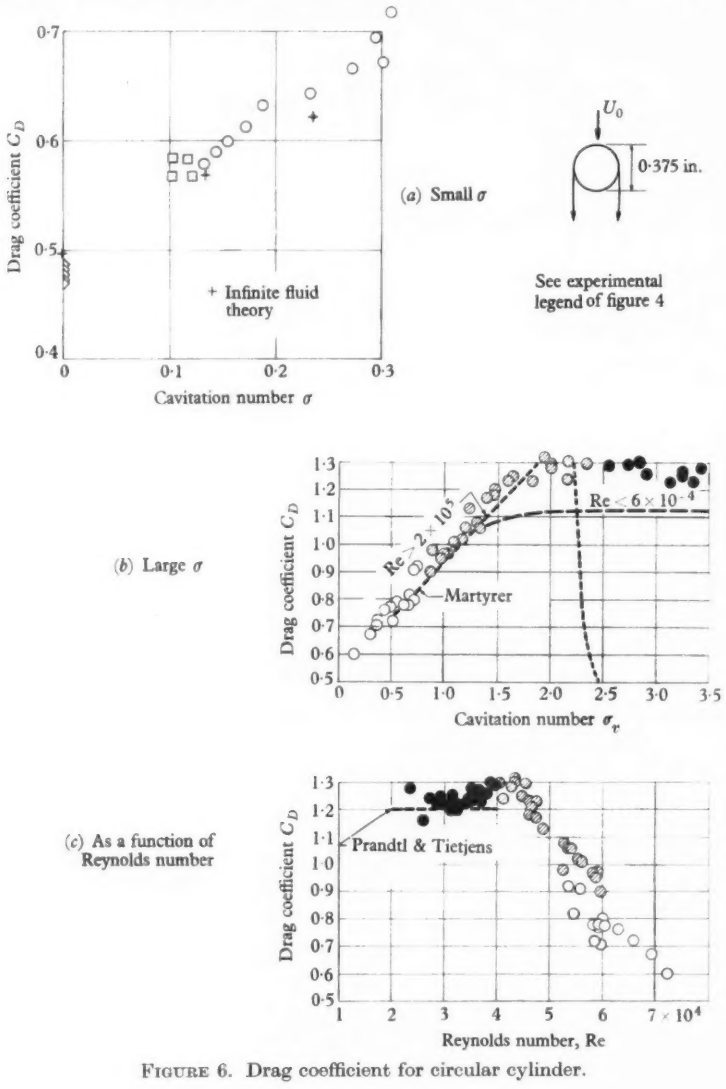

FIGURE 6. Drag coefficient for circular cylinder.

flow became turbulent within about 1 chord length or less from the trailing ends of the bodies. Transition appeared to occur along a fixed ragged line across the span on each cavity wall.

4. Effect of gravity

It is desirable to compare the experimental results with theoretical computations. As has already been mentioned in describing the equipment, the uniformity of the velocity across the jet makes it possible to treat the flow as that of an ideal, two-dimensional, infinite jet. A possible limitation on this treatment is the effect

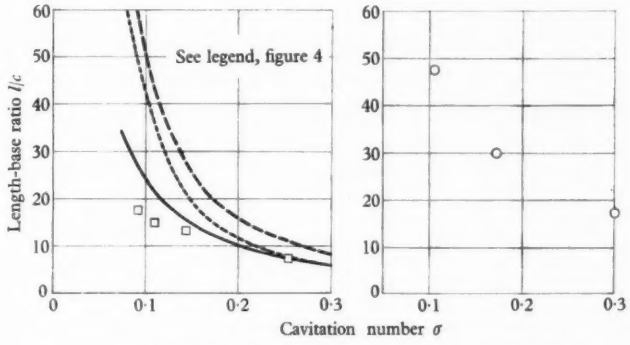
Length-base ratio l/c
See legend, figure 4
Cavitation number σ
(a) Symmetrical wedge, $\gamma = 15$ deg.
(b) Circular cylinder
Length-chord ratio l/c
Infinite fluid theories
— Wu
--- Tulin (linear)
Cavitation number σ
(c) Flat plate, $\alpha = 8$ deg.
(d) Flat plate, $\alpha = \tan^{-1} 0{\cdot}2$

FIGURE 7. Typical cavity length measurements.

of gravity, because the jet is vertical and contracts as it falls. (The contraction effect attributable to gravity is, however, at least partially balanced by boundary-layer growth on the two-dimensional side plates.)

The magnitude of the gravitational effect depends on the Froude number of the jet. This is apparent from the continuity equation, which may be written

$$\frac{db}{dh} = -\frac{b}{U}\frac{dU}{dh}, \tag{5}$$

and from the momentum equation

$$U\frac{dU}{dh} = g, \tag{6}$$

where h is the depth from the origin of the jet to any point in the test section, U is the velocity at depth h, b is the breadth of the jet at depth h, and g is the acceleration due to gravity. Thus, we have

$$\frac{db}{dh} = -\frac{bg}{U^2}, \tag{7}$$

where the quantity on the right-hand side is the inverse square of the Froude number. For the test jet, b is 10 in.; with $U = 40$ ft./sec, the theoretical rate of contraction is approximately 0·2 in./ft. of fall, while at 20 ft./sec it is 0·8 in./ft.

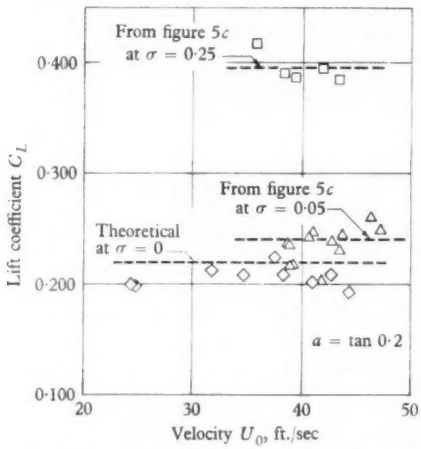

FIGURE 9. Effect of gravity on flat-plate lift coefficient.

In order to estimate the gravitational effect on force coefficients, the flat plate at an incidence of $\tan^{-1}(0{\cdot}2)$ was operated over a range of velocities at each of several cavitation numbers. The resulting lift coefficients are plotted in figure 9. Similar results were obtained for drag coefficients. It may be concluded from the figure that, within the range of velocities studied, there is no recognizable effect on force coefficients attributable to gravity. Another similar experiment was performed using the wedge of 12·5° semi-angle at zero cavitation number. These results are included in figure 4*c*. A definite decrease in drag coefficient was observed when the velocity was decreased from 27·6 to 19·4 ft./sec, but at higher velocities any change may be within the experimental error.

No experimental investigation has been made as to the effect of gravity on cavity shape. The definition for cavitation number given by (1) may be looked upon as the ratio of transverse momentum change produced by pressure difference to longitudinal momentum change. Considering that, for a given cavitation number, $p_0 - p_k$ is constant along the jet while U_0 increases because of gravity, it would be expected that a cavity in the vertical free jet would be longer than predicted by a theory obtained without considering gravity.

5. Comparison with theory and with measurements by others

In each of figures 3 to 8, one or more comparable theoretical or experimental results have been introduced.

In figure 3, for the two-dimensional cup, the theoretical drag is calculated by assuming that stagnation pressure exists uniformly over the upstream surface of the cup and that cavity pressure exists uniformly over the downstream surface. Then

$$C_D = \frac{q+p_0-p_k}{q} = 1+\sigma. \tag{8}$$

This prediction is independent of the tunnel boundary conditions (but may be influenced by the depth of the cup). The comparison between (8) and the experimental results shown in figure 3 serves to verify the drag dynamometer.

For the wedges at zero cavitation number in an infinite jet, the free-streamline theory has been worked out by Siao & Hubbard (1953). Calculations have been made from Siao & Hubbard's paper; the theoretical results for drag are indicated on the graphs of figure 4 and for shape, for the 15° wedge, by crosses on the photograph in figure 8*a* (plate 2). Agreement between measurement and theory is very satisfactory. The cavity walls seen in the downstream portion of the photograph in figure 8*a* (plate 2) have already attained their theoretical direction at infinity—6·42° with the axis of symmetry.

Cohen & Tu (1956) have developed a linearized theory for drag and cavity length of a symmetrical wedge in a free jet at non-zero cavitation numbers. The computations required to obtain drag coefficient from the paper are quite involved; but one of the authors, in a private communication, supplied the curve reproduced in figure 4*a* for the 15° semi-angle wedge. There is good agreement with the experimental data for cavitation numbers above 0·1.* Also reproduced in figure 4*a* are the results obtained on the basis of infinite-fluid theory by Plesset & Shaffer (1948) using the Riabouchinsky method and by Wu (1957) using a linearized theory. Wu's results are also plotted in figure 4*c* for comparison with the experimental results for the 12·5° semi-angle wedge. In the non-cavitating range (figure 4*b*), comparison is made with the experimental results of Lindsey (1938) obtained in a closed wind tunnel. The present results are uniformly about 13 % below those of Lindsey (which include skin friction).

Theoretical results for cavity length for the 15° semi-angle wedge are plotted with the experimental data in figure 7*a*. The effective shortening of the cavity in the free jet, as compared to a cavity in an infinite fluid, is clearly shown. The measured cavity lengths are even shorter than predicted by the linear free-jet theory, although they might have been expected to be longer because of the gravitational effect discussed in § 4. Actually, as may be seen in figures 8*c* and 8*d* (plate 2), there is considerable uncertainty in measuring cavity length; and this,

* Linear theories depend on the introduction of a perturbation potential to produce the cavity. It must be assumed that the perturbation potential will not affect the flow at infinity. However, with an infinitely long cavity, there is no way to avoid interference with the flow at infinity and the linear method must fail at zero cavitation number.

together with the breakdown of the linear theory at small cavitation numbers, may account for the discrepancies between experiment and theory.

Although the free-streamline theory for an inclined flat plate in a jet at zero cavitation number is fairly straightforward, no solution which had been carried to the point of computational usefulness could be found in the literature. Accordingly, such a solution is given in Appendix B. The calculated lift and drag coefficients are shown on the graphs in figure 5, and the resulting cavity shape for the angle of attack of $\tan^{-1}(0{\cdot}2)$ is shown on the photograph in figure 8*b* (plate 2). Agreement between experiment and theory may again be considered very satisfactory. In the downstream portion of the photograph in figure 8*b* (plate 2), the cavity walls have already become essentially straight and have attained their theoretical directions at infinity, 4·01 degrees with the axis of symmetry for the wall originating from the leading edge and 6·43 degrees for the other.

There is no available theory for the inclined plate in a jet at non-zero cavitation numbers.* For comparative purposes, the results of the free-streamline theory (non-linear) for an infinite fluid given by Wu (1956) are shown on the graphs in figure 5. The data fall below the infinite-fluid theory at small cavitation numbers, as is to be expected, and appear to approach the infinite-fluid results as the cavitation number increases. It should be observed that Wu's theoretical results agree well with experimental measurements in a closed tunnel at a chord-tunnel-width ratio of about 1/8 as reported by Parkin (1958). The experimental measurements in the closed tunnel were carried down to a cavitation number of about 0·15 at an angle of attack of 8°, down to about 0·2 at 11°, down to about 0·35 at 20°, and down to about 0·45 at 25°. In so far as lift is concerned, it appears from the present data, from Wu's theory, and from Parkin's data that wall corrections are important only at small cavitation numbers (of the order of 0·12 or less) for the narrow cavities associated with small angles of attack.

Wu's theory for the plate in an infinite fluid does not yield a precise definition of cavity length. However, lengths obtained using the definition given by Wu are shown for comparative purposes on the graphs in figures 7*c* and 7*d*. Also shown on these graphs are the cavity lengths predicted by Tulin's (1956) linear theory for the inclined plate in infinite fluid. (Lift and drag predicted by Tulin's theory were not shown in figure 5, as the curves are only a little higher than Wu's curves at zero cavitation number and approach Wu's curves closely at higher cavitation numbers.) As in the case of the wedge, there is difficulty in selecting the closing point of the cavities from the flat-plate photographs, so the experimental cavity lengths shown in the figures are subject to some error. The results look reasonable, however, when compared with the infinite-fluid theory.

Three theoretical drag coefficients computed for the circular cylinder in infinite fluid, presented by Birkhoff & Zarantonello (1957, p. 148) are shown for comparison with the experimental data in figure 6*a*. The agreement with free-jet data is quite good at all three points. At higher cavitation numbers, shown in figure 6*b*, comparison is made with Martyrer's experimental data (1932) obtained in a closed

* There is a fundamental obstacle to the development of a suitable linear theory for a lifting surface in a jet because of the absence of symmetry in both the cavity and the jet walls.

tunnel. Again agreement between the free-jet and closed-tunnel results is reasonably good. For the non-cavitating flow past the circular cylinder (figure 6*c*), the accepted value for the drag coefficient at Reynolds numbers from 2 to 4×10^4 is about 1·2, as given in Prandtl & Tietjens (1934, figure 50, p. 96). Small discrepancies between free-jet and closed-tunnel results may be accounted for by variations in the point of separation on the cylinder.

6. Conclusion

Good agreement has been obtained between measurements in the free-jet tunnel and theoretical prediction for a free jet, where theoretical predictions were available. At the operating speeds of the tunnel, gravity has no appreciable effect on the measured force coefficients. The tunnel and measuring equipment are, therefore, believed to be operating satisfactorily.

Comparison between the present results and theoretical results for an infinite fluid, and with measurements by others in closed tunnels, indicates that wall corrections for converting measured results in the free jet to infinite-fluid conditions are negligibly small for all but the smallest cavitation numbers. At zero cavitation number, force coefficients and cavity lengths measured in the free jet can be expected to be less than those in infinite fluid. The exact relation depends on the shape of the body and its position in the jet. For the flat plate at several angles of attack, the difference between the measurements in the jet and the theoretical predictions for infinite fluid all but disappeared for cavitation numbers greater than about 0·12.

The work described herein was undertaken at the St Anthony Falls Hydraulic Laboratory with support of the Office of Naval Research, United States Department of the Navy, under contract Nonr 710(24) with the University of Minnesota. Robert L. Gordier has been responsible for operating the tunnel and obtaining the experimental data. John F. Ripken has been of material assistance in perfecting the experimental equipment and in offering advice on other phases of the work.

Appendix A

Drag corrections

Two subtractive corrections were made to the measured drag coefficients. The first of these, the end-disk drag, was calculated by assuming a turbulent (dictated by the Reynolds number) flat-plate boundary layer from the leading edge of each side plate. The local shear stress was then integrated over the area of each disk less an average area occupied by the body plus cavity or wake. No allowance was made for pressure drag on the disks even though there was a little leakage around their edges. The final expression for the correction to the drag coefficient for the two end disks was

$$\Delta C_D = -\frac{0{\cdot}0605}{\mathrm{Re}^{\frac{1}{5}}}\left(\frac{R}{c}\right)^{\frac{4}{5}}, \tag{A 1}$$

where R is the radius of the end disk—i.e. 1·27 in.

The calculations were partially checked by measurements in the tunnel. A flat plate of 2 in. chord and at an incidence of $\tan^{-1}(0{\cdot}2)$ was mounted rigidly as a cantilever beam from the lift side plate with the lift dynamometer removed. A dummy end disk was mounted in the drag dynamometer; about 0·004 in. separated the disk from the flat plate. Drag measurements obtained with this arrangement were about 25 % lower than given by the above formula. It was later realized, however, that pressure differences over the face of the disk caused the disk to twist out of the plane of the wall, twisting the dynamometer and producing false readings which could be expected to be low.

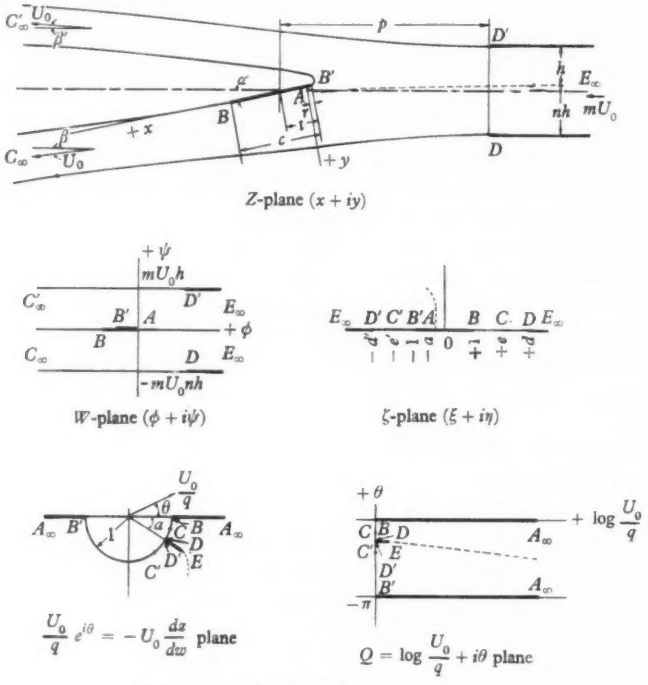

FIGURE 10. Conformal mapping planes.

The second correction was for skin-friction drag on the test bodies. The wedges, being of 1 in. chord, possessed laminar boundary layers. Drag was calculated using the wedge-flow solution as outlined in Schlichting (1955, p. 128). For application of this solution, the velocity was taken in the form

$$U(x) = U_k x^m = U_0(1+\sigma)^{\frac{1}{2}} x^m, \tag{A 2}$$

where x is the distance along the wedge from the front stagnation point, in inches ($0 \leqslant x \leqslant 1$), $U(x)$ is the velocity at any x, U_k is the constant velocity at the edge of the cavity given by $(U_k/U_0)^2 = 1+\sigma$, and $m = \gamma/(\pi-\gamma)$ where γ is the wedge semi-angle. Integration of the wall shear stress over both surfaces resulted in the expression

$$\Delta C_D = -C\frac{(1+\sigma)^{\frac{1}{2}}}{\mathrm{Re}^{\frac{1}{2}}}, \tag{A 3}$$

where the constant C has the value 1·91 for the 12·5° semi-angle wedge and 2·20 for the 15° semi-angle wedge. It is noted in passing that if each wedge surface had been considered a flat plate at zero pressure gradient in a stream of velocity U_0, the constants would have been 1·77 and 1·94, respectively, at zero cavitation number.

In view of the wedge solution and the comparison with the flat plate at zero pressure gradient just discussed, skin friction on the inclined flat plates (one side only) was based on the skin friction of the flat plate at zero pressure gradient. For laminar boundary layers, equation (A 3) was used, C having the value 1·328. For turbulent boundary layers, which occurred on the 2 in. chord plate, $0{\cdot}074/\mathrm{Re}^{\frac{1}{5}}$ was substituted for $C/\mathrm{Re}^{\frac{1}{2}}$ in equation (A 3).

Only the end-disk skin-friction correction was applied to the cup and circular cylinder data.

Appendix B

Free-streamline solution for an inclined flat plate in an infinite jet

The upper diagram in figure 10 represents the flow from a jet from a nozzle about an inclined flat plate. The corresponding complex-potential plane and other mapping planes are shown in the remaining diagrams. The origin in the physical plane is taken at the stagnation point A. The angle of attack is α and the velocity on the free streamline is U_0. The transformations are

$$\left.\begin{aligned} W &= \frac{mU_0h}{\pi}\left[n\log\frac{\zeta-e}{e+a}+\log\frac{\zeta+e'}{e'-a}-i\pi n\right], \\ n &= \frac{e+a}{e'-a}. \end{aligned}\right\} \tag{B 1}$$

$$\frac{dQ}{d\zeta} = \frac{K}{(\zeta+a)\,[(\zeta^2-1)\,(\zeta-d)\,(\zeta+d')]^{\frac{1}{2}}}. \tag{B 2}$$

Equation (B 2) is readily integrated when points D and D' are at infinity in the ζ plane (p goes to infinity in the physical plane while $h+nh$ remains constant). This corresponds to the case of the infinite jet with $m = 1$. Then

$$Q = -\cosh^{-1}\left(\frac{1+a\zeta}{\zeta+a}\right) = -\log\left\{\frac{1+a\zeta}{\zeta+a}-\left[\left(\frac{1+a\zeta}{\zeta+a}\right)^2-1\right]^{\frac{1}{2}}\right\}, \tag{B 3}$$

$$-U_0\frac{dz}{dw} = \frac{1+a\zeta+i[(1-a^2)\,(\zeta^2-1)]^{\frac{1}{2}}}{\zeta+a}, \tag{B 4}$$

$$a = \cos\alpha, \tag{B 5}$$

$$\left.\begin{aligned} \beta &= -\alpha+\tan^{-1}\left[\frac{(e^2-1)^{\frac{1}{2}}\sin\alpha}{1+e\cos\alpha}\right], \\ \beta' &= -\alpha+\tan^{-1}\left[\frac{(e'^2-1)^{\frac{1}{2}}\sin\alpha}{e'\cos\alpha-1}\right], \end{aligned}\right\} \tag{B 6}$$

$$\frac{dz}{d\zeta} = -\frac{h(n+1)}{\pi}\,\frac{1+a\zeta+(1-a^2)^{\frac{1}{2}}\,(1-\zeta^2)^{\frac{1}{2}}}{(\zeta+e')\,(\zeta-e)}; \tag{B 7}$$

and, for $\zeta^2 \leqslant 1$,

$$\frac{z}{h(n+1)} = \frac{1}{\pi(e'+e)}\left[(ae+1)\log\frac{a+e}{e-\zeta} - (ae'-1)\log\frac{e'+\zeta}{e'-a}\right] + \frac{\sin\alpha}{\pi}\left\{\pi - \alpha - \cos^{-1}\zeta\right.$$
$$+ 2\frac{(e'^2-1)^{\frac{1}{2}}}{e'+e}\tan^{-1}\frac{[(1-a)(1-\zeta)]^{\frac{1}{2}} - [(1+a)(1+\zeta)]^{\frac{1}{2}}}{[(1-a)(1+\zeta)(e'+1)/(e'-1)]^{\frac{1}{2}} + [(1+a)(1-\zeta)(e'-1)/(e'+1)]^{\frac{1}{2}}}$$
$$\left. + 2\frac{(e^2-1)^{\frac{1}{2}}}{e'+e}\tan^{-1}\frac{[(1-a)(1-\zeta)]^{\frac{1}{2}} - [(1+a)(1+\zeta)]^{\frac{1}{2}}}{[(1-a)(1+\zeta)(e-1)/(e+1)]^{\frac{1}{2}} + [(1+a)(1-\zeta)(e+1)/(e-1)]^{\frac{1}{2}}}\right\}. \tag{B 8}$$

The constant was evaluated so that $z = 0$ when $\zeta = -a$. Noting that the chord length is given by $c = z_{B'} - z_B$, the chord-length to jet-width ratio is found to be

$$\frac{c}{h(n+1)} = \left[1 - \frac{(e'^2-1)^{\frac{1}{2}} + (e^2-1)^{\frac{1}{2}}}{e'+e}\right]\sin\alpha - \frac{ae'-1}{\pi(e'+e)}\log\frac{e'+1}{e'-1} + \frac{ae+1}{\pi(e'+e)}\log\frac{e+1}{e-1}. \tag{B 9}$$

For $\zeta^2 \geqslant 1$, the integral of (B 7) may be written

$$\frac{z}{h(n+1)} = \frac{1}{\pi(e'+e)}\left[(ae'-1)\log\frac{e'-a}{e'+\zeta} - (ae+1)\log\frac{e-\zeta}{a+e}\right] - \frac{\alpha}{\pi}\sin\alpha$$
$$+ \frac{2\sin\alpha}{\pi(e'+e)}\left[(e'^2-1)^{\frac{1}{2}}\tan^{-1}\left(\frac{e'+1}{e'-1}\frac{1-a}{1+a}\right)^{\frac{1}{2}} + (e^2-1)^{\frac{1}{2}}\tan^{-1}\left(\frac{e-1}{e+1}\frac{1-a}{1+a}\right)^{\frac{1}{2}}\right]$$
$$+ i\frac{\sin\alpha}{\pi}\left\{\cosh^{-1}(-\zeta) - \frac{2}{e'+e}\left[(e'^2-1)^{\frac{1}{2}}\tanh^{-1}\left(\frac{e'+1}{e'-1}\frac{\zeta+1}{\zeta-1}\right)^{\frac{1}{2}}\right.\right.$$
$$\left.\left. + (e^2-1)^{\frac{1}{2}}\tanh^{-1}\left(\frac{e-1}{e+1}\frac{\zeta+1}{\zeta-1}\right)^{\frac{1}{2}}\right]\right\}. \tag{B 10}$$

The positions of the upper and lower jet walls at E with respect to A in the physical plane are given by

$$\tfrac{1}{2}h(n+1) - (t-r)\sin\alpha = -x_{E(-\infty)}\sin\alpha - y_{E(-\infty)}\cos\alpha, \tag{B 11}$$

$$\tfrac{1}{2}h(n+1) + (t-r)\sin\alpha = x_{E(+\infty)}\sin\alpha + y_{E(+\infty)}\cos\alpha. \tag{B 12}$$

Subtracting (B 11) from (B 12), we find

$$\frac{t}{h(n+1)} = \tfrac{1}{2}\sin\alpha + \frac{\cos\alpha}{\pi}\log 2 + \frac{1}{e'+e}\left\{\cot\alpha - (e'-e)\frac{\sin\alpha}{2}\right.$$
$$- (e'^2-1)^{\frac{1}{2}}\sin\alpha - \frac{1}{\pi}\log\frac{e'-1}{e+1} - \frac{\cos\alpha}{(e'+e)\pi}\left[2(e'^2-1)^{\frac{1}{2}}\tanh^{-1}\left(\frac{e'-1}{e'+1}\right)^{\frac{1}{2}}\right.$$
$$\left.\left. - e'\log(e'-1) + 2(e^2-1)^{\frac{1}{2}}\tanh^{-1}\left(\frac{e-1}{e+1}\right)^{\frac{1}{2}} - e\log(e+1)\right]\right\}. \tag{B 13}$$

Equations (B 9) and (B 13) are a pair of simultaneous equations for e and e', given c, t, $h(n+1)$, and α. Once e and e' are determined, lift and drag may be obtained from the momentum equation using (B 6) or by integrating the pressure

Elevation

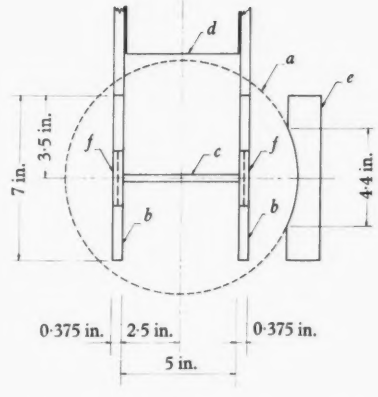

Plan

FIGURE 2 (plate 1). Views of two-dimensional test section. *a*, 10 in. diameter free jet nozzle; *b*, two-dimensional side plates; *c*, test body and integral end disks; *d*, side plate support structure; *e*, viewing window (Plexiglass), *f*, dynamometers; *g*, piezometer tubes for measuring cavity pressure; *h*, housing that rises to seal test section.

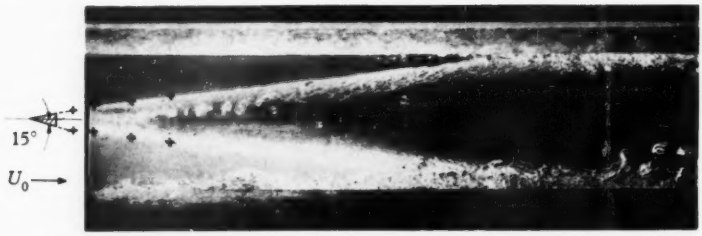

+Theoretical points

(*a*) Symmetrical wedge, $\sigma = 0$

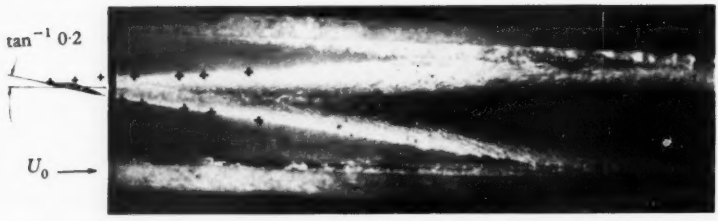

+Theoretical points

(*b*) Flat plate, $\sigma = 0$

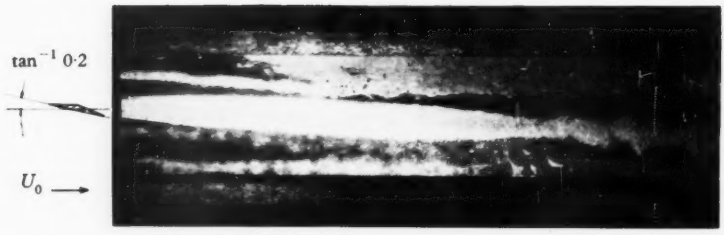

(*c*) Flat plate, $\sigma = 0{\cdot}063$

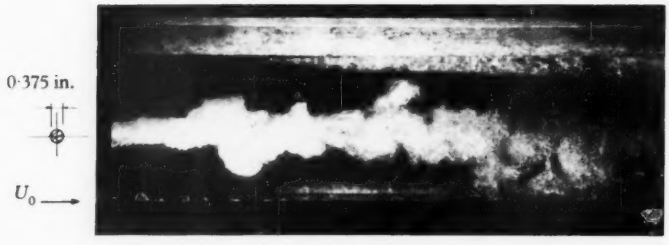

(*d*) Circular cylinder, $\sigma = 0{\cdot}301$

FIGURE 8 (plate 2). Typical cavities.

o
c

a

W

F

F
t

F

F

F

C

C

F

over the plate. Performing either of these operations, and reducing the results to coefficient form, we obtain

$$C_L = \frac{\pi \sin 2\alpha}{\pi \sin \alpha + \dfrac{(ae'-1)\log[(e'+1)/(e'-1)] - (ae+1)\log[(e+1)/(e'-1)]}{(e^2-1)^{\frac{1}{2}} + (e'^2-1)^{\frac{1}{2}} - e' - e}}, \tag{B 14}$$

and

$$C_D = C_L \tan \alpha. \tag{B 15}$$

When the fluid is infinite, h, e and $e' \to \infty$, and

$$C_{L\infty} = \frac{\pi \sin 2\alpha}{\pi \sin \alpha + 4}. \tag{B 16}$$

Hence

$$\frac{C_L}{C_{L\infty}} = \frac{C_D}{C_{D\infty}} = \frac{h(n+1)}{c}(4/\pi + \sin\alpha)\left[1 - \frac{(e'^2-1)^{\frac{1}{2}} + (e^2-1)^{\frac{1}{2}}}{e'+e}\right]. \tag{B 17}$$

Equation (B 17) is plotted in figure 11 for several angles of attack for the case $t/c = \frac{1}{3}$. Small changes in t/c have negligible effect on the force coefficients.

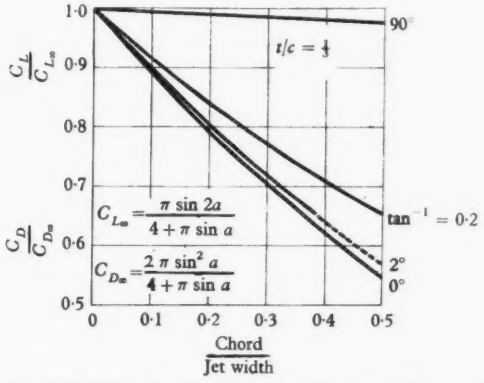

FIGURE 11. Force coefficients for flat plates in free jet at zero cavitation number.

REFERENCES

BIRKHOFF, G., PLESSET, M. S. & SIMMONS, N. 1950 Wall effects in cavity flow. Part I. *Quart. Appl. Math.* **8**, 151.

BIRKHOFF, G., PLESSET, M. S. & SIMMONS, N. 1952 Wall effects in cavity flow. Part II. *Quart. Appl. Math.* **9**, 413.

BIRKHOFF, G. & ZARANTONELLO, E. H. 1957 *Jets, Wakes and Cavities.* New York: Academic Press.

CHRISTOPHERSON, C. D. 1953 Description of a ten-inch free-jet water tunnel. *St Anthony Falls Hydraulic Laboratory, University of Minnesota, Project Rep.* no. 35. (Available on interlibrary loan from the University of Minnesota Library, Minneapolis 14, Minnesota.)

COHEN, H. & TU, Y. 1956 A comparison of wall effects on supercavitating flows past symmetric bodies in solid wall channels and jets. *Proc. 9th Int. Congr. Appl. Mech., Brussels*, p. 359.

LINDSEY, W. F. 1938 Drag of cylinders of simple shapes. *Nat. Adv. Comm. Aero., Wash., Rep.* no. 619.

MARTYRER, E. 1932 Kraftsmessungen an Widerstandskörpern und Flügelprofilen in Wasserstrom beim Kavitation, Article in *Hydromechanische Probleme des Schiffsentriebs* (Ed. Kempf & Foerster). Hamburg: Schiffbau–Versuchsanstalt.

PARKIN, B. R. 1958 Experiments on circular arc and flat plate hydrofoils in noncavitating and full cavity flows. *J. Ship. Res.* **1**, 34.

PLESSET, M. S. & SHAFFER, P. A., JR. 1948 Cavity drag in two and three dimensions. *J. Appl. Phys.* **19**, 934.

PRANDTL, L. & TIETJENS, O. G. 1934 *Applied Hydro and Aeromechanics.* New York: McGraw-Hill.

SCHLICHTING, H. 1955 *Boundary Layer Theory.* New York: McGraw-Hill.

SIAO, T. T. & HUBBARD, P. G. 1953 Deflection of jets, Part I. Symmetrically placed V-shaped obstacle. *Free Streamline Analyses of Transition Flow and Jet Deflection, State University of Iowa, Bulletin* no. 35, p. 33.

TULIN, M. P. 1956 Supercavitating flow past foils and struts. *Proc. Symposium on Cavitation in Hydrodynamics, National Physical Laboratory, Teddington, England.*

WU, T. Y. 1956 A free streamline theory for two-dimensional fully cavitated hydrofoils. *J. Math. Phys.* **25**, 236.

WU, T. Y. 1957 A simple method for calculating the drag in the linear theory of cavity flows. *California Institute of Technology, Rep.* no. 85.

Steady flow through non-uniform gauzes of arbitrary shape

By J. W. ELDER†
Cavendish Laboratory, University of Cambridge

(Received 18 July 1958)

The steady, two-dimensional flow through an arbitrarily-shaped gauze, of non-uniform properties, placed in a parallel channel is considered for the case in which viscosity can be ignored except in the immediate vicinity of the gauze. The equations are linearized by requiring departures from uniformity both in the flow and in the gauze parameters to be small. Knowledge of any three of the upstream profile, the downstream profile, the shape of the gauze, and the gauze parameters, allows the other to be calculated from a linear relation between these four quantities. Particular solutions are given for the production of a uniform shear and the flow through linear and parabolic gauzes. The validity of the solution is verified by experiment. It is shown that the method can also be applied to two-dimensional flow in a diverging channel, axisymmetric flow in a circular pipe and in a circular cone, and to flow through multiple gauzes.

1. Introduction

When a stream of fluid passes through a wire gauze the stream may be deflected and the static pressure of the stream reduced. An adequate description of these properties of the gauze can be given in terms of a drag coefficient, K, and a lift coefficient, B, and many, largely empirical attempts, have been made to relate these coefficients to the numerical parameters of the gauze (e.g. Wieghardt 1953).

The present paper is concerned principally with the steady two-dimensional flow in a parallel channel in which an arbitrarily-shaped gauze is placed. The flow through a gauze placed normal to the incident stream was first solved by Taylor & Batchelor (1949), who showed that departures from uniformity in the incident stream were attenuated by a factor $(2-K-B+KB)/(2+K-B)$. This solution was also obtained by Bonneville & Harper (1951), in a manner similar to that employed by Bragg & Hawthorne (1950), who considered the perturbation to the stream function by gauzes that deflected the streamlines by small amounts. Davis (1957) applied the method to flow through two normal, interfering gauzes, while Owen & Zienkiewicz (1957) showed that a gauze, with a linear variation of drag across its surface, placed normal to a uniform incident stream produced a linear profile downstream. All these investigations rely on the departures of the flow from uniformity being small. A similar perturbation solution will be obtained

† Present address: Department of Scientific and Industrial Research, Wellington, New Zealand.

below for the flow through a single or a pair of arbitrarily shaped, non-uniform gauzes; the equations being linearized by requiring both the departures of the gauze parameters from uniformity and the angle of incidence of the flow on the gauze to be small. The principal result of the paper is a linear relation between the upstream velocity profile, the downstream profile, the shape of the gauze, and the variation of K across the gauze. This relation can be manipulated to give any one of these four quantities in terms of the other three and contains all the hitherto known solutions as particular cases.

Although in principle the solution also applies to a gauze which only partially fills the channel, it is found by experiment to be invalid unless $K \ll 1$. For higher values of K the only solution so far known is that given by Taylor (1944), which consists in replacing the gauze by a sheet of sources. Throughout this paper only gauzes which fill the channel will be considered.

1.1. *A gauze as a surface of discontinuity*

For the present purpose any regular or nearly regular spatial distribution of obstructions which lie on or near a single surface will be regarded as a gauze. Typical examples are: a row of cylinders, a plane rectangular mesh of circular wires, a perforated plate, a sheet of cloth, a cascade of aerofoils, a honeycomb of parallel tubes, etc. Combinations of more than one, and possibly different, gauzes can under certain conditions be regarded as a single gauze. The definition implies and requires that the extent of the gauze is large in the directions parallel and small in the direction normal to the surface. As the following treatment is largely two-dimensional, a gauze may be thought of as a row of equal cylinders, not necessarily lying in a plane nor necessarily equally spaced.

Although 'gauze' is quite a broad concept, investigations are usually restricted to gauzes of simple geometrical form which can be specified by a few numbers, such as the wire spacing l and the wire diameter d of a square mesh wire gauze. The flow will then be determined by a velocity scale U_1, the kinematic viscosity ν, l, and d, from which the dimensionless parameters $\beta = (1-d/l)^2$, the proportion of open area presented to the stream, and the Reynolds number $R = U_1 d/\nu$, may be constructed.

Consider now a gauze placed in a steady-flow field, and use the suffices 1 and 2 to indicate the regions upstream and downstream of the gauze. Some distance away from the gauze, the exact nature of the flow near it will be of little importance, particularly for $R \gg 1$. On this basis the gauze may be replaced by a surface of discontinuity across which discontinuities in the velocity and pressure fields occur. It remains to describe how the fields immediately on either side of the surface are related.

Let the velocity at the gauze be resolved into a normal component U_n, and a tangential component V_s (see figure 1). The mass flux ρU_n of fluid of density ρ through the gauze is conserved, and since the fluid is incompressible the velocity change

$$\Delta U_n \equiv U_{n1} - U_{n2} = 0.$$

Similarly, the momentum flux along the normal to the gauze is conserved, so that the drag per unit area is given solely by Δp, the loss of pressure across the

gauze. It is convenient to express this in terms of a dimensionless resistance coefficient K defined by

$$\Delta p = \tfrac{1}{2}\rho K U_n^2. \tag{1.2}$$

K may take all values $\geqslant 0$. By Bernoulli's theorem it follows that Δp is also given by the change in total pressure, $p + \frac{1}{2}\rho U^2$, from far upstream to that far downstream along a streamline.

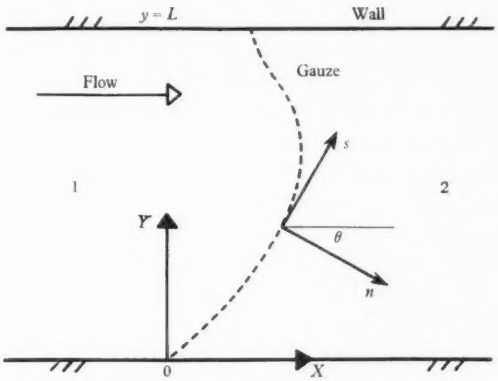

FIGURE 1. Diagram of the co-ordinate systems and the flow boundaries.

The screen also, in general, experiences a lift force, so that $V_{s1} \neq V_{s2}$, and we can define B such that

$$\Delta V_s \equiv V_{s1} - V_{s2} = BV_{s1}. \tag{1.3}$$

A streamline is usually bent towards the normal so that $0 \leqslant B \leqslant 1$. It may be that $B = B(\phi)$, where ϕ is the angle between V_{s1} and some characteristic direction in the gauze, such as a wire direction. However, it will be assumed in this paper, as hitherto, that B is independent of ϕ, and further that U_n, V_{s1} and V_{s2} lie in the same plane.

Davis (1957) has found by experiment that K varies with the Reynolds number R in the manner

$$K \doteq K_0 + 88(1-\beta)/R. \tag{1.4}$$

K_0 is independent of R and can be related to β by a mixing-jet model, similar to that proposed by Taylor & Davies (1944), with the result that

$$K_0 = [(1 - 0{\cdot}95\beta)/0{\cdot}95\beta]^2, \tag{1.5}$$

where 0·95 is an empirical constant.

The mechanism responsible for B is not yet understood. If, however, the flow is equivalent to a uniform stream past a row of equally spaced vortices of circulation k, then $V_1 = V_2 + 2\pi k/l$. Hence, by definition, $B = 2\pi k/lV_1$. If such a circulation exists it must be generated in the vicinity of the cylinder so that on dimensional grounds $k = AdV_1$, where A is a constant. That is, $B = 2\pi Ad/l$. For a square mesh wire gauze,

$$\beta = (1-d/l)^2 \quad \text{and} \quad K \doteq [(1-\beta)/\beta]^2$$

by (1.5), so that,

$$B = 1 - (1+\sqrt{K})^{-\frac{1}{2}}, \tag{1.6}$$

where we have placed $2\pi A = 1$ to satisfy the assumption that $B = 1$ for $K = \infty$. This formula is similar to one proposed on empirical grounds by Taylor & Batchelor (1949), and although it may be considerably in error for a particular gauze, it is sufficiently realistic to provide a convenient choice of pairs of values of K, B for use in theoretical discussion. B will be assumed independent of both R and the angle of incidence of the flow.

K and B may, of course, be functions of position on the gauze, but there is no real significance in changes of K and B over distances much less than l.

1.2. *The linearized boundary conditions at the gauze*

Consider the flow through a gauze placed in a parallel channel with walls at $y = 0$, L such that every velocity vector lies in the Cartesian co-ordinate plane XOY and such that the flow at infinity is parallel to OX and given by $U_\infty(y)$. Let the angle XOn be θ (see figure 1). If the effect of viscosity be neglected except in the vicinity of the gauze, vorticity is conserved along streamlines. If, further, the flow perturbation due to the presence of the gauze is sufficiently small so that streamlines are deflected by a small amount only, then the vorticity $\boldsymbol{\zeta} = \zeta\mathbf{k}$, where $\mathbf{k}$ is unit vector normal to XOY, is such that ζ is unchanged by the presence of the gauze except for a discontinuity at the gauze. Thus $\zeta = \zeta(y) = -\partial U_\infty/\partial y$.

It is necessary to establish that, in practice, it is possible to realize flows in which the assumption of a perfect fluid is valid. For the purpose of taking into account the diffusion of momentum by viscosity, consider as an extreme example the flow given by $U_{\infty 2} = V + U_0 \operatorname{erf}(Vy^2/4\nu x)^{\frac{1}{2}} \quad (U_0 \ll V)$.

This can be shown to correspond to the flow produced by the laminar mixing of two parallel streams of slightly different speeds, $V \pm U_0$, such as would be produced by a gauze made up of two parts of slightly different resistance coefficient. The half-width of the viscous region is required to be less than aL, say, where for practical purposes a lies between 0·01 and 0·05, and L is the width of the channel. Hence we require $x/L < 0{\cdot}28a^2VL/\nu$.

This condition can normally be satisfied without difficulty. For example, in the Cavendish wind tunnel with $L = 40$ cm and $V = 500$ cm/sec, $x/L < 4$ even for $a = 0{\cdot}01$, and for $a = 0{\cdot}05$, $x/L < 100$. On the other hand, a uniform shear can be expected to persist almost indefinitely until viscous effects encroach into the flow from the wall boundary layers. Thus the assumption of a perfect fluid is a good one.

Write $U_1 = U, \quad T = \tan\theta, \quad \gamma = K\cos^2\theta, \tag{1.7}$

and substitute into equations (1.1), (1.2) and (1.3), obtaining

$$U_2 = U - (V_1 - V_2)\,T,$$
$$\Delta p = \tfrac{1}{2}\rho\gamma(U^2 + V_1^2T^2),$$
$$BUT = (1-B)\,V_1 - V_2 + (V_1 - V_2)\,T^2.$$

Except at the gauze, the fluid obeys the equation of motion

$$-\frac{1}{\rho}\nabla p = \tfrac{1}{2}\nabla\mathbf{U}^2 - \mathbf{U}\times\boldsymbol{\zeta}, \quad \boldsymbol{\zeta} = \nabla\times\mathbf{U},$$

from the y-component of which

$$-\frac{1}{\rho}\frac{\partial}{\partial y}\Delta p = \frac{1}{2}\frac{\partial}{\partial y}\Delta \mathbf{U}^2 + (U_1\zeta_1 - U_2\zeta_2),$$

since $\zeta_1 = -\partial U_{\infty 1}/\partial y, \zeta_2 = -\partial U_{\infty 2}/\partial y$. The largest of the above terms involving T is $(V_1 - V_2)\,T$. For T near zero $(V_1 - V_2)\,T$ is small compared to U_1 so that neglecting such terms (a first step towards complete linearization) and making the equations dimensionless by means of a suitable mean velocity V by defining

$$q = U/V, \quad u = U_{\infty 1}/V, \quad u^* = U_{\infty 2}/V,$$
$$u_1 = U_1/V, \quad u_2 = U_2/V, \quad v_1 = V_1/V, \quad v_2 = V_2/V.$$

we have at the gauze,

$$\left.\begin{aligned} u_1 = u_2 = q, &\qquad (a)\\ BqT = (1-B)\,v_1 - v_2, &\qquad (b)\\ \frac{\partial}{\partial y}\gamma q^2 = 2q(u' - u^{*\prime}) \quad (' = d/dy). &\qquad (c) \end{aligned}\right\} \tag{1.8}$$

Now $B \leqslant 1$ and BT is small over a range of θ near zero. If the departures of q from uniformity are also small, the product of BT and the variation of q can be neglected so that we can write $q = 1$ in BTq. The linearization is completed by writing

$$\gamma = \gamma_0[1 + s(y)], \tag{1.9}$$

where γ_0 is a constant and $|s| \ll 1$. Substituting (1.9) into (1.8*c*) and neglecting second-order quantities, we obtain after an immediate integration

$$u - u^* = \gamma_0(q-1) + \tfrac{1}{2}\gamma_0 s, \tag{1.10}$$

where to satisfy continuity we require $\int_0^L s(y)\,dy = 0$ if V is the mean velocity.

The derivation of (1.8) and (1.10) has required the following quantities to be small: the displacement of a streamline by the gauze, the variation of resistance s, $(V_1 - V_2)\,T$, BT, and the variation of velocity across the channel. It is found experimentally that it is normally sufficient to have the dimensionless shear $L\,du/dy$ or $L\,du^*/dy$ less than 0·5.

For low values of R, such that K behaves as in (1.4), equation (1.10) remains valid provided we write

$$\gamma = \cos^2\theta\, d(KV^2)/dV^2.$$

2. Two-dimensional flow in a parallel channel

The problem is to find the transformation relating the velocity profiles upstream and downstream of an arbitrary gauze. The fluid is assumed to be perfect, have zero-normal velocity on the channel walls and satisfy (1.8*a*, *b*) and (1.10) at the gauze. The velocity field will be formulated in terms of a stream function ψ which is perturbed in the vicinity of the gauze. The perturbation is determined by the assumption that vorticity is conserved along a streamline except for a discontinuity at the gauze.

The formulation is simplest for two-dimensional motion where (see, for example, Lamb 1932),

$$\zeta = \nabla^2\psi. \tag{2.1}$$

Suppose the gauze produces a perturbation ψ^* to a main flow ψ^0 such that $\psi = \psi^0 + \psi^*$, then, provided the gauze produces only small transverse displacements of the streamlines,

$$\nabla^2\psi^* = 0. \tag{2.2}$$

A finite solution of (2.2) which satisfies the boundary conditions at the walls is

$$\left.\begin{aligned}\frac{\psi^*}{LV} &= \sum_{n=1}^{\infty}\frac{1}{n\pi}P_n e^{n\pi x/L}\sin n\pi y/L \quad (x<0),\\ &= \sum_{n=1}^{\infty}\frac{1}{n\pi}Q_n e^{-n\pi x/L}\sin n\pi y/L \quad (x>0).\end{aligned}\right\} \tag{2.3}$$

Thus,

$$\left.\begin{aligned}u_1 &= u - \sum_1^{\infty} P_n e^{n\pi x/L}\cos n\pi y/L,\\ u_2 &= u - \sum_1^{\infty} Q_n e^{-n\pi x/L}\cos n\pi y/L,\\ v_1 &= \sum_1^{\infty} P_n e^{n\pi x/L}\sin n\pi y/L,\\ v_2 &= \sum_1^{\infty} Q_n e^{-n\pi x/L}\sin n\pi y/L.\end{aligned}\right\} \tag{2.4}$$

The velocities given by these equations must satisfy the boundary conditions (1.8) and (1.10) on the gauze. Assuming that the gauze is everywhere nearly coincident with the plane $x = 0$, these conditions are

$$q = u - \sum_1^{\infty} P_n \cos nw = u^* - \sum_1^{\infty} Q_n \cos nw, \tag{2.5}$$

$$BT = \sum_1 [(1-B)P_n + Q_n]\sin nw, \tag{2.6}$$

$$u - u^* = \gamma_0(q-1) + \tfrac{1}{2}\gamma_0 s, \tag{2.7}$$

where $w = \pi y/L$ and from (2.7) and (2.9),

$$\gamma_0(u-1) + \tfrac{1}{2}\gamma_0 s = \sum_1^{\infty}[(1+\gamma_0)P_n - Q_n]\cos nw. \tag{2.8}$$

It is convenient to define

$$\left.\begin{aligned}\alpha_n &= (1-B)P_n + Q_n,\\ \beta_n &= (1+\gamma_0)P_n - Q_n,\end{aligned}\right\} \tag{2.9}$$

so that,

$$\left.\begin{aligned}BT &= \sum_1^{\infty}\alpha_n \sin nw,\\ \tfrac{1}{2}\gamma_0 s + \gamma_0(u-1) &= \sum_1^{\infty}\beta_n\cos nw.\end{aligned}\right\} \tag{2.10}$$

Then

$$P_n = \frac{\alpha_n + \beta_n}{2+\gamma_0 - B}, \quad Q_n = \frac{-(1+\gamma_0)\alpha_n + (1-B)\beta_n}{2+\gamma_0 - B}, \tag{2.11}$$

so that substituting q from (2.5) in (2.7),

$$u^*-1 = A(u-1)+\tfrac{1}{2}(1-A)s+E\sum_1^\infty \alpha_n \cos nw, \tag{2.12}$$

where

$$E = \gamma_0(2+\gamma_0-B) \quad \text{and} \quad A = (2-\gamma_0-B+\gamma_0 B)/(2+\gamma_0-B) = 1-\gamma_0(1-E).$$

Hardy & Rogosinski (1944) discuss the relation between two functions $g(w)$, $g^*(w)$ defined in the range $0 < w < \pi$ such that

$$g(w) = \sum_1^\infty h_n \sin nw \quad \text{and} \quad g^*(w) = \sum_1^\infty h_n \cos nw.$$

This relation is denoted by $g^* = \mathscr{H}(g)$ and $g = \mathscr{H}^*(g^*)$, and they show that

$$\mathscr{H}(g) = \frac{1}{2\pi}\int_0^\pi [g(w+t)-g(w-t)]\cot \tfrac{1}{2}t\,dt. \tag{2.13}$$

Hence, since $BT = \sum_1^\infty \alpha_n \sin nw$, we can write finally

$$u^*-1 = A(u-1)-\tfrac{1}{2}(1-A)s+E\mathscr{H}(BT). \tag{2.14}$$

Notice that the factor A is the attenuation of an upstream flow variation by a uniform gauze normal to the stream, and that the remaining terms represent the disturbances introduced respectively by the variations of resistance coefficient and by variations of inclination to the stream. The separation of these effects is a consequence of the linearization of the equations. Equation (2.14) is a linear relation between the upstream velocity distribution, u, the downstream distribution, u^*, and the two properties of the gauze, and it may be used to relate any one of these quantities to the other three. For example, if the velocity distributions u and u^* are known, then there are two distinct cases of interest, corresponding to a shaped gauze of uniform resistance or a gauze of non-uniform resistance placed normal to the stream.

If, first, the distribution of inclination, T, is required explicitly, it is readily obtained from (2.14) by applying the transformation $\mathscr{H}^*$ to give

$$EBT = \mathscr{H}^*\left[\frac{u^*-u}{E}+(2-B)(u-1)+\tfrac{1}{2}(1-A)s\right]. \tag{2.15}$$

Provided u, u^*, K and B are given, (2.15) can be integrated to give the gauze shape, $x-x_0 = \int_{y_0}^{y} T(y)\,dy$, required to produce a prescribed velocity distribution.

Secondly, for a gauze placed normal to the stream so that $T = 0$, (2.14) gives the variation of resistance required to produce a prescribed velocity distribution as

$$s = 2[A(u-1)-(u^*-1)]/(1-A). \tag{2.16}$$

If this variation of s is produced by the variable spacing of a row of cylinders for which $\beta = 1-d/l$, then by (1.5)

$$K \doteq \left(\frac{d}{l}\right)^2\left(1-\frac{d}{l}\right)^{-2} = K_1(1+s). \tag{2.17}$$

It is assumed that K_1 is given; hence (2.16) and (2.17) can be solved for d/l. A restriction is imposed by the requirement $d/l > 0$, so that

$$(u^*-1) < \tfrac{1}{2}(1-A)+A(u-1).$$

In particular, to produce the linear gradient $u^*-1 = \lambda(y/L-\frac{1}{2})$ from a uniform, incident flow with $u = 1$ requires

$$s = -2\lambda(y/L-\tfrac{1}{2})/(1-A). \tag{2.18}$$

This particular result has already been derived and verified experimentally by Owen & Zienkiewicz (1957).

3. Axisymmetric and diffuser flow

The simplest extension of the above results is to nearly radial, two-dimensional flow. Use polar co-ordinates (r, θ). For potential flow in a channel with walls at $\theta = 0, \alpha$, the velocity, distant from the gauze, is radial and of the form $u = f(\theta)/r$. The gauze produces a perturbation ψ^* to the stream function ψ^0, where again $\nabla^2\psi^* = 0$. Appropriate eigenfunctions for ψ^* are $r^k \sin k\theta$, where $k = n\pi/\alpha$. The solution proceeds exactly as in section 2, except that y, u_1, u_2 are replaced by $\theta, f_1(\theta), f_2(\theta)$. Equation (2.14) becomes

$$f^*-1 = A(f-1)+E\mathscr{H}(BT)-\tfrac{1}{2}(1-A)s, \tag{3.1}$$

where A, E, s, and the operator $\mathscr{H}$ have the same meaning as in § 2, but T is the tangent of the angle between the radius vector and the gauze normal. The solution (2.15) also applies, but $x-x_0$ is replaced by $\log r/r_0$, so that

$$\log\frac{r}{r_0} = \frac{\alpha}{\pi}\int_{\theta_0}^{\theta}\frac{1}{B}\mathscr{H}^*[(f^*-f)/E+(2-B)(f-1)]\,dw. \tag{3.2}$$

A further extension can be made to the axisymmetric flow in a circular pipe of radius a. Use cylindrical polar co-ordinates (r, θ, z), where $\partial/\partial\theta \equiv 0$ and $\mathbf{U} = (V, 0, U)$. The equation of continuity is satisfied by introducing a stream function defined by $rU = -\partial\psi/\partial r$, $rV = \partial\psi/\partial z$. As before, we assume that vorticity is conserved along a streamline, except for a discontinuity introduced at the gauze. Hence, the vorticity $\boldsymbol{\zeta}$ is of the form $(0, \zeta, 0)$, where

$$r\zeta = \frac{\partial^2\psi}{\partial r^2}-\frac{1}{r}\frac{\partial\psi}{\partial r}+\frac{\partial^2\psi}{\partial z^2} = L(\psi), \text{ say.} \tag{3.3}$$

If the gauze produces a perturbation ψ^* to the stream function ψ^0, then $L(\psi^*) = 0$. This equation can be separated to yield the finite solutions $\psi^* = re^{-m|z|}J_1(mr)$, where $J_1(ma) = 0$. The solution now proceeds as before except that $J_0(mr)$ replaces $\cos mw$, $J_1(mr)$ replaces $\sin nw$, and the summations are over all roots m such that $J_1(ma) = 0$. The previous solution (2.16) applies except that the transformation $\mathscr{H}$ is now defined in terms of the Bessel functions J_0 and J_1 by

$$\left.\begin{aligned} g(r) = \sum_m h_m J_1(mr), \quad g^*(r) = \sum_m h_m J_0(mr), \quad J_1(ma) = 0 \\ \text{and} \qquad g^* = \mathscr{H}(g), \quad g = \mathscr{H}^*(g^*). \end{aligned}\right\} \tag{3.4}$$

The properties of the transformation represented by these Fourier–Bessel series can be expected to be similar to the corresponding Fourier series.

The solution for the axisymmetric flow in a circular pipe can be extended to the case of flow in a circular-cone diffuser, in a manner similar to that used for radial two-dimensional flow. Use spherical polar co-ordinates (r, θ, ϕ), so that $\partial/\partial\phi = 0$ and $\mathbf{U} = (U, V, 0)$. For potential flow within the cone $\theta = \alpha$, the velocity, distant from the gauze, is radial and of the form $u = f(\theta)/r^2$. As before, solution (2.16) with the modification (3.2) applies here, except that $f(\theta)$ replaces $u(y)$.

4. Multiple gauzes

A further simple extension of the previous results is to the common practical case of two or more gauzes placed in series. Consider a gauze A placed at $x = 0$ and a gauze B placed at $x = x_0$ and define

$$\eta_n = \coth \xi_n, \quad \zeta_n = \operatorname{coshec} \xi_n,$$

where $\xi_n = n\pi x_0/L$ and n is an integer. As before, it is possible to express the velocity field in terms of trigonometric series so that with, in an obvious notation,

$$u - 1 = \sum_{n=1}^{\infty} H_n \cos nw,$$

$$B_A T_A = \sum_{n=1}^{\infty} G_n \sin nw,$$

$$u^* - 1 = \sum_{n=1}^{\infty} L_n \cos nw,$$

$$B_B T_B = \sum_{n=1}^{\infty} M_n \sin nw,$$

then it can be shown that

$$D_n L_n = P_n H_n + Q_n G_n + R M_n,$$

where
$$D_n = -\gamma_A \gamma_B \zeta_n + [(1+\gamma_A)(1+\gamma_B) + (1-B_A)(1-B_B)]\eta_n + (1+\gamma_A)(1-B_B) + (1+\gamma_B)(1-B_A),$$

$$P_n = -\gamma_A \gamma_B (1-B_A)(1-B_B)\zeta_n + [1 + (1-\gamma_A)(1-\gamma_B)(1-B_A) \times (1-B_B)]\eta_n + (1-\gamma_A)(1-B_A) + (1-\gamma_B)(1-B_B),$$

$$Q_n = \gamma_A + (1-B_B)[\gamma_B(1+\gamma_A)\zeta_n + \gamma_A(1-\gamma_B)\eta_n],$$

$$R_n = \gamma_B(1-B_A) + [\gamma_A(1-\gamma_B)\zeta_n + \gamma_B(1+\gamma_A)\eta_n].$$

For ξ_1 large, it can be shown that the solution corresponds to the result that would be obtained by assuming the gauzes did not interfere and using (2.16) twice. In general, although P_n can be zero, due to the presence of ζ_n and η_n in each coefficient, two interfering gauzes cannot remove all variations in $u - 1$ but can merely remove a particular harmonic component. The case of two normal interfering gauzes has already been solved by Davis (1957).

5. The linear gauze

A linear gauze, inclined at a uniform angle to the stream, provides both theoretically and experimentally one of the simplest flows through a gauze inclined to the stream and at the same time reveals all the consequences of the

ability of a gauze to deflect the stream. Consider the uniform flow incident on a gauze for which both T and K are uniform over the gauze surface and, therefore, s is zero. By (2.14),

$$u^* - 1 = EBT\mathscr{H}(1).$$

The transform $\mathscr{H}(1)$ can be evaluated by elementary analysis, giving

$$u^* - 1 = \frac{2EBT}{\pi} \log \cot \tfrac{1}{2}w. \tag{5.1}$$

In figure 2, the curve of $(u^* - 1)/EBT$ as a function of y is drawn together with experimental values. The agreement is good even close to the walls where the present theory gives an infinite value.

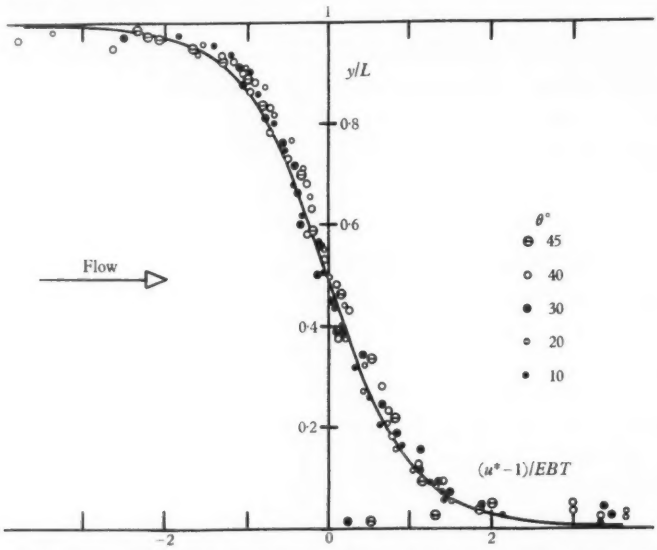

FIGURE 2. The velocity profile downstream of a gauze inclined at a uniform angle to a uniform incident stream. Theoretical curve from equation (5.1). Experimental points for $\theta = 10°, 20°, 30°, 40°, 45°$.

Apart from some qualitative observations in a water channel, the experiments were performed, in collaboration with Dr G. Davis of the Australian Atomic Energy Commission, in the wind tunnel of the Heat Research Laboratory of the Engineering Laboratory, Cambridge. The tunnel provided a velocity of 30 m/sec in a polished wood-working section of 5 in. × 10 in. Velocity measurements were made with a 0·125 in., 3-hole probe and an inclined tube manometer. The tunnel boundary layer was 0·05 in. thick. Velocity variations across the section, outside the boundary layers, was less than $\pm 1\%$ and flow direction variations were less than $\pm 15'$. The screens were mounted on wooden frames and clamped to the adjustable tunnel walls which provided a range of θ up to 45°. The data of figure 1 were with values of l, β, K, B of 0·0194 in., 0·395, 2·20 and 0·220, while the values for figure 4 were 0·0117 in., 0·348, 3·20 and 0·286.

Notice that the coefficient

$$ET = \sin 2\theta/(M + \cos 2\theta), \tag{5.2}$$

where

$$M = 1 + (4 - 2B)/K,$$

has a maximum at $\cos 2\theta = -1/M$, where its value is $(M^2 - 1)^{-\frac{1}{2}}$. ET is plotted in figure 3, for a series of values of K and corresponding values of B taken from (1.6). It is seen that near $\theta = 0$ there is an extensive region where $ET \propto \theta$, that the extent of this region increases with K, and that the maximum occurs for $\theta \geqslant \frac{1}{4}\pi$. Although the maximum values of ET suggested here occur at values of

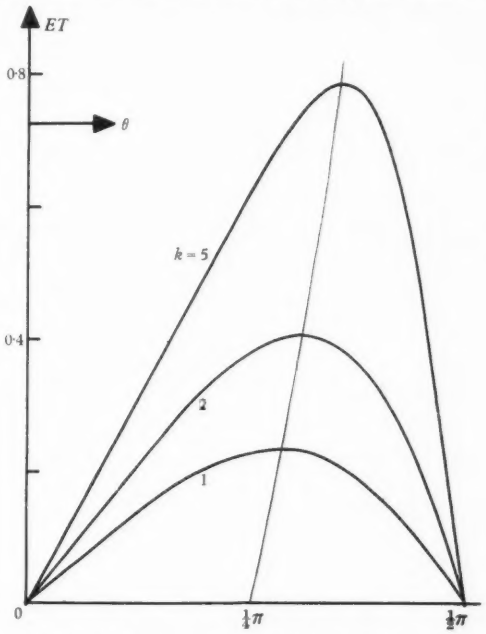

FIGURE 3. The deflexion parameter ET for various values of K as a function of the gauze inclination.

the inclination outside the range of the linearized solution, qualitative experiments in a water channel, in which we observe the deflexion of a dye stream on passing through the gauze, clearly show a maximum deflexion for $\frac{1}{4}\pi < \theta < \frac{1}{2}\pi$. Since the deflexion is proportional to ET, these observations suggest that the qualitative conclusions of the linearized theory apply even for $\theta > \frac{1}{4}\pi$.

It is important to evaluate the stream function in order to verify directly the fundamental assumption that the deflexion of a streamline in passing through the gauze is small. The deflexion $Y(x, y)$ of a streamline which passes through y and originates at y_∞ is

$$Y \equiv y - y_\infty,$$

and is related to the perturbation stream-function, to the first order, by

$$Y/L = \psi^*/V.$$

From (2.3) and (2.11) we obtain

$$\psi^* = [4EBT/\gamma_0\pi^2]\,S(x,y) \quad (x<0)$$
$$= -[4EBT(1+\gamma_0)/\gamma_0\pi^2]\,S(x,y) \quad (x>0),$$

where
$$S = \sum_{n\ \mathrm{odd}}^{\infty} \frac{1}{n^2} e^{-n|x|/L} \sin nw.$$

The form of the mid-stream line, for which $y_\infty = \frac{1}{2}L$, has been computed and is shown in figure 4. The bulk of the change occurs in $|x| < L$. Near $y = \frac{1}{2}L$ the final displacement
$$Y(\infty, y)/L \doteqdot EBT[-0{\cdot}371 + (y/L - \tfrac{1}{2})^2].$$

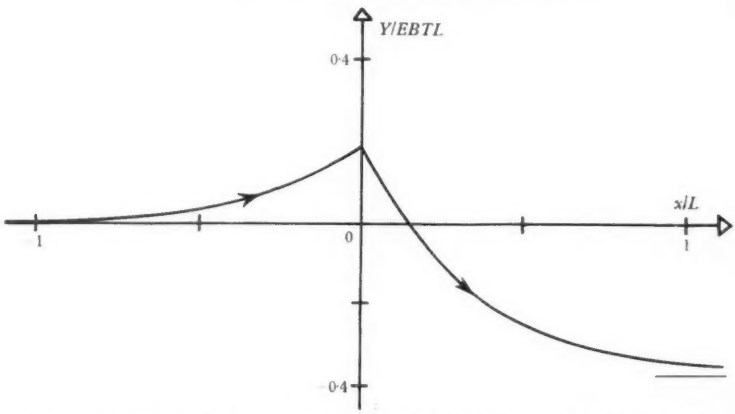

FIGURE 4. The middle streamline through a linear gauze placed at $x = 0$.

It is also of interest to observe that the stress coefficient is

$$p \equiv L\left\{\frac{\partial u^*}{\partial y}\right\}_{y=\frac{1}{2}L} = -2EBT,$$

and that the terms neglected in deriving the boundary conditions at the gauze are of order
$$[(V_1 - V_2)\,T]_{y=\frac{1}{2}L} = -EBT^2.$$

The experiments here were with values of p up to 0·2, whereas in the measurements of Owen & Zienkiewicz (1957) the stress reached 0·45. It thus appears that the linearized equations may be used with confidence up to $p = 0{\cdot}5$ and $T = 1$.

6. The parabolic gauze

A second simple flow through a non-normal gauze is that through a parabolic gauze. This introduces the additional feature that $K\cos^2\theta$ is no longer independent of y. Consider the gauze $(y - \frac{1}{2}L)^2 = L(kL - x)/4k$, of sag k, so that $T = dx/dy = -8k(w - \frac{1}{2}\pi)/\pi$. Hence by (2.14), with $u = 1$, $K =$ constant, but $s \neq 0$, and evaluating the transform $\mathscr{H}(w - \frac{1}{2}\pi)$ by elementary analysis,

$$(u^* - 1) - \Delta u = -\frac{8kEB}{\pi} \log 2 \sin w, \tag{6.1}$$

where
$$\Delta u = \tfrac{1}{2}(1 - A)\,(1 - 4k\cos^2\theta/\tan^{-1}k).$$

In figure 5, $(u^* - 1 - \Delta u)/kEB$ is plotted together with experimental values. The agreement is not quite so good as for the linear screen, due to the difficulty of bending an accurate parabola.

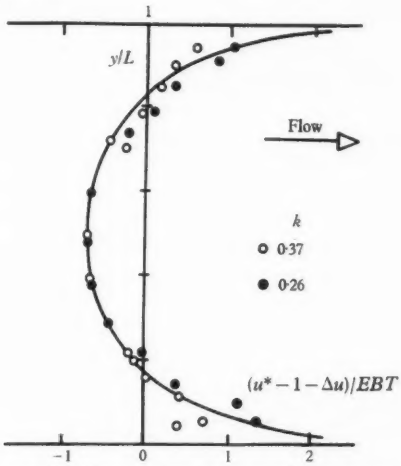

FIGURE 5. The velocity profile downstream of a parabolic gauze in a uniform stream. Theoretical curve from equation (6.1). Experimental points for sag $k = 0{\cdot}26$ and $0{\cdot}37$.

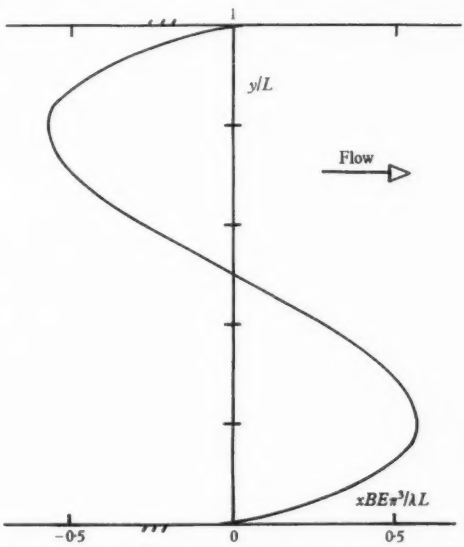

FIGURE 6. The gauze shape to produce a uniform shear from a uniform incident stream.

7. The production of a uniform shear

The production of a linear velocity gradient by means of a linear variation of resistance across the gauze as in (2.18) has already been investigated by Owen & Zienkiewicz (1957). The alternative physical method of bending a uniform gauze

to an appropriate shape has some practical convenience. Consider the particular case of (2.15) required to produce the linear profile $u^* - 1 = \lambda(y/L - \frac{1}{2})$ from $u = 1$; it is

$$x(y) = \frac{\lambda L}{BE\pi^2} \int_0^a \mathscr{H}^*(a)\, da \quad (a = w - \tfrac{1}{2}\pi). \tag{7.1}$$

It can be shown by elementary analysis that

$$\mathscr{H}^*(w - \tfrac{1}{2}\pi) = \frac{2}{\pi} \int_0^w \log \tan \tfrac{1}{2}t\, dt,$$

$$= \frac{1}{\pi}(-C + a^2 + \tfrac{1}{12}a^4 + \tfrac{1}{240}a^6 + \ldots), \tag{7.2}$$

where $$C = -\frac{1}{2} \int_0^{\frac{1}{2}\pi} \log \tan \tfrac{1}{2}t\, dt = 0{\cdot}915,$$

so that $$BE\pi^3 x/\lambda L = -0{\cdot}915a + \tfrac{1}{3}a^3 + \tfrac{1}{60}a^5 + \tfrac{1}{1680}a^7 + \ldots. \tag{7.3}$$

This series can be used with confidence right up to the wall since x becomes small there. The required gauze shape, given by $BE\pi^3 x/\lambda L$ as a function of y, is shown in figure 6. This shape is to be expected in view of the result for a linear screen where in the centre of the channel the shear is uniform and only the flow near the walls would need to be adjusted to produce a completely uniform flow.

I gratefully acknowledge that my period of research at Cambridge has been made possible by my employers, the New Zealand Defence Scientific Corps.

REFERENCES

Bonneville, J. M. & Harper, D. B. 1951 *An analysis and investigation of two-dimensional flow through wire screens.* M.S. Thesis, Massachusetts Institute of Technology.

Bragg, S. L. & Hawthorne, W. R. 1950 *J. Aero. Sci.* **17**, 243.

Davis, G. 1957 *Non-uniform flow through wire screens.* Ph.D. Dissertation, University of Cambridge.

Hardy, G. H. & Rogosinski, W. W. 1944 *Fourier Series. Math. Tracts*, **38**. Cambridge University Press.

Lamb, H. 1932 *Hydrodynamics.* Cambridge University Press.

Owen, P. R. & Zienkiewicz, H. K. 1957 *J. Fluid Mech.* **2**, 521.

Taylor, G. I. 1944 *Aero. Res. Coun. R. & M.* no. 2236.

Taylor, G. I. & Batchelor, G. K. 1949 *Quart. J. Mech. Appl. Math.* **2**, 1.

Taylor, G. I. & Davis, R. M. 1944 *Aero. Res. Coun. R. & M.* no. 2237.

Weighardt, K. E. G. 1953 *Aero. Quart.* **4**, 186.

A new approach to problems of shock dynamics

Part 2. Three-dimensional problems

By G. B. WHITHAM
Institute of Mathematical Sciences, New York University

(Received 15 September 1958)

This paper gives the extension of the approximate theory developed in Part 1 (Whitham 1957) to three-dimensional problems. The basic equations are derived in § 1, using the original assumption of a functional relation between the strength of the shock wave at any point and the area of the ray tube. An analogy with steady supersonic flow is found. For the diffraction of a plane shock wave by an obstacle, the equations and boundary conditions are exactly the same as those for steady supersonic potential flow past that obstacle, with a special choice of the density-speed relation. The successive positions of the shock wave are the equipotential surfaces of the supersonic flow. The 'shock-shocks' introduced in Part 1, i.e. discontinuities in the slope and Mach number of the shock wave, correspond to the steady oblique shock waves in the supersonic flow problem. They arise when Mach reflexion occurs.

In § 2 the theory is applied in detail to the diffraction of a plane shock wave by a cone. Then, in § 3, a small perturbation theory is applied to the two typical problems of (i) diffraction by a slender axi-symmetrical body of general shape, and (ii) the stability of a plane shock. Many further applications would be possible and some brief comments on these are made in § 4.

1. General theory

The theory of shock dynamics developed in Part 1 (Whitham 1957) is extended in this paper to include general three-dimensional problems. The extension is only a matter of manipulating equations; the basic assumption remains the same. We introduce the rays, which are curves orthogonal to the successive positions of the shock wave, and consider a portion of the shock wave moving along a narrow tube of neighbouring rays. Then the assumption is that the Mach number M of the shock and the area A of the ray tube are functionally related. This is suggested by the similarity of the propagation in a ray tube to the propagation of a shock wave in a tube with *solid* walls, and the function $M(A)$ is taken from the results obtained by Chisnell (1957) for that problem. The assumption and its implications have been considered in detail in Part 1. It may be added that further investigations of Chisnell's function $M(A)$ have been made since Part 1 was written; these include an alternative derivation of the formula and further discussion of its validity (see Whitham 1958).

Although the rays are not known in advance and have to be deduced as part of the solution, the relation $A = A(M)$ is sufficient to determine the motion of the

shock wave without any further discussion of the dynamics of the flow. For two-dimensional problems, appropriate equations were formulated in the following way. The shock wave positions, α = constant, and the rays, β = constant, form a set of orthogonal co-ordinates (α, β) in the plane. The co-ordinate α is chosen to be $a_0 t$, where t is the time at which the shock occupies that position and a_0 is the sound speed in the undisturbed gas ahead of the shock. Then the line elements in the directions of the co-ordinate curves are $M\delta\alpha$ and $A\,\delta\beta$. For purely geometrical reasons, M and A must satisfy the relation

$$\frac{\partial}{\partial\alpha}\left(\frac{1}{M}\frac{\partial A}{\partial\alpha}\right)+\frac{\partial}{\partial\beta}\left(\frac{1}{A}\frac{\partial M}{\partial\beta}\right)=0, \tag{1}$$

or, in more convenient form, the two relations

$$\left.\begin{aligned}\frac{\partial\theta}{\partial\beta}-\frac{1}{M}\frac{\partial A}{\partial\alpha}&=0,\\ \frac{\partial\theta}{\partial\alpha}+\frac{1}{A}\frac{\partial M}{\partial\beta}&=0,\end{aligned}\right\} \tag{2}$$

where $\theta(\alpha, \beta)$ is the angle made by the ray with a fixed direction. The dynamics assumption,

$$A = A(M), \tag{3}$$

completes a determinate set of equations for M, A, θ as functions of α and β. From the solution of these equations the motion of the shock is easily determined: for example, by integration along rays, the position of the shock at time $t = \alpha/a_0$ is given in terms of the parameter β by

$$\left.\begin{aligned}x&=x_0(\beta)+\int_0^\alpha M\cos\theta\,d\alpha,\\ y&=y_0(\beta)+\int_0^\alpha M\sin\theta\,d\alpha,\end{aligned}\right\} \tag{4}$$

where x, y are Cartesian co-ordinates, $x_0(\beta)$, $y_0(\beta)$ describe the initial shock position at $t = 0$ and θ is measured from the x-axis.

The choice of ind pendent variables based on the shock positions and the rays is particularly convenient for two-dimensional problems, and at first it was assumed that this would be true for three-dimensional problems. It seemed natural to introduce a third co-ordinate γ so that a ray would be specified by β, γ; then, relations corresponding to (1) for the line elements together with (3) would determine the motion. In fact, this procedure was rashly indicated in Part 1 as the one to be followed. It can be done, of course, but the amount of formal manipulation becomes prohibitive. The main snag is that a set of surfaces, such as the shock positions here, cannot in general be one family of a system of orthogonal co-ordinates (see, for example, Weatherburn 1931, p. 218); that is, β and γ can not be orthogonal in general. Accordingly, such a co-ordinate system becomes a positive disadvantage in three dimensions, and we revert to the Cartesian co-ordinates (x, y, z). Then the formulation becomes surprisingly simple.

The motion of the shock can be described by

$$a_0 t = \varkappa(x, y, z) \tag{5}$$

and the problem now is to determine the function $\alpha(x, y, z)$. The distance δs along a ray between the shock positions at t and $t+\delta t$ is given by

$$a_0 \delta t = \delta s |\nabla \alpha|,$$

since the ray is normal to the shock. Hence, the Mach number M is given by

$$M = \frac{1}{|\nabla \alpha|}. \tag{6}$$

Next, let $\mathbf{i}(x, y, z)$ be the unit vector in the ray direction; since it is normal to the surfaces (5), it may be expressed as

$$\mathbf{i} = \frac{\nabla \alpha}{|\nabla \alpha|} = M \nabla \alpha. \tag{7}$$

Now, consider a small length of a narrow ray tube with end sections parts of surfaces $\alpha =$ constant, and let A be proportional to the cross-sectional area of the tube (measured by the area of the surface $\alpha =$ constant inside the tube at that section). Applying the divergence theorem to the vector $\mathbf{i}/A$ and the volume V inside the ray tube, we have

$$\int_V \nabla . \left(\frac{\mathbf{i}}{A}\right) d\tau = \int_S \frac{\mathbf{i} . \boldsymbol{\nu}}{A} dS, \tag{8}$$

where $\boldsymbol{\nu}$ is the outward normal to the surface S of the ray tube. On the sides of the tube, $\mathbf{i} . \boldsymbol{\nu} = 0$; on the ends, $\mathbf{i} . \boldsymbol{\nu} = \pm 1$ respectively and $\int A^{-1} dS = 1$, so that the contributions from the ends cancel. Hence the right-hand side of (8) vanishes. Therefore, since the elementary ray tube can be taken arbitrarily, the usual argument of continuity shows that

$$\nabla . \left(\frac{\mathbf{i}}{A}\right) = 0$$

everywhere. From (7), we have

$$\nabla . \left(\frac{M}{A} \nabla \alpha\right) = 0, \quad M = \frac{1}{|\nabla \alpha|}. \tag{9}$$

Since the basic assumption is that A is a known function of M, this is an equation to determine α.

A typical problem is the diffraction of an initially plane shock by a solid obstacle. If the initial Mach number of the shock is M_0 then we require

$$\alpha \sim \frac{x}{M_0} \text{ at infinity}, \tag{10}$$

and, since the shock must be normal to the surface of the obstacle, the normal derivative of α must vanish on it, i.e.

$$\frac{\partial \alpha}{\partial n} = 0 \quad \text{on the obstacle.} \tag{11}$$

For this problem the solution of (9) is required subject to the boundary conditions (10) and (11).

Analogy with steady supersonic flow

There is an immediate analogy between this problem and that of determining the velocity potential in irrotational supersonic flow past a body. For, in steady compressible flow, the continuity of mass requires

$$\nabla.(\rho\mathbf{q}) = 0, \tag{12}$$

where $\mathbf{q}$ is the velocity vector and ρ is the density. If the flow is irrotational with velocity potential ϕ then $\mathbf{q} = \nabla\phi$. Furthermore, from Bernoulli's equation, ρ is a function of the speed q; for a polytropic gas with pressure-density relation $p = \kappa\rho^\gamma$, Bernoulli's equation is

$$\frac{\gamma\kappa\rho^{\gamma-1}}{\gamma-1} + \tfrac{1}{2}q^2 = \frac{\gamma\kappa\rho_\infty^{\gamma-1}}{\gamma-1} + \tfrac{1}{2}q_\infty^2, \tag{13}$$

where ρ_∞, q_∞ refer to values in the uniform stream at infinity. Therefore, we have

$$\nabla.(\rho\nabla\phi) = 0, \tag{14}$$

where ρ is a known function of $q = |\nabla\phi|$. This corresponds exactly to (9), the precise correspondence being

$$\phi \to \alpha, \quad q \to 1/M, \quad \rho \to M/A. \tag{15}$$

The difference is that the dependence of ρ on $|\nabla\phi|$ is not the same as that of M/A on $|\nabla\alpha|$. This difference accounts for the fact that (9) is always hyperbolic, corresponding to wave motions, whereas (14) may be hyperbolic or elliptic depending upon whether the flow is supersonic or subsonic. Turning to the boundary conditions in the steady-flow problem, we require

$$\phi \sim q_\infty x \quad \text{at infinity}$$

and

$$\frac{\partial\phi}{\partial n} = 0 \quad \text{on the body.}$$

These correspond precisely to (10) and (11), so the analogy is complete.

In view of this analogy, for any problem in supersonic flow there is a corresponding one of shock diffraction which can be solved by the same method. The difference in the dependence of the functions ρ and M/A on $|\nabla\phi|$ and $|\nabla\alpha|$, respectively, will mean in general that the details of the solutions will differ. However, in the special case of a small perturbation theory, the solution can be taken over directly from the corresponding *linearized* supersonic flow with a mere change in interpretation! *Thus, any solution of a linearized supersonic flow problem solves the corresponding shock diffraction problem at the same time.* To show this we substitute

$$\alpha = \frac{1}{M_0}(x + \alpha') \tag{16}$$

in (9), and linearize the equation on the assumption that the perturbations α' are small. First,

$$M = \frac{1}{|\nabla\alpha|} = M_0 - M_0\alpha_x' + O(\alpha'^2), \tag{17}$$

and

$$\frac{M}{A} = \left[\frac{M}{A}\right]_{M=M_0} + \left[\frac{d}{dM}\left(\frac{M}{A}\right)\right]_{M=M_0}(-M_0\alpha_x') + O(\alpha'^2)$$

$$= \left[\frac{M}{A}\right]_{M=M_0} - \left[\frac{M}{A} - \frac{M^2}{A^2}\frac{dA}{dM}\right]_{M=M_0}\alpha_x' + O(\alpha'^2). \tag{18}$$

Then, substituting (16) and (18) in (9), we have

$$\alpha'_{yy}+\alpha'_{zz}-B^2\alpha'_{xx}=0, \quad B^2=\left[-\frac{M}{A}\frac{dA}{dM}\right]_{M=M_0}. \tag{19}$$

In supersonic flow, the velocity potential is taken in the form

$$\phi = q_\infty(x+\phi'), \tag{20}$$

and the linearized equation satisfied by ϕ' is found to be

$$\phi'_{yy}+\phi'_{zz}-B^2\phi'_{xx}=0, \quad B^2=\mathscr{M}_\infty^2-1, \tag{21}$$

where $\mathscr{M}_\infty$ is the Mach number of the stream at infinity. At infinity, α' and ϕ' tend to zero, and on the obstacle the normal derivatives of $x+\alpha'$ and $x+\phi'$ must both vanish. Therefore, the problems to be solved for α' and ϕ' are exactly the same. The interpretations of the solution are different, and the coefficients B have different definitions in terms of the given parameters. *The equipotentials of the supersonic flow problem are the shock positions of the diffraction problem; the streamlines are the rays.*

Solutions obtained by use of this analogy will be presented in § 3.

Two-dimensional problems

The analogy with supersonic flow also provides a useful way of comparing the formulation (9) with (2) for two-dimensional problems. As noted above, (9) corresponds to the equation for ϕ in Cartesian co-ordinates (x, y). Now, (2) corresponds to the equations for speed q and flow direction θ as functions of the velocity potential ϕ and stream function ψ. The latter equations are

$$\left.\begin{aligned}\frac{\partial\theta}{\partial\phi}&=\frac{\rho}{q}\frac{\partial q}{\partial\psi},\\ \frac{\partial\theta}{\partial\psi}&=q\frac{\partial}{\partial\phi}\left(\frac{1}{\rho q}\right);\end{aligned}\right\} \tag{22}$$

the correspondence with (2) is

$$\phi\to\alpha, \quad \psi\to\beta, \quad \theta\to\theta, \quad q\to 1/M, \quad \rho\to M/A, \tag{23}$$

in agreement with (15). (Equations (22) can be derived from the geometry of equipotentials and streamlines in exactly the same way that equations (2) were obtained in Part 1 from the geometry of shocks and rays.)

Equations (2) are more convenient than (9) for the problems of Part 1, just as, for many purposes, equations (22) are more convenient than (12) for two-dimensional flow. This is particularly true in finding the characteristic form of the equations. It was found in Part 1, that the characteristic form of equations (2) is

$$\theta\pm\int\frac{dM}{Ac}=\text{constant} \tag{24}$$

on curves

$$\frac{d\beta}{d\alpha}=\pm c, \tag{25}$$

where $c(M)$, the propagation speed in the (α, β) co-ordinates, is given by

$$c(M) = \sqrt{\left(-\frac{M}{A}\frac{dM}{dA}\right)}. \tag{26}$$

(See equations (10), (11) and (12) of Part 1.) The variables M and θ are given in terms of the derivatives of α by

$$\alpha_x^2 + \alpha_y^2 = 1/M^2, \quad \alpha_y/\alpha_x = \tan\theta, \tag{27}$$

which allows the Riemann invariants $\theta \pm \int dM/Ac$ to be written in terms of α_x, α_y. To write the slopes of the characteristics in terms of x and y, we note that

$$\frac{dy}{dx} = \frac{y_\alpha + y_\beta(d\beta/d\alpha)}{x_\alpha + x_\beta(d\beta/d\alpha)},$$

and $$x_\alpha = M\cos\theta, \quad y_\alpha = M\sin\theta, \quad x_\beta = -A\sin\theta, \quad y_\beta = A\cos\theta. \tag{28}$$

Therefore, the characteristics $d\beta/d\alpha = \pm c$ become

$$\frac{dy}{dx} = \tan(\theta \pm m) \quad \text{where} \quad \tan m = \frac{Ac}{M} = \sqrt{\left(-\frac{A}{M}\frac{dM}{dA}\right)}. \tag{29}$$

The angle m corresponds to the Mach angle in supersonic flow. It is observed that the coefficient B which appears in the linearized equation (19) is $\cot m_0$, where m_0 is the angle of the characteristic in the undisturbed region ahead of the obstacle, where $\theta = 0$, $M = M_0$. Equations (24), (27) and (29) provide the characteristic form of (9) in two-dimensional problems. Clearly, even when using the (x, y) plane, it is often convenient to work with M and θ as dependent variables.

The simplest problem treated in Part 1 was the motion of an initially plane shock along a curved wall. It will be useful, perhaps, to indicate how the solution is obtained directly in the (x, y) plane. By the usual argument, the solution must be a simple wave with

$$\theta = \int_{M_0}^{M} \frac{dM}{Ac} \tag{30}$$

holding throughout the flow (since all the negative characteristics start in the undisturbed region where $M = M_0, \theta = 0$). This gives the Mach number M_w at the wall in terms of the angle θ_w of the wall without further calculation. In the complete solution, θ and M remain constant on each positive characteristic; as a consequence these characteristics are straight lines. The solution may be written in terms of a characteristic parameter ξ as

$$\theta = \theta_w(\xi), \quad M = M_w(\xi), \tag{31}$$

$$y = y_w(\xi) + (x - \xi)\tan\{\theta_w(\xi) + m_w(\xi)\}, \tag{32}$$

where $y = y_w(x)$ describes the shape of the wall, $\theta_w(x) = \tan^{-1}y_w'(x)$, $M_w(x)$ is found from (30) and $m_w(x)$ is the corresponding value of m. If the wall turns away from the flow region, the solution is an 'expansion wave' with diverging characteristics as shown in figure 1. If the wall turns into the flow region a 'compression wave' results and the characteristics converge as shown in figure 2. The shock positions are lines of constant α. Since $\alpha_x = \cos\theta/M$, α is given by

$$\alpha = \int_{x_0}^{x} \frac{\cos\theta}{M}\,dx, \tag{33}$$

where $x = x_0$ is the initial position of the shock at $t = 0$; the curve $\alpha = a_0 t$ gives the position at time t. Shock positions are indicated by the broken lines in figures 1 and 2; it should be remembered that they correspond to the equipotentials of supersonic flow. The characteristics in the (x, y) plane give the locus of the waves as they move along the shock.

In the case of a compression wave, the characteristics form an envelope and the continuous solution given in (31) and (32) breaks down. This corresponds precisely to the 'breaking' of the waves propagating along the shock and the formation of a *shock-shock* as described in Part 1. The formation of a shock-shock indicates Mach reflexion as explained in Part 1. In the (x, y)-plane the shock-shock will be represented as a curve across which M and θ are discontinuous. This curve will be the locus of the shock-shock as it moves along the shock wave;

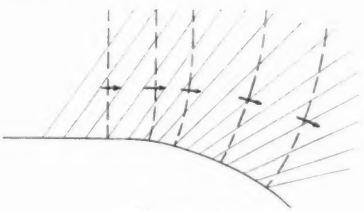

FIGURE 1

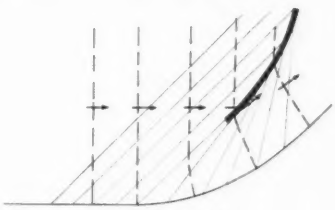

FIGURE 2

FIGURE 1. Motion of a shock wave along a convex wall; the full lines are characteristics and the broken lines are successive shock-wave positions.

FIGURE 2. Motion of a shock wave along a concave wall.

although there is a slight difference in sense, this locus will simply be called a shock-shock. It corresponds to the steady oblique shock which appears in similar circumstances in steady supersonic flow. It is shown as a thicker line in figure 2. The relations connecting the values of M and θ on the two sides of a shock-shock with its velocity have been established in Part 1. Here, they are required in the form of relations to be satisfied across the shock-shock curve in the (x, y) plane. In addition, the general form of the relations for three-dimensional problems must be established.

Shock-shock relations

First of all, since the portions of the shock wave must be connected, α must be continuous across the shock-shock. Hence, it follows that the tangential derivatives of α on the two sides of the shock-shock must be equal. If $\mathbf{n}$ is the unit vector normal to the surface of the shock-shock, this condition may be written

$$\mathbf{n} \times (\nabla \alpha)_0 = \mathbf{n} \times (\nabla \alpha)_1, \tag{34}$$

where subscripts 0 and 1 denote values on the two sides of the shock-shock. The other condition concerns the jump in the normal derivative of α, and it may be found as follows. Consider a narrow ray tube which intersects a small portion of the shock-shock surface. If $\mathbf{i}_0$, $\mathbf{i}_1$ are the directions of the ray on the two sides and A_0, A_1 are corresponding cross-sectional areas of the ray tube, it is clear that the

area intercepted on the shock-shock has a projection A_0 in the $\mathbf{i}_0$ direction and a projection A_1 in the $\mathbf{i}_1$ direction. Therefore,

$$\frac{\mathbf{n}.\mathbf{i}_0}{A_0} = \frac{\mathbf{n}.\mathbf{i}_1}{A_1}.$$

In terms of α, this condition may be written

$$\frac{M_0}{A_0}\mathbf{n}.(\nabla\alpha)_0 = \frac{M_1}{A_1}\mathbf{n}.(\nabla\alpha)_1. \tag{35}$$

It may be remarked that (9) shows that the flux of $M\nabla\alpha/A$ through a closed surface is zero in regions where $M\nabla\alpha/A$ is continuous; equation (35) shows that the flux of $M\nabla\alpha/A$ is conserved even across discontinuities. This gives a quick

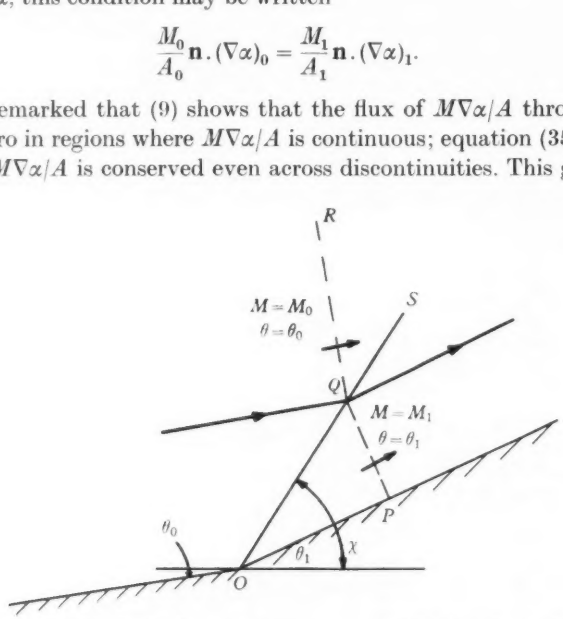

FIGURE 3. Shock-shock at a concave corner; OS is the shock-shock and PQR represents a typical shock-wave position.

way of guessing the appropriate shock condition from an equation of motion in divergence form, but it must always be verified independently that the quantity is indeed conserved across a discontinuity. For example, in continuous regions of a supersonic flow the entropy S is conserved, i.e.

$$\nabla.(\rho\mathbf{q}S) = 0,$$

but it is *not* true that the normal flux of entropy on the two sides of a shock are the same.

Equations (34) and (35) constitute the shock-shock relations for the three-dimensional problem. Remembering that $\nabla\alpha$ corresponds to $\mathbf{q}$ and M/A corresponds to ρ in steady supersonic flow, we see that (34) corresponds to the continuity of tangential velocity across an oblique shock wave and (35) corresponds to the conservation of mass flux. In supersonic flow a further relation is added (involving the normal component of momentum) since the entropy changes across the shock wave and so the function $\rho(q)$ is modified. The extra relation is required to determine this modification. In the shock dynamics, this would correspond to a change in the functional dependence of A on M and it will be

ignored; but it is an important point and is discussed in detail in Part 1, pp. 155–6. It corresponds to ignoring the entropy changes in supersonic flow and continuing to assume potential flow behind a shock wave.

It may be verified that (34) and (35) reduce to the relations found in Part 1 for the two-dimensional case. In that case, we may consider the oblique shock-shock separating the two uniform regions as shown in figure 3. The shock-shock is the line OS and a typical position of the shock wave is PQR. (This shows the Mach reflexion of the shock wave when it is diffracted by a wedge.) If the angle of the shock-shock to the x-axis is χ, then remembering that $\nabla\alpha = \mathbf{i}/M$, (34) and (35) give

$$\frac{\cos(\chi-\theta_0)}{M_0} = \frac{\cos(\chi-\theta_1)}{M_1}, \tag{36}$$

$$\frac{\sin(\chi-\theta_0)}{A_0} = \frac{\sin(\chi-\theta_1)}{A_1}. \tag{37}$$

These relations can be solved to give θ_1 and χ in terms of M_0, θ_0, M_1 as follows:

$$\tan(\theta_1-\theta_0) = \frac{(M_1^2-M_0^2)^{\frac{1}{2}}(A_0^2-A_1^2)^{\frac{1}{2}}}{A_1M_1+A_0M_0}, \tag{38}$$

$$\tan(\chi-\theta_0) = \frac{A_0}{M_0}\left(\frac{M_1^2-M_0^2}{A_0^2-A_1^2}\right)^{\frac{1}{2}}. \tag{39}$$

These agree with the form found in Part 1; (39) corresponds to the relation

$$C = \left(\frac{M_1^2-M_0^2}{A_0^2-A_1^2}\right)^{\frac{1}{2}}$$

for the shock-shock velocity C in the (α, β) co-ordinates.

The A-M relation

Before proceeding to applications of this basic theory to specific problems, it is convenient to repeat the main properties of the function $A(M)$ for purposes of reference. All the information has been given in Part 1. The function $A(M)$ may be written

$$A = A_0\exp\left\{-\int_{M_0}^{M}\frac{2M}{(M^2-1)K(M)}\,dM\right\}, \tag{40}$$

where

$$K(M) = 2\left[\left(1+\frac{2}{\gamma+1}\frac{1-\mu^2}{\mu}\right)(2\mu+1+M^{-2})\right]^{-1}, \quad \mu^2 = \frac{(\gamma-1)M^2+2}{2\gamma M^2-(\gamma-1)}. \tag{41}$$

The function $K(M)$ decreases slowly from 0·5 at $M = 1$ to 0·3941 (for $\gamma = 1{\cdot}4$) as $M \to \infty$. Thus, for weak shocks,

$$\frac{A}{A_0} \sim \left(\frac{M_0-1}{M-1}\right)^2, \quad M-1 \ll 1, \tag{42}$$

and for strong shocks

$$\frac{A}{A_0} \sim \left(\frac{M_0}{M}\right)^n, \quad n = \frac{2}{K(\infty)} = 5{\cdot}0743 \quad (M \gg 1). \tag{43}$$

The strong shock formula is particularly useful because it simplifies all the expressions, and also it covers the most important range of shock strengths. It becomes a good approximation for $M > 3$, say. It should also be noted that when this approximation applies, the expressions for α/M_0, M/M_0, θ in any problem will be independent of M_0. Thus, a single calculation for a given geometry is sufficient for all M_0. *The shock wave will go through the same sequence of positions for all M_0; only the time scale will be modified.*

A graph of the function $\int_1^M dM/Ac$, which appears in the Riemann invariants (24), has been given in Part 1. We note the limiting values

$$\int_{M_0}^{M} \frac{dM}{Ac} \sim 2^{\frac{3}{2}}\{(M-1)^{\frac{1}{2}} - (M_0-1)^{\frac{1}{2}}\} \quad (M-1 \ll 1), \tag{44}$$

$$\int_{M_0}^{M} \frac{dM}{Ac} \sim n^{\frac{1}{2}} \log \frac{M}{M_0} \quad (M \gg 1). \tag{45}$$

The angle m between the characteristic direction and the ray direction can be determined from (29) and (40). It is found to be given by

$$\tan m = \left\{\frac{(M^2-1)\,K(M)}{2M^2}\right\}^{\frac{1}{2}}. \tag{46}$$

For weak shocks,

$$\tan m \sim \left(\frac{M-1}{2}\right)^{\frac{1}{2}} \quad (M-1 \ll 1); \tag{47}$$

for strong shocks,

$$\tan m \to n^{-\frac{1}{2}} = 0{\cdot}4439, \quad m \to 23{\cdot}9^\circ, \quad M \to \infty. \tag{48}$$

The coefficient B that appears in the linearized equation (19) is just $\cot m_0$; hence, $B \to n^{\frac{1}{2}} = 2{\cdot}253$ as $M \to \infty$.

2. Diffraction by a cone

The simplest three-dimensional problem is the diffraction of a plane shock wave by a cone; this corresponds to the well-known Taylor–Maccoll problem of flow past a cone in supersonic flow. For axi-symmetrical problems such as this, it is still possible to use independent variables based on the shock positions and rays. The only modification of (2) would be the replacement of A by A/r, where x is the distance from the axis of symmetry, and the addition of the equation

$$\frac{\partial r}{\partial \alpha} = M \cos\theta$$

to determine r. But, it will be more convenient to work directly from (9) in the (x, r) plane.

In terms of M and θ,

$$\alpha_x = \frac{\cos\theta}{M}, \quad \alpha_r = \frac{\sin\theta}{M}, \tag{49}$$

so that

$$\frac{\partial}{\partial x}\left(\frac{\sin\theta}{M}\right) - \frac{\partial}{\partial r}\left(\frac{\cos\theta}{M}\right) = 0, \tag{50}$$

and, from (9),

$$\frac{\partial}{\partial x}\left(\frac{r\cos\theta}{A}\right)+\frac{\partial}{\partial r}\left(\frac{r\sin\theta}{A}\right)=0. \tag{51}$$

In the problem of diffraction by a cone, the only parameters prescribed in the problem are the initial Mach number M_0 and the cone angle θ_w; there is no length. Hence in the solution, M and θ must be functions of the single variable $\eta=\tan^{-1}r/x$. Then, (50) and (51) become

$$\frac{1}{M}\frac{dM}{d\eta}=\tan(\eta-\theta)\frac{d\theta}{d\eta}, \tag{52}$$

$$-\frac{1}{A}\frac{dA}{d\eta}=\left(-\frac{M}{A}\frac{dA}{dM}\right)\frac{1}{M}\frac{dM}{d\eta}=\left\{\frac{d\theta}{d\eta}+\frac{\tan\theta}{\sin\eta\cos\eta\,(1+\tan\eta\tan\theta)}\right\}\cot(\eta-\theta). \tag{53}$$

The disturbed region is separated from the uniform region in which $M=M_0$, $\theta=0$ by a shock-shock at which η is equal to the shock-shock angle χ and the relations (38), (39) must be satisfied. So the solution of (52) and (53) is required such that

$$\left.\begin{aligned}&\theta=\theta_1,\quad M=M_1\\ &\tan\theta_1=\frac{(M_1^2-M_0^2)^{\frac{1}{2}}(A_0^2-A_1^2)^{\frac{1}{2}}}{A_1M_1+A_0M_0}\\ &\tan\chi=\frac{A_0}{M_0}\left(\frac{M_1^2-M_0^2}{A_0^2-A_1^2}\right)^{\frac{1}{2}}\end{aligned}\right\}\quad\text{at }\eta=\chi, \tag{54}$$

and

$$\theta=\theta_w\text{ at the cone }\eta=\theta_w. \tag{55}$$

These are essentially two boundary conditions since χ is not known in advance. The procedure for finding solutions for given M_0 is to choose a value for M_1, then χ and θ_1 can be found from (54) and the pair of equations (52) and (53) integrated from $\eta=\chi$ down to the point where it is found that $\theta=\eta$. This point must be the surface of the cone and it gives the value of the cone angle θ_w which corresponds to the chosen value of M_1.

If the strength of the shock wave is fairly large ($M_0>3$, say) the asymptotic form (43) may be used for the A-M relation and there is considerable simplification in the whole calculation. Most important of all, only the Mach number ratio M/M_0 is significant, and one calculation gives the solution for a given cone *for all* M_0. We set $M/M_0=R$, then $A/A_0=R^{-n}$ and

$$-\frac{M}{A}\frac{dA}{dM}=n.$$

Hence, a single equation for $\theta(\eta)$ can be obtained from (52) and (53). We have

$$\frac{d\theta}{d\eta}=\frac{\tan\theta}{\sin\eta\cos\eta\,(1+\tan\eta\tan\theta)\{n\tan^2(\eta-\theta)-1\}} \tag{56}$$

and

$$\frac{1}{R}\frac{dR}{d\eta}=\tan(\eta-\theta)\frac{d\theta}{d\eta}. \tag{57}$$

The shock-shock relations become

$$\left.\begin{aligned}\tan\theta_1 &= \frac{(R_1^2-1)^{\frac{1}{2}}(1-R_1^{-2n})^{\frac{1}{2}}}{1+R_1^{1-n}}\\ \tan\chi &= \left(\frac{R_1^2-1}{1-R_1^{-2n}}\right)^{\frac{1}{2}}\end{aligned}\right\} \quad \text{at } \eta=\chi. \tag{58}$$

To solve the problem a value of R_1 is chosen, the starting value of θ at $\eta=\chi$ is found from (58), and (56) is integrated to the point where $\theta=\eta$. This common value is the cone angle θ_w. The Mach number ratio R can then be found from an integration of (57).

The position of the shock wave at any time can be found from the solution for $\theta(\eta)$, $R(\eta)$ without any further integration. For α takes the form $xf(\eta)/M_0$, so

$$\alpha_x = \frac{1}{M_0}\{f(\eta)-\sin^2\eta f'(\eta)\} = \frac{\cos\theta}{R},$$

$$\alpha_r = \frac{1}{M_0}\sin\eta\cos\eta\, f'(\eta) = \frac{\sin\theta}{R}.$$

Therefore,

$$f(\eta) = \frac{\cos\theta+\sin\theta\tan\eta}{R}. \tag{59}$$

Hence, at time t after the shock strikes the vertex of the cone, $\alpha = a_0 t$ and

$$\left.\begin{aligned}\frac{x}{U_0 t} &= \frac{1}{f(\eta)} = \frac{R}{\cos\theta+\sin\theta\tan\eta},\\ \frac{r}{U_0 t} &= \frac{x}{U_0 t}\tan\eta,\end{aligned}\right\} \tag{60}$$

gives the position of the shock wave in terms of the parameter η. It should be especially noted that x/U_0t, r/U_0t, the shock-shock angle χ and the distributions of θ and M/M_0 with η are all independent of M_0. *Thus, for a given cone, all shock waves go through exactly the same sequence of positions*; the differences in U_0 affect only the time scale.

The calculation has been carried out* for $R_1 = M_1/M_0 = 1{\cdot}2$, corresponding to $\theta_1 = 22{\cdot}4°$ and a shock-shock angle $\chi = 35{\cdot}8°$. The corresponding cone is found to be $\theta_w = 28{\cdot}8°$. The change in R is very small; it rises only to 1·216 at the cone. The position of the shock is shown in figure 4, and the distributions of θ and M/M_0 with η are given in figures 5 and 6. It should be remarked that since θ and R do not change very much, this solution is quite close to the corresponding two-dimensional one of diffraction by a wedge in which θ and M/M_0 remain constant. As $R_1 = M_1/M_0$ increases further, θ_w increases and the changes in θ and M/M_0 between the shock-shock and the cone get smaller. At the same time, the angle between the shock-shock and the cone decreases (from (58), $\chi \to \theta_1$ as $R_1 \to \infty$). As explained in Part 1 for the wedge problem, there is no critical angle at which Mach reflexion goes over into regular reflexion when the simple dependence of A on M is used across shock-shocks.

* The author is indebted to Mr J. Engelhardt for this calculation.

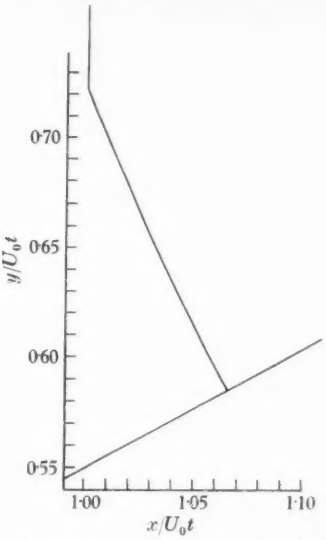

FIGURE 4. Calculated position of shock wave in diffraction by a cone.

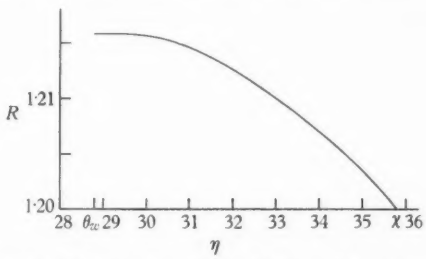

FIGURE 5. Distribution of $R = M/M_0$ with $\eta = \tan^{-1} r/x$ for shock wave in figure 4.

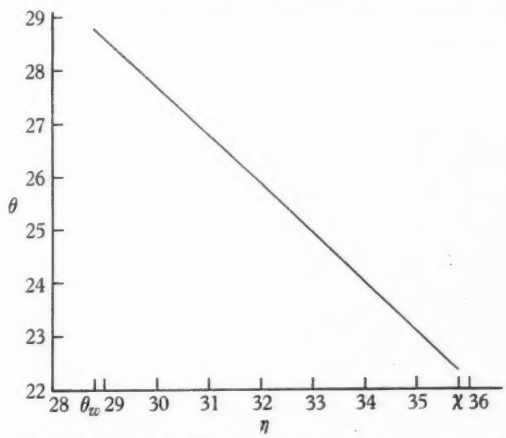

FIGURE 6. Distribution of θ with $\eta = \tan^{-1} r/x$ for shock wave in figure 4.

As R_1 decreases, the solution becomes less like the two-dimensional. When $R_1 - 1$ is small, corresponding to a slender cone with small angle θ_w, the changes in M/M_0 and θ across the shock-shock are of much smaller order in θ_w than the changes between the shock-shock and the cone surface. An analytic expression for the solution can be found in this case; it is included in the next section where the general solution is found for a slender axi-symmetrical obstacle of arbitrary shape. The jumps in M/M_0 and θ across the shock-shock are found to be

$$\left.\begin{aligned} \frac{M_1}{M_0} - 1 &= 18{\cdot}2\theta_w^4, \\ \theta_1 &= 41{\cdot}0\theta_w^4, \end{aligned}\right\} \tag{61}$$

whereas at the cone $\theta = \theta_w$ and

$$\frac{M_w}{M_0} - 1 = \theta_w^2 \left\{ \log \frac{1}{\theta_w} - 0{\cdot}619 \right\}. \tag{62}$$

Finally, it should be remarked that the shock-shock represents Mach reflexion, but the reflected shock wave is suppressed in this work. However, the strength and angle of the reflected shock wave at the triple point can be calculated from the values of θ_1 and M_1 using the shock-wave relations.

3. Small perturbation problems

For perturbations to a plane shock wave moving in the x-direction with Mach number M_0,

$$\alpha = \frac{1}{M_0}(x + \alpha'),$$

where α'/x is small. The linearized equation to be satisfied by α' is the wave equation

$$\alpha'_{yy} + \alpha'_{zz} - B^2 \alpha'_{xx} = 0$$

as found in (19). There are two main types of perturbation problem: (i) diffraction by thin or slender obstacles, and (ii) stability problems in which the initial shape and strength of the shock wave are given. An example of each is now considered.

(i) *Diffraction by a slender body*

If the perturbations are produced by a thin or slender obstacle, the boundary conditions are $\partial(x + \alpha')/\partial n = 0$ on the obstacle, and $\alpha' = 0$ at infinity. As explained already the solutions can be taken over from the theory of linearized supersonic flow. There is no point in copying down a long list of these. One example will be discussed here and the full range of possibilities can be seen by looking through a standard book on supersonic flow (for example, Ward (1955) or Sears (1955)).

It is worth noting in some detail the important special case of diffraction by an axi-symmetrical slender body. If the cross-sectional area of the body at a distance x from the nose is $S(x)$, the solution of (19), satisfying the boundary conditions, is

$$\alpha' = -\frac{1}{2\pi} \int_0^{x - Br} \frac{S'(\xi)}{\sqrt{[(x-\xi)^2 - B^2 r^2]}} d\xi. \tag{63}$$

(This assumes that $S'(x)$ is continuous.) In deriving M and θ from this solution it is important to notice that α'_x and α'_r are not of the same order near the body. If the maximum slope δ of the surface of the body is taken as a measure of the slenderness, $\alpha'_r \propto \delta$, while $\alpha'_x \propto \delta^2 \log 1/\delta$ near the body. Therefore, in calculating M, the approximate expression

$$\frac{M-M_0}{M_0} = -\alpha'_x - \tfrac{1}{2}\alpha'^2_r + O\left(\delta^4 \log^2 \frac{1}{\delta}\right) \tag{64}$$

should be used, instead of the simple linearized expression (17). This appears to be inconsistent since (17) was used in deriving (19), but the corresponding procedure has been fully investigated in supersonic flow and shown to give valid approximations. There is no trouble with θ; it is simply given by α'_r. Away from the body, both α'_x and α'_r are $O(\delta^2)$ and the α'_r term in (64) can be dropped.

The linearized solution does not include an adequate description of the shock-shock. Due to the linearization, the shock-shock degenerates into the characteristic $x - Br = 0$, but an inspection of (63) shows that α', α'_x, α'_r are continuous there. When $(x-Br)/r$ is small, the expressions for α'_x and α'_r may be approximated as

$$\left.\begin{aligned} \alpha'_x &= -\frac{M-M_0}{M_0} = -\frac{F(x-Br)}{\sqrt{(2Br)}}, \\ \alpha'_r &= \theta = \frac{BF(x-Br)}{\sqrt{(2Br)}}, \end{aligned}\right\} \tag{65}$$

where

$$F(x) = \frac{1}{2\pi}\int_0^x \frac{S''(\xi)\,d\xi}{\sqrt{(x-\xi)}}. \tag{66}$$

Since $F(x) \to 0$ as $x \to 0$, $M - M_0$ and θ vanish at $x - Br = 0$ and so there is no shock-shock. This result arises because the true values of $M - M_0$ and θ at the shock-shock are of smaller order in δ than the typical ones and they get neglected in the linearized theory. The linearized theory can be improved to include results for the shock-shock by the method used in supersonic flow (see Whitham 1952). The improved solution has

$$\left.\begin{aligned} \frac{M-M_0}{M_0} &= \frac{F(\tau)}{\sqrt{(2Br)}}, \\ \theta &= \frac{BF(\tau)}{\sqrt{(2Br)}}, \end{aligned}\right\} \tag{67}$$

in place of (65), where $\tau(x, r)$ has to give a more accurate approximation to the true characteristic than the linear $\tau = x - Br$. On the characteristic curve τ = constant, we have from (29),

$$\frac{dx}{dr} = \cot(\theta+m) = \cot m_0 - \frac{1}{\sin^2 m_0}\left\{\theta + \left(\frac{dm}{dM}\right)_0 (M-M_0)\right\} + O\left\{\theta^2, \left(\frac{M-M_0}{M_0}\right)^2\right\}.$$

Substituting from (67) and using $B = \cot m_0$, we have

$$\frac{dx}{dr} = B - \tfrac{1}{2}kF(\tau)\,r^{-\frac{1}{2}} + O\left(\frac{F^2}{r}\right),$$

where

$$k = (2B)^{\frac{1}{2}}(B^2+1)\left\{1 + \frac{M_0}{B}\left(\frac{dm}{dM}\right)_{M=M_0}\right\}. \tag{68}$$

Hence, the improved approximation for τ is

$$x = Br - kF(\tau)\, r^{\frac{1}{2}} + \tau. \tag{69}$$

The shock-shock can be determined from the characteristics (69) exactly as in the supersonic flow problem. At the shock-shock η and r are related by

$$r^{\frac{1}{2}} = \frac{2}{kF^2(\tau)} \int_0^\tau F(\tau')\, d\tau'. \tag{70}$$

Together with (69), this gives the shock-shock curve; (67) gives the values M_1 and θ_1 at the shock-shock.

To supplement the results of the last section we may specialize the results of this small perturbation theory to the case of a slender cone. If the cone angle is θ_w, then $S(x) = \pi\theta_w^2 x^2$. The linearized solution (63) becomes

$$\alpha' = x\theta_w^2 \left\{ \frac{\sqrt{[(x/Br)^2 - 1]}}{x/Br} - \cosh^{-1}(x/Br) \right\}; \tag{71}$$

hence,

$$\left.\begin{aligned} \alpha'_x &= -\theta_w^2 \cosh^{-1}(x/Br), \\ \alpha'_r &= \theta_w^2 B \sqrt{[(x/Br)^2 - 1]}. \end{aligned}\right\} \tag{72}$$

These quantities vanish at $x/Br = 1$, and become

$$\begin{aligned} \alpha'_x &= -\theta_w^2 \log \frac{2}{B\theta_w}, \\ \alpha'_r &= \theta_w, \end{aligned}$$

at the cone where $x/Br \sim 1/B\theta_w$. Therefore, according to (64), the Mach number at the surface of the cone is given by

$$\frac{M_w - M_0}{M_0} = \left(\theta_w^2 \log \frac{2}{B\theta_w} - \tfrac{1}{2}\theta_w^2 \right) + O\left(\theta_w^4 \log^2 \frac{1}{\theta_w} \right). \tag{73}$$

In the improved theory near the shock-shock, $F(\tau) = 2\theta_w^2 \tau^{\frac{1}{2}}$; hence, (70) gives

$$\tau = \frac{9k^2\theta_w^4 r}{4},$$

and the shock-shock is the straight line

$$x = (B - \tfrac{3}{4}k^2\theta_w^4)\, r.$$

The shock-shock angle χ is

$$\chi = m_0 + \tfrac{3}{2}B(B^2+1) \left\{ 1 + \frac{M_0}{B} \left(\frac{dm}{dM} \right)_0 \right\}^2 \theta_w^4, \tag{74}$$

and the values of θ and M at the shock-shock are

$$\theta_1 = 3B(B^2+1) \left\{ 1 + \frac{M_0}{B} \left(\frac{dm}{dM} \right)_0 \right\} \theta_w^4, \tag{75}$$

$$\frac{M_1 - M_0}{M_0} = 3(B^2+1) \left\{ 1 + \frac{M_0}{B} \left(\frac{dm}{dM} \right)_0 \right\} \theta_w^4. \tag{76}$$

If M_0 is large, $m_0 \sim 23{\cdot}9^\circ$, $B \sim 2{\cdot}253$ and $M_0 (dm/dM)_0 \sim 0$ (see (48)). The results for this case have been given in (61) and (62).

(ii) *Stability of a plane shock wave*

In the stability problem, the initial position and Mach number distribution of the shock wave are given, and the problem is to determine the subsequent motion. Here, it is assumed that the initial position is

$$x = -f(y,z)$$

and the initial strength is $M = M_0\{1-g(y,z)\}$,

where f and g are small. Then, with

$$\alpha = M_0(x+\alpha'),$$

we have (using (17)) $\alpha' = f(y,z), \quad \alpha'_x = g(y,z),$

initially. Strictly speaking, these are the values on $x = -f(y,z)$, but it is consistent with the linearization already used to apply these initial conditions at $x = 0$. The solution of

$$B^2\alpha'_{xx} = \alpha'_{yy} + \alpha'_{zz}$$

must be found subject to these initial values.

The analogy with the two-dimensional initial value problem of acoustics is obvious, and the solution is well known. It can be written as

$$\alpha' = \frac{B^2}{2\pi}\left\{\frac{\partial}{\partial x}\iint \frac{f(\eta,\zeta)\,d\eta\,d\zeta}{\sqrt{[x^2 - B^2(\eta-y)^2 - B^2(\zeta-z)^2]}} + \iint \frac{g(\eta,\zeta)\,d\eta\,d\zeta}{\sqrt{[x^2 - B^2(\eta-y)^2 - B^2(\zeta-z)^2]}}\right\}, \tag{77}$$

where the integrations are over the interior of the circle

$$B^2(\eta-y)^2 + B^2(\zeta-z)^2 = x^2.$$

In general, the disturbance given by (77) decays as it spreads out on the shock wave; if the disturbance is initially confined to a finite region, the decay is ultimately like $x^{-\frac{1}{2}}$ for large x. For the two-dimensional disturbance discussed in Part 1 there is no decay according to the linearized theory. But certain non-linear features, related to the formation of shock-shocks become crucially important after a sufficient time. When they were included in the two-dimensional problem a decay like $x^{-\frac{1}{2}}$ was found (see Part 1). Similar effects arise here and modify the ultimate decay law for an initially finite region from $\alpha' \propto x^{-\frac{1}{2}}$ to $\alpha' \propto x^{-\frac{3}{4}}$ for large x. No details will be given, since a very full treatment for the closely similar problems of sound waves has been presented in a previous paper (Whitham 1956). The linearized expression (77) should give a good approximation in general until x becomes quite large.

4. Further applications

As explained above, many problems could be posed and solved for the small perturbation theory simply by re-interpreting the large number of solutions available in linearized supersonic flow and acoustics. Two of the simpler examples have been given in § 3, and others can be worked out as required. Generally speaking, however, these solutions for small disturbances will probably be of less

practical value here than in supersonic flow or acoustics, and the main emphasis should be on the solution of the full non-linear equations. For axi-symmetrical problems the numerical solution of quite complicated cases would be straightforward. But even for the full three-dimensional problems, numerical methods become feasible in the approximate theory of this paper, since there are only three independent variables x, y, z. (This would seem to be out of the question in the exact formulation which involves all four variables x, y, z and t.) Furthermore, there are special cases other than axi-symmetrical problems, where similarity solutions apply and the three variables can be reduced to two. For example, in the diffraction of a plane shock wave by a flat plate delta wing at incidence, the solution must take the form

$$\alpha = xf\left(\frac{y}{x}, \quad \frac{z}{x}\right),$$

since there is no fundamental length prescribed in the problem. This type of example corresponds to cone field theory in supersonic flow.

For genuine three-variable problems, the theory developed in § 1 leads to partial differential equations which are very similar to those in the *exact* formulation of *two-dimensional* time-dependent gas dynamics and numerical methods devised for such problems could be used here.

This paper represents results obtained at the Institute of Mathematical Sciences, New York University, under the sponsorship of the Office of Naval Research, Contract N6ori-201, T.O. 1.

REFERENCES

Chisnell, R. F. 1957 *J. Fluid Mech.* **2**, 286.

Sears, W. R. (ed.) 1955 *General Theory of High Speed Aerodynamics. High Speed Aerodynamics and Jet Propulsion*, vol. VI. Princeton University Press.

Ward, G. N. 1955 *Linearized Theory of Steady High-Speed Flows.* Cambridge University Press.

Weatherburn, C. E. 1931 *Differential Geometry*, vol. I. Cambridge University Press.

Whitham, G. B. 1952 *Comm. Pure Appl. Math.* **6**, 301.

Whitham, G. B. 1956 *J. Fluid Mech.* **1**, 290.

Whitham, G. B. 1957 *J. Fluid Mech.* **2**, 145.

Whitham, G. B. 1958 *J. Fluid Mech.* **4**, 337.

The propagation of small disturbances in hydromagnetics

By G. S. S. LUDFORD
University of Maryland and Harvard University

(Received 20 August 1958)

This paper is concerned with the propagation of small initial disturbances in a conducting gas under the influence of a uniform external magnetic field.

For a perfect conductor, there are three types of plane waves, each of which depends strongly on the angle at which the magnetic field is crossed. The modifying effects of finite conductivity are determined and, in the case of these waves, this is done uniformly for all angles. A general disturbance may be resolved into two parts, one of which satisfies a fourth-order equation and the other a fifth; for a perfect conductor these reduce to second- and fourth-order equations, respectively.

The free oscillations of the gas are examined when it is contained in a rectangular box, and, in particular, when the external field is very weak or very strong. For vanishingly weak fields the idealization of infinite conductivity proves to be inadequate. Finally, the initial-value problem is discussed.

1. Introduction

In this paper we consider the small perturbations of an electrically conducting inviscid gas at rest in the presence of a uniform external magnetic field. The main interest lies in fluids of high (but not infinite) conductivity, and in order to obtain all effects we do not neglect displacement currents.

The system of eleven first-order linear differential equations governing the motion possesses two integrals (invariants in time) so that the effective order is nine. First we discuss plane waves which, in the context of forced oscillations, have been previously considered by van de Hulst (1951) and by Baños (1955), but in each case with certain important limitations. The equations are found to divide into two sets, one leading to a quartic for the frequency as a function of the wavelength and the other to a quintic. Two of the roots of the quartic and one of the quintic give pure decay of which the main effect is the reduction of the initial electrical field, as measured in the local frame, to zero; this being required in a perfect conductor. For such a conductor the remaining two and four roots give the three possible modes of propagation of sinusoidal disturbances. One of these can be identified as an Alfvén wave; the other two cannot in general be distinguished except on the basis of velocity.† The damping effect of finite conductivity on these waves is determined (uniformly) for all inclinations of the wave front to the undisturbed magnetic field. For small inclinations the damping predominates in two of the modes and the disturbances decay exponentially.

Returning to the general perturbation equations, we show that, by suitable

† These correspond to Friedrichs's (1957) transverse, fast and slow disturbance waves.

transformation, these also can be split into sets of four and five. Each set leads, on elimination of all but any one of the independent variables, to a partial differential equation of the same order. These orders reduce to two and four, respectively, for a perfect conductor; the second-order equation then being a one-dimensional wave equation and the fourth-order equation exhibiting similar strong anisotropy in the direction of the external field.

We next examine a simple boundary-value problem in detail, namely, the standing waves in the fluid when it is confined in a rectangular box made of perfectly conducting material into which a uniform magnetic field perpendicular to two of the faces has been frozen. These waves, which consist of combinations of plane waves, are of three types: those corresponding to an infinity of frequencies associated with the Alfvén velocity, and two others distinguished by their symmetry properties about the median plane and having separate frequency equations. The resulting pair of distributions of frequencies are sketched for the two extreme cases of very weak and very strong external fields. In the former case the ordinary acoustic frequencies are obtained in the limit, half from one equation and half from the other, while all other frequencies tend to zero.

The limiting forms of the waves themselves for the two extreme cases are also discussed, and here we encounter two interesting phenomena for a vanishingly weak external field. First, the last two types of waves become indeterminate if the conductivity has been taken infinite, but tend to definite limits for any finite conductivity (which may then tend to infinity). Secondly, for all waves the tangential component of velocity is zero on the two walls perpendicular to the external field, while no such condition need be satisfied in the absence of an external field. Such initial discontinuities in the latter case cling to the walls as vortex sheets, while in the presence of a (non-parallel) external field they immediately move away. We conclude that, however large the conductivity of the fluid may be, the idealization of its being perfectly conducting is not good in the case of sufficiently weak external fields; and that however weak the field, a vortex sheet can only remain adjacent to walls which are parallel to the field.

We conclude with a discussion of the general initial-value problem and the determination of Fourier coefficients appropriate to the orthogonal system defined by the standing waves.

2. The equations of motion

We consider the motion of an electrically conducting inviscid gas in the absence of body forces and heat conduction. Further we shall assume that the material coefficients μ (permeability), ϵ (dielectric constant), and σ (conductivity) are constant. Then the equations governing the motion are

$$\left.\begin{aligned} \mu\frac{\partial \mathbf{H}}{\partial t} &= -\operatorname{curl}\mathbf{E}, \quad \frac{1}{\sigma}(\mathbf{J}-\rho_e\mathbf{v}) = \mathbf{E}+\mu\mathbf{v}\times\mathbf{H}, \\ \rho\frac{d\mathbf{v}}{dt} &= -\operatorname{grad}p+\rho_e\mathbf{E}+\mu\mathbf{J}\times\mathbf{H}, \\ \frac{\partial\rho}{\partial t}+\operatorname{div}\rho\mathbf{v} &= 0, \quad \rho T\frac{dS}{dt} = \frac{1}{\sigma}(\mathbf{J}-\rho_e\mathbf{v})^2. \end{aligned}\right\} \tag{1}$$

Here the temperature T and the specific entropy S are given functions of the pressure p and density ρ, while ρ_e (charge density) and $\mathbf{J}$ (current density) are related to the electric field $\mathbf{E}$ and the magnetic field $\mathbf{H}$ by

$$\rho_e = \epsilon \operatorname{div} \mathbf{E}, \quad \mathbf{J} = \operatorname{curl} \mathbf{H} - \epsilon \frac{\partial \mathbf{E}}{\partial t}.$$

The system (1) consists of eleven first-order equations for $\mathbf{E}, \mathbf{H}, \mathbf{v}, p, \rho$ and we only admit solutions for which

$$\operatorname{div} \mathbf{H} = 0, \tag{2}$$

this condition being satisfied at all times if it is satisfied at any one instant since $\partial \mathbf{H}/\partial t$ is solenoidal.

If the deviation from a given uniform state $\mathbf{E} = 0$, $\mathbf{H} = \mathbf{H}_0$, $\mathbf{v} = 0$, $p = p_0$, $\rho = \rho_0$ is small, so that we may neglect squares and products of disturbance quantities, the system (1) reduces to

$$\left.\begin{aligned} &(a)\quad \mu \frac{\partial \mathbf{H}}{\partial t} = -\operatorname{curl} \mathbf{E}, \quad (b)\quad \frac{1}{\sigma}\mathbf{J} = \mathbf{E} + \mu \mathbf{v} \times \mathbf{H}_0, \\ &(c)\quad \rho_0 \frac{\partial \mathbf{v}}{\partial t} = -\operatorname{grad} p + \mu \mathbf{J} \times \mathbf{H}_0, \\ &(d)\quad \frac{\partial \rho}{\partial t} + \rho_0 \operatorname{div} \mathbf{v} = 0, \quad (e)\quad \frac{\partial p}{\partial t} - a_0^2 \frac{\partial \rho}{\partial t} = 0, \end{aligned}\right\} \tag{3}$$

where $\mathbf{H}, p, \rho$ now denote deviations from $\mathbf{H}_0$, p_0, ρ_0 and

$$a_0^2 = \left(\frac{\partial S/\partial \rho}{\partial S/\partial p}\right)_{p_0, \rho_0} = \left(\frac{dp}{d\rho}\right)_{S=S_0}.$$

From (3e) we see that, except for a function independent of t,

$$\rho = \frac{1}{a_0^2} p. \tag{4}$$

In view of the integrals (2) and (4) the effective order of the system (3) is nine.

3. Plane waves

These were considered in detail first by van de Hulst (1951) and later by Baños (1955) for the simpler case of forced oscillations. Since neither of their treatments is readily adaptable to the present discussion we shall briefly derive the salient features here *ab initio*. In particular, we shall contrast the case of a good conductor (σ large) with that of the more familiar poor conductor (σ small).

Take the x-axis along the direction of propagation and let the x, y-plane contain $\mathbf{H}_0$: then $\mathbf{H}_0 = (H_0 \cos\phi, H_0 \sin\phi, 0)$ where ϕ is the angle at which the waves cross the undisturbed magnetic field. With all variable proportional to $\exp i(\omega t - \kappa x)$ and the same symbols used for the factors, the equations (3) divide into two sets, I and II, involving†

$$\text{I: } E_1, E_2, H_3, v_3 \quad \text{and} \quad \text{II: } E_3, H_2, v_1, v_2, p \text{ (and } \rho), \tag{5}$$

† Subscripts 1, 2, 3 denote x-, y-, z-components consistently throughout this paper.

respectively. Thus we find from equations $(3b_1)$,† $(3a_3)$, $(3b_2)$, and $(3c_3)$:

$$\text{(I)}\quad \begin{cases} E_1 = \dfrac{\mu H_0 \sin\phi}{(1+i\eta\omega/c^2)}\, v_3, \quad E_2 = \dfrac{\mu\omega}{\kappa} H_3, \\ \left[\omega - i\eta\left(\kappa^2 - \dfrac{\omega^2}{c^2}\right)\right] H_3 + \kappa H_0 \cos\phi v_3 = 0, \\ \left(\kappa^2 - \dfrac{\omega^2}{c^2}\right)\left(1 + \dfrac{i\eta\omega}{c^2}\right) A_0^2 \cos\phi H_3 + \omega\kappa H_0 \left(1 + \dfrac{i\eta\omega}{c^2} + \dfrac{A_0^2}{c^2}\sin^2\phi\right) v_3 = 0, \end{cases}$$

respectively, where $c^2 = 1/\mu\epsilon$, $A_0^2 = \mu H_0^2/\rho_0$, and $\eta = 1/\mu\sigma$ (magnetic diffusivity). Similarly, from $(3a_2)$, $(3d)$, $(3b_3)$, $(3c_1)$, and $(3c_2)$ we obtain

$$\text{(II)}\quad \begin{cases} E_3 = -\dfrac{\mu\omega}{\kappa} H_2, \quad p = \dfrac{a_0^2 \rho_0 \kappa}{\omega} v_1, \\ \left[\omega - i\eta\left(\kappa^2 - \dfrac{\omega^2}{c^2}\right)\right] H_2 - \kappa H_0 \sin\phi v_1 + \kappa H_0 \cos\phi v_2 = 0, \\ \omega\left(\kappa^2 - \dfrac{\omega^2}{c^2}\right) A_0^2 \sin\phi H_2 + \kappa(a_0^2\kappa^2 - \omega^2) H_0 v_1 = 0, \\ \left(\kappa^2 - \dfrac{\omega^2}{c^2}\right) A_0^2 \cos\phi H_2 + \omega\kappa H_2 v_2 = 0, \end{cases}$$

respectively. The remaining equation $(3a_1)$ gives $H_1 = 0$, in agreement with the requirement (2).

The dispersion relations corresponding to these two systems are

$$\text{(i)}\quad \frac{\eta^2}{c^4}\omega^4 - \frac{i\eta}{c^2}\left(2 + \frac{A_0^2}{c^2}\right)\omega^3 - \left(1 + \frac{A_0^2}{c^2} + \frac{\eta^2\kappa^2}{c^2}\right)\omega^2 + i\eta\kappa^2\left(1 + \frac{A_0^2}{c^2}\right)\omega + A_0^2\kappa^2\cos^2\phi = 0,$$

$$\text{(ii)}\quad \frac{i\eta}{c^2}\omega^5 + \left(1 + \frac{A_0^2}{c^2}\right)\omega^4 - i\eta\kappa^2\left(1 + \frac{a_0^2}{c^2}\right)\omega^3 - \kappa^2\left(a_0^2 + A_0^2 + \frac{a_0^2 A_0^2}{c^2}\cos^2\phi\right)\omega^2 + i\eta\kappa^4 a_0^2\omega + \kappa^4 a_0^2 A_0^2 \cos^2\phi = 0.$$

In the first case there are, in general, four possible values of ω for each given κ, ϕ, and in the second case five. The total of nine corresponds to the eleven original equations less the two t-integrals (2) and (4). We shall see that two of the roots in (i) and one of those in (ii) correspond to pure decays; the remainder (two and four) represent damped sinusoidal waves, which are in general neither transverse nor longitudinal.

From (5) we note that **E** is always perpendicular to both **H** and **v**, these being parallel vectors in case I.

4. The extreme cases

(*a*) *Insulator.* For a perfect insulator $\eta = \infty$, and we find

$$\text{I:}\quad \omega = \pm c\kappa; \quad E_2 = \pm\sqrt{(\mu/\epsilon)}\, H_3, \quad E_1 = v_3 = 0,$$

$$\text{II:}\quad \begin{cases} \omega = \pm c\kappa; & E_3 = \mp\sqrt{(\mu/\epsilon)}\, H_2, & v_1 = v_2 = p = 0, \\ \omega = \pm a_0\kappa; & p = \pm\rho_0 a_0 v_1, & E_3 = H_2 = v_2 = 0. \end{cases}$$

† $(3b_1)$ is the x-component of equation $(3b)$, etc.

The field $\mathbf{H}_0$ is purely additive. I and the first of II are ordinary (transverse) electromagnetic waves and can be added. The second of II is an ordinary (longitudinal) acoustic wave.

For a good insulator and all but very small wave numbers (i.e. when the non-dimensional quantity $\eta\kappa/c$ is large) these frequencies become (to order $1/\eta^2$)

$$\text{I:} \quad \omega = \pm c\kappa + ic^2/2\eta,$$

$$\text{II:} \quad \begin{cases} \omega = \pm c\kappa + ic^2/2\eta, \\ \omega = \pm a_0\kappa + iA_0^2 \sin^2\phi/2\eta. \end{cases}$$

The damping of the electromagnetic waves is independent of the undisturbed state and is the same as for a rigid body. On the other hand, the (much slower) damping of the acoustic wave does depend on the undisturbed state and in particular is zero for $\phi = 0$. In addition, three other roots now occur, given (to order $1/\eta^3$) by†

$$\text{I:} \quad \begin{cases} \omega = i\alpha_1 c^2/\eta; \quad E_1 = [\mu H_0 \sin\phi/(1-\alpha_1)]\, v_3 \doteqdot (\rho_0 c^2/H_0 \sin\phi)\, v_3, \\ \omega = i\alpha_2 c^2/\eta; \quad E_1 = [\mu H_0 \sin\phi/(1-\alpha_2)]\, v_3 \doteqdot \mu H_0 \sin\phi v_3, \end{cases}$$

$$\text{II:} \quad \omega = iA_0^2 \cos^2\phi/\eta; \quad v_2 \text{ predominates},$$

where

$$\alpha_1, \alpha_2 = \frac{1}{2}\left(1 + \frac{A_0^2}{c^2}\right)\left[1 \pm \sqrt{\left(1 - \frac{4c^2 A_0^2 \cos^2\phi}{(c^2 + A_0^2)^2}\right)}\right] \doteqdot 1 - \frac{A_0^2}{c^2}\sin^2\phi, \frac{A_0^2}{c^2}\cos^2\phi.$$

The first of I reduces to the familiar charge decay for small H_0 (or ϕ). The other two are then essentially (much slower) velocity decays.

(*b*) *Conductor.* For a perfect conductor $\eta = 0$, and we find

$$\text{I:} \quad \omega \doteqdot \pm (A_0 \cos\phi)\kappa; \quad E_1/\mu H_0 \sin\phi = -E_2/\mu H_0 \cos\phi = \mp (A_0/H_0) H_3 = v_3 \text{ (approx.)},$$

$$\text{II:} \quad \begin{Bmatrix} \omega = \pm V^{(1)}\kappa \\ \omega = \pm V^{(2)}\kappa \end{Bmatrix}; \quad \frac{E_3}{\mu H_0 V} = \frac{\mp H_2}{H_0} = \frac{(a_0^2 - V^2)\, v_1}{A_0^2 V \sin\phi} = \frac{V v_2}{A_0^2 \cos\phi}$$

$$= \pm \frac{(a_0^2 - V^2)\, p}{a_0^2 A_0^2 \rho_0 V \sin\phi} \text{ (approx.)},$$

where $V = V^{(1)}, V^{(2)}$ are the positive roots of (approx.)

$$V^4 - (a_0^2 + A_0^2)\, V^2 + a_0^2 A_0^2 \cos^2\phi = 0.$$

A sketch of $V^{(1)}$ and $V^{(2)}$ as functions of ϕ is given in figure 1. I gives so-called Alfvén waves which progress along the $\mathbf{H}_0$-direction with velocity $\pm A_0$ and with $\mathbf{E}$ perpendicular to $\mathbf{H}_0$ as well as to $\mathbf{H}$. For $\phi = 0$, II represents the same Alfvén waves, now transverse and rotated through 90° about the x-axis, and (longitudinal) acoustic waves with velocity $\pm a_0$. For other values‡ of ϕ such a distinction has meaning only when

$$A_0 \ll a_0: \quad V^{(1)} = a_0, \quad V^{(2)} = A_0 \cos\phi. \tag{6}$$

In fact for

$$A_0 \gg a_0: \quad V^{(1)} = A_0, \quad V^{(2)} = a_0 \cos\phi, \tag{7}$$

† Of the quantities (5), only those of lowest order are listed here [e.g. in I, $H_3/v_3 = O(1/\eta)$ and hence H_3 is omitted]. Also A_0^2/c^2 will be neglected in comparison with unity whenever appropriate (indicated by 'approx.' or '$\doteqdot$').

‡ For fixed ϕ and $\sqrt{(a_0^2 + A_0^2)}$, the root $V^{(1)}$ has a minimum and the root $V^{(2)}$ a maximum when $a_0 = A_0$ (cf. figure 1). At this point the two waves for $\phi = 0$ interchange.

the velocities a_0, A_0 have changed roles, without however a corresponding interchange of the other characteristics of the waves.

For a good conductor and all but very large wave numbers (i.e. when the non-dimensional quantity $\eta\kappa/c$ is small) the damping is determined (approx.) by:

$$\omega^2 - i\eta\kappa^2\omega - \kappa^2 A_0^2 \cos^2\phi = 0,$$
$$\omega^4 - i\eta\kappa^2\omega^3 - (a_0^2 + A_0^2)\kappa^2\omega^2 + i\eta\kappa^4 a_0^2\omega + \kappa^4 a_0^2 A_0^2 \cos^2\phi = 0, \tag{8}$$

respectively. From the first of these we find immediately:

$$\text{I:}\quad \omega \doteqdot \begin{cases} \frac{1}{2}\kappa[\pm\sqrt{(4A_0^2\cos^2\phi - \eta^2\kappa^2)} + i\eta\kappa] & (\cos\phi > \eta\kappa/2A_0). \\ \frac{1}{2}i\kappa[\eta\kappa \pm \sqrt{(\eta^2\kappa^2 - 4A_0^2\cos^2\phi)}] & (\cos\phi < \eta\kappa/2A_0). \end{cases}$$

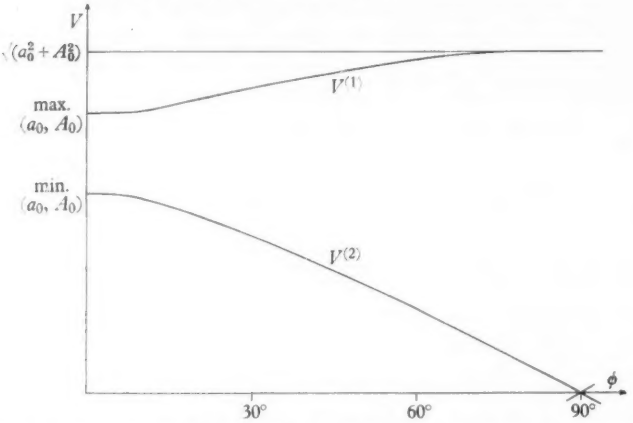

FIGURE 1. The velocities $V^{(1)}$ and $V^{(2)}$ as functions of the angle ϕ between the undisturbed magnetic field and the direction of propagation.

The second yields the damping of the $V^{(1)}$-waves as an η-perturbation. Having found this perturbation, we take out the corresponding factor from the left-hand side of the equation and are left with

$$\omega^2 - i\eta\kappa^2 F(\phi)\,\omega - V^{(2)2} = 0,$$

where
$$F(\phi) = \frac{V^{(1)2} - A_0^2}{2V^{(1)2} - a_0^2 - A_0^2} = \frac{a_0^2 - V^{(2)2}}{a_0^2 + A_0^2 - 2V^{(2)2}},$$

as the equation governing the damping of the $V^{(2)}$-waves. Hence we find

$$\text{II:}\quad \begin{cases} \omega \doteqdot \pm V^{(1)}\kappa + \frac{1}{2}i\eta\kappa^2(1-F), \\ \omega \doteqdot \begin{cases} \frac{1}{2}\kappa[\pm\sqrt{(4V^{(2)2} - \eta^2\kappa^2F^2)} + i\eta\kappa F] & (V^{(2)}/F > \frac{1}{2}\eta\kappa),\dagger \\ \frac{1}{2}i\kappa[\eta\kappa F \pm \sqrt{(\eta^2\kappa^2F^2 - 4V^{(2)2})}] & (V^{(2)}/F < \frac{1}{2}\eta\kappa).\dagger \end{cases} \end{cases}$$

For I and the second of II there is a range of values near $\phi = \frac{1}{2}\pi$ where the damped waves turn into pure decays. In all cases, when ϕ is small the damping factor changes rapidly near $a_0 = A_0$.‡ There is no damping of the acoustic wave ($\phi = 0$), and for $\phi = \frac{1}{2}\pi$ two of the four decays stop. These last results are in fact exact, see (i) and (ii).

† Using the approximation $V^{(2)} = a_0 A_0 \cos\phi/\sqrt{(a_0^2 + A_0^2)}$ near $\phi = \frac{1}{2}\pi$ these conditions become $\cos\phi \gtrless \eta\kappa a_0/2A_0\sqrt{(a_0^2 + A_0^2)}$.

‡ At $\phi = 0$, F jumps discontinuously from 1 to zero.

As before, there are three more roots now, given (to order η) by

$$\text{I:}\quad \begin{cases} \omega = ic^2/\eta; \quad E_1/\cos\phi = E_2/\sin\phi, \\ \omega = ic^2(1+A_0^2/c^2)/\eta \doteq ic^2/\eta; \quad E_1/\sin\phi = -E_2/\cos\phi = -(\rho_0 c^2/H_0)\, v_3 \end{cases}$$

$$\text{II:}\quad \omega = ic^2(1+A_0^2/c^2)/\eta \doteq ic^2/\eta; \quad (H_0/\rho_0 c^2)\, E_3 = v_1/\sin\phi = -v_2/\cos\phi.$$

Together these correspond to (very fast) decays in $\mathbf{E}$ and $\mathbf{v}\times\mathbf{H}_0$ in which the total momentum $\rho_0\mathbf{v}+(\mathbf{E}\times\mathbf{H}_0)/c^2$ remains constant (zero). We shall return to this point later.

5. Splitting of the general linearized equations

The division of plane waves into two sets has its counterpart for the general flow governed by equations (3). To show this we introduce new Cartesian co-ordinates, where now the y-axis lies along $\mathbf{H}_0$. Also we denote by θ, δ, Δ the divergences of $\mathbf{E}$, $\mathbf{H}$, $\mathbf{v}$ using x- and z-components only:

$$\theta = \frac{\partial E_1}{\partial x}+\frac{\partial E_3}{\partial z}, \quad \delta = \frac{\partial H_1}{\partial x}+\frac{\partial H_3}{\partial z}, \quad \Delta = \frac{\partial v_1}{\partial x}+\frac{\partial v_3}{\partial z}.$$

Then for E_2, θ, $\operatorname{curl}_2\mathbf{H}$, $\operatorname{curl}_2\mathbf{v}$ the following four equations hold:

$$\left.\begin{aligned} \left(\nabla^2-\frac{\partial^2}{\partial y^2}\right)E_2-\frac{\partial\theta}{\partial y}-\mu\frac{\partial}{\partial t}\operatorname{curl}_2\mathbf{H} &= 0, \\ \left(\frac{\eta}{c^2}\frac{\partial}{\partial t}+1\right)E_2-\mu\eta\operatorname{curl}_2\mathbf{H} &= 0, \\ \left(\frac{\eta}{c^2}\frac{\partial}{\partial t}+1\right)\left(\frac{\partial E_2}{\partial y}+\theta\right)+\mu H_0\operatorname{curl}_2\mathbf{v} &= 0, \\ \frac{1}{c^2}\frac{\partial\theta}{\partial t}+\mu\frac{\partial}{\partial y}\operatorname{curl}_2\mathbf{H}-\frac{\rho_0}{H_0}\frac{\partial}{\partial t}\operatorname{curl}_2\mathbf{v} &= 0. \end{aligned}\right\} \tag{9}$$

The first and fourth of these are the y-components of the curl of $(3a)$ and the curl of $(3c)$, respectively; the second is the same component of $(3b)$ and the third is the divergence of that equation.

Similarly, for $\operatorname{curl}_2\mathbf{E}$, H_2, δ, v_2, Δ, p we find the six equations

$$\left.\begin{aligned} \operatorname{curl}_2\mathbf{E}+\mu\frac{\partial H_2}{\partial t} &= 0, \\ \left(\frac{\eta}{c^2}\frac{\partial}{\partial t}+1\right)\operatorname{curl}_2\mathbf{E}+\mu\eta\nabla^2 H_2-\mu H_0\Delta &= 0, \\ \rho_0\frac{\partial v_2}{\partial t}+\frac{\partial p}{\partial y} &= 0, \\ \frac{1}{c^2}\frac{\partial}{\partial t}\operatorname{curl}_2\mathbf{E}+\mu\nabla^2 H_2+\frac{\rho_0}{H_0}\frac{\partial}{\partial t}\left(\frac{\partial v_2}{\partial y}+\Delta\right)+\frac{1}{H_0}\nabla^2 p &= 0, \\ \rho_0 a_0^2\left(\frac{\partial v_2}{\partial y}+\Delta\right)+\frac{\partial p}{\partial t} &= 0, \\ \frac{\partial H_2}{\partial y}+\delta &= 0. \end{aligned}\right\} \tag{10}$$

Here the first and third equations are the y-components of (3a) and (3c) respectively, and the second is the same component of the curl of (3b). The fourth is the divergence of (3c). The fifth is just (3d), after (3e) has been used, and the six this the integrated form of the divergence of (3a) (see equation (2)).

Thus each of (3a)—(3d) has given rise to as many equations in (9) and (10) as it has components, and the order (nine) of these in the t-derivative is just two less than that (eleven) of the original system.

By eliminating the other three variables from (9), we find that each of $u = E_2$, θ, $\mathrm{curl}_2 \mathbf{H}$, $\mathrm{curl}_2 \mathbf{v}$ satisfies

$$\left[\frac{\partial}{\partial t}\left(\frac{\eta}{c^2}\frac{\partial}{\partial t}+\overline{1+\frac{A_0^2}{c^2}}\right)\left(\eta\overline{\frac{1}{c^2}\frac{\partial^2}{\partial t^2}-\nabla^2}+\frac{\partial}{\partial t}\right)-A_0^2\frac{\partial^2}{\partial y^2}\right]u=0; \tag{11}$$

note that for $\eta = 0$ this is a one-dimensional wave equation. Similarly, by eliminating all but one of $u = \mathrm{curl}_2 \mathbf{E}$, H_2, δ, v_2, Δ, p from (10) we find

$$\left[\eta\frac{\partial}{\partial t}\left(\frac{1}{c^2}\frac{\partial^2}{\partial t^2}-\nabla^2\right)\left(\frac{\partial^2}{\partial t^2}-a_0^2\nabla^2\right)+\left(1+\frac{A_0^2}{c^2}\right)\frac{\partial^4}{\partial t^4}\right.$$
$$\left.-\left(\overline{a_0^2+A_0^2}\nabla^2+\frac{a_0^2A_0^2}{c^2}\frac{\partial^2}{\partial y^2}\right)\frac{\partial^2}{\partial t^2}+a_0^2A_0^2\nabla^2\frac{\partial^2}{\partial y^2}\right]u=0.$$

The two operators reduce to the left-hand sides of equations (i) and (ii), respectively, on setting $\partial/\partial t = i\omega$, $\nabla^2 = -\kappa^2$, $\partial^2/\partial y^2 = -\kappa^2\cos^2\phi$, as they should. For $\eta = 0$, the order of the first in the t-derivative reduces from four to two, while that of second changes from five to four. The combined loss of three corresponds to the fact that (3b) reduces to the algebraic relation

$$\mathbf{E}+\mu\mathbf{v}\times\mathbf{H}_0=0 \tag{12}$$

for a perfect conductor, so that $\mathbf{E}$ can no longer be initially prescribed independently of $\mathbf{v}$. For small η the corresponding relaxation of the initial conditions is asymptotically represented by the three modes of decay discussed at the end of the preceding section.†

6. Standing waves in a rectangular box

Suppose the gas fills a rectangular cavity ($x = 0, a$; $y = 0, b$; $z = 0, c$)‡ in a perfectly conducting rigid body into which is 'frozen'§ a uniform magnetic field; let the corresponding external field in the cavity be H_0. Since we must allow the possibility of surface currents for a perfect conductor, the tangential component of $\mathbf{H}$ is not necessarily continuous across the walls of the cavity. Thus, whether or not the gas is considered to be perfect, the complete set of boundary conditions is

$$\left.\begin{aligned} E_2 = E_3 = H_1 = v_1 = 0 \quad &\text{on} \quad x = 0, a, \\ E_3 = E_1 = H_2 = v_2 = 0 \quad &\text{on} \quad y = 0, b, \\ E_1 = E_2 = H_3 = v_3 = 0 \quad &\text{on} \quad z = 0, c, \end{aligned}\right\} \tag{13}$$

† A fuller account has been given by Ludford (1959).

‡ No confusion arises from this second use of c since the old A_0^2/c^2 will be automatically neglected in the remainder of this paper.

§ For a perfect solid conductor Maxwell's equations integrate to give $\mathbf{E} = 0$ and $\mathbf{H}$ independent of t. In the present case this has the effect of isolating the oscillating gas.

expressing the continuity of the tangential component of **E** and of the normal components of $\mu\mathbf{H}$ and **v**.

By virtue of Maxwell's equation (3*a*) the conditions on **H** are satisfied whenever those on **E** are satisfied. Moreover, for a perfectly conducting gas: $E_2 \equiv 0$, the vanishing of E_3 on the x-faces is implied by the vanishing of v_1, and similarly for E_1 and v_3 on the z-faces [see (12)]. Thus for $\eta \neq 0$ there are only eighteen effective conditions in (13), of which eight are automatically satisfied by virtue of the other ten when $\eta = 0$.

Since the modifying effects of non-zero η have already been sketched in § 4 we restrict the discussion now to $\eta = 0$. Separation of variables then leads to the following solutions of (9):

$$\left.\begin{aligned} H_1 &= \frac{m\pi}{b} H_0 F_z(x,z) \cos m\frac{\pi y}{b} e^{i\omega t}, \\ H_3 &= -\frac{m\pi}{b} H_0 F_x(x,z) \cos m\frac{\pi y}{b} e^{i\omega t}, \\ v_1 &= -\frac{E_3}{\mu H_0} = i\omega F_z(x,z) \sin m\frac{\pi y}{b} e^{i\omega t}, \\ v_3 &= \frac{E_1}{\mu H_0} = -i\omega F_x(x,z) \sin m\frac{\pi y}{b} e^{i\omega t}, \end{aligned}\right\} \tag{14}$$

where in agreement with (i) $$\omega = \frac{m\pi}{b} A_0; \tag{15}$$

in addition $E_2 = H_2 = v_2 = p = 0$. In order to satisfy the boundary conditions on v_1 and v_3, the otherwise arbitrary function $F(x,z)$ must vanish on $x = 0$, a and $z = 0, c$; the $\sin m\pi y/b$, with m a non-negative integer, in E_1 and E_3 follows for a similar reason. Note that H and v are 90° out of phase, and that we have ensured $\operatorname{curl}_2 \mathbf{E} = \delta = \Delta = 0$ [equations (10) must also be satisfied].

Similarly, we find product solutions of (10):

$$\left.\begin{aligned} H_1 &= -i\frac{l}{\omega a} H_0 g'(y) \sin l\frac{\pi x}{a} \cos n\frac{\pi z}{c} e^{i\omega t}, \\ H_2 &= \frac{i\pi}{\omega}\left(\frac{l^2}{a^2}+\frac{n^2}{c^2}\right) H_0 g(y) \cos l\frac{\pi x}{a} \cos n\frac{\pi z}{c} e^{i\omega t}, \\ H_3 &= -i\frac{n}{\omega c} H_0 g'(y) \cos l\frac{\pi x}{a} \sin n\frac{\pi z}{c} e^{i\omega t}, \\ v_1 &= -\frac{E_3}{\mu H_0} = \frac{l}{a} g(y) \sin l\frac{\pi x}{a} \cos n\frac{\pi z}{c} e^{i\omega t}, \\ v_2 &= \pi\left(\frac{l^2}{a^2}+\frac{n^2}{c^2}\right) f(y) \cos l\frac{\pi x}{a} \cos n\frac{\pi z}{c} e^{i\omega t}, \\ v_3 &= \frac{E_1}{\mu H_0} = \frac{n}{c} g(y) \cos l\frac{\pi x}{a} \sin n\frac{\pi z}{c} e^{i\omega t}, \\ p &= \frac{i\pi}{\omega}\rho_0 a_0^2\left(\frac{l^2}{a^2}+\frac{n^2}{c^2}\right)[f'(y)+g(y)] \cos l\frac{\pi x}{a} \cos n\frac{\pi z}{c} e^{i\omega t}, \end{aligned}\right\} \tag{16}$$

where
$$a_0^2 f'' + \omega^2 f + a_0^2 g' = 0,$$
$$\pi^2 \left(\frac{l^2}{a^2} + \frac{n^2}{c^2}\right) a_0^2 f' - A_0^2 g'' + \left[\pi^2 \left(\frac{l^2}{a^2} + \frac{n^2}{c^2}\right)(a_0^2 + A_0^2) - \omega^2\right] g = 0, \Bigg\} \tag{17}$$

and
$$f(0) = f(b) = g(0) = g(b) = 0, \tag{17'}$$

by virtue of the boundary conditions (13) on v_2 and H_2; also $E_2 \equiv 0$. Here l and n are non-negative integers and the $\sin l\pi x/a$, $\sin n\pi z/c$ in v_1, v_3 follow from the boundary conditions, while this time we have to take $\theta = \operatorname{curl}_2 \mathbf{H} = \operatorname{curl}_2 \mathbf{v} = 0$. Note that $\mathbf{H}$ and p are 90° out of phase with $\mathbf{v}$.

On setting f and g proportional to e^{iky} in (17), we find that (ii), with $\eta = 0$, $\kappa^2 = k^2 + \pi^2 \left(\frac{l^2}{a^2} + \frac{n^2}{c^2}\right)$, and $\kappa^2 \cos^2 \phi = k^2$, must be satisfied. For each ω (to be determined), l, n, there are four possible k's, say $\pm k^{(1)}$, $\pm k^{(2)}$, given by the roots of

$$k^4 + \left[\pi^2 \left(\frac{l^2}{a^2} + \frac{n^2}{c^2}\right) - \left(\frac{1}{a_0^2} + \frac{1}{A_0^2}\right) \omega^2\right] k^2 + \omega^2 \left[\frac{\omega^2}{a_0^2 A_0^2} - \left(\frac{1}{a_0^2} + \frac{1}{A_0^2}\right) \pi^2 \left(\frac{l^2}{a^2} + \frac{n^2}{c^2}\right)\right] = 0. \tag{18}$$

In order to satisfy the boundary conditions (17') with a linear combination of the four pairs of corresponding functions these roots $k^{(1)}$, $k^{(2)}$ must either satisfy

$$\frac{\tan \frac{1}{2} k^{(1)} b}{\tan \frac{1}{2} k^{(2)} b} = \frac{k^{(2)}(a_0^2 k^{(1)2} - \omega^2)}{k^{(1)}(a_0^2 k^{(2)2} - \omega^2)}, \tag{19}$$

in which case (except for an arbitrary constant factor)

$$\left.\begin{aligned} f &= \sin \tfrac{1}{2} k^{(2)} b \sin k^{(1)}(\tfrac{1}{2} b - y) - \sin \tfrac{1}{2} k^{(1)} b \sin k^{(2)}(\tfrac{1}{2} b - y), \\ g &= \frac{a_0^2 k^{(1)2} - \omega^2}{a_0^2 k^{(1)}} \sin \tfrac{1}{2} k^{(2)} b \cos k^{(1)}(\tfrac{1}{2} b - y) - \frac{a_0^2 k^{(2)2} - \omega^2}{a_0^2 k^{(2)}} \sin \tfrac{1}{2} k^{(1)} b \cos k^{(2)}(\tfrac{1}{2} b - y), \end{aligned}\right\} \tag{19'}$$

or else
$$\frac{\tan \frac{1}{2} k^{(1)} b}{\tan \frac{1}{2} k^{(2)} b} = \frac{k^{(1)}(a_0^2 k^{(2)2} - \omega^2)}{k^{(2)}(a_0^2 k^{(1)2} - \omega^2)}, \tag{20}$$

when

$$\left.\begin{aligned} f &= \cos \tfrac{1}{2} k^{(2)} b \cos k^{(1)}(\tfrac{1}{2} b - y) - \cos \tfrac{1}{2} k^{(1)} b \cos k^{(2)}(\tfrac{1}{2} b - y), \\ g &= -\frac{a_0^2 k^{(1)2} - \omega^2}{a_0^2 k^{(1)}} \cos \tfrac{1}{2} k^{(2)} b \sin k^{(1)}(\tfrac{1}{2} b - y) + \frac{a_0^2 k^{(2)2} - \omega^2}{a_0^2 k^{(2)}} \cos \tfrac{1}{2} k^{(1)} b \sin k^{(2)}(\tfrac{1}{2} b - y). \end{aligned}\right\} \tag{20'}$$

Each of the solutions given above involves surface currents, given by the tangential component of $\mathbf{H}$ rotated in the face through 90°, and surface charges, measured by the value of the normal component of $\mathbf{E}$.

7. Distribution of frequencies

The values of ω for the standing waves (14) are given explicitly by (15); they do not depend on a_0, nor on the form of F. On the other hand, the two sets of values of ω for the waves (16) are determined implicitly by (19) and (20), and depend on l, n, a_0, A_0; we shall now determine the nature of these last distributions for the two extreme cases of very weak and very strong magnetic fields $\mathbf{H}_0$.

When $l = n = 0$ equation (18) gives $k^{(1)} = \omega/a_0$, $k^{(2)} = \omega/A_0$ and then (19) and (20) together yield

$$\tan \tfrac{1}{2}k^{(1)}b = 0, \infty; \quad \omega = \frac{m\pi}{b}a_0, \tag{21a}$$

$$\tan \tfrac{1}{2}k^{(2)}b = \infty, 0; \quad \omega = \frac{m\pi}{b}A_0, \tag{21b}$$

where m is a non-negative integer. With these in mind we consider in turn:

(*a*) $A_0 \ll a_0$. For the frequencies with $\omega b/a_0$ of order A_0/a_0 we find from (18)

$$k^{(2)} = \frac{\omega}{A_0}, \quad k^{(1)} = i\pi\sqrt{\left(\frac{l^2}{a^2}+\frac{n^2}{c^2}\right)} = \frac{iK}{b} \quad \text{(say)},$$

correct to $O(A_0/a_0)$. Thus when l and n are not both zero, equations (19) and (20) reduce to

$$\omega = \frac{A_0}{b}\tilde{\omega}, \quad \tilde{\omega}\begin{matrix}\cot\\ \tan\end{matrix}\tfrac{1}{2}\tilde{\omega} = \pm K\begin{matrix}\coth\\ \tanh\end{matrix}\tfrac{1}{2}K. \tag{22}$$

Graphs of $\tilde{\omega}\cot\frac{1}{2}\tilde{\omega}$ and $\tilde{\omega}\tan\frac{1}{2}\tilde{\omega}$ show that for each l, n there is alternately a root of one of this last pair of equations in every interval $(\pi, 2\pi)$, $(2\pi, 3\pi)$, ..., and that in each interval the roots converge monotonically towards the left end-point as K increases. The large roots must be excluded in forming the corresponding ω's and to the latter we must add (21*b*) which correspond to $l = n = 0$.

On the other hand, when $\omega b/a_0 = O(1)$ we have

$$k^{(1)} = \frac{\omega}{A_0}, \quad k^{(2)} = \sqrt{\left[\frac{\omega^2}{a_0^2} - \pi^2\left(\frac{l^2}{a^2}+\frac{n^2}{c^2}\right)\right]}, \tag{23}$$

correct to $O(1)$. The right-hand side of (19) is now $O(a_0/A_0)$ and may be taken infinite; similarly, the right-hand side of (20) is effectively zero. Thus either

$$\tan \tfrac{1}{2}k^{(1)}b = \infty, 0; \quad \omega = \frac{m\pi}{b}A_0 \quad \text{for all } l, n, \tag{24}$$

or else

$$\tan \tfrac{1}{2}k^{(2)}b = 0, \infty; \quad \frac{\omega^2}{a_0^2} = \pi^2\left(\frac{l^2}{a^2}+\frac{m^2}{b^2}+\frac{n^2}{c^2}\right). \tag{25}$$

The frequencies (24) apply when m is $O(a_0/A_0)$ (according to our assumption) and give the continuation of (22). The second set (25) is the same as for ordinary acoustic waves in the region.

(*b*) $A_0 \gg a_0$. If $\omega b/a_0$ is $O(1)$ compared with a_0/A_0, we have

$$k^{(1)} = \frac{\omega}{a_0}, \quad k^{(2)} = i\pi\sqrt{\left(\frac{l^2}{a^2}+\frac{n^2}{c^2}\right)},$$

correct to $O(a_0/A_0)$. Now (19) and (20) become $\tan\frac{1}{2}k^{(1)}b = 0$ and $\tan\frac{1}{2}k^{(1)}b = \infty$, respectively, and so

$$\omega = \frac{m\pi}{b}a_0, \quad \text{for all } l, n. \tag{26}$$

However, when $\omega b/a_0 = O(A_0/a_0)$ the wave numbers are

$$k^{(1)} = \frac{\omega}{a_0}, \quad k^{(2)} = \sqrt{\left[\frac{\omega^2}{A_0^2} - \pi^2\left(\frac{l^2}{a^2}+\frac{n^2}{c^2}\right)\right]},$$

correct to $O(1)$. As before, but this time to a higher degree of accuracy, we may take

$$\tan \tfrac{1}{2}k^{(1)}b = 0, \infty; \quad \omega = \frac{m\pi}{b}a_0 \quad \text{for all } l, n, \tag{27}$$

$$\tan \tfrac{1}{2}k^{(2)}b = \infty, 0; \quad \frac{\omega^2}{A_0^2} = \pi^2\left(\frac{l^2}{a^2}+\frac{m^2}{b^2}+\frac{n^2}{c^2}\right). \tag{28}$$

In the first of these m must, for consistency, be large, and we obtain the continuation of (26).

The most important point to notice is that a_0 and A_0 have now changed roles [compare the remarks concerning (6) and (7)].

8. Limiting forms of the waves

It is of some interest to sketch the forms of the standing waves for the two extreme cases (a) and (b) discussed in the last section.

(a) $A_0 \ll a_0$. The waves (14) give no trouble. From (15) we find $\omega \to 0$ as $A_0 \to 0$ for every m, so that the pairs H_1, H_3 and v_1, v_3 become independent of t (we factor out H_0 to avoid all except E_1 and E_3 becoming zero) and of each other. This is in agreement with the integrals: curl $\mathbf{v}$ = const. (in time) and $\mathbf{H}$ = const. (in time) of equations (3) for $\sigma = \infty$ and $H_0 = 0$. However, we note that in the limit v_1 and v_3 still vanish† on $y = 0, b$ whereas no such boundary conditions are required for $H_0 = 0$ (ordinary acoustic equations govern $\mathbf{v}$). The corresponding vortex sheet which clings to a y-face when $H_0 = 0$ propagates as a transverse wave discontinuity [in the sense of Friedrichs (1957)] with velocity $\pm A_0$ along the y-direction when $H_0 \neq 0$, and suffers successive reflexions at $y = 0, b$. This follows immediately from the fact that $\text{curl}_2\,\mathbf{v}$ satisfies (11), which for $\eta = 0$ is the one-dimensional wave equation.

A similar thing happens in the limit, for the frequencies of order A_0, with the waves (16). The triples H_1, H_2, H_3 and v_1, v_2, v_3 become independent of t and of each other, while E_1, E_3 and p tend to zero, the last ($p \to 0$) following from the fact that $f' + g$ tends to zero like A_0^2 [see the first of equations (17)]. Again the vanishing of v_1 and v_3 on the y-faces occurs and is reconciled with ordinary acoustics in a similar way.

More care is required with the frequencies which are of order unity. According to (23) these involve values of $k^{(1)}$ which tend to infinity like $1/A_0$, so that f and g become indeterminate. The difficulty is due to the order of the limits: $\eta \to 0$, $H_0 \to 0$ and is resolved by interchanging them. Thus for small $\eta \neq 0$ and $A_0 \to 0$, the dispersion relation (8) with $\kappa^2 = \pi^2(l^2/a^2 + n^2/c^2) + k^2$ and $\kappa^2 \cos^2\phi = k^2$ yields

$$k^{(1)} = \sqrt{\frac{\omega}{2\eta}}(1-i), \quad k^{(2)} = \sqrt{\left[\frac{\omega^2}{a_0^2} - \pi^2\left(\frac{l^2}{a^2}+\frac{n^2}{c^2}\right)\right]}$$

in place of (23). With these, the frequencies in (24) are replaced by

$$\omega = i\frac{m^2\pi^2}{b^2}\eta. \tag{29}$$

† From (12) and the fact that the tangential component of $\mathbf{E}$ must be zero, we see that $\mathbf{v}$ vanishes at any perfectly conducting rigid wall not parallel to $\mathbf{H}_0$.

while (25) are effectively unaltered. The values of ω given by (29) decrease with η and can be expected to tend to zero, so as to give the same results as in the last paragraph. For the remaining values of ω the forms (19′) and (20′) are still correct in the limit $\eta \to 0$, and on dividing through by the exponentially large $\sin k^{(1)}b$, and $\cos k^{(1)}b$, respectively, we find the limiting forms

$$f = -\sin k^{(2)}(\tfrac{1}{2}b - y), \quad -\cos k^{(2)}(\tfrac{1}{2}b - y),$$

$$g = \frac{\pi^2(l^2/a^2 + n^2/c^2)}{k^{(2)}} \cos k^{(2)}(\tfrac{1}{2}b - y), \quad \frac{\pi^2(l^2/a^2 + n^2/c^2)}{k^{(2)}} \sin k^{(2)}(\tfrac{1}{2}b - y),$$

except for $y = 0, b$. Then L_1, E_3, H_1, H_2, H_3 vanish in (16) and v_1, v_2, v_3, p are related in the same way as for acoustic waves ($\sin k^{(2)}b$ and $\cos k^{(2)}b$ are respectively zero). Again the limit forms of v_1 and v_3 do not vanish as the y-faces are approached.

(*b*) $A_0 \gg a_0$. The situation here is more straightforward. In (14) the components E_1, E_3 dominate for large H_0, and a high-frequency electric wave results. Similarly, for the frequencies (26), g is $O(a_0/A_0)$ and $f = O(1)$ so that in (16) v_1 and v_3 may be ignored in comparison with the others. For the higher frequencies (27) the component H_2 may be dropped as well. In either case the result is a wave for which the fluid essentially oscillates in the direction of the undisturbed magnetic field. Finally, the frequencies (28) lead to functions f and g which are both $O(1)$. Again the components E_1 and E_3 predominate so that a high frequency electric wave results.

In particular we note that the pressure fluctuations are still carried by the waves with velocity a_0.

9. Orthogonality and the three types of wave

We conclude with a few remarks concerning the solution of the general initial-value problem for the present case.

It follows from the work of Bernstein, Frieman, Kruskal & Kulsrud (1958) that velocity vectors $\mathbf{v}^{(1)}$, $\mathbf{v}^{(2)}$ of standing waves with different frequencies are orthogonal,† i.e.

$$\int_0^a \int_0^b \int_0^c [v_1^{(1)} v_1^{(2)} + v_2^{(1)} v_2^{(2)} + v_3^{(1)} v_3^{(2)}]\, dx\, dy\, dz = 0. \tag{30}$$

Thus, assuming that we are dealing with a complete set of functions, we can in principle solve any initial-value problem by expanding the (assumed) given values of $\mathbf{v}$ and $\partial\mathbf{v}/\partial t$ at $t = 0$ in (vector) Fourier series, making use of this set. Note that the initial value of $\partial\mathbf{v}/\partial t$ follows from (3*c*) when H_1, H_2, H_3 are specified (consistently) together with p.

Such an expansion can be broken down into three separate ones, each of which has a different interpretation. From the initial values we first form $\mathrm{curl}_2 \mathbf{H}$ and $\mathrm{curl}_2 \mathbf{v}$ and expand them in half-range $(0, b)$ cosine and sine series, respectively, in y. The pairs of coefficients (functions of x, z) then determine separately the pairs of arbitrary functions F in the general standing waves formed from (14): each F is determined by a two-dimensional Poisson equation and zero boundary values on $x = 0, a$ and $z = 0, c$. In this way we find the contribution to the complete solution arising from the frequencies (15).

Next we note that the functions f and g in (19′) are odd and even, respectively.

† This is approximate. In the exact relation the first and last terms in the integrand are multiplied by $(1 + A_0^2/c^2)$, where c has its original meaning.

about $y = \frac{1}{2}b$, that the reverse is true for the functions (20′), and that H_2, v_2, Δ, $\partial p/\partial y$ as given by (16) have factors g and f alternately (from the first of equations (17) the factor $f'' + g'$ in $\partial p/\partial y$ is a multiple of f). Moreover, H_2 is in phase (or 180° out of phase) with p and both are 90° out of phase with v_2 and Δ, so that initial values of H_2 and p correspond to one of the coefficients in the general standing wave formed from (16) and initial values of v_2 and Δ correspond to the other.

The procedure is now clear. We form v_2 and Δ from the given initial values and take their odd and even parts (about $y = \frac{1}{2}b$), respectively. The resulting functions are then expanded in half-range $(0, a; 0, c)$ cosine series in x and z, the coefficients being functions of y. Each pair of coefficients $v_2(y; l, n)$ and $\Delta(y; l, n)$ must now be expanded in series whose general terms are of the form $\alpha f(y)$, $\alpha g(y)$ with f and g given by (19′). The value of α is obtained by multiplying the first series by $\pi^2(l^2/a^2 + n^2/c^2)\,f(y)$ and the second by $g(y)$, adding, and integrating from 0 to b

$$\alpha = \frac{\int_0^b \left[\pi^2\left(\frac{l^2}{a^2}+\frac{n^2}{c^2}\right) v_2(y; l, n)\, f(y) + \Delta(y; l, n)\, g(y)\right] dy}{\int_0^b \left[\pi^2\left(\frac{l^2}{a^2}+\frac{n^2}{c^2}\right) f^2(y) + g^2(y)\right] dy}.$$

This follows from the orthogonality relation (30), which for velocity vectors corresponding to pairs of functions $f^{(1)}$, $g^{(1)}$ and $f^{(2)}$, $g^{(2)}$ with the same l, n reduces to†

$$\int_0^b \left[\pi^2\left(\frac{l^2}{a^2}+\frac{n^2}{c^2}\right) f^{(1)} f^{(2)} + g^{(1)} g^{(2)}\right] dy = 0.$$

The value of α determines one of the coefficients mentioned at the end of the last paragraph and the other follows from a similar analysis of the even part of H_2 and the odd part of $\partial p/\partial y$.

In this way we determine the contribution arising from the frequencies satisfying (19). The remaining part of the solution, corresponding to the frequencies satisfying (20), is obtained from the even parts of v_2, $\partial p/\partial y$ and the odd parts of H_2, Δ using now (20′) for f and g.

The author is indebted to S. Goldstein for suggesting this investigation and for valuable discussion at each stage of it. This research was supported in part by the U.S. Air Force under Contract AF 49 (638)–154 monitored by the Office of Scientific Research of A.R.D.C. Support from the Guggenheim Foundation is gratefully acknowledged.

REFERENCES

Baños, Jr., A. 1955 Magneto-hydrodynamic waves in incompressible and compressible fluids. *Proc. Roy. Soc.* A, **233**, 350–66.

Bernstein, I. B., Frieman, E. A., Kruskal, M. D. & Kulsrud, R. M. 1958 An energy principle for hydromagnetic stability problems. *Proc. Roy. Soc.* A, **244**, 17–40.

Friedrichs, K. O. 1957 Nonlinear wave motion in magneto-hydrodynamics. *Los Alamos Rep.* no. 2105.

van de Hulst, H. C. 1951 Interstellar polarization and magneto-hydrodynamic waves. *Problems of Cosmical Aerodynamics*, p. 45 (*Proc. Symposium Int. Union of Theor. and Appl. Mech., Paris* 1949). Dayton, Ohio: Central Air Documents Office.

Ludford, G. S. S. 1959 On initial conditions in hydromagnetics. *Proc. Camb. Phil. Soc.* **55**, 141.

† This relation is easily checked directly from the definitions of f and g.

Cellular convection with finite amplitude in a rotating fluid

By G. VERONIS

Woods Hole Oceanographic Institution, Woods Hole, Massachusetts

(Received 3 July 1958)

When a rotating layer of fluid is heated uniformly from below and cooled from above, the onset of instability is inhibited by the rotation. The first part of this paper treats the stability problem as it was considered by Chandrasekhar (1953), but with particular emphasis on the physical interpretation of the results. It is shown that the time-dependent (overstable) motions occur because they can reduce the stabilizing effect of rotation. It is also shown that the boundary of a steady convection cell is distorted by the rotation in such a way that the wavelength of the cell measured along the distorted boundary is equal to the wavelength of the non-rotating cell. This conservation of cellular wavelength is traced to the constancy of horizontal vorticity in the rotating and non-rotating systems. In the finite-amplitude investigation the analysis, which is pivoted about the linear stability problem, indicates that the fluid can become unstable to finite-amplitude disturbances before it becomes unstable to infinitesimal perturbations. The finite-amplitude motions generate a non-linear vorticity which tends to counteract the vorticity generated by the imposed constraint of rotation. Under experimental conditions the two fluids, mercury and air, which are considered in this paper, will not exhibit this finite amplitude instability. However, a fluid with a sufficiently small Prandtl number will become unstable to finite-amplitude perturbations. The special role of viscosity as an energy releasing mechanism in this problem and in the Orr-Sommerfeld problem suggests that the occurrence of a finite-amplitude instability depends on this dual role of viscosity (i.e. as an energy releasing mechanism as well as the more familiar dissipative mechanism). The relative stability criterion developed by Malkus & Veronis (1958) is used to determine the preferred type of cellular motions which can occur in the fluid. This preferred motion is a function of the Prandtl number and the Taylor number. In the case of air it is shown that overstable square cells become preferred in finite amplitude, even though steady convective motions occur at a lower Rayleigh number.

Introduction

The columnar structure in figure 1 represents the manner in which the boundary of a hexagonal convection cell in a fluid is distorted by an imposed uniform rotation of the entire system. The distortion plays an important role in the determination of the finite amplitude effects in the convecting fluid. We shall study this geometry of cellular convection as part of a more general investigation into the nature of cellular convection in a rotating fluid.

The constraint of rotation is, of course, only one of a large number of externally imposed constraints to which a fluid may be subjected. Yet a detailed knowledge of the constraining effect of rotation and of the finite-amplitude behaviour of the rotating fluid may provide an insight into the mechanism of a broad class of problems in which the system is constrained externally.

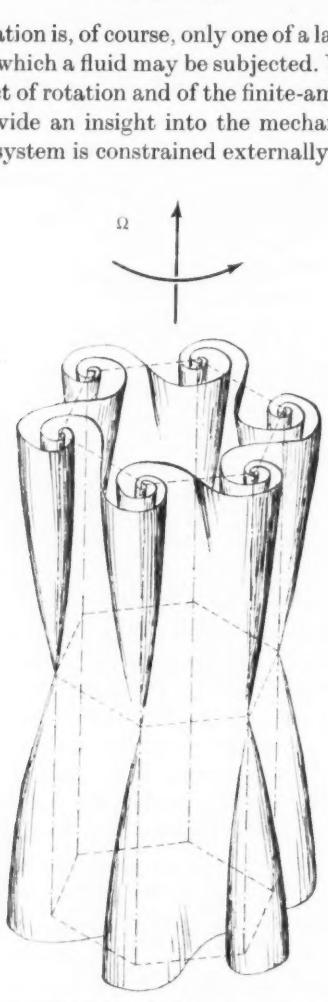

FIGURE 1. A perspective sketch of a hexagonal convection cell as it is distorted by an imposed rotation of the fluid.

As a starting-point for this discussion, we have available several previous studies. The stability problem has been investigated theoretically by Chandrasekhar (1953) and by Nakagawa & Frenzen (1955) (hereafter these papers will be referred to as II and III respectively), and experimentally by Nakagawa & Frenzen (1955) and by Fultz & Nakagawa (1955). Finite amplitude cellular convection in a non-rotating fluid has been considered by Malkus & Veronis (1958) (hereafter referred to as I). The questions which we may hope to answer in this paper may be posed more clearly in the light of these investigations.

When a horizontally infinite layer of fluid is heated uniformly from below and cooled from above, the system is stable to infinitesimal disturbances for values of

the Rayleigh number λ below a critical value λ_0. Here, $\lambda = \alpha g \beta_m d^4/\kappa\nu$, where g is the gravitational acceleration; α, ν and κ are respectively the coefficients of expansion, kinematic viscosity and thermometric diffusivity of the fluid; d is the depth of the fluid; and $\beta_m = (T_H - T_C)/d$, where T_H and T_C are respectively the temperatures at the bottom and top surfaces of the layer. When $\lambda \geqslant \lambda_0$, the fluid is unstable and convective motions occur leading to a distortion of the mean (horizontally averaged) temperature field. Experimentally, convection is observed to set in as a fairly regular cellular pattern in the horizontal.

The specific value of λ_0 depends on the boundary conditions. In the non-rotating system, λ_0 is constant for a particular set of boundary conditions. In the rotating fluid, the specific value of the critical Rayleigh number depends on the value of the Taylor number $\mathscr{T}^2 = 4\Omega^2 d^4/\nu^2$ (where Ω is the uniform angular velocity of the system) and on the value of the Prandtl number $\sigma\,(\equiv \nu/\kappa)$. The general effect of the rotation is to increase λ_0 and to decrease the horizontal scale of the cells. For large, but experimentally realizable, values of $\mathscr{T}^2$, the value of λ_0 may be as high as 10^5 times the critical Rayleigh number corresponding to the non-rotating system. It has been noted both experimentally and theoretically (cf. II and III) that for a range of values of the parameters σ and $\mathscr{T}^2$, instability can arise as a time-periodic motion. In the greater part of the range, this so-called 'overstability' occurs before steady convective instability.

A number of interesting questions arise from the study of the stability problem. Although the horizontal scale of the cells diminishes with rotation, what similarities exist between the motions of the constrained and unconstrained systems? What physical mechanism causes overstability to occur and to be preferred to steady convective instability? Is it possible that the initial instability occurs as convection, but that overstability can enter and become the preferred state of motion in finite amplitude? Is the reverse possible?

As we have noted, the constraining effect of rotation manifests itself principally by making the system more stable, i.e. by increasing the value of λ_0. That the rotating system will behave differently from the non-rotating fluid in finite amplitude is indicated by the fact that viscosity plays a dual role here. In addition to its more familiar role of dissipating the kinetic energy of the fluid, the viscosity serves also as the energy releasing mechanism. The fluid particles are constrained by the rotation to move in the direction of the rotation vector $\boldsymbol{\Omega}$. Only through the presence of viscosity do they find a means for achieving cross-isobar flow through which potential energy is released. This dual role of viscosity as a function of rotation is no more evident than it is in the fact that (cf. II) for sufficiently high rotation rates, a fluid confined by rigid boundaries becomes unstable for a value of λ_0 lower than the λ_0 corresponding to a fluid confined by free boundaries where viscous effects are smaller. In the non-rotating case, the free boundary conditions have always led to lower λ_0.

As a further guide to the finite amplitude study we turn to the analysis of finite amplitude convection in the non-rotating system (I).

After the fluid has become unstable, the convective motions lead to a distortion of the mean temperature profile. When the Prandtl number is large, the amount of heat which is transported vertically by convection is determined principally by

this distortion of the mean temperature field. For $\sigma < 1$, the self-distortion of the cellular structure plays an important role in the determination of the vertical heat transport. Since the constraint of rotation adds to the distortion of the cellular structure, we can anticipate that in the present study the self-distortion of the cell will be more important in determining the heat transport.

All close-packed cellular patterns (rectangles, hexagons, triangles and two-dimensional rolls) are mathematically possible in finite amplitude. A relative stability criterion was developed in I to determine which of the many possible steady solutions will actually be realized. When the system has vertical symmetry and free boundaries, square cells are the preferred pattern for $\sigma > 0{\cdot}8$, and limiting rectangles (one side becomes infinitely long) for $\sigma \leqslant 0{\cdot}8$. When a vertical asymmetry is present (e.g. free upper boundary, rigid lower boundary), hexagonal cells are preferred when λ exceeds λ_0 by a small amount.

The qualitative results relating to symmetrical and asymmetrical systems ought not to be altered by the presence of rotation. However, is the preferred cellular pattern for a symmetric system a function of the rotation rate? What effect has overstability on the geometrical pattern of the flow?

More general questions are the following. What is the mechanism through which the constraint manifests itself in the flow? Does the fluid organize itself so as to minimize the effects of the externally imposed constraint? Indeed, is it possible for the fluid to generate its own 'constraint' to offset the imposed one?

1. Equations and boundary conditions

This problem is one of a large class of convection problems in which the Boussinesq (1903) approximation may be applied. The density is considered to be constant everywhere in the equations except in the buoyant force term. The equations for the local conservation of heat, momentum and mass are then

$$\frac{\partial \bar{T}}{\partial t} - \kappa \nabla^2 \bar{T} = -\mathbf{v} \cdot \nabla \bar{T}, \tag{1.1}$$

$$\frac{\partial \mathbf{v}}{\partial t} + \mathbf{v} \cdot \nabla \mathbf{v} + 2\Omega \mathbf{k} \times \mathbf{v} = -\frac{1}{\rho_m} \nabla p + \gamma \bar{T} \mathbf{k} + \nu \nabla^2 \mathbf{v}, \tag{1.2}$$

$$\nabla \cdot \mathbf{v} = 0, \tag{1.3}$$

where the equation of state

$$\rho = \rho_m (1 - \alpha \bar{T}) \tag{1.4}$$

has been used in the buoyancy term. In these equations $\bar{T}$ is the deviation of the temperature from its mean value, ρ_m is the mean density of fluid, $\mathbf{v}$ is the three-dimensional velocity field (u, v, w) in the directions (x, y, z) respectively, t is the time, $\mathbf{k}$ is the unit vector in the vertical (z) direction, ∇^2 is the three-dimensional Laplacean operator, $p = \tilde{p} - gz$, where $\tilde{p}$ is the pressure, $\gamma = \alpha g$, and the remaining terms have been defined in the introduction.

We consider an ensemble of systems with the given fixed boundary conditions. These systems will have arbitrary phases in time and horizontal space. An ensemble average denotes an average over these arbitrary phases, and, consequently, $\bar{T}$ can be subdivided into a portion which is a function only of the vertical co-ordinate and a fluctuation which is a function of x, y, z and t.

Let
$$\tilde{T} = T(z) + T(x, y, z, t), \tag{1.5}$$
where $T(z)$ denotes the ensemble-average temperature. Thus, letting a bar over a quantity denote the ensemble-average, we have
$$\overline{\tilde{T}} = T(z), \quad \overline{T(x, y, z, t)} = 0.$$
The substitution of (1.5) into (1.1) yields
$$\frac{\partial T}{\partial t} - \kappa \frac{\partial^2 T(z)}{\partial z^2} - \kappa \nabla^2 T = \beta w - \mathbf{v} \cdot \nabla T, \tag{1.6}$$
where $\beta = -\partial T(z)/\partial z$ is the negative vertical gradient of mean temperature. By taking an ensemble-average of (1.6), one gets
$$-\kappa \frac{\partial^2 T(z)}{\partial z^2} = -\frac{\partial}{\partial z}(\overline{wT}), \tag{1.7}$$
which can be integrated once to yield
$$\kappa\beta + \overline{wT} = H, \tag{1.8}$$
where H is the vertical heat flux in the fluid and is constant for an ensemble of systems with given fixed boundary conditions. Thus, taking a vertical average $\left(= \frac{1}{d}\int_0^d H\,dz\right)$ yields
$$\kappa\beta_m + \{wT\}_m = H, \tag{1.9}$$
where $\{\}_m$ denotes both an ensemble and a vertical average.

From (1.8) and (1.9), we have
$$\frac{\beta}{\beta_m} = 1 + \frac{\{wT\}_m - \overline{wT}}{\kappa\beta_m}. \tag{1.10}$$
Equation (1.10) provides a means for determining the distortion of the mean temperature field from the values of the fluctuation quantities w and T.

Substituting (1.7) into (1.6) and making use of (1.10), we have
$$\frac{\partial T}{\partial t} - \kappa \nabla^2 T - \beta_m w = \frac{\{wT\}_m - \overline{wT}}{\kappa} - h, \tag{1.11}$$
where $h = \mathbf{v} \cdot \nabla T - \partial(\overline{wT})/\partial z$ represents the zero-average heat advection terms.

The pressure p (relative to hydrostatic pressure) can be eliminated from (1.2) to yield
$$\frac{\partial}{\partial t}\nabla^2 w + 2\Omega \frac{\partial \zeta}{\partial z} - \gamma \nabla_1^2 T = \nu \nabla^4 w + L, \tag{1.12}$$
where $$L = \frac{\partial}{\partial z}\left[\frac{\partial}{\partial x}(\mathbf{v} \cdot \nabla u) + \frac{\partial}{\partial y}(\mathbf{v} \cdot \nabla v)\right] - \nabla_1^2(\mathbf{v} \cdot \nabla w), \quad \nabla_1^2 = \frac{\partial^2}{\partial x^2} + \frac{\partial^2}{\partial y^2},$$
and $\zeta = \partial v/\partial x - \partial u/\partial y$ is the vertical component of vorticity. From the first two equations of (1.2), an additional relation between ζ and w can be derived:
$$\frac{\partial \zeta}{\partial t} - \nu \nabla^2 \zeta - 2\Omega \frac{\partial w}{\partial z} = -Z, \tag{1.13}$$
where $Z = \frac{\partial}{\partial x}(\mathbf{v} \cdot \nabla v) - \frac{\partial}{\partial y}(\mathbf{v} \cdot \nabla u)$. The terms L and Z appearing in (1.12) and (1.13) are both zero-average non-linear terms.

Because the subsequent analysis will be based on an expansion of each of the variables, it is convenient to work with the equations in dimensionless form. Thus, letting $\mathbf{v} = \nu\mathbf{v}'/d$, $\mathbf{r} = d\mathbf{r}'$, $\nabla = d^{-1}\nabla'$, $T = \kappa\nu T'/\gamma d^3$, $t = d^2\tau/\kappa$, $\sigma = \nu/\kappa$, one has

$$\left(\frac{\partial}{\partial\tau} - \nabla^2\right) T - \sigma\lambda w = \sigma^2[\{wT\}_m - \overline{wT}]\, w - \sigma h, \tag{1.11 bis}$$

$$\left(\frac{1}{\sigma}\frac{\partial}{\partial\tau} - \nabla^2\right)\nabla^2 w + \mathscr{T}\frac{\partial\zeta}{\partial z} - \frac{1}{\sigma}\nabla_1^2 T = L, \tag{1.12 bis}$$

$$\left(\frac{1}{\sigma}\frac{\partial}{\partial\tau} - \nabla^2\right)\zeta - \mathscr{T}\frac{\partial w}{\partial z} = -Z, \tag{1.13 bis}$$

where the primes have been dropped from the variables. *Throughout the remainder of the work, unprimed quantities will denote dimensionless variables unless otherwise noted.* In these equations $\mathscr{T} = 2\Omega d^2/\nu$ is the square root of the Taylor number.

The analysis will be pivoted about the linear stability solution and it is therefore convenient to eliminate all but one of the variables in the linear operators. Elimination of T and ζ from the left-hand sides of (1.11), (1.12) and (1.13) gives

$$\left(\frac{1}{\sigma}\frac{\partial}{\partial\tau} - \nabla^2\right)^2\left(\frac{\partial}{\partial\tau} - \nabla^2\right)\nabla^2 w + \mathscr{T}^2\left(\frac{\partial}{\partial\tau} - \nabla^2\right)\frac{\partial^2 w}{\partial z^2} - \left(\frac{1}{\sigma}\frac{\partial}{\partial\tau} - \nabla^2\right)\lambda\nabla_1^2 w$$
$$= \sigma\left(\frac{1}{\sigma}\frac{\partial}{\partial\tau} - \nabla^2\right)[\{wT\}_m - \overline{wT}]\,\nabla_1^2 w$$
$$+ \mathscr{T}\left(\frac{\partial}{\partial\tau} - \nabla^2\right)\frac{\partial Z}{\partial z} - \left(\frac{1}{\sigma}\frac{\partial}{\partial\tau} - \nabla^2\right)\nabla_1^2 h + \left(\frac{\partial}{\partial\tau} - \nabla^2\right)\left(\frac{1}{\sigma}\frac{\partial}{\partial\tau} - \nabla^2\right) L. \tag{1.14}$$

Equations (1.3), (1.11), (1.13) and (1.14) are the basic equations of our analysis. A perturbation method similar to that employed in I is used to derive approximate solutions.

Let

$$\left.\begin{aligned} w &= \epsilon w_0 + \epsilon^2 w_1 + \epsilon^3 w_2 + \epsilon^4 w_3 + \ldots, \\ T &= \epsilon T_0 + \epsilon^2 T_1 + \epsilon^3 T_2 + \epsilon^4 T_3 + \ldots, \\ u &= \epsilon u_0 + \epsilon^2 u_1 + \epsilon^3 u_2 + \epsilon^4 u_3 + \ldots, \\ v &= \epsilon v_0 + \epsilon^2 v_1 + \epsilon^3 v_2 + \epsilon^4 v_3 + \ldots. \end{aligned}\right\} \tag{1.15}$$

The parameter ϵ must be identified with the amplitude. Since the value of λ determines the amplitude, a relation between λ and ϵ must also be deduced. As in I, λ is also expanded in terms of ϵ: thus

$$\lambda = \lambda_0 + \epsilon\lambda_1 + \epsilon^2\lambda_2 + \epsilon^3\lambda_3 + \epsilon^4\lambda_4 + \ldots, \tag{1.16}$$

where the λ_i are to be determined.

If the expansions (1.15) and (1.16) are introduced into equations (1.3), (1.11), (1.13) and (1.14), and if the coefficients of each order of ϵ are equated, a series of equations is derived involving the variables w_i, T_i, u_i and v_i. We shall postpone writing the resulting relations explicitly until we come to the specific sections on finite-amplitude steady convection and finite-amplitude overstability.

An additional equation, which we shall find useful, results from multiplying (1.2) by $\mathbf{v}$ and averaging. This yields in non-dimensional form

$$\sigma\{\mathbf{v}.\nabla^2\mathbf{v}\}_m + \{wT\}_m = \frac{\partial}{\partial\tau}\{\tfrac{1}{2}\mathbf{v}.\mathbf{v}\}_m. \tag{1.17}$$

Equation (1.17) asserts that the rate of change of kinetic energy is equal to the rate of release of potential energy minus the rate of viscous dissipation of kinetic energy (the first term on the left is negative definite). In our problems the right-hand side will vanish.

Boundary conditions

If the boundary at the top or the bottom surface is considered 'free', the conditions on the velocities are

$$w = 0, \quad \frac{\partial v}{\partial z} = \frac{\partial u}{\partial z} = \frac{\partial^2 w}{\partial z^2} = 0 \tag{1.18}$$

at the boundary. At rigid boundaries, the conditions are

$$w = 0, \quad u = v = \frac{\partial w}{\partial z} = 0. \tag{1.19}$$

In the present investigation both boundaries are considered 'free'. Although this is an idealization, nevertheless it permits one to determine most of the qualitative features of the flow. The rigid boundary conditions lead to such a formidable computational problem (cf. I) that the present method of solution is practically useless.

Thermally, the boundaries are considered perfect conductors. For air or water, most metal boundaries will by comparison be nearly perfect conductors. For a fluid such as mercury, silver or copper boundaries approximate the ideal boundary material. Hence, at the bounding surfaces, we take

$$T = 0. \tag{1.20}$$

If we evaluate the basic equations (1.11) and (1.12) at a free boundary where $T = 0$, then (1.12) becomes

$$\frac{\partial^4 w}{\partial z^4} = 0. \tag{1.21}$$

2. Stability problem

The equations for the stability problem can be determined either by substituting the expansions (1.15) and (1.16) in equations (1.3), (1.11), (1.13) and (1.14), and then taking only the first-order terms in ϵ, or alternatively by simply neglecting all the non-linear terms in the equations. In either case, the equations are

$$\left(\frac{\partial}{\partial \tau} - \nabla^2\right) T_0 - \sigma \lambda_0 w_0 = 0, \tag{2.1a}$$

$$\left(\frac{1}{\sigma}\frac{\partial}{\partial \tau} - \nabla^2\right) \zeta_0 - \mathscr{T}^{\frac{1}{2}} \frac{\partial w_0}{\partial z} = 0, \tag{2.1b}$$

$$\left(\frac{1}{\sigma}\frac{\partial}{\partial \tau} - \nabla^2\right)^2 \left(\frac{\partial}{\partial \tau} - \nabla^2\right) \nabla^2 w_0 + \mathscr{T}^{\frac{1}{2}} \left(\frac{\partial}{\partial \tau} - \nabla^2\right) \frac{\partial^2 w_0}{\partial z^2} - \left(\frac{1}{\sigma}\frac{\partial}{\partial \tau} - \nabla^2\right) \lambda_0 \nabla_1^2 w_0 = 0, \tag{2.1c}$$

$$\frac{\partial u_0}{\partial x} + \frac{\partial v_0}{\partial y} + \frac{\partial w_0}{\partial z} = 0, \tag{2.1d}$$

where the subscript zero has been included in order to identify the variables with the stability problem.

Experimentally, convection is seen to occur as a close-packed cellular regime. This indicates that a useful analytical approach to the stability problem is to assume separability of horizontal and vertical dependence and to assume a periodic horizontal structure. These two simplifications are written as

$$w_0 = e^{p_0\tau} f(x,y)\, g(z), \quad \nabla_1^2 f(x,y) = -\alpha^2 \pi^2 f(x,y), \tag{2.2}$$

where α is the effective horizontal wave number and the time dependence is chosen as $e^{p_0\tau}$ as is customary in linear stability theory.

The stability problem can now be solved immediately (cf. II) since the free boundary conditions on w_0 are satisfied by $g(z) = \sin n\pi z$. If

$$w_0 = e^{p_0\tau} f(x,y) \sin n\pi z \tag{2.3}$$

is substituted into (2.1*c*), it is found that

$$(\alpha^2+n^2)[p_0+\pi^2(\alpha^2+n^2)][p_0/\sigma+\pi^2(\alpha^2+n^2)]^2+\mathscr{T}^2 n^2[p_0+\pi^2(\alpha^2+n^2)] - \alpha^2\lambda_0[p_0/\sigma+\pi^2(\alpha^2+n^2)] = 0,$$

hence, on rearrangement,

$$p_0^3+(2\sigma+1)\pi^2(\alpha^2+n^2)\,p_0^2+[\pi^4(\alpha^2+n^2)^2(\sigma^2+2\sigma)+(\mathscr{T}^2 n^2\sigma-\alpha^2\lambda_0)\sigma/(\alpha^2+n^2)]p_0 + \sigma^2\pi^6(\alpha^2+n^2)^3+\sigma^2\pi^2(\mathscr{T}^2 n^2-\alpha^2\lambda_0) = 0. \tag{2.4}$$

A. *Steady convective instability*

If p_0 is real, marginal instability occurs when $p_0 = 0$, i.e. when

$$\frac{\lambda_0}{\pi^4} = \frac{(\alpha^2+n^2)^3+\mathscr{T}_1^2 n^2}{\alpha^2}, \tag{2.5}$$

where $\mathscr{T}_1^2 = \mathscr{T}^2/\pi^4$. From

$$\frac{\partial\lambda_0}{\partial\alpha^2} = 2\alpha^6+3\alpha^4 n^2-n^6-\mathscr{T}_1^2 n^2 = 0, \tag{2.6}$$

we can find that value of α^2, as a function of $\mathscr{T}_1^2$ and n^2, which minimizes λ_0/π^4.

We note immediately from (2.6) and (2.5) that $\lambda_0/\pi^4 \to 3(\frac{1}{2}\mathscr{T}_1^2 n^2)^{\frac{2}{3}}$ and $\alpha^2 \to (\frac{1}{2}\mathscr{T}_1^2 n^2)^{\frac{1}{3}}$ as $\mathscr{T}_1^2 \to \infty$. Thus, as the Taylor number increases, λ_0 increases and the cellular diameter decreases. It is evident also that λ_0/π^4 attains its minimum value when $n = 1$ (neglecting the trivial case $n = 0$ when there is no motion). A curve of λ_0/π^4 *vs* $\mathscr{T}_1^2$ is plotted in figure 5.

Since $\mathscr{T}_1^2$ is inversely proportional to the square of the viscosity, the asymptotic expression, $\lambda_0/\pi^4 \to 3(\frac{1}{2}\mathscr{T}_1^2 n^2)^{\frac{2}{3}}$ asserts that both the critical Rayleigh number and the actual critical temperature difference $T_H - T_C$ decreases with increasing viscosity. This destabilizing effect of viscosity plays an important role in the finite-amplitude behaviour of the fluid, and we shall refer to it again later.

The motions associated with the point of instability depend on the particular cellular pattern which is postulated. These motions will be presented here in some detail because a knowledge of them provides some insight into the finite-amplitude behaviour of the fluid.

B. *Geometry of the fluid motion*

The possible horizontal patterns for close-packed cells are limited to two-dimensional rolls, hexagons, triangles and rectangles. Though the first of these cannot occur in an experimental investigation, it represents the simplest type of motion and will be discussed first.

Rolls. Let w_0 be independent of the y-co-ordinate. The solution (2.2) which satisfies the symmetry condition $\partial w_0/\partial x = 0$ at the walls of the cell is

$$w_0 = 2\cos\pi\alpha x \sin\pi z, \tag{2.7}$$

where, for reasons which will appear later, w_0 has been normalized, i.e. $\{w_0^2\}_m = 1$. (The normalization does not affect the present discussion.)

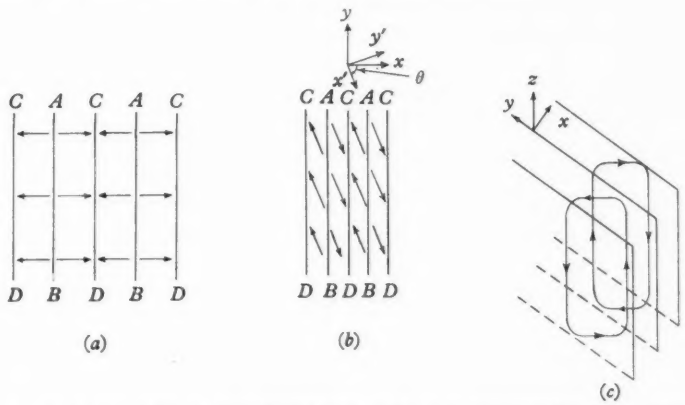

FIGURE 2. (*a*) A top view of two-dimensional rolls in a non-rotating fluid. The arrows indicate the direction of motion of the fluid. (*b*) The same in a system rotating counter-clockwise. (*c*) A perspective view of fluid particle motions in a role when the fluid is rotated.

From equations (2.1), the temperature T_0 and the velocity components u_0, v_0 are

$$T_0 = \frac{2\sigma\lambda_0}{\pi^2(\alpha^2+1)}\cos\pi\alpha x\sin\pi z, \quad u_0 = -\frac{2}{\alpha}\sin\pi\alpha x\cos\pi z,$$
$$v_0 = \frac{2\mathscr{T}_1}{\alpha(\alpha^2+1)}\sin\pi\alpha x\cos\pi z. \tag{2.8}$$

When $\mathscr{T}_1 = 0$, we have $v_0 = 0$ and the fluid motion is in the x-direction only. In figure 2*a* a view of the top of a non-rotating fluid layer is shown. The fluid has maximum upward velocity along lines AB and maximum downward velocity along lines CD.

When the system is rotated, the coriolis force introduces a velocity component parallel to the isobars (isotherms in this case), i.e. in the y-direction. Therefore, the streamlines are oriented at an oblique angle to the y-axis (figure 2*b*).

The wave-number α of the cell is a function of $\mathscr{T}_1^2$ as given by (2.6). The wave number corresponding to the oblique cell, i.e. in the direction of the orientation of

the cell, can be computed from (2.8). Let θ be the angle from the x-axis to the streamline path as indicated in figure 2*b*. Then

$$\theta = \tan^{-1}\left(\frac{v_0}{u_0}\right) = -\tan^{-1}\left(\frac{\mathscr{T}_1}{\alpha^2+1}\right). \tag{2.9}$$

The square of the wave-number of the oblique cell is given by

$$\alpha^2\cos^2\theta = \frac{\alpha^2(\alpha^2+1)^2}{\mathscr{T}_1^2+(\alpha^2+1)^2}. \tag{2.10}$$

With (2.6), this expression reduces to

$$\alpha^2\cos^2\theta = \alpha^2(1/2\alpha^2) = \tfrac{1}{2}. \tag{2.11}$$

In other words, although the wavelength of the cell decreases with rotation, the wavelength of the cell measured in the direction of the orientation of the cell is the same as in the non-rotating case.

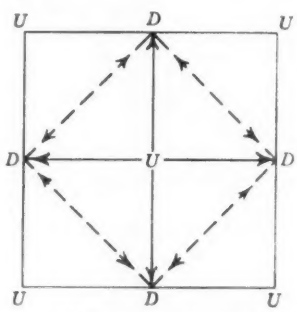

FIGURE 3*a*. A top view of square cells in a non-rotating fluid. Points marked U are points of maximum upward velocity; those marked D are points of maximum downward velocity. The region within the dotted lines would be seen as a cell in an experiment.

Square cells. From the analysis of the non-rotating system we anticipate that square cells will be the preferred form for a system with vertical symmetry. Paralleling the argument for rolls, we can write

$$\left.\begin{aligned} w_0 &= 2\sqrt{2}\cos\frac{\pi\alpha x}{\sqrt{2}}\cos\frac{\pi\alpha y}{\sqrt{2}}\sin\pi z, \quad T_0 = \frac{\sigma\lambda_0}{\pi^2(\alpha^2+1)}w_0, \\ u_0 &= -\left[\frac{2\mathscr{T}_1}{\alpha(\alpha^2+1)}\cos\frac{\pi\alpha x}{\sqrt{2}}\sin\frac{\pi\alpha y}{\sqrt{2}}+\frac{2}{\alpha}\sin\frac{\pi\alpha x}{\sqrt{2}}\cos\frac{\pi\alpha y}{\sqrt{2}}\right]\cos\pi z, \\ v_0 &= \left[-\frac{2}{\alpha}\cos\frac{\pi\alpha x}{\sqrt{2}}\sin\frac{\pi\alpha y}{\sqrt{2}}+\frac{2\mathscr{T}_1}{\alpha(\alpha^2+1)}\sin\frac{\pi\alpha x}{\sqrt{2}}\cos\frac{\pi\alpha y}{\sqrt{2}}\right]\cos\pi z. \end{aligned}\right\} \tag{2.12}$$

When $\mathscr{T}_1 = 0$, both the horizontal and the vertical motions form a square pattern. A top view of the fluid is illustrated in figure 3*a*, where U and D define points of maximum upward and downward motions respectively. The cell is shown with fluid rising in the centre, but the pattern can equally as well be displaced by a half wavelength in the x- or y-direction to yield a cell with sinking at the centre. In actuality the region within the dotted lines is what one would see as a cell in an experiment.

When $\mathscr{T}_1 > 0$, the coriolis force causes the fluid to turn as it moves toward or from the centre so that part of the flow is parallel to the isobars. The spiral curves in figure 3*b* correspond to the straight lines shown in figure 3*a*. As the spiral crosses the x- and y-axes, it coincides with the inverse logarithmic spiral $r = \alpha^{-1}\exp\{\mathscr{T}_1\theta/(\alpha^2+1)\}$ (in polar co-ordinates r, θ), but the regions intermediate to the axes, it deviates from the logarithmic spiral. (The actual spiral is not equiangular, i.e. it does not cross all radial lines with the same angle at each traversal. The logarithmic spiral was used to construct the figure and to compute the half wavelength along the path.) By computing the length of the spiral, one can derive expression (2.11) for the horizontal 'wave-number' along the spiral. The wavelength measured along the distorted cellular boundary is again equal to that of the non-rotating case.

Figure 3*c* is a perspective sketch of a complete trajectory of a particle which travels from the centre of the cell to the edge and back again. The particle spirals upward and clockwise (for counterclockwise Ω) from the centre of the cell, crosses to the corner near the top of the cell and spirals downward and counterclockwise. Halfway down it reverses its direction of rotation, spirals downward and clockwise crosses back toward the middle of the cell, and begins a counterclockwise upward motion toward the centre.

The reversal of rotation as a particle crosses the middle plane is due to the fact that at this point the horizontal divergence of the fluid changes sign. As the fluid moves outward, it is deflected to the right by the coriolis force and spirals in a clockwise manner. Converging fluid spirals counterclockwise when deflected to the right.

The square cell shown in the diagram corresponds to the basic geometry of the vertical velocity. The actual cell is distorted by the rotation and is not reproduced here.

Hexagonal cells. The preferred pattern for the vertical velocity is the hexagonal pattern when the boundary conditions provide a vertical asymmetry. Since most experimental observations of cells are made when the upper surface is free, hexagonal cells will ordinarily occur.

The discussion parallels that for square cells. The analytical form as proposed by Christopherson (1940) is

$$w_0 = \frac{2}{\sqrt{3}}\left(2\cos\frac{2\pi x}{\sqrt{3}L}\cos\frac{2\pi y}{3L} + \cos\frac{4\pi y}{3L}\right)\sin\pi z, \tag{2.13a}$$

where $L = 4/(3\alpha)$ is the length of one side of the regular hexagon. The remaining variables have the form

$$\left.\begin{aligned} T_0 &= \frac{\sigma\lambda_0}{\pi^2(\alpha^2+1)}w_0, \\ u_0 &= -\left[\frac{3L}{2}\sin\frac{2\pi x}{\sqrt{3}L}\cos\frac{2\pi y}{3L} + \frac{\sqrt{3}L\mathscr{T}_1}{2(\alpha^2+1)}\left(\cos\frac{2\pi x}{\sqrt{3}L}\sin\frac{2\pi y}{3L} + \sin\frac{4\pi y}{3L}\right)\right]\cos\pi z, \\ v_0 &= \left[\frac{3L\mathscr{T}_1}{2(\alpha^2+1)}\sin\frac{2\pi x}{\sqrt{3}L}\cos\frac{2\pi y}{3L} - \frac{\sqrt{3}L}{2}\left(\cos\frac{2\pi x}{\sqrt{3}L}\sin\frac{2\pi y}{3L} + \sin\frac{4\pi y}{3L}\right)\right]\cos\pi z. \end{aligned}\right\} \tag{2.13b}$$

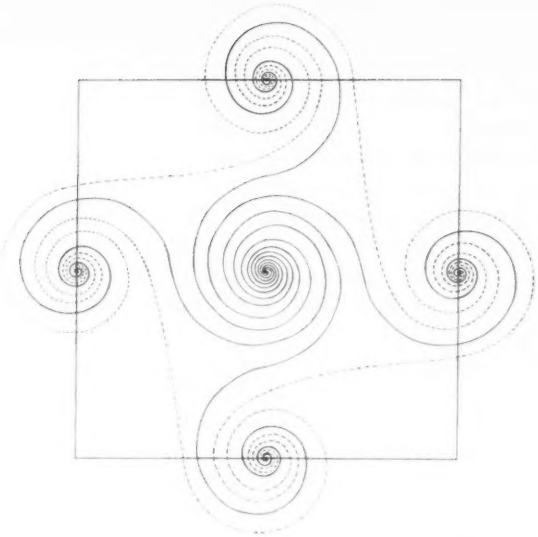

FIGURE 3*b*. A square cell in a rotating fluid. The particle motions from the centre outward follow the spiral curves. The dashed curves form the boundary of the square cell.

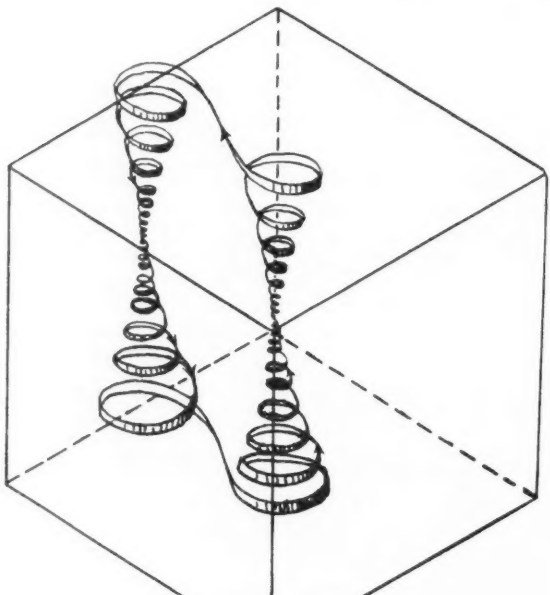

FIGURE 3*c*. A perspective sketch of a fluid particle motion in the square cell.

Figure 4*a* illustrates the particle motion at the top of a non-rotating-cell. Figure 4*b* is a top view of a rotating cell and of the six adjacent cells. The dashed spirals form the upper boundary of the centre cell. Each centre is surrounded by six corners and each corner receives fluid from the three adjacent centres.

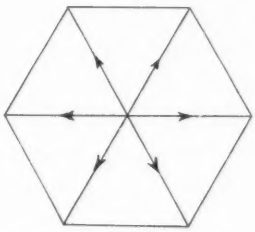

FIGURE 4*a*. Top view of a non-rotating hexagonal cell. The fluid rises in the centre and spreads outward to the six corners where it descends.

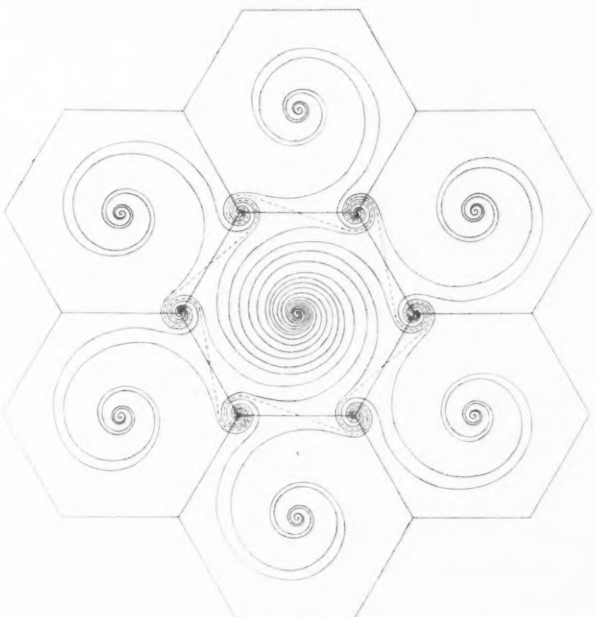

FIGURE 4*b*. A top view of seven rotating hexagonal cells. The fluid particles follow spiral paths from the centre toward the corners. The dashed lines form the boundaries of the centre cell.

A perspective sketch of a fluid particle path in three dimensions is shown in figure 4*c*. Figure 1 illustrates the manner in which the cell is distorted by the rotation.

The effective wave-number of the non-rotating cell is again equal to the wave-number measured along the spiral curve.

The three cases discussed here indicate that the wave-number measured along the curved path is invariant. It is clear that such an invariance must be intimately coupled with a physical property of the fluid which is unaffected by the imposed constraint. The one property of the fluid which is not affected by a rotation about a vertical axis is the horizontal vorticity. We shall show here how the constancy of horizontal vorticity preserves the wave-number measured in the direction of flow for the simplest type of motion, viz. that of rolls.

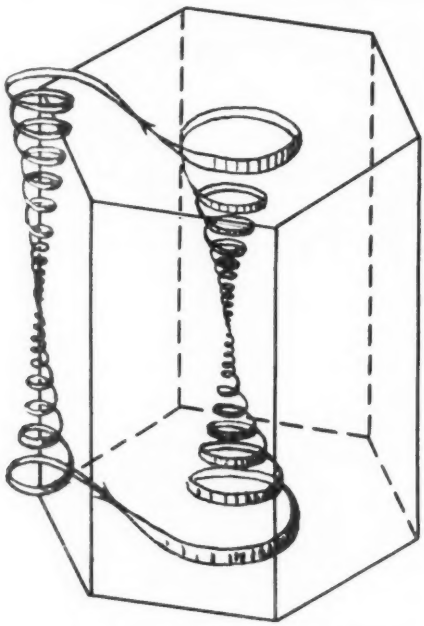

FIGURE 4c. A perspective sketch of a fluid particle path which passes through the centre of the cell.

Consider a rotation of the horizontal co-ordinates so that the x'-direction is measured along the direction of flow (figure 2*b*). Then the horizontal vorticity about the y-axis is given by $\partial u'/\partial z - \partial w/\partial x'$, where the primes correspond to a measure of the quantities along the new axes. Since the horizontal vorticity is constant, we have

$$\left\{\left(\frac{\partial u'}{\partial z}-\frac{\partial w}{\partial x'}\right)^2\right\}_m = \left\{\left(\frac{\partial u}{\partial z}-\frac{\partial w}{\partial x}\right)^2\right\}_m = \text{const.}, \tag{2.14}$$

where the middle expression corresponds to the non-rotating system, i.e. when x' is parallel to x. From the equation of continuity, we have

$$\frac{\partial u'}{\partial x'}+\frac{\partial w}{\partial z}=0, \quad \frac{\partial u}{\partial x}+\frac{\partial w}{\partial z}=0. \tag{2.15}$$

Since w is normalized and since the z-distance is fixed, equation (2.15) yields a relation between the wave-number measured in the x (or x') direction and the

amplitude of u (or u'). From (2.14) we then note that the wave-number must be the same in the two systems. When the vertical velocity is normalized the amplitudes of the horizontal velocities are equal.

C. *Overstability*

Though p_0 must be real in the non-rotating system, p_0 may be complex when $\mathscr{T}^2 > 0$. The coefficients of (2.4) are real; therefore, in general p_0 will have one real and two complex conjugate roots. These can be written in the form

$$(p_0 - p')(p_0 - p_r - ip_i)(p_0 - p_r + ip_i) = 0,$$

or
$$p_0^3 - (p' + 2p_r)p_0^2 + (2p_r p' + p_i^2 + p_r^2)p_0 - p'(p_i^2 + p_r^2) = 0,$$

where p', p_i and p_r are real.

For marginal stability $p_r = 0$, and

$$p_0^3 - p'p_0^2 + p_i^2 p_0 - p'p_i^2 = 0. \tag{2.16}$$

Hence, for marginal stability, the product of the coefficients of p_0^2 and p_0 must equal the coefficient of p_0^0. By (2.4) this condition becomes

$$\frac{\lambda_0}{\pi^4} = 2(\sigma+1)\left[\frac{(\alpha^2+n^2)^3 + \dfrac{\sigma^2}{(\sigma+1)^2}n^2\mathscr{T}_1^2}{\alpha^2}\right], \tag{2.17}$$

which has a minimum when $\partial\lambda_0/\partial\alpha^2 = 0$, i.e. when

$$2\alpha^6 + 3\alpha^4 n^2 = n^6 + \frac{\sigma^2}{(\sigma+1)^2}n^2\mathscr{T}_1^2. \tag{2.18}$$

Thus $\alpha^2 \to 2^{-\frac{1}{3}}[\sigma n\mathscr{T}_1/(\sigma+1)]^{\frac{2}{3}}$ and $\lambda_0/\pi^4 \to 2^{\frac{1}{3}}3(\sigma+1)[\sigma n\mathscr{T}_1/(\sigma+1)]^{\frac{2}{3}}$ as $\mathscr{T}_1^2 \to \infty$. (The above results do not obtain for $\sigma = 0$, but this case is physically uninteresting and will not be considered.)

The remainder of the discussion will be confined to the lowest eigenvalue, i.e. to the case $n = 1$.

When p_0 is imaginary, the coefficient of p_0 in (2.16) is real and positive. From (2.4), we find that

$$p_i^2 = \pi^4(\alpha^2+1)^2(\sigma^2+2\sigma) + \frac{\sigma}{\alpha^2+1}(\mathscr{T}^2\sigma - \alpha^2\lambda_0) \geqslant 0,$$

or, using (2.17), that

$$p_i^2 = -\sigma^2\pi^4(\alpha^2+1)^2 + \frac{\mathscr{T}^2\sigma^2(1-\sigma)}{(\alpha^2+1)(1+\sigma)} \geqslant 0. \tag{2.19}$$

Therefore, a necessary condition for overstability is

$$\mathscr{T}_1^2 \geqslant \frac{\sigma+1}{-\sigma+1}(\alpha^2+1)^3. \tag{2.20}$$

Eliminating $\mathscr{T}_1^2$ from (2.18) and the equality of (2.20), we can find the value of α^2 at which overstability can just occur, i.e. when $p_i = 0$. This value satisfies

$$(2-3\sigma^2)\alpha^2 + 3(1-2\sigma^2)\alpha^4 - 3\sigma^2\alpha^2 - 1 = 0. \tag{2.21}$$

When $\sigma = \sqrt{\frac{2}{3}}$, $\alpha^2 = \infty$. Therefore $\sigma = \sqrt{\frac{2}{3}}$ represents the (upper) limiting value of the Prandtl number for which overstability can occur.*

Equation (2.17) together with (2.18) determines the minimum value of λ_0 for each pair of values of $\mathscr{T}_1^2$ and σ. The curves in figure 5 show the dependence of λ_0/π^4 on $\mathscr{T}_1^2$ for a number of values of σ. The curve C corresponds to steady convective instability.

It is possible, of course, that the fluid may become unstable in a steady convective manner and that overstability may occur in finite amplitude or that overstability may occur first and convection be preferred in finite amplitude. Figure 6 shows three divided regions in the $(\sigma, \mathscr{T}_1^2)$-plane. In region A overstability cannot arise because (2.20) cannot be satisfied. In region B convection occurs first but overstability may be the preferred state in finite amplitude.

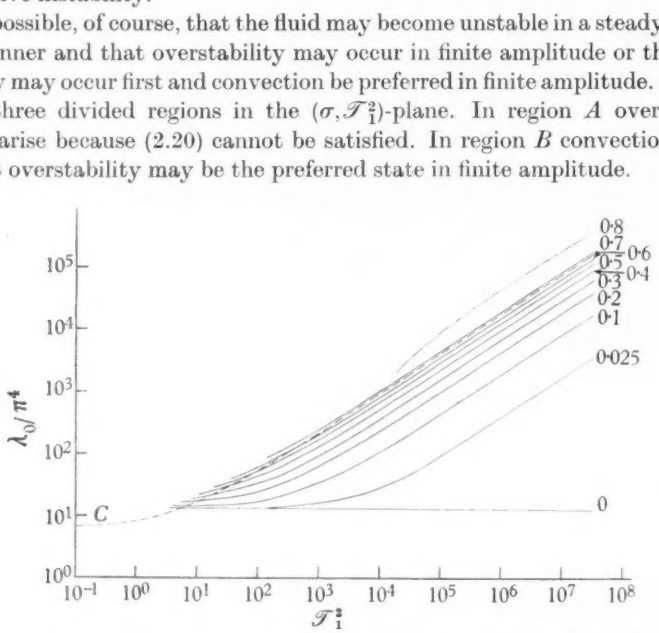

FIGURE 5. The λ_0/π^4 *vs* $\mathscr{T}_1^2$ relations for marginal stability. The dashed curve corresponds to steady convective instability. The solid curves correspond to instability in the form of time-periodic motions. The numbers on the curves are the values of the Prandtl numbers.

The curve between regions B and C marks the points at which overstability and convection occur simultaneously. The system will become overstable to infinitesimal disturbances when σ and $\mathscr{T}_1^2$ have values in the region C. Here, however, convection may come in at finite amplitude.

Why can overstability occur in the rotating systems and not when $\mathscr{T} = 0$? To answer this question we shall look into the energetics of the fluid.

For the two-dimensional case the solution to (2.1*c*) is

$$w_0 = 2\sqrt{2}\cos p_0 \tau \cos \pi\alpha x \sin \pi z, \tag{2.22}$$

where p_0^2 is equal to p_i^2 in (2.19). The remaining variables T_0, u_0, v_0 can be determined from equations (2.1) and are listed in § 4. If these expressions are substi-

* Nakagawa & Frenzen (III) show in figure 7 the value of λ_0 for overstability (R_c^* in their notation) in water ($\sigma \doteq 6$). That overstability cannot occur for $\sigma \geqslant \sqrt{\frac{2}{3}}$ is clear from the above argument. In addition, they derive the value $\lambda_0 = 2(\sigma+1)\,\alpha^{-2}\,(\alpha^2+1)^3$ when $\mathscr{T}_1^2 = 0$. However, condition (2.20) is violated so that this result is also incorrect.

tuted into the power integral expression (1.17) (with the right-hand side equal to zero). and if we use (2.19) for p_0^2, we have

$$\frac{\lambda_0/\pi^4}{(1+\sigma)\left[(\alpha^2+1)^2+\dfrac{\sigma^2}{(\sigma+1)^2}\dfrac{\mathscr{T}_1^2}{(\alpha^2+1)}\right]}=2\frac{\alpha^2}{\alpha^2+1}, \tag{2.23}$$

where the left-hand side represents the rate of release of potential energy, $\{wT\}_m$, and the right-hand side the rate of dissipation of kinetic energy $\{\mathbf{v}.\nabla^2\mathbf{v}\}_m$. Equation (2.23) is equivalent to (2.17). Therefore the eigenvalue equation is a statement that a balance of the rate of viscous dissipation and the rate of release of potential energy is achieved by the fluid at the point of instability. The equivalent expression for the steady case is given by (2.5).

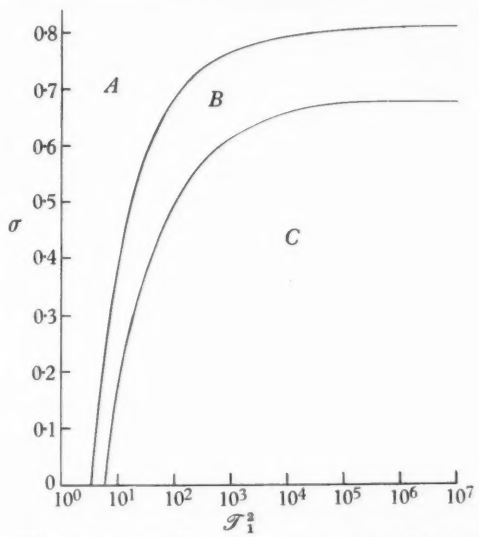

FIGURE 6. The $(\sigma, \mathscr{T}_1^2)$-plane is divided into three regions which are significant in the stability problem. In A instability occurs as steady convection. In B steady convective instability occurs first but overstability is possible for higher λ_0. In C overstability occurs before steady convection.

For fixed values of the convective heat transport, $\{wT\}_m$, and the rate of dissipation of kinetic energy, a decrease of σ in the overstable case reduces the effect of the external constraint $\mathscr{T}^2$. To compensate for the reduction of σ it is necessary that λ_0 be decreased. In the steady system the energy balance at the point of instability is unaltered by a change of σ. Therefore, in the overstable case, it is possible for the value of the Rayleigh number to be smaller than the value corresponding to the steady regime because the effect of the constraint is small when the Prandtl number is small.

From the stability problem, we have derived information concerning the onset of steady convective instability and of overstability. However, the amplitude of the motions for a given value of λ, the energetics of the fluid, the preferred

motions for a given set of external parameters, and still other features are unknowns which can be determined only in a finite-amplitude study. Therefore, we shall now go on to a study of finite-amplitude steady convection.

3. Finite-amplitude steady convection

The equations which govern steady convection are given by (1.3), (1.11), (1.13) and (1.14) with $\partial/\partial\tau \equiv 0$. Thus, the following equations are obtained by collecting terms in ϵ, ϵ^2 and ϵ^3 respectively: equations corresponding to ϵ^4, etc., can be found in the same way:

$$\left.\begin{aligned} \mathscr{L}w_0 &\equiv \left[\nabla^6 + \mathscr{T}^2\frac{\partial^2}{\partial z^2} - \lambda_0\nabla_1^2\right]w_0 = 0, \\ \mathscr{L}w_1 &= \lambda_1\nabla_1^2 w_0 - \nabla^2 L_{00} + \mathscr{T}\frac{\partial Z_{00}}{\partial z} - \nabla_1^2 h_{00}, \\ \mathscr{L}w_2 &= \lambda_2\nabla_1^2 w_0 + \lambda_1\nabla_1^2 w_1 - \nabla^2(L_{01}+L_{10}) + \mathscr{T}\frac{\partial}{\partial z}(Z_{01}+Z_{10}) \\ &\quad - \nabla_1^2(h_{01}+h_{10}) + \sigma[\{w_0 T_0\}_m - \overline{w_0 T_0}]\nabla_1^2 w_0; \end{aligned}\right\} \tag{3.1}$$

$$\left.\begin{aligned} -\nabla^2 T_0 &= \sigma\lambda_0 w_0, \\ -\nabla^2 T_1 &= \sigma\lambda_0 w_1 + \sigma\lambda_1 w_0 - \sigma h_{00}, \\ -\nabla^2 T_2 &= \sigma\lambda_0 w_2 + \sigma\lambda_1 w_1 + \sigma\lambda_2 w_0 + \sigma^2[\{w_0 T_0\}_m - \overline{w_0 T_0}]w_0 - \sigma(h_{01}+h_{10}); \end{aligned}\right\} \tag{3.2}$$

$$\left.\begin{aligned} -\nabla^2\zeta_0 &= \mathscr{T}\frac{\partial w_0}{\partial z}, \\ -\nabla^2\zeta_1 &= \mathscr{T}\frac{\partial w_1}{\partial z} - Z_{00}, \\ -\nabla^2\zeta_2 &= \mathscr{T}\frac{\partial w_2}{\partial z} - (Z_{01}+Z_{10}); \end{aligned}\right\} \tag{3.3}$$

$$\frac{\partial u_i}{\partial x} + \frac{\partial v_i}{\partial y} + \frac{\partial w_i}{\partial z} = 0 \quad (i = 0, 1, 2, \ldots). \tag{3.4}$$

Here the subscripts i, j correspond to the order of the variables to be substituted into each expression: e.g. $h_{ij} = \mathbf{v}_i \cdot \nabla T_j - \dfrac{\partial}{\partial z}(\overline{w_i T_j})$.

The method of solution is the same as the method used in the non-rotating problem (I). A brief outline of the method is given below.*

The form of w_0 can be determined by inspection from (3.1). Expressions for T_0, u_0 and v_0 are derived from the normalized expression for w_0 by means of equations (3.2), (3.3) and (3.4). The right-hand side of the second equation of (3.1) can then be computed directly since it is composed of zero-order functions only. However, two difficulties appear at this point. The inhomogeneous term in the w_1 equation will, in general, contain terms of the form of w_0 as well as the unknown parameter λ_1. In solving for the particular solution for w_1, one will obtain secular terms in addition to terms which are spatially periodic. In addition, the homogeneous solution of w_1 will contain the form of w_0 with an arbitrary amplitude.

* *Note added in proof.* A method for treating the finite-amplitude range has also been proposed by L. P. Gor'kov (1957). His method and that of Malkus & Veronis yield the same finite-amplitude results for λ_2.

Since λ_1 multiplies a term of the form of w_0 in the inhomogeneous term, we can evaluate λ_1 to cancel the remaining amplitudes of w_0. Secular terms are thereby eliminated and the assumed periodicity of the solution is maintained. Furthermore, by specifying that ϵ be the total amplitude of that part of w which contains w_0, we can write $\{ww_0\}_m = \epsilon$ or $\{w_i w_0\}_m = 0$ for $i > 0$, i.e. the homogeneous part of $w_i\,(i > 0)$ which has the form of w_0 has zero amplitude. The system of equations can now be solved for the w_i, T_i, u_i, v_i and λ_i. We shall apply the method first to determine an approximate finite-amplitude solution for the two-dimensional rolls. Though this case is unrealistic, it is the only case which, with a reasonable amount of effort, can be carried beyond the second approximation. Because the roll is not truly descriptive of the actual physical system, we shall discuss certain qualitative features of this case only. Later, in the analysis for the square cell, additional observable features of the flow will be presented.

(*a*) *Rolls*

The solution to the stability problem is given by equations (2.7) and (2.8). This is

$$\left.\begin{aligned} w_0 &= 2\cos\pi\alpha x\sin\pi z, & T_0 &= \frac{2\sigma\lambda_0}{\pi^2(\alpha^2+1)}\cos\pi\alpha x\sin\pi z,\\ u_0 &= -\frac{2}{\alpha}\sin\pi\alpha x\cos\pi z, & v_0 &= \frac{2\mathscr{T}_1}{\alpha(\alpha^2+1)}\sin\pi\alpha x\cos\pi z, \end{aligned}\right\} \tag{3.5}$$

where the value of α corresponding to a given value of $\mathscr{T}_1$ is given by (2.6), and λ_0 is given by (2.5)

The inhomogeneous term for w_1 can be evaluated directly; thus

$$Z_{00} = \frac{\partial}{\partial x}(\mathbf{v}_0.\nabla v_0) - \frac{\partial}{\partial y}(\mathbf{v}_0.\nabla u_0) = -\frac{4\mathscr{T}}{\alpha^2+1}\cos 2\pi\alpha x,$$

$$L_{00} = \frac{\partial}{\partial z}\left[\frac{\partial}{\partial x}(\mathbf{v}_0.\nabla u_0) + \frac{\partial}{\partial y}(\mathbf{v}_0.\nabla v_0)\right] - \nabla_1^2(\mathbf{v}_0.\nabla w_0) = 0,$$

$$h_{00} = \mathbf{v}_0.\nabla T_0 - \frac{\partial}{\partial z}(\overline{w_0 T_0}) = 0.$$

Therefore, $\mathscr{L}w_1 = -\pi^2\alpha^2\lambda_1 w_0$.

Now λ_1 is evaluated so as to cancel the form of w_0 from the right-hand side. Since the only term containing the form of w_0 is $\lambda_1\nabla_1^2 w_0$, it is necessary that $\lambda_1 = 0$. Thus,

$$\lambda_1 = 0, \quad w_1 = 0, \quad T_1 = 0, \quad u_1 = 0. \tag{3.6}$$

The second equation of (3.3) gives

$$v_1 = \frac{\mathscr{T}_1}{2\pi\alpha^3(\alpha^2+1)}\sin 2\pi\alpha x. \tag{3.7}$$

To solve for w_2, we note that $L_{01} = L_{10} = h_{01} = h_{10} = Z_{10} = 0$, and

$$\mathscr{T}\frac{\partial Z_{01}}{\partial z} = \frac{\mathscr{T}^2}{\alpha^2(\alpha^2+1)}[3\cos 3\pi\alpha x - \cos\pi\alpha x]\sin\pi z,$$

$$\sigma[\{w_0 T_0\}_m - \overline{w_0 T_0}]\nabla_1^2 w_0 = -\frac{\alpha^2\sigma^2\lambda_0}{\alpha^2+1}\cos\pi\alpha x(\sin 3\pi z - \sin\pi z),$$

$$\lambda_2\nabla_1^2 w_0 = -2\pi^2\alpha^2\lambda_2\cos\pi\alpha x\sin\pi z.$$

Thus, $$\mathscr{L}w_2 = \left[-2\pi^2\alpha^2\lambda_2 + \frac{\alpha^2\sigma^2\lambda_0}{\alpha^2+1} - \frac{\mathscr{T}^2}{\alpha^2(\alpha^2+1)}\right]\cos\pi\alpha x \sin\pi z + \frac{3\mathscr{T}^2}{\alpha^2(\alpha^2+1)}\cos 3\pi\alpha x \sin\pi z - \frac{\alpha^2\sigma^2\lambda_0}{\alpha^2+1}\cos\pi\alpha x \sin 3\pi z. \quad (3.8)$$

The first term on the right-hand side has the form of w_0 and must vanish. Hence,

$$\lambda_2 = \frac{\sigma^2\lambda_0}{2\pi^2(\alpha^2+1)} - \frac{\mathscr{T}^2}{2\pi^2\alpha^4(\alpha^2+1)}. \quad (3.9)$$

The evaluation of λ_2 provides the first finite-amplitude result. From the expression (1.9) for the heat transport, we can write

$$\frac{H}{\kappa\beta_m} = 1 + \frac{\sigma}{\lambda}\{wT\}_m, \quad (3.10)$$

where w and T are non-dimensional. Expanding w and T as in (1.15), we have

$$\{wT\}_m = \epsilon^2[\{w_0T_0\}_m + \epsilon\{w_0T_1 + w_1T_0\}_m + \epsilon^2\{w_0T_2 + w_1T_1 + w_2T_0\}_m + \epsilon^3\{w_0T_3 + w_1T_2 + w_2T_1 + w_3T_0\}_m + \epsilon^4\{w_0T_4 + w_1T_3 + w_2T_2 + w_3T_1 + w_4T_0\}_m + \ldots]. \quad (3.11)$$

Therefore, to the ϵ^2 approximation for the convective heat transport, we get

$$\frac{\sigma}{\lambda}\{wT\}_m = \frac{\sigma}{\lambda}\epsilon^2\{w_0T_0\}_m. \quad (3.12)$$

To the same approximation (1.16) becomes

$$\epsilon^2 = \frac{\lambda - \lambda_0}{\lambda_2}. \quad (3.13)$$

Hence,
$$\frac{\sigma}{\lambda}\{wT\}_m = \frac{\sigma}{\lambda_2}\left(1 - \frac{\lambda_0}{\lambda}\right)\{w_0T_0\}_m = \frac{\sigma^2\lambda_0}{\pi^2(\alpha^2+1)\lambda_2}\left(1 - \frac{\lambda_0}{\lambda}\right). \quad (3.14)$$

We can see from (3.14) that to the ϵ^2 approximation the convective heat transport varies inversely as λ_2. Table 1 contains values of the convective heat transport $\sigma\{wT\}_m/(\lambda - \lambda_0)$ of rolls for various values of σ and $\mathscr{T}_1^2$. The range of σ is restricted to the values for which overstability can also occur. Not that λ_2 and therefore $\sigma\{wT\}_m/(\lambda - \lambda_0)$ are negative for small Prandtl numbers and positive for larger values. In most of the range where λ_2 is negative overstability will occur before steady convection. However, for sufficiently low rotation rates, overstability cannot arise and the flow will be steady.

Since $\epsilon^2 > 0$, it is clear from (3.13) that negative λ_2 implies that $\lambda < \lambda_0$. According to this analysis, which is pivoted about the linear stability problem,

the system will behave as follows. As λ increases toward λ_0, heat is transported by pure conduction (figure 7). When $\lambda = \lambda_0$ convection will occur but now λ can be decreased below λ_0 and convection will be maintained. According to the ϵ^2 approximation, one could decrease λ indefinitely and convection would continue; therefore, one must go to a higher approximation to determine when the curve begins to turn up again.

	$\mathscr{T}_1^2$					
σ	0·1	0·5	1	5	10	10^2
0·025	−0·0239	−0·00702	−0·00487	−0·00377	−0·00406	−0·00724
0·1	−0·569	−0·117	−0·0808	−0·0619	−0·0671	−0·122
0·2	−6·01	−0·562	−0·365	−0·274	−0·0299	−0·600
0·3	4·87	−1·94	−1·07	−0·735	−0·827	−2·16
0·4	2·99	−14·36	−3·24	−1·81	−2·17	−24·2
0·5	2·54	7·39	−63·0	−5·60	−8·68	6·51
0·6	2·34	4·06	7·10	40·1	13·7	3·85
0·687	2·25	3·26	4·41	6·77	5·75	3·16
0·7	2·23	3·19	4·23	6·56	5·37	3·09
0·8	2·18	2·80	3·37	4·40	3·86	2·74

	$\mathscr{T}_1^2$					
σ	10^3	10^4	10^5	10^6	10^7	10^8
0·025	−0·0150	−0·0326	−0·0715	−0·168	−0·382	−1·06
0·1	−0·270	−0·690	−2·47	11·2	3·28	2·44
0·2	−1·82	77·6	3·66	2·55	2·21	2·09
0·3	29·6	3·53	2·50	2·23	2·09	2·04
0·4	4·20	2·64	2·25	2·14	2·05	2·02
0·5	3·01	2·37	2·16	2·10	2·03	2·01+
0·6	2·60	2·25	2·11	2·07	2·02	2·01−
0·687	2·43	2·18	2·09	2·04	2·01+	2·01−
0·7	2·41	2·16	2·08	2·03	2·01	2·01−
0·8	2·29	2·14	2·06	2·02	2·01−	2·00+

TABLE 1. Values of $\dfrac{\sigma\{wT\}_m}{\lambda-\lambda_0} = \dfrac{\sigma^2\lambda_0}{\pi^2(\alpha^2+1)\lambda_2}$ for rolls.

Experimentally, one would not observe the sequence of events described above. If a finite-amplitude perturbation were present, the system would become unstable at λ_U (figure 7), and the motions would grow very quickly from C to A, i.e. until the fluid transported the amount of heat corresponding to point A. A further increase in λ would be needed to increase H. On the other hand, if no finite-amplitude disturbance were present, instability would occur at λ_0, but the motions would grow very rapidly with $\lambda = \lambda_0$ until the heat transport corresponded to point B. If the system were allowed to 'run down', i.e. if λ were decreased from a value above λ_0, then the system would always follow the path $BACO$.

The onset of instability as a finite-amplitude disturbance in the rotating system marks a definite point of departure from the results of the non-rotating

system. In the latter case, convective heat transport is possible only for values of $\lambda > \lambda_0$. Why does the rotating system respond so differently in finite amplitude? What is the mechanism for the occurrence of finite amplitude instability?

The answers to these questions can be found in equation (1.14). For the steady convective case, we have

$$\nabla^6 w + \mathscr{T}^2 \frac{\partial^2 w}{\partial z^2} - \lambda \nabla_1^2 w = \sigma[\{wT\}_m - \overline{wT}]\nabla_1^2 w + \mathscr{T}\frac{\partial Z}{\partial z} - \nabla_1^2 h - \nabla^2 L. \quad (3.15)$$

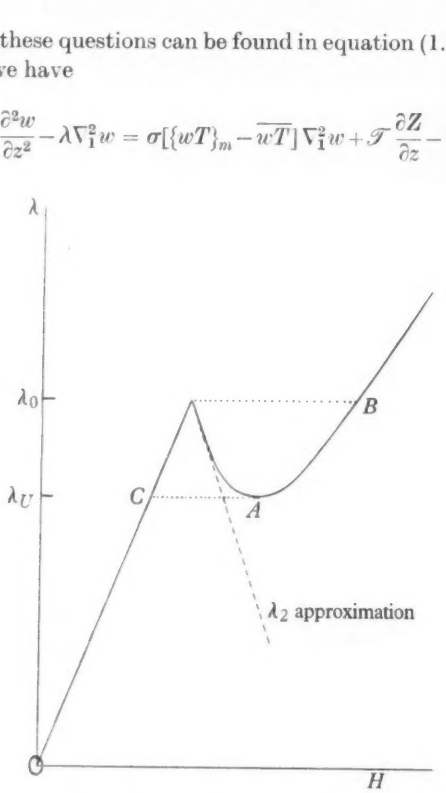

FIGURE 7. The λ *vs* H curve when λ_2 is negative.

The term

$$Z = \frac{\partial}{\partial x}(\mathbf{v}.\nabla v) - \frac{\partial}{\partial y}(\mathbf{v}.\nabla u)$$

can be written in the form

$$Z = \mathbf{v}_1.\nabla_1\zeta - \boldsymbol{\omega}_1.\nabla_1 w = \nabla_1.[\mathbf{v}_1\zeta - \boldsymbol{\omega}_1 w], \quad (3.16)$$

where the subscript 1 corresponds to the horizontal vectors and $\boldsymbol{\omega}_1$ is the horizontal vorticity vector. If the term $\mathscr{T}(\partial Z/\partial z)$ is taken to the left-hand side of the equation (3.15), the second term can be written (with the aid of (1.3))

$$\mathscr{T}\frac{\partial}{\partial z}\nabla_1.\{\mathbf{v}_1\mathscr{T} - \mathbf{v}_1\zeta + \boldsymbol{\omega}_1 w\}. \quad (3.17)$$

The individual terms within the brackets correspond respectively to the horizontal transport of imposed vertical vorticity, the horizontal transport of local

vertical vorticity, and the vertical transport of horizontal vorticity. In finite amplitude, therefore, the fluid can generate a local vorticity whose net effect is to decrease the role of the constraining first term in (3.17). When the viscosity is large, the generation of local vorticity is accompanied by strong viscous dissipation so that the non-linear terms will stabilize the system.

It is important to note that the possibility of a finite-amplitude instability is brought about by interactions of the zero-average non-linear terms which do not contribute *per se* to the distortion of the mean temperature profile. These terms play an increasingly important role as the Prandtl number diminishes. In the non-rotating system, the heat transport curve of a fluid with small Prandtl number breaks away from the conduction line with a slope one-third greater than that of pure conduction, whereas when the Prandtl number is large the slope of the heat transport curve is twice the conduction slope. When an external constraint is present, the heat convected by the fluid varies as a function of the constraint.

When λ_2 is positive, heat is transported by convection only when λ is increased beyond λ_0. We shall discuss this case in some detail in a subsection on square cells.

When $\lambda_2 < 0$, it is necessary to consider the next approximation in order to find the point at which the λ *vs* H curve turns upward. We can feel fairly confident that the ϵ^2 approximation is valid only in a very limited range, otherwise the λ, H curve would cross the H axis, i.e. the fluid would transport a finite amount of heat in the absence of a temperature gradient.

λ_4 *for rolls.* Because of the vertical symmetry, $\lambda_i = 0$ for odd i. Hence, it is necessary to go to the ϵ^4 approximation to determine the higher-order effect on the heat transport.

The equations governing the ϵ^4 approximation can be determined from equation (3.15) and from the expansions (1.15) and (1.16). The results only will be listed here:

$$\left.\begin{aligned} w_2 &= w_{20}\cos\pi\alpha x\sin 3\pi z + w_{21}\cos 3\pi\alpha x\sin\pi z,\\ T_2 &= \frac{\sigma\lambda_0 w_{20}+\sigma^2 N_0}{\pi^2(\alpha^2+9)}\cos\pi\alpha x\sin 3\pi z+\frac{\sigma\lambda_0 w_{21}}{\pi^2(9\alpha^2+1)}\cos 3\pi\alpha x\sin\pi z\\ &\qquad -\frac{\sigma\mathscr{T}_1^2}{\alpha^4(\alpha^2+1)^2}\cos\pi\alpha x\sin\pi z; \end{aligned}\right\} \tag{3.18}$$

$$\left.\begin{aligned} \lambda_3 &= 0,\\ \lambda_4 &= -\frac{\sigma^2}{4}\left[\frac{\mathscr{T}_1^2}{\alpha^4(\alpha^2+1)^2}+\frac{\sigma^2 N_0}{\alpha^2+9}\left(\frac{\alpha^2\lambda_0/\pi^4}{A}+1\right)\right]\\ &\qquad -\frac{\sigma^4 N_0^2\alpha^2}{2A}+\frac{\mathscr{T}_1^2}{4\alpha^6(\alpha^2+1)}\left[\frac{1}{9\alpha^2+1}\left(1-\frac{\mathscr{T}_1^2}{B}\right)+\frac{1}{\alpha^2+1}\right], \end{aligned}\right\} \tag{3.19}$$

where
$$w_{20}=\frac{\sigma\alpha^2 N_0}{\pi^4 A},\quad w_{21}=-\frac{3\mathscr{T}_1^2}{\pi^2\alpha^2(\alpha^2+1)B},\quad N_0=\frac{\lambda_0}{\pi^2(\alpha^2+1)},$$

$$A=(\alpha^2+9)^3+9\mathscr{T}_1^2-\alpha^2\frac{\lambda_0}{\pi^4},\quad B=(9\alpha^2+1)^3+\mathscr{T}_1^2-9\alpha^2\frac{\lambda_0}{\pi^4}$$

Values of λ_4 for mercury ($\sigma = 0{\cdot}025$) and air ($\sigma = 0{\cdot}687$) are given in table 2.

We can now determine the range of validity of the ϵ^2 approximation. To the ϵ^4 approximation, (1.16) becomes

$$\epsilon^2 = -\frac{\lambda_2 + \sqrt{[\lambda_2^2 + 4\lambda_4(\lambda - \lambda_0)]}}{2\lambda_4}, \tag{3.20}$$

where the positive sign in front of the radical has been chosen so that $\epsilon^2 \to 0$ as $\lambda \to \lambda_0$. Only when $\lambda_2^2 > |4\lambda_4(\lambda - \lambda_0)|$ is the ϵ^2 approximation valid. From the values of λ_2 and λ_4 for air, $\lambda - \lambda_0 = -\frac{1}{4}\lambda_2^2/\lambda_4$ when $\lambda - \lambda_0 \doteqdot \lambda_0$ in the range $0 \leqslant \mathscr{T}_1^2 \leqslant 0{\cdot}1$. As $\mathscr{T}_1^2$ increases, the limiting value of $\lambda - \lambda_0$ decreases to $0{\cdot}03\lambda_0$ at $\mathscr{T}_1^2 \doteqdot 10$ and then asymptotically approaches $0{\cdot}16\lambda_0$. For mercury the value of $\lambda - \lambda_0$ beyond which the λ_4 approximation is no longer valid is λ_0 when $\mathscr{T}_1^2 = 0$, decreases to $0{\cdot}005\lambda_0$ when $\mathscr{T}_1^2 = 0{\cdot}5$, rises to $0{\cdot}14\lambda_0$ when $\mathscr{T}_1^2 = 10^4$ and then steadily decreases to $0{\cdot}09\lambda_0$ at $\mathscr{T}_1^2 = 10^8$. Therefore, the ϵ^4 approximation is valid for a rather limited range of λ. The λ_2 curve describes the system accurately in a slightly smaller range of λ.

$\mathscr{T}_1^2$	λ_4 (air)	λ_4 (mercury)	$\mathscr{T}_1^2$	λ_4 (air)	λ_4 (mercury)
0·1	0·0495	0·0971	10^3	−0·164	$0{\cdot}956 \times 10^{-2}$
0·5	0·168	0·286	10^4	−0·203	$0{\cdot}195 \times 10^{-2}$
1	0·230	0·354	10^5	−0·229	$0{\cdot}410 \times 10^{-3}$
5	0·122	0·277	10^6	−0·245	$0{\cdot}797 \times 10^{-4}$
10	0·042	0·196	10^7	−0·253	$0{\cdot}168 \times 10^{-5}$
10^2	−0·101	0·0499	10^8	−0·257	$0{\cdot}280 \times 10^{-5}$

TABLE 2. λ_4 for rolls.

In the non-rotating system (I), the ϵ^2 approximation for rolls is accurate for $\lambda - \lambda_0 \leqslant \lambda_0$. The more limited range of validity of λ_2 for air in the rotating problem can be traced to the stability problem itself. The system becomes unstable to a disturbance with the form of the second mode, i.e. $\sin 2\pi z$, at a relatively smaller value of λ. It was shown in § 2 that $(\lambda_0)_{n=2}/(\lambda_0)_{n=1} \to (16)^{\frac{1}{3}} = 2{\cdot}52$ as $\mathscr{T}_1^2 \to \infty$, whereas in the non-rotating system the ratio equals 16. Since the finite-amplitude solution is based on the linear stability problem, it can describe the system only in the range in which the fluid is not unstable to other disturbances. This range is ten times smaller in the rotating case (for large $\mathscr{T}_1^2$); therefore the corresponding approximation is accurate in an equally limited range. This reasoning does not apply to mercury where λ_2 is negative. In this case, the range of validity of the second-order approximation must be limited for the reason mentioned earlier. Nor can we apply the above reasoning to account for the extremely small range of validity of the ϵ^2 approximation for air when $\mathscr{T}_1^2 \doteqdot 10$. As we shall see later, the fluid behaves quite differently for these smaller values of $\mathscr{T}_1^2$ than it does either for zero rotation or for higher rotation rates.

From the expressions for the heat transport (3.10) and (3.11), we have to fourth order

$$\frac{H}{\kappa\beta_m} = 1 + \frac{\sigma\epsilon^2}{\lambda}[\{w_0 T_0\}_m + \epsilon^2\{w_0 T_2\}_m], \tag{3.21}$$

where the remaining terms in (3.11) vanish. Therefore,

$$\frac{H}{\kappa\beta_m} = 1 + \frac{\sigma\epsilon^2}{\lambda}\left[\frac{\sigma\lambda_0}{\pi^2(\alpha^2+1)} - \frac{\sigma\mathscr{T}_1^2}{2\alpha^4(\alpha^2+1)}\epsilon^2\right]. \tag{3.22}$$

For mercury, $\lambda_2 < 0$ and $\lambda_4 > 0$. Therefore, from (3.20), we note that the amplitude ϵ^2 increases as a result of the higher approximation. H increases with ϵ^2 so that the net effect of λ_4 is to turn the λ *vs* H curve (figure 7) toward the right, i.e. toward point A. In order to determine the actual behaviour of the system as the λ *vs* H curve is turned upward again, it would be necessary to consider the next approximation.

The most important result which we have obtained from this study of finite-amplitude convection for rolls is that fluids with a sufficiently small Prandtl number can become unstable to a finite-amplitude disturbance at a lower value of λ than λ_0. The non-linear vorticity generated by the finite-amplitude motions enables the fluid to reduce the effect of the external constraint and thereby become unstable at lower values of the external parameters.

(*b*) λ_2 *for rectangular cells*

Using the method outlined earlier, we can determine λ_2 for the rectangular cell. The detailed analysis is rather tedious and lengthy, so that only the results will be given.

The stability solution is

$$\left.\begin{aligned} w_0 &= 2\sqrt{2}\cos\pi lx\cos\pi my\sin\pi z, \quad T_0 = 2\sqrt{2}\,\sigma N_0\cos\pi lx\cos\pi my\sin\pi z,\\ u_0 &= -\left[\frac{2\sqrt{2}\,m\mathscr{T}_1}{\alpha^2(\alpha^2+1)}\cos\pi lx\sin\pi my + \frac{2\sqrt{2}\,l}{\alpha^2}\sin\pi lx\cos\pi my\right]\cos\pi z,\\ v_0 &= \left[\frac{2\sqrt{2}\,l\mathscr{T}_1}{\alpha^2(\alpha^2+1)}\sin\pi lx\cos\pi my - \frac{2\sqrt{2}\,m}{\alpha^2}\cos\pi lx\sin\pi my\right]\cos\pi z, \end{aligned}\right\} \tag{3.23}$$

where $2\sqrt{2}$ is the normalization constant for w_0, $N_0 = \dfrac{\lambda_0}{\pi^2(\alpha^2+1)}$ and $l^2+m^2 = \alpha^2$. Equations (2.5) and (2.6) again determine λ_0 and α^2 as functions of $\mathscr{T}_1$. The first-order functions are

$$\left.\begin{aligned} w_1 &= [a_1(l,m)\cos 2\pi lx + a_2(l,m)\cos 2\pi my]\sin 2\pi z,\\ T_1 &= [b_1(l,m)\cos 2\pi lx + b_2(l,m)\cos 2\pi my]\sin 2\pi z,\\ v_1 &= \left[\frac{\alpha_1\mathscr{T}_1}{4l(l^2+1)}\sin 2\pi lx - \frac{a_2}{m}\sin 2\pi my\right]\cos 2\pi z + \frac{\mathscr{T}_1}{2\pi l\alpha^2(\alpha^2+1)}\sin 2\pi lx\\ &\qquad + \frac{l\mathscr{T}_1}{2\pi\alpha^4(\alpha^2+1)}\sin 2\pi lx\cos 2\pi my,\\ u_1 &= -\left[\frac{a_1}{l}\sin 2\pi lx + \frac{a_2\mathscr{T}_1}{4m(m^2+1)}\sin 2\pi my\right]\cos 2\pi z\\ &\qquad - \frac{\mathscr{T}_1}{2\pi m\alpha^2(\alpha^2+1)}\sin 2\pi my - \frac{m\mathscr{T}_1}{2\pi\alpha^4(\alpha^2+1)}\cos 2\pi lx\sin 2\pi my, \end{aligned}\right\} \tag{3.24}$$

where $\lambda_1 = 0,$

$$a_1(l,m) = \frac{\dfrac{8\pi^3 l^2 m^2 \sigma N_0}{\alpha^2} + \dfrac{32\pi^5 l^2 m^2 (l^2+1)}{\alpha^4}\left[\alpha^2 + 1 + \dfrac{\mathscr{T}_1^2}{(\alpha^2+1)^2}\right]}{-4\pi^6[16(l^2+1)^3 + \mathscr{T}_1^2 - l^2\lambda_0/\pi^4]},$$

$$b_1(l,m) = \sigma\frac{\lambda_0 a_1 - 2\pi\sigma N_0 m^2/\alpha^2}{4\pi^2(l^2+1)},$$

$$a_2(l,m) = a_1(m,l), \quad b_2(l,m) = b_1(m,l).$$

From these zero- and first-order functions and from (3.1), an expression for λ_2 can be obtained:

$$\lambda_2 = \frac{\sigma^2 N_0}{2} - \frac{\pi}{2\alpha^2}(m^2 b_1 + l^2 b_2) + \frac{\pi^3}{2\alpha^4}(m^2 a_1 + l^2 a_2)\left[\frac{\mathscr{T}_1^2}{\alpha^2+1} - (\alpha^2+1)^2\right] + \frac{\mathscr{T}_1^2\pi^3}{2\alpha^4}\left[\frac{l^2 a_2}{m^2+1} + \frac{m^2 a_1}{l^2+1} + \frac{3}{2\pi(\alpha^2+1)}\right]. \quad (3.25)$$

As a function of the parameters σ, $\mathscr{T}_1$ and the ratio l/m, expression (3.25) for λ_2 has a triply infinite set of values. We shall restrict our attention here to the values of $\mathscr{T}_1^2$ which were considered in the subsection on rolls. Furthermore, we shall consider only two values of σ, those corresponding to mercury ($\sigma = 0{\cdot}025$) and air ($\sigma = 0{\cdot}687$). The ratio l/m cannot be chosen arbitrarily, of course, for it is a parameter whose value is determined by the physics of the system. In order to decide which of the infinite number of values of l/m is chosen by the fluid we turn now to the relative stability criterion which was developed in I.

The relative stability criterion is the answer to the following question. If all of the mathematically possible solutions of a statistically steady physical system are known, which of the solutions is stable to disturbances which have the form of any of the other solutions? When all of the solutions are orthogonal to each other (as in the present case), the criterion takes a particularly simple form. The fluid chooses that solution which has the maximum value of $\{\beta^2\}_m$. From (1.10) in non-dimensional form, $\{\beta^2\}_m$ can be written

$$1 + \frac{\sigma^2}{\lambda^2}\{[\{wT\}_m - \overline{wT}]^2\}_m. \quad (3.26)$$

To the ϵ^2 approximation, (3.26) is equal to

$$1 + \frac{\sigma^2\epsilon^4}{\lambda^2}\{[\{w_0 T_0\}_m - \overline{w_0 T_0}]^2\}_m = 1 + \frac{\sigma^4 N_0^2 \epsilon^4}{2\lambda^2} = 1 + \frac{\sigma^4 N_0^2(\lambda-\lambda_0)^2}{2\lambda^2\lambda_2^2}, \quad (3.27)$$

where (3.13) was used to derive the last equality. Since N_0 is not a function of l/m, the solution with maximum $\{\beta^2\}_m$ at a given value of λ is the solution with minimum λ_2 or maximum heat transport.

For this problem λ_2 as given by (3.25) has a minimum at* $l/m = \infty$ for small $\mathscr{T}_1^2$ and at* $l/m = 1$ for large $\mathscr{T}_1^2$. The value of $\mathscr{T}_1^2$ at which the preferred shape crosses over from $l/m = \infty$ to $l/m = 1$ depends upon the Prandtl number. Values of the

* When $l/m = \infty$, the cellular geometry is that of limiting rectangles, i.e. the cells take the form of rolls in the limit. When $l/m = 1$, the cells are square.

convective heat transport for air and mercury are given in table 3 for square cells and for limiting rectangles.

A result which is immediately evident upon comparing tables 1 and 3 is that the value of the heat transport for limiting rectangles differs markedly from the value for rolls. This difference was found also in the non-rotating case. Again the only conclusion which we can draw from these results is that one must use the limiting rectangle in the description of the two-dimensional case. Though neither the roll nor the limiting rectangle can satisfy lateral experimental boundary conditions, nevertheless the limiting rectangle can approximate long thin rectangular cells.

	Air		Mercury			Air		Mercury	
$\mathscr{T}_1^2$	Square	LR	Square	LR	$\mathscr{T}_1^2$	Square	LR	Square	LR
0·1	1·15	1·20	0·00623	0·0155	10^3	1·95	1·11	−0·0448	0·00993
0·5	0·971	0·961	0·00340	0·00455	10^4	2·06	1·23	−0·0361	0·0209
1	0·900	0·862	0·00275	0·00322	10^5	2·05	1·29	−0·0587	0·0445
5	0·896	0·782	0·00262	0·00244	10^6	2·03	1·31	−0·118	0·0924
10	0·983	0·807	0·00329	0·00270	10^7	2·02	1·32	−0·249	0·184
10^2	1·49	1·02	0·0126	0·00481	10^8	2·01	1·33	−0·608	0·342

TABLE 3. Convective heat transport $(\sigma\{wT\}_m)/(\lambda-\lambda_0)$ for steady square cells and limiting rectangles.

An additional fact which emerges from a comparison of tables 1 and 3 is that for air the heat transport of squares exactly coincides with that of rolls when $\mathscr{T}_1^2$ is large. Whether this is a chance coincidence or has some deeper significance has not been determined. Clearly the physical factors which enter into the determination of λ_2 are quite different in the two cases.

A definite qualitative difference between the two-dimensional and three-dimensional cases is illustrated by the heat transport for mercury. For rolls a finite-amplitude instability can occur throughout the range of $\mathscr{T}_1^2$ considered, whereas limiting rectangles will not become unstable to finite-amplitude perturbations.

We may note from table 3 that steady convective instability in mercury will set in the form of limiting rectangles for the range $0 \leqslant \mathscr{T}_1^2 \leqslant 3$. For higher values of $\mathscr{T}_1^2$, convection occurs in the form of square cells. Since overstability can occur (though at a higher Rayleigh number) when $\mathscr{T}_1^2 \doteqdot 4$, further discussion about the expected nature of convection must be postponed until the finite-amplitude effects of overstability are presented.

One can predict the cellular structure of air over a much larger range of $\mathscr{T}_1^2$. It is evident from table 3 that limiting rectangles will be preferred only when $\mathscr{T}_1^2 < 0{\cdot}5$. Since overstability cannot set in until $\mathscr{T}_1^2 \doteqdot 108$, convection will take place in the form of steady square cells in the range $0{\cdot}5 \leqslant \mathscr{T}_1^2 \leqslant 108$.

It should be noted also that the very small amplitude of heat convection in mercury indicates that the heat transport curve in the H *vs* λ graph starts off practically tangent to the conduction line when instability occurs.

In air the convective heat transport is much larger than it is in mercury. An interesting property for air exhibited by table 3 is that the convective heat transport for both the limiting rectangle and the square approach asymptotic values for large $\mathscr{T}_1^2$. The asymptotic value for square cells is equal to the value for rolls. Furthermore, the non-rotating roll has precisely the same value $(\sigma\{wT\}_m/(\lambda-\lambda_0)=2)$ for all fluids. The value of the heat transport for limiting rectangles at large $\mathscr{T}_1^2$, approaches the same value $\frac{4}{3}$ as it has in the non-rotating system.

The results for large $\mathscr{T}_1^2$ must be reconsidered in the light of finite-amplitude overstable motions. However, for small values of the Taylor number ($\leqslant 10^2$ for air, $\leqslant 10$ for mercury) it ought to be possible to check the above results experimentally. For instance, one ought to be able to see whether the limiting rectangle is actually the preferred cellular shape in air at very low rotation rates. The slope of the heat transport *vs* λ curve ought to be much steeper for low rotation rates than it is for zero rotation. Finally, the λ_4 values for rolls in air are positive when $\mathscr{T}_1^2$ is small. If this result bears even a qualitative significance to the realizable square or limiting rectangle, it would mean that for small $\mathscr{T}_1^2$ the heat transport is smaller than the value given by the λ_2 approximation.

To summarize the results of this section, we have found that in a fluid with a small Prandtl number it is possible that a finite-amplitude instability can occur before the fluid becomes unstable to infinitesimal perturbations. In this case, the finite-amplitude motions partially cancel the effect of the imposed constraint. For realizable cellular patterns in mercury this finite-amplitude instability will occur only in the range where overstability occurs first. It is, therefore, necessary to look into finite-amplitude overstable motions to determine whether the fluid can indeed be unstable to finite-amplitude disturbances.

4. Finite-amplitude overstable motions

In the analysis of these motions, the method of solution outlined in the previous section is inadequate. The difficulty which arises in the present case can be demonstrated by the following argument.

Let $w_0=\cos p_0\tau f(x,y)\,g(z)$ be the solution to (2.1*c*). Then u_0, v_0 and T_0 can be determined from the remaining equations of (2.1). The inhomogeneous terms of the equations for w_1, w_2, etc., contain products of the lower-order functions, and the individual inhomogeneous terms are operated on by operators such as $(\partial/\partial\tau)-\nabla^2$. As a result, terms of the type $\sin p_0\tau f(x,y)\,g(z)$ may appear as forcing terms but they do not contribute to the evaluation of the λ_i since they are orthogonal to the basic solution. Therefore, they remain as inhomogeneous terms and will give rise to secular terms in w_1, w_2, etc., because they satisfy the basic homogeneous equation. One cannot avoid the difficulty by introducing an arbitrary phase since the same difficulty arises regardless of the phase of the basic solution, i.e. out of phase components are always generated.

The present difficulty is not unique to the overstable problem. Indeed, one can conceive of examples in the steady problem in which the same problem arises. For example, in the basic roll solution, $w_0=\cos\pi\alpha x\,g(z)$, there are instances when a generated inhomogeneous term has the form $\sin\pi\alpha x\,g(z)$. In the examples of the

previous section these 'resonant' terms always cancelled identically. However, it is possible that in some problems this fortuitous cancellation will not occur.

To reduce the equations to a soluble sequence once again we add an additional expansion. Specifically, let

$$\tau = t/p, \tag{4.1}$$

so that $\dfrac{\partial}{\partial \tau} = \dfrac{\partial}{\partial t}\dfrac{\partial t}{\partial \tau} = p\dfrac{\partial}{\partial t}$. We now expand p in powers of ϵ as

$$p = p_0 + \epsilon p_1 + \epsilon^2 p_2 + \ldots. \tag{4.2}$$

where the p_i are to be determined.

If we add (4.1) and (4.2) to the expansions (1.15) and (1.16), the equations (1.11), (1.13) and (1.14) take the form (where we give only the ϵ^1 terms (a) and ϵ^2 terms (b))

$$\mathscr{L}w_0 \equiv \left[\left(\frac{p_0}{\sigma}\frac{\partial}{\partial t} - \nabla^2\right)^2\left(p_0\frac{\partial}{\partial t} - \nabla^2\right)\nabla^2 + \mathscr{T}^2\left(p_0\frac{\partial}{\partial t} - \nabla^2\right)\frac{\partial^2}{\partial z^2} - \lambda_0\left(\frac{p_0}{\sigma}\frac{\partial}{\partial t} - \nabla^2\right)\nabla_1^2\right] w_0 = 0, \tag{4.3a}$$

$$\begin{aligned}\mathscr{L}w_1 = -\Big\{p_1\Big[\frac{3p_0^2}{\sigma^2}\frac{\partial^3}{\partial t^3} - 2p_0\left(\frac{1}{\sigma^2}+\frac{2}{\sigma}\right)\frac{\partial^2}{\partial t^2}\nabla^2 + \left(1+\frac{2}{\sigma}\right)\frac{\partial}{\partial t}\nabla^4\Big]\nabla^2 + p_1\frac{\partial}{\partial t}\left(\mathscr{T}^2\frac{\partial^2}{\partial z^2} - \frac{\lambda_0}{\sigma}\nabla_1^2\right)\\ - \lambda_1\left(\frac{p_0}{\sigma}\frac{\partial}{\partial t} - \nabla^2\right)\nabla_1^2\Big\} w_0 + \mathscr{T}\left(p_0\frac{\partial}{\partial t} - \nabla^2\right)\frac{\partial Z_{00}}{\partial z} - \left(\frac{p_0}{\sigma}\frac{\partial}{\partial t} - \nabla^2\right)\nabla_1^2 h_{00}\\ + \left(p_0\frac{\partial}{\partial t} - \nabla^2\right)\left(\frac{p_0}{\sigma}\frac{\partial}{\partial t} - \nabla^2\right)L_{00};\end{aligned} \tag{4.3b}$$

$$\left(\frac{p_0}{\sigma}\frac{\partial}{\partial t} - \nabla^2\right)\zeta_0 = \mathscr{T}\frac{\partial w_0}{\partial z}, \tag{4.4a}$$

$$\left(\frac{p_0}{\sigma}\frac{\partial}{\partial t} - \nabla^2\right)\zeta_1 = \mathscr{T}\frac{\partial w_1}{\partial z} - \frac{p_1}{\sigma}\frac{\partial \zeta_0}{\partial t} - Z_{00}; \tag{4.4b}$$

etc.

$$\left(p_0\frac{\partial}{\partial t} - \nabla^2\right)T_0 = \sigma\lambda_0 w_0. \tag{4.5a}$$

$$\left(p_0\frac{\partial}{\partial t} - \nabla^2\right)T_1 = \sigma\lambda_0 w_1 - p_1\frac{\partial T_0}{\partial t} + \sigma\lambda_1 w_0 - \sigma h_{00}; \tag{4.5b}$$

etc.

The continuity equation has the form (3.4).

One can now proceed in the same manner as in the steady case. However, both sets of undetermined coefficients p_i and λ_i are used to eliminate the resonant terms whose forms are $\cos tf(x,y)\,g(z)$ and $\sin tf(x,y)\,g(z)$. Using this method we find that the frequency p of the overstable oscillation changes with amplitude. It is clear that if out-of-phase resonant terms had been generated in the steady case, one would have had to expand α in powers of ϵ, i.e. the basic spatial wave number would have been a direct function of amplitude also.

The algebra involved in the solution of the overstable case is so extremely tedious and lengthy that only the solution to the stability problem and the method of procedure will be outlined here. The expressions for w_1, T_1, etc.. and for λ_2, p_2 will not be written explicitly.

For the general rectangle, the solution of the stability problem is*

$$\left.\begin{aligned}
w_0 &= 4\cos t\cos\pi lx\cos\pi my\sin\pi z,\\
T_0 &= \frac{4\pi^2\sigma\lambda_0/\pi^4}{p_0^2/\pi^4+(\alpha^2+1)^2}[(\alpha^2+1)\cos t+p_0/\pi^2\sin t]\cos\pi lx\cos\pi my\sin\pi z,\\
u_0 &= -4\left\{\frac{l}{\alpha^2}\cos t\sin\pi lx\cos\pi my\right.\\
&\qquad\left.+\frac{m}{\alpha^2}\mathscr{T}_1\frac{[\sigma^2(\alpha^2+1)\cos t+\sigma(p_0/\pi^2)\sin t]}{p_0^2/\pi^4+\sigma^2(\alpha^2+1)^2}\cos\pi lx\sin\pi my\right\}\cos\pi z.\\
v_0 &= 4\left\{\frac{l}{\alpha^2}\mathscr{T}_1\frac{\sigma^2(\alpha^2+1)\cos t+\sigma(p_0/\pi^2)\sin t}{p_0^2/\pi^4+\sigma^2(\alpha^2+1)^2}\sin\pi lx\cos\pi my\right.\\
&\qquad\left.-\frac{m}{\alpha^2}\cos t\cos\pi lx\sin\pi my\right\}\cos\pi z.
\end{aligned}\right\}\tag{4.6}$$

The inhomogeneous term in (4.3*b*) can be determined as a function of p_1, λ_1 and the remaining (known) parameters of the problem. We now have an expression with non-resonant forcing terms plus terms of the type

$$[(ap_1+b\lambda_1+c)\cos t+(dp_1+e\lambda_1+f)\sin t]\cos\pi lx\cos\pi my\sin\pi z.$$

The coefficients a, b, c, d, e and f are functions of previously determined parameters. One evaluates p_1 and λ_1 so that the coefficients of the resonant term vanish. It is then possible to go on and determine the higher order λ_i and p_i in the same manner.

As in the steady case, λ_1 vanishes and $p_1 \equiv 0$ here. Therefore, we must consider ϵ^2 terms to determine the first finite-amplitude effects. This evaluation was carried out for the case of the general rectangle and numerical results were computed for square cells and limiting rectangles in air and mercury. The results for the convection heat transport (as given by the ϵ^2 approximation (3.14)) for overstability are shown in table 4.

A comparison of the values of the convective heat transport for air in tables 3 and 4 indicates that heat is convected in air by steady cellular motions for $\mathscr{T}_1^2 < 10^6$. However, for $\mathscr{T}_1^2 \geqslant 10^6$, overstable oscillations with a cellular pattern of squares will become the preferred motion *in finite amplitude* even though instability occurs as steady convection. The preference for overstability is very slight, and experimentally one may expect either type of motion to occur. The sequence of preferred finite-amplitude motions in air is: steady convective

* We can, of course, include arbitrary phases in the horizontal co-ordinate dependence and in the time dependence. However, no loss of generality is involved in writing the solution as given by (4.6). The ensemble average is now an average over the horizontal space and time periods, i.e. $\dfrac{1}{8\pi lm}\displaystyle\int_{-l}^{l}\int_{-m}^{m}\int_{0}^{2\pi}\{\ \}\,dx\,dy\,dt$.

limiting rectangles for $\mathscr{T}_1^2 < 0{\cdot}5$, steady convective squares for $0{\cdot}5 \leqslant \mathscr{T}_1^2 < 10^6$, and overstable square cells for $\mathscr{T}_1^2 \geqslant 10^6$.

The cross-over from steady convection to overstability in mercury takes place at lower values of $\mathscr{T}_1^2$ and is indeed much more definite. As we noted earlier, steady limiting rectangles occur for $\mathscr{T}_1^2 < 3$ and the system changes over to

	Mercury		Air	
$\mathscr{T}_1^2$	Square	LR	Square	LR
5	0·00416	0·0016	—	—
10	0·00431	0·00303	—	—
10^2	0·0136	0·0207	—	—
10^3	0·0394	0·0444	1·14	1·31
10^4	0·0733	0·0728	1·66	1·55
10^5	0·107	0·105	1·95	1·59
10^6	0·128	0·126	2·07	1·60
10^7	0·138	0·136	2·13	1·61
10^8	0·146	0·144	2·16	1·62

TABLE 4. Convective heat transport for overstable square cells and limiting rectangles.

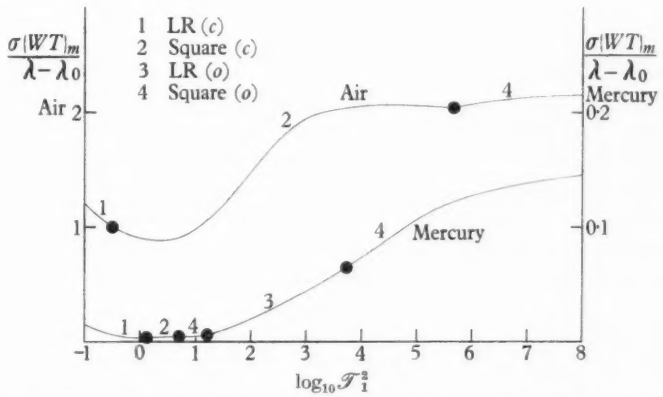

FIGURE 8. The convective heat transport values for air and mercury as functions of $\mathscr{T}_1^2$. The numbers on the portions of the curves lying between the dots mark the type of convective motions which occur in the specified ranges of $\mathscr{T}_1^2$. (*c*) corresponds to steady convective motions, (*o*) to overstable motions.

steady square cells when $\mathscr{T}_1^2 \geqslant 3$. Overstable square cells are preferred when $\mathscr{T}_1^2 \doteqdot 4{\cdot}5$ and remain as the preferred motion until $\mathscr{T}_1^2 \doteqdot 20$. However, at this point overstable limiting rectangles come in and are preferred to squares until $\mathscr{T}_1^2 \doteqdot 7 \times 10^3$, when overstable square cells become preferred again. These results are summarized in figure 8. It should be noted that the preference for square cells over limiting rectangles at large Taylor numbers is based on a very small

difference in heat transport (1 to 2 %). It may therefore be very difficult to obtain any recognizable stable pattern unless one were to make the determination at larger λ where higher order effects may conceivably solidify the preference.

The convective heat transport for mercury is a small fraction of the conductive heat transport throughout the range of $\mathscr{T}_1^2$ considered, and one may expect the H *vs* λ curve for $\lambda \geqslant \lambda_0$ to be practically tangent to the conduction line until higher order effects become important. In air the heat transport curve breaks away quite sharply after instability and has about twice the slope of the pure conduction line.

	Mercury		Air	
$\mathscr{T}_1^2$	Square	LR	Square	LR
5	11·3	0·735	—	—
10	2·30	1·80	—	—
10^2	0·332	1·18	—	—
10^3	$6{\cdot}28 \times 10^{-2}$	0·263	−2·14	1·33
10^4	$5{\cdot}46 \times 10^{-3}$	$6{\cdot}03 \times 10^{-2}$	−1·16	0·466
10^5	$-2{\cdot}48 \times 10^{-3}$	$2{\cdot}13 \times 10^{-2}$	−0·558	0·160
10^6	$-1{\cdot}93 \times 10^{-3}$	$8{\cdot}61 \times 10^{-3}$	−0·292	0·0616
10^7	$-9{\cdot}91 \times 10^{-4}$	$4{\cdot}20 \times 10^{-3}$	−0·138	0·0260
10^8	$-5{\cdot}80 \times 10^{-4}$	$1{\cdot}80 \times 10^{-3}$	−0·0645	0·0115

TABLE 5. The coefficient $p_2\lambda_0/p_0\lambda_2$ for mercury and air.

One of the most important results in the finite-amplitude study of overstable convection is that neither mercury nor air become unstable to finite-amplitude perturbations. Since the overstable oscillations in mercury take place at a much lower value of λ_0 than does steady convective instability, the fact that the latter can become unstable to finite-amplitude perturbations will not be observed experimentally.

The finite-amplitude effects on the frequency of the oscillation can be determined by (4.2) which, to the ϵ^2 approximation, has the form

$$\frac{p}{\pi^2} = \frac{p_0}{\pi^2} + \frac{\epsilon^2}{\pi^2} p_2. \tag{4.7}$$

Using (3.13), equation (4.7) can be written

$$\frac{p}{\pi^2} = \frac{p_0}{\pi^2}\left\{1 + \frac{p_2\lambda_0}{p_0\lambda_2}\left(\frac{\lambda}{\lambda_0} - 1\right)\right\}. \tag{4.8}$$

The coefficient $p_2\lambda_0/p_0\lambda_2$ is shown in table 5 for air and mercury. When the change in the frequency is negative, the correction decreases the convective heat transport (since λ_2 is a function of p_2). One of the most surprising features exhibited by the change in the frequency is the magnitude of effect on the heat transport even when the change in the frequency is extremely small, as it is for higher rotation rates in mercury. Indeed, the value of λ_2 in mercury without the

p_2 correction is negative for $10^4 \leqslant \mathscr{T}_1^2 \leqslant 10^7$. The change in frequency causes λ_2 to become positive, and the system is stable to finite-amplitude perturbations. Thus, the non-linear change in frequency effectively stabilizes the system in this part of the range. Where p_2 is positive, the non-linear change in frequency makes the system less stable.

5. Summary and conclusions

The most important conclusion in the stability investigation is that overstability occurs because the fluid is thereby able to reduce the constraint of the imposed rotation. A second conclusion of considerable interest is that in steady convective instability the wavelength of the cell measured along the boundary (as it is distorted by the rotation) is equal to the wavelength of the non-rotating cell. Other results (which are explicitly or implicitly contained in Chandrasekhar's original investigation (1953)) are that overstability cannot occur in a fluid with a Prandtl number greater than $\sqrt{\frac{2}{3}}$ because the rate of dissipation of kinetic energy always exceeds the rate of release of potential energy for larger σ, and that overstability cannot occur for sufficiently low rotation rates because the tendency of the fluid to undo the external constraint is more than offset by the increased dissipation due to the time-dependent motions.

For a range of the external parameters it is possible for the fluid, through finite-amplitude growth, to decrease the effect of the external constraint by generating a motion to counteract the effects of the imposed constraint. In cases where this happens, the fluid may become unstable to finite-amplitude disturbances before it becomes unstable to infinitesimal perturbations. Neither air nor mercury, the two fluids considered here, will exhibit this finite-amplitude behaviour under laboratory conditions.

More particular results in the finite-amplitude study are as follows. As the rotation rate is increased, the preferred cellular pattern for convection in air changes from steady limiting rectangles to steady squares to overstable squares (overstable square cells are preferred in finite amplitude even though the fluid first becomes unstable to steady convective motions). In mercury the sequence of preferred cellular shapes changes with increasing Taylor numbers from steady limiting rectangles, to steady squares, to overstable squares, to overstable limiting rectangles, and finally, when $\mathscr{T}_1^2 \doteq 10^6$, to overstable squares again. The heat convected by mercury after instability is only a small fraction of the conducted heat, and consequently the H *vs* λ curve will not show the very sharp breaks which are exhibited in the non-rotating system. In air the convective heat transport is at least as large as the conductive transport for all rotation rates, and the H *vs* λ curve will show a sharp break at the point of instability.

The frequency of the oscillations in overstable motions is a direct function of the amplitude. The change in frequency is too small to be noticeable in mercury when $\mathscr{T}_1^2 > 50$. However, even when small, the change in frequency has a marked effect on the heat transport.

According to the present investigation the fluid reacts to the imposed constraint by generating internal motions which counteract the external constraint. This result hints rather strongly that in general, when a fluid is subjected to

external constraints, it may generate motions which tend to offset the constraint.* In particular, in an electrically conducting fluid it is possible that a magnetic disturbance will grow so as to offset even further the constraint of the imposed rotation. In such a case the preferred convective state would be one with a self-generated magnetic field.

An additional suggested result with fairly broad application is the reason for the possible occurrence of a finite-amplitude instability. In other problems, such as shear flow in a channel, a finite amplitude instability can also occur (Meksyn & Stuart 1951). The one feature which these problems have in common is the dual role of viscosity mentioned in the introduction. Viscosity acts as an energy-releasing mechanism as well as a dissipative mechanism. Since finite-amplitude growth is invariably accompanied by increased viscous dissipation, one would not expect a finite-amplitude instability to occur unless the fluid were able to release even more potential energy. The fact that viscosity can fulfil the role as the energy-releasing mechanism suggests that this dual role of viscosity is essential to finite-amplitude instability.

It is interesting to note that the information concerning the appearance of a finite-amplitude instability is a consequence of an investigation which is pivoted about the linear stability problem. Application of the method described here to other problems, such as shear flow in a channel, may yield important results concerning the possible occurrence of finite-amplitude instability. One still feels, however, that the tools which we possess for treating finite-amplitude problems are woefully inadequate and that a more direct approach to non-linear stability problems should be sought.

A note should be added about an alternative, integral, technique for determining finite-amplitude effects. The method employed by Stuart (1958) and discussed in I is based on the power integral which can be derived by multiplying (1.11) by T and averaging. If quantities with the form of the stability solution are substituted into the power integral, one can then deduce the amplitude of w or T as a function of the external parameter λ. However, in the present problem this type of evaluation would yield results which are misleading because the principal effects in the determination of amplitude are those which result from the zero-average non-linear terms. These terms do not appear in the power integral.

Finally, what are the possible applications of these results to the fields of geophysics and astrophysics? (*a*) The formal technique described here together with the relative stability criterion provides a means for determining the

* The first finite-amplitude result (λ_2) for rolls was computed for an electrically conducting fluid subjected to heating from below and cooling from above and with an imposed magnetic field. As Chandrasekhar (1952) has shown, the imposed magnetic field acts as a constraint on the system in much the same manner as does the rotation. In the finite-amplitude computation, λ_2 is negative for a restricted range of the parameter η/κ, where η is the magnetic diffusivity. The range lies within the range of values of η/κ within which overstability can occur. Therefore, the possibility of finite amplitude instability exists also for this case, although it cannot occur in experiments realizable in the laboratory. The parametric values correspond to those which can exist in stellar atmospheres as Chandrasekhar has shown.

preferred finite-amplitude configuration of any statistically steady system with a solved stability problem. The principal limitation of the method lies in the formidable computations which may be required to carry out the analysis. (*b*) The very important role of viscosity as the energy releasing mechanism in a gyroscopically constrained system indicates that one ought to exercise some care in using such approximations as that of geostrophic flow in discussing the energetics of the fluid. (*c*) The ability of a fluid to react to externally imposed conditions may lead to a fuller understanding of the mechanistic behaviour of large-scale systems such as the atmosphere or the ocean.

A number of the ideas which are presented in this paper were a direct result of discussions with W. V. R. Malkus, and I wish to acknowledge his many valuable suggestions. The work was performed under the auspices of the Office of Naval Research and is Contribution no. 985 from the Woods Hole Oceanographic Institution.

REFERENCES

Boussinesq, J. 1903 *Theorie Analytique de la Chaleur*, **2**, 172. Paris: Gauthier-Villars.

Chandrasekhar, S. 1952 On the inhibition of convection by a magnetic field. *Phil. Mag.* (7), **43**, 501.

Chandrasekhar, S. 1953 The instability of a layer of fluid heated below and subject to coriolis forces. *Proc. Roy. Soc.* A, **217**, 306.

Christopherson, D. G. 1940 *Quart. J. Math.* **11**, 63.

Fultz, D. & Nakagawa, Y. 1955 *Proc. Roy. Soc.* A, **231**, 198.

Gor'kov, L. P. 1957 *J. Exptl. Theor. Phys.* (*U.S.S.R.*), **33**, 402.

Malkus, W. V. R. & Veronis, G. 1958 Finite amplitude cellular convection. *J. Fluid Mech.* **4**, 225.

Meksyn, D. & Stuart, J. T. 1951 *Proc. Roy. Soc.* A, **208**, 517.

Nakagawa, Y. & Frenzen, P. 1955 A theoretical and experimental study of cellular convection in rotating fluids. *Tellus*, **7**, 1.

Stuart, J. T. 1958 On the non-linear mechanics of hydrodynamic stability. *J. Fluid Mech.* **4**, 1.

Ring vortices generated electromagnetically

By CHIA-SHUN YIH
Department of Engineering Mechanics, University of Michigan

(Received 9 September 1958)

If an electric current of uniform density j_0 is passed axially through a stationary fluid between concentric cylinders of radii r_1 and r_2 ($> r_1$), the fluid is stable to axisymmetric disturbances only if the damping provided by viscosity and electrical resistivity is sufficiently large. It is shown herein that the fluid may also be stabilized by passing a line current J along the axis, sufficient conditions for stability being

$$J \leqslant -\pi j_0(r_2^2 - r_1^2), \quad \text{or} \quad \geqslant J\ \pi j_0 r_1^2.$$

The values of J needed to stabilize the fluid when the fluid has non-zero viscosity and finite conductivity are calculated for the case $r_2 - r_1 \ll r_1$. In this latter case, the ring vortices which exist under conditions of neutral stability are exactly the same as those for flow between rotating cylinders if J and j_0 have the same sign, and if J is not very small compared with $\pi j_0 r^2$.

1. Introduction

In a remarkable paper (Taylor 1923), Taylor presented the results of his analytical and experimental investigation of the stability of a viscous fluid between two rotating cylinders. The vortices which he found in the fluid for unstable conditions have since been found to be present in many fluid flows with curved streamlines. The cause of these vortices is here dynamical in nature, i.e. it is due to the centripetal acceleration of the fluid which is tantamount to a centrifugal force. Can similar ring vortices be created in a quiescent fluid? The answer is in the affirmative if electromagnetic forces are allowed. In the following sections, it will be shown that Taylor vortices can occur in a fluid between concentric cylinders if a longitudinal electric current passes along the axis of the cylinders and another passes through the fluid. Specific results are given for small differences in radii. The cause of instability is the *centripetal* electromagnetic body force acting on the fluid in the undisturbed state.

2. The undisturbed state

The relationship between magnetic field strength $\mathbf{H}$ and current density $\mathbf{j}$ is

$$\operatorname{curl} \mathbf{H} = 4\pi \mathbf{j}. \tag{1}$$

In cylindrical co-ordinates (r, θ, z), a current J along the centre line (z-axis) of the cylinders will give rise to a circular magnetic field equal to $2J/r$, current being counted as positive if it is in the positive z-direction. The circular magnetic field due to a current of density j_0 passing between the cylinders in the axial direction

is $2\pi j_0(r^2-r_1^2)/r$, if the radii of the cylinders are denoted by r_1 and $r_2(>r_1)$. Thus the undisturbed state is characterized by

$$\bar{H}_r=\bar{H}_z=0, \quad \bar{H}_\theta=2\pi\left(\frac{J'}{\pi r}+j_0 r\right), \quad J'=J-\pi j_0 r_1^2. \tag{2}$$

It can be shown that a quiescent state of the fluid is consistent with the magnetic field given by equations (2), and that the only effect the field has is to change the (hydrostatic) pressure by an amount consistent with the equation of equilibrium.

The electromagnetic body force per unit volume of the fluid is $-\mu j_0 H_\theta$ acting in the (outward) radial direction. Since this body force is similar to the pseudo-body-force (so-called centrifugal force) in the case of a fluid under rotation, instability of the fluid can be expected to occur under suitable conditions.

3. Formulation of the problem

With (u, v, w) and (H_r, H_θ, H_z) denoting the components of the velocity and of the magnetic field strength in the directions of the (r, θ, z)-co-ordinate lines, the equations of motion for an incompressible fluid are

$$\rho\left(\frac{Du}{D\tau}-\frac{v^2}{r}\right)=-\frac{\partial\chi}{\partial r}+\rho\nu\left(\nabla^2 u-\frac{u}{r^2}-\frac{2}{r^2}\frac{\partial v}{\partial\theta}\right)+\frac{\mu}{4\pi}\left(\frac{\mathscr{D}H_r}{\mathscr{D}\tau}-\frac{H_\theta^2}{r}\right),$$

$$\rho\left(\frac{Dv}{D\tau}+\frac{uv}{r}\right)=-\frac{1}{r}\frac{\partial\chi}{\partial\theta}+\rho\nu\left(\nabla^2 v-\frac{v}{r^2}+\frac{2}{r^2}\frac{\partial u}{\partial\theta}\right)+\frac{\mu}{4\pi}\left(\frac{\mathscr{D}H_\theta}{\mathscr{D}\tau}+\frac{H_r H_\theta}{r}\right),$$

$$\rho\frac{Dw}{D\tau}=-\frac{\partial\chi}{\partial z}+\rho\nu\nabla^2 w+\frac{\mu}{4\pi}\frac{\mathscr{D}H_z}{\mathscr{D}\tau},$$

in which

$$\chi=p+\frac{\mu|\mathbf{H}|^2}{8\pi}+\rho\Omega,$$

$$\frac{\mathscr{D}}{\mathscr{D}\tau}\equiv H_r\frac{\partial}{\partial r}+\frac{H_\theta}{r}\frac{\partial}{\partial\theta}+H_z\frac{\partial}{\partial z},$$

$$\frac{D}{D\tau}\equiv\frac{\partial}{\partial\tau}+u\frac{\partial}{\partial r}+\frac{v}{r}\frac{\partial}{\partial\theta}+w\frac{\partial}{\partial z},$$

$$\nabla^2\equiv\frac{\partial^2}{\partial r^2}+\frac{1}{r}\frac{\partial}{\partial r}+\frac{1}{r^2}\frac{\partial^2}{\partial\theta^2}+\frac{\partial^2}{\partial z^2},$$

and ρ is the density, τ the time, ν the kinematic viscosity, μ the magnetic permeability, and Ω the gravitational potential per unit mass. The equations for the magnetic field are

$$\frac{DH_r}{D\tau}=\frac{\mathscr{D}u}{\mathscr{D}\tau}+\eta\left(\nabla^2 H_r-\frac{H_r}{r^2}-\frac{2}{r^2}\frac{\partial H_\theta}{\partial\theta}\right),$$

$$\frac{DH_\theta}{D\tau}+\frac{vH_r}{r}=\frac{\mathscr{D}v}{\mathscr{D}\tau}+\frac{H_\theta u}{r}+\eta\left(\nabla^2 H_\theta-\frac{H_\theta}{r^2}+\frac{2}{r^2}\frac{\partial H_r}{\partial\theta}\right),$$

$$\frac{DH_z}{D\tau}=\frac{\mathscr{D}w}{\mathscr{D}\tau}+\eta\nabla^2 H_z,$$

in which η is the magnetic diffusivity.

A disturbance of the stationary fluid will give rise to small velocity components (u, v, w), and a deviation from the equilibrium magnetic field denoted by (h_r, h_θ, h_z). The total magnetic field is then given by

$$h_r, \quad 2\pi\left(\frac{J'}{\pi r}+j_0 r\right)+h_\theta, \quad h_z.$$

If these are substituted in the equations of motion and the equations of magnetic diffusion and all quadratic terms in u, v, w, and the h's are neglected, and if axisymmetry is assumed, the following linearized equations are obtained:

$$\rho\frac{\partial u}{\partial \tau}=-\frac{\partial \chi'}{\partial r}+\rho\nu\left(\nabla^2 u-\frac{u}{r^2}\right)-\mu\left(\frac{J'}{\pi r^2}+j_0\right)h_\theta, \tag{3}$$

$$\rho\frac{\partial v}{\partial \tau}=\rho\nu\left(\nabla^2 v-\frac{v}{r^2}\right)+\mu j_0 h_r, \tag{4}$$

$$\rho\frac{\partial w}{\partial \tau}=-\frac{\partial \chi'}{\partial z}+\rho\nu\nabla^2 w, \tag{5}$$

$$\frac{\partial h_r}{\partial \tau}=\eta\left(\nabla^2 h_r-\frac{h_r}{r^2}\right), \tag{6}$$

$$\frac{\partial h_\theta}{\partial \tau}=\frac{4J'}{r^2}u+\eta\left(\nabla^2 h_\theta-\frac{h_\theta}{r^2}\right), \tag{7}$$

$$\frac{\partial h_z}{\partial \tau}=\eta\nabla^2 h_z. \tag{8}$$

in which $$\nabla^2\equiv\frac{\partial^2}{\partial r^2}+\frac{1}{r}\frac{\partial}{\partial r}+\frac{\partial^2}{\partial z^2}, \quad \chi'=p'+\frac{\mu}{4\pi}\bar{H}_\theta h_\theta,$$

with p' denoting the pressure perturbation. The equation of continuity is

$$\frac{\partial(ru)}{\partial r}+\frac{\partial(rw)}{\partial z}=0, \tag{9}$$

since compressibility can be neglected.

From the form of equations (6) and (8) we can conclude that h_r and h_z will be damped out if they are not initially everywhere zero (see Yih 1959). Then from equation (4) we conclude further that v will also be damped out. The differential equations to be dealt with are then equations (3), (5) and (7). Eliminating χ' from equations (3) and (5), we have

$$\rho\frac{\partial}{\partial \tau}\left(\frac{\partial w}{\partial r}-\frac{\partial u}{\partial z}\right)=\rho\nu\left(\nabla^2-\frac{1}{r^2}\right)\left(\frac{\partial w}{\partial r}-\frac{\partial u}{\partial z}\right)+\mu\left(\frac{J'}{\pi r^2}+j_0\right)\frac{\partial h_\theta}{\partial z}. \tag{10}$$

We define dimensionless variables

$$(r', z')=\left(\frac{r}{r_1}, \frac{z}{r_1}\right), \quad t=\frac{\tau\nu}{r_1^2},$$

$$(u_1, w_1)=\left(\frac{ur_1}{\nu}, \frac{wr_1}{\nu}\right), \quad h_1=\frac{h_\theta}{j_0 r_1},$$

where r_1 and r_2 are the radii of the inner and outer cylinders. Then, on dropping the primes on r and z, we can write equations (10) and (7) as

$$\frac{\partial}{\partial t}\left(\frac{\partial w_1}{\partial r}-\frac{\partial u_1}{\partial z}\right)=\left(\nabla^2-\frac{1}{r^2}\right)\left(\frac{\partial w_1}{\partial r}-\frac{\partial u_1}{\partial z}\right)+A\left(\frac{B}{r^2}+1\right)\frac{\partial h_1}{\partial z}, \tag{11}$$

$$\frac{\partial h_1}{\partial t}=\frac{\eta}{\nu}\left(\nabla^2-\frac{1}{r^2}\right)h_1+\frac{4\pi B}{r^2}u_1, \tag{12}$$

in which

$$A=\frac{\mu j_0^2 r_1^4}{\rho\nu^2}, \quad B=\frac{J'}{\pi j_0 r_1^2}. \tag{13}$$

Following Taylor, we can make the following substitutions:

$$(u_1, w_1, h_1)=[U(r)\cos mz, \quad W(r)\sin mz, \quad h(r)\cos mz]\,e^{\sigma t},$$

in which m is the wave number for the z-direction. The equation of continuity then becomes

$$rU'+U+mrW=0, \tag{14}$$

and equations (11) and (12) become

$$(L-m^2-\sigma)(L-m^2)\,U=-m^2A\left(\frac{B}{r^2}+1\right)h, \tag{15}$$

$$\left(L-m^2-\frac{\sigma\nu}{\eta}\right)h=-\frac{4\pi B\nu}{\eta r^2}U, \tag{16}$$

in which

$$L=D\left\{\frac{1}{r}D(r\ )\right\}, \quad D=\frac{d}{dr}.$$

With

$$U=-m^2Af \quad \text{and} \quad N=\frac{4\pi AB\nu}{\eta},$$

equations (15) and (16) can be written as

$$(L-m^2-\sigma)(L-m^2)f=\left(\frac{B}{r^2}+1\right)h, \tag{17}$$

$$\left(L-m^2-\frac{\sigma\nu}{\eta}\right)h=m^2N\frac{f}{r^2}. \tag{18}$$

The boundary conditions corresponding to

$$U=W=0 \quad \text{at} \quad r=1 \quad \text{and} \quad r=\frac{r_2}{r_1}=\alpha$$

are

$$f=Df=0 \quad \text{at} \quad r=1 \text{ and } r=\alpha. \tag{19}$$

The simplest realistic boundary condition for h is that which corresponds to zero electrical conductivity of the walls, that is, to $j_r=0$. But

$$j_r=\frac{1}{r}\frac{\partial h_3}{\partial\theta}-\frac{\partial h_\theta}{\partial z}=-\frac{\partial h_\theta}{\partial z} \quad \text{(for axisymmetry)},$$

and so the boundary condition for h is

$$h=0 \quad \text{at} \quad r=1 \text{ and } r=\alpha \tag{20}$$

for non-conducting walls. The task is to find the relationship between N and m for a given value of B, from the differential system consisting of equations (17) and (20).

4. Sufficient condition for stability

A sufficient condition for stability can be given on physical grounds, in the manner of Rayleigh (1916), or on mathematical grounds, in the manner of Synge (1938). The physical proof relies upon the fact that for a magnetically non-diffusive fluid ($\eta = 0$) the lines of force move with the fluid. The proof for this well-known fact is identical with the proof for vorticity lines in an inviscid fluid (Lamb 1945, p. 204), and is available elsewhere. In § 3 of this paper it has been shown that H_r and H_z (or h_r and h_z) will be damped out. In a discussion of the sufficient condition for stability it can thus be assumed that only H_θ is different from zero. Since the total magnetic flux round a thin material ring of fluid is constant, and since by continuity the volume of this ring must be constant, so that its cross-section varies inversely as its radius r', H_θ must be equal to kr' (r' dimensional), with k as the constant (for the ring as it moves) of proportionality. The body force per unit volume in the r-direction, which is in general (Yih 1959)

$$\frac{\mu}{4\pi}\left(-\frac{\frac{1}{2}\partial(\partial|\mathbf{H}|^2)}{\partial r}+H_r\frac{\partial H_r}{\partial r}+\frac{H_\theta}{r}\frac{\partial H_r}{\partial \theta}+H_z\frac{\partial H_r}{\partial z}-\frac{H_\theta^2}{r}\right),$$

can in the present discussion be written as

$$-\frac{\mu}{4\pi}H_\theta\left(\frac{\partial H_\theta}{\partial r}+\frac{H_\theta}{r}\right).$$

Now imagine the thin material ring with a magnetic flux in the θ-direction to be instantaneously situated at the position indicated by r'. The sole effect of the term

$$-\frac{\mu}{4\pi}H_\theta\frac{\partial H_\theta}{\partial r}$$

is to reduce the pressure throughout the ring by an amount $\mu H_\theta^2/8\pi$, and therefore has no effect on the work done by the ring against pressure applied externally on the surface of the ring. Consequently, the only force acting on the ring which can be properly counted as a body force is

$$-\frac{\mu}{4\pi}\frac{H_\theta^2}{r}.$$

Since the instantaneous value for r is r' for the thin ring, and since $H_\theta = kr'$, this force can be written as

$$-\frac{\mu}{4\pi}k^2r'.$$

The potential energy due to this centripetal force is then $\mu k^2 r'^2/8\pi$, which increases with r' for any particular value of k.

Returning to the distribution of the mean field $\bar{H}_\theta$ specified earlier in this paper, we can imagine the fluid in its mean configuration to be composed of thin shells, each with a different value for k given by

$$k=\frac{\bar{H}_\theta}{r}=2\pi\left(\frac{J'}{\pi r^2}+j_0\right).$$

Since a higher value of k^2 corresponds to a 'heavier' fluid, and since stability will ensue if a 'heavier' fluid shell occupies a position of lower potential energy (hence smaller r), one concludes that a sufficient condition for stability is that the quantity

$$\left(\frac{J'}{\pi r^2}+j_0\right)^2$$

does not increase outwards—a situation which is possible only if

$$J \leqslant -\pi j_0(r_2^2-r_1^2) \quad \text{or} \quad J \geqslant j_0 r_1^2.$$

In this physical proof magnetic diffusivity has been neglected. It is tacitly assumed that, if a fluid with no magnetic diffusivity is stable, one with magnetic diffusivity will be so *a fortiori*. For the type of instability under discussion, this is a valid assumption, as will be demonstrated by a mathematical proof (of the sufficient conditions just reached), in which the effects of viscosity and magnetic diffusivity are not neglected. Whether magnetic diffusivity can have a destabilizing effect on certain flows, in the manner that viscosity can sometimes be destabilizing, is not known. An investigation of this possibility would be highly interesting.

For a mathematical proof of the same result one turns to the dimensionless equations (17) to (20). Multiplying equation (17) by $r\bar{f}$ ($\bar{f}$ being the complex conjugate of f) and integrating (by parts if necessary) with respect to r between 1 and α, we have, upon utilization of the boundary conditions on f,

$$I_2+(2m^2+\sigma)I_1+m^2(m^2+\sigma)I_0=\int_1^\alpha\left(\frac{B}{r^2}+1\right)rh\bar{f}\,dr, \tag{21}$$

in which

$$I_0=\int_1^\alpha r|f|^2dr, \quad I_1=\int_1^\alpha\frac{1}{r}|Drf|^2dr, \quad I_2=\int_1^\alpha r|Lf|^2dr.$$

Similarly, by multiplying equation (18) by $r\bar{h}$ and $r^3\bar{h}$ and integrating, one obtains, respectively,

$$H_1+\left(m^2+\frac{\nu\sigma}{\eta}\right)H_0=-m^2N\int_1^\alpha\frac{f\bar{h}}{r}dr, \tag{22}$$

$$H_3+\left(m^2+\frac{\nu\sigma}{\eta}\right)H_2+2\int_1^\alpha r\bar{h}D(rh)\,dr=-m^2N\int_1^\alpha rf\bar{h}\,dr, \tag{23}$$

in which

$$H_0=\int_1^\alpha r|h|^2dr, \quad H_1=\int_1^\alpha\frac{1}{r}|Drh|^2dr, \quad H_2=\int_1^\alpha r^3|h|^2dr, \quad H_3=\int_1^\alpha r|Drh|^2dr.$$

Equations (21) to (23) can be suitably combined to eliminate the integrals on the right-hand sides. The result is

$$m^2N(I_2+2m^2I_1+m^4I_0)+B(H_1+m^2H_0)+(H_3+m^2H_2)$$
$$-2\int_1^\alpha r\bar{h}D(rh)\,dr+\sigma\left(m^2NI_1+m^4NI_0+\frac{B\nu}{\eta}H_0+\frac{\nu}{\eta}H_2\right)=0. \tag{24}$$

But since

$$\int_1^\alpha r\bar{h}D(rh)\,dr+\int_1^\alpha rhD(r\bar{h})\,dr=r^2h\bar{h}\,|_1^\alpha=0,$$

the real part of the integral in equation (24) is zero. Taking the real part of (24), we have

$$m^2N(I_2+2m^2I_1+m^4I_0)+B(H_1+m^2H_0)+(H_3+m^2H_2)$$
$$+\sigma_r\left(m^2NI_1+m^4NI_0+\frac{B\nu}{\eta}H_0+\frac{\nu}{\eta}H_2\right)=0. \quad (25)$$

Now from the definitions of the integrals denoted by H, it is evident that

$$\alpha^2H_0 > H_2, \quad \text{and} \quad \alpha^2H_1 > H_3.$$

Thus, since N and B are of the same sign, if

$$-B \geqslant \alpha^2, \quad \text{or} \quad B > 0, \quad (26)$$

it follows from equation (25) that σ_r is negative, and the fluid is stable. With the definition of B given by (13), the sufficient condition of stability is therefore again found to be

$$J \leqslant -\pi j_0(r_2^2-r_1^2) \quad \text{or} \quad J \geqslant \pi j_0 r_1^2. \quad (27)$$

5. Solution for small spacings

For small spacings of the cylinders, the operator L in (17) and (18) can be replaced by D^2. If the dimensionless parameters are now re-defined as

$$t=\frac{\tau\nu}{d^2}, \quad \xi=\frac{r-r_1}{d}\,(r \text{ dimensional}), \quad m=\frac{2\pi d}{\lambda},$$

in which d is r_2-r_1, and λ is the wavelength in the z-direction, equations (17) and (18) can be replaced by

$$(D^2-m^2-\sigma)(D^2-m^2)f=\left(\frac{d}{r_1}\right)^4\left[(B+1)-\frac{2Bd}{r_1}\xi\right]h, \quad (28)$$

$$\left(D^2-m^2-\frac{\nu\sigma}{\eta}\right)h=m^2N\left(1-\frac{2d}{r_1}\xi\right)f, \quad (29)$$

where D stands now for $d/d\xi$. The boundary conditions are

$$f=Df=0 \quad \text{at} \quad \xi=0 \text{ and } 1, \quad (30)$$

$$h=0 \quad \text{at} \quad \xi=0 \text{ and } 1. \quad (31)$$

We shall investigate the stability for the cases in which the two currents are in the same direction ($-B<1$), so that the electromagnetic body force on the undisturbed state is contripetal. If B is not nearly equal to -1, equations (28) and (29) become (since d/r_1 is assumed to be very small)

$$(D^2-m^2-\sigma)(D^2-m^2)f=(B+1)\left(\frac{d}{r_1}\right)^4h, \quad (32)$$

$$\left(D^2-m^2-\frac{\nu\sigma}{\eta}\right)h=m^2Nf. \quad (33)$$

Effectively the same equations with the same boundary conditions as for the problem at hand have been solved exactly by Pellew & Southwell (1940), who also proved that for neutral stability σ is zero and not purely imaginary. Comparing

equations (32) and (33) with Pellew & Southwell's equations (see Lin 1955, p. 108), we find that the parameter corresponding to Pellew & Southwell's R (Rayleigh number) is

$$T \equiv -(1+B)N\left(\frac{d}{r_1}\right)^4 = \frac{\mu J(\pi j_0 r_1^2 - J)}{\pi\rho\nu\eta}\left(\frac{d}{r_1}\right)^4.$$

According to Pellew & Southwell's solution, then,

$$T = 1707{\cdot}8. \tag{34}$$

If $1+B$ is positive but of the same magnitude as d/r_1, and if the principle of exchange of stabilities is assumed, equations (28) and (29) become

$$(D^2-m^2)^2 f = (1+B)\left(\frac{d}{r_1}\right)^4 (1+\beta\xi)h, \tag{35}$$

$$(D^2-m^2)h = m^2 N f. \tag{36}$$

where

$$\beta = -\frac{2dB}{r_1(1+B)}. \tag{37}$$

The boundary conditions are still specified by (30) and (31). Solution of the differential system for three values of β by the method of Chandrasekhar (1954) yields the corresponding critical values of T as given in table 1.

β ...	0·25		0·5		1·0	
m ...	3·12	3·13	3·12	3·13	3·12	3·13
T (1st approx.)	1524·5	1524·6	1372·1	1372·1	1143·4	1143·4
T (2nd approx.)	1524·4	1524·4	1371·6	1371·7	1142·4	1142·4
T (3rd approx.)	1518·0	1518·0	1365·9	1366·0	1137·7	1137·7

TABLE 1

Computation for the case of negative $J(1+B<0)$ has not been performed. However, from the definition of N it can be seen that N is negative for negative J, and from the forms of (35) and (36) it can be seen that the fluid is probably stable for negative J unless $|1+B|$ is very small and β large. For very small $|1+B|$, the modified parameter

$$T' = \beta T$$

can be advantageously used instead of T. A table for T' can be easily constructed from table 1. The value of T' for negative J of small magnitude or for small $|1+B|$ is not much different from that for small positive J, so that a rough measure of it can be obtained by extrapolation from the table for T'. This measure can be improved by extending the range of β in Table 1, and hence in the T'-table derived therefrom.

6. Feasibility of experiment

For an experiment the most favourable value of B for the occurrence of ring vortices is of course $-1/2$. If d/r_1 is 0·1, for the critical case

$$\frac{\mu}{4}\frac{\pi j_0^2 r_1^4}{\rho\nu\eta} = 1707{\cdot}8\times 10^4.$$

For mercury, we have, in e.m.u.,

$$\eta = \frac{1}{4\pi\mu\sigma} = 8000\,\text{cm}^2/\text{sec}, \quad \mu = 1\,\text{e.m.u.},$$

$$\nu = 1{\cdot}12 \times 10^{-3}\,\text{cm}^2/\text{sec}, \quad \rho = 13{\cdot}6\,g/\text{c.c.}$$

For r_1 equal to 10 cm and d equal to 1 cm,

$$j_0 = 257\,\text{e.m.u.} = 2570\,\text{amp/cm}^2.$$

The total current through the annular space is then

$$20\pi j_0 = 1{\cdot}62 \times 10^5\,\text{amp},$$

which is obviously a tremendous current. However, this current is the same (for the same d/r_1) regardless of the size of the apparatus, and the total power per metre (which is roughly 4160 kW for $r = 10$ cm) decreases in inverse proportion to the square of the lateral dimension of the apparatus. Furthermore, the heat capacity of mercury per metre of length increases in direct proportion to the square of the lateral dimension. Thus the danger of boiling decreases rapidly as the lateral size increases. For highly ionized gases with a density much smaller than that of mercury and with very high conductivity, the necessary current for ring vortices to occur will be very much reduced. Unfortunately a simple experiment with a small apparatus does not appear feasible.

This work was jointly sponsored by the University of Michigan and the Office of Ordnance Research of the U.S. Army. The computational service of Mr Wei Lai was supplied through a faculty research fund by the Rackham Graduate School of the University of Michigan.

REFERENCES

Chandrasekhar, S. 1954 The stability of viscous flow between rotating cylinders. *Mathematika*, **1**, 5–13.

Lamb, H. 1945 *Hydrodynamics*. New York: Dover.

Lin, C. C. 1955 *The Theory of Hydrodynamic Stability*. Cambridge University Press.

Pellew, A. & Southwell, R. V. 1940 On maintained convective motion in a fluid heated from below. *Proc. Roy. Soc.* A, **176**, 312–343.

Rayleigh, Lord 1916 On the dynamics of revolving fluids. *Scientific Papers*, **6**, 447–453. Cambridge University Press.

Synge, J. L. 1938 On the stability of a viscous liquid between two rotating coaxial cylinders. *Proc. Roy. Soc.* A, **167**, 250–256.

Taylor, G. I. 1923 Stability of a viscous liquid contained between two rotating cylinders. *Phil. Trans.* A, **223**, 289–343.

Yih, C.-S. 1959 Inhibition of hydrodynamic instability by an electric current. (To be published.)

The supersonic flow past a leading edge separation bubble

By A. W. SHARP
Department of the Mechanics of Fluids, University of Manchester

(Received 24 August 1958)

The supersonic flow field outside a leading edge separation bubble has been computed in detail by a special application of the method of characteristics. Experimental observations on a two-dimensional square-nosed flat plate at $M = 1{\cdot}96$ formed the initial data, and base points were established on the plate surface. Computations proceeded outwards and upstream to the sonic line and bow wave, the bow wave entropy gradient being taken into account. The shape of the sonic line was found to be very sensitive to the conditions along the plate surface. Streamlines and iso-Mach lines have been interpolated and are presented. Good agreement was found at the intersection of the network and the bow wave between computed values and those given directly by the shock wave equations. A comparison has been made with interferometric results from France.

1. Introduction

The two-dimensional supersonic flow past a square-nosed flat plate involves a detached bow shock wave with a resulting region of mixed flow. Also, the boundary layer on the front face of the plate is unable to negotiate the right-angle corner and separates, reattaching to the plate some distance downstream. The region enclosed between the separated boundary layer, or mixing region, and the solid boundary is termed a separation bubble. Such bubbles have been noted previously, for instance by Holder & Chinneck (1954), who photographed and pressure-plotted the region at Mach numbers below that of the present work. Separation bubbles have also been observed to occur on the leading edge of thin aerofoils.

After traversing the bow shock wave, the flow close to the centre line is subsonic, but accelerates to supersonic speed, attaining a Mach number of unity at the sonic line which joins the bow wave sonic point to the sonic point on the plate. Of these two end-points, the former is easily determined from the bow wave slope, and the latter is generally accepted to lie at the corner of the plate. However, the shape of the sonic line between them and the interdependence between its shape and the conditions along the separated region and the solid boundary farther downstream are not known.

It appeared possible that the supersonic portion of the external flow field might be computed by the method of characteristics if the flow conditions along the plate were known. It was hoped that the shape and location of the sonic line might be determined, and that its relationship with the boundary conditions

would be clarified. The procedure followed is described in the present paper, the basic data being the experimentally determined pressure distribution and bubble profile. On suitably spaced base points a characteristics network has been constructed, which extends upstream to the inboard portion of the sonic line, and outwards to the bow wave. In this way, it has proved possible to determine the inboard part of the sonic line, and also the streamlines and iso-Mach lines in the supersonic region.

In § 2 below the basic experimental results are described, whilst their conversion to usable form is discussed in § 3. Details of the actual computation follow in § 4 and a discussion of the resultant flow field is given in § 5.

2. The basic experimental data

The flat plate of $\frac{9}{32}$ in. thickness was mounted at zero incidence in an intermittent vacuum-operated wind tunnel of working section dimensions 5 in. × 4 in.; this wind tunnel has been described previously by Bardsley & Mair (1951). The plate spanned the entire 4 in. width of the working section and was supported

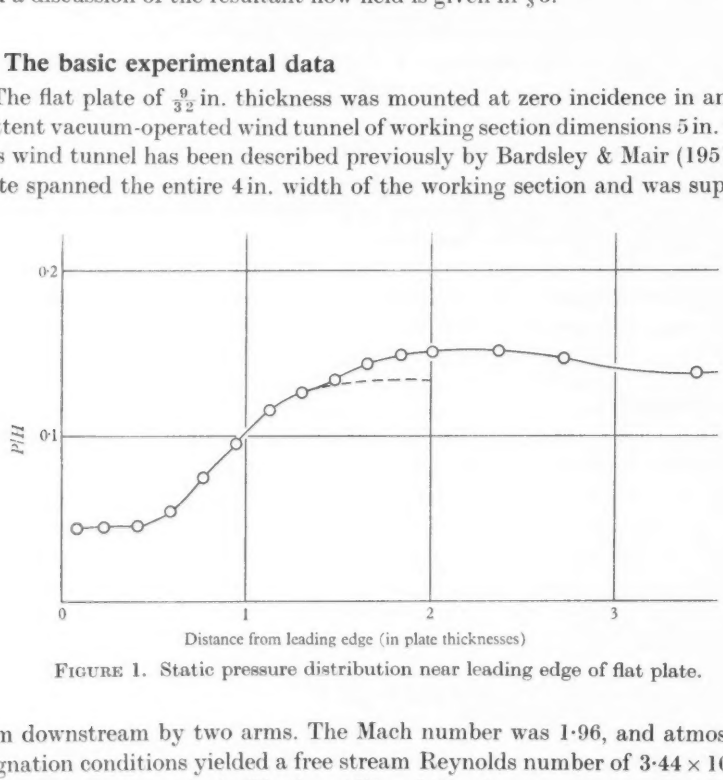

FIGURE 1. Static pressure distribution near leading edge of flat plate.

from downstream by two arms. The Mach number was 1·96, and atmospheric stagnation conditions yielded a free stream Reynolds number of $3{\cdot}44 \times 10^5$ with a length scale of one inch. The humidity of the air was maintained well below 0·2 g/kg in order to avoid condensation effects. Pressure tappings of 0·015 in. diameter in the surface of the plate communicated, via a buried tube, with an absolute mercury manometer of accuracy ± 0·1 mm of mercury.

The measured pressure distribution on the plate is shown in figure 1. P is the static pressure and H the free stream stagnation pressure. The broken curve at the downstream end indicates the expected return to free stream static pressure. The upward kink in the observed curve is thought to be due to compression and rarefaction disturbances propagated downstream from the bow wave-boundary layer interaction on the tunnel window, and has been ignored in what follows. As

would be expected, the pressure inside the front portion of the bubble is constant, but is followed by a rapid pressure rise through the recompression fan.

The flow pattern was photographed, using a conventional two-mirror schlieren system with a flash-tube as light source. A photograph of the nose region is shown in figure 2 (plate 1). The apparent thickness of the shock waves and separated boundary layer is due to interaction with the window boundary layer, and to the flow not being truly two-dimensional.

3. Conversion of data

The static pressure distribution was first converted into the surface Mach number distribution, allowance being made for the loss of stagnation pressure suffered when the stagnation streamline traversed the normal bow wave. The pressure across the separated region was assumed to be constant at each station. The schlieren photograph was then enlarged to eight times natural size, and the ordinates of the bubble profile were carefully measured at a number of stations. Similar measurements were taken of the bow wave location and shape. It was now necessary to fit analytic curves to these profiles in order that the ordinates and slopes could be calculated at all points.

The bow wave co-ordinates were fitted very well by a cubic over the range required. From this curve, the slope of the bow wave at any ordinate could be calculated, so that the bow wave sonic point was located precisely. The fitting of curves to the bubble profile proved to be rather more difficult. The initial direction of the separated layer was calculated, assuming sonic conditions at the corner, and knowing the bubble static pressure. The photographic ordinates were well fitted by a combination of three curves, namely an ellipse from the leading edge to just beyond the point of maximum height, followed by a straight line down towards the surface, and a circular arc between the line and the surface. Of these curves, the ellipse had the correct slope at the leading edge, the straight line was tangential to both the ellipse and the circular arc, and the plate surface was tangential to the arc. A trial set of computations based on this boundary, however, produced kinks in the iso-Mach lines and flaws in the recompression shock wave. These flaws were traced back to the concave portion of the profile, and it was realized that a smooth distribution of $(\theta+t)$ along the boundary had not been obtained, although both θ, the flow direction, and t, a function of Mach number, individually had smooth distributions. This requirement for a smooth $(\theta+t)$ distribution proved difficult to satisfy, but was eventually achieved by fitting a parabola and a quintic to the recompression region. The condition that $(\theta+t)$ must vary smoothly along the boundary therefore severely limited the choice of curves available for fitting, and also demonstrated the close relationship between surface conditions and sonic line shape.

4. Details of the computations

4.1. *The first approximation*

The information available, namely the distributions of flow direction, Mach number, and bubble height along the surface made it possible to commence the calculations after selecting suitably spaced base points. These were selected to

coincide with the static holes over most of the bubble region, but this spacing was varied where necessary. Thus, close to the leading edge the bubble curvature is much increased, and the base points are accordingly much closer together; conversely, far downstream conditions become almost constant, and a much wider spacing is acceptable. The data were sufficient to permit the computation, by the method of characteristics, of the flow field enclosed by the first minus Mach line from the leading corner and the plus Mach line from any surface point downstream. (Plus and minus Mach lines are defined in figure 3.) Since the surface static pressure becomes constant downstream of the bubble, the flow field may be investigated as far downstream, and hence as far outwards as is required, the conditions on all plus Mach lines being known.

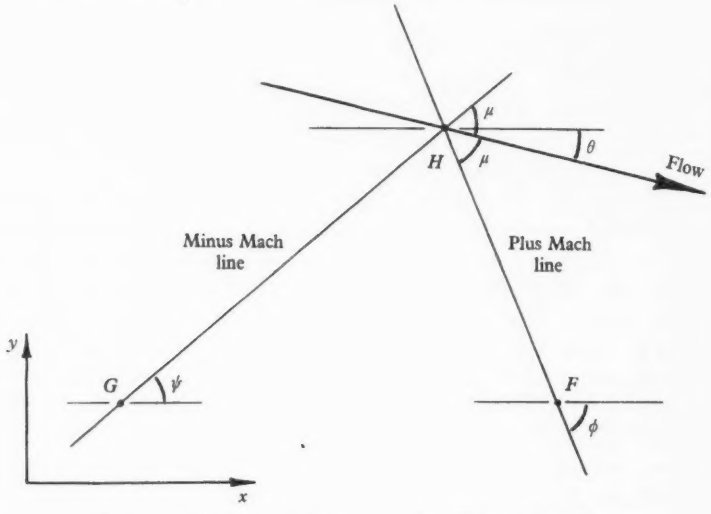

FIGURE 3. Angles used in computing H from F and G.

Using Cartesian co-ordinates x, y, the characteristic equations for the Mach lines may be written (see Meyer 1948),

$$\frac{dy}{dx} = \tan(\theta \mp \mu), \tag{1}$$

$$d\theta \mp \frac{\sin\mu\cos\mu}{\rho a^2}\,dp = 0, \tag{2}$$

where the upper and lower signs refer to plus and minus Mach lines respectively. (μ is the Mach angle, θ the angle between the x-axis and the velocity vector, ρ the density, a the velocity of sound, and p the pressure.) Equation (2) may be rewritten in the form

$$d(t \pm \theta) + d\sigma \sin 2\mu = 0,$$

where
$$dt = \frac{dq}{q}\cot\mu \quad \text{and} \quad d\sigma = \frac{ds}{2\gamma R}. \tag{3}$$

FIGURE 2 (plate 1). The separation bubble.

Here, q is the velocity magnitude, s the specific entropy, γ the ratio of specific heats, and R the gas constant. It may be shown that

$$t = \mu - \tfrac{1}{2}\pi + \lambda^{-1}\cot^{-1}(\lambda^{-1}\tan\mu), \tag{4}$$

where $$\lambda = [(\gamma-1)/(\gamma+1)]^{\frac{1}{2}}.$$

The function $(1000-t)$, normally referred to as the pressure number, has been tabulated for $\gamma = 1{\cdot}400$ by Herbert & Older (1946).

As a first approximation, the difference in entropy change between adjacent streamlines across the curved bow wave was neglected, so that equation (3) became

$$d(t \pm \theta) = 0. \tag{5}$$

From equations (1) and (5), a network of points was constructed by the usual method of characteristics, extending upstream and outwards and based on the surface points. In the expansion fan at the leading corner, minus Mach lines were chosen at intervals of 5° in θ. Iso-Mach lines were drawn in by interpolation for Mach numbers, M, equal to 1·1, 1·2, 1·3, and were found to be kinked, due to an irregular surface distribution of $(\theta+t)$. The mechanism of this effect may be explained as follows. In figure 4, ignoring entropy differences,

$$(\theta+t)_A = (\theta+t)_B.$$

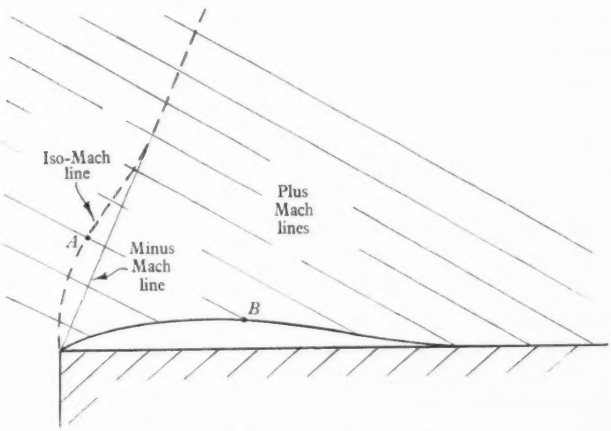

FIGURE 4. Shape of iso-Mach lines.

Along the iso-Mach line, by definition, M = constant, so that μ and t are also constant. Thus using suffixes M, B, to denote conditions on the iso-Mach line and boundary respectively, and since $(\theta+t)_M = (\theta+t)_B$, we have

$$\theta_M = (\theta+t)_B - t_M = (\theta+t)_B - \text{constant}.$$

Hence, once $(\theta+t)_B$ has settled down to its constant value, it follows that θ_M = constant. Moreover, we now have θ_M and t_M both constant so that $(\theta-t)_M$ = constant, i.e. the iso-Mach line is also a minus Mach line. Also, since μ_M, θ_M are constant along this line, $\psi_M = (\theta+\mu)_M$ = constant, and the iso-Mach lines and minus Mach lines are therefore straight in this region.

It can thus be seen that kinks in $(\theta+t)_B$ would give rise to corresponding kinks in the distribution of θ_M along the iso-Mach line, leading, in turn, to kinks in the line itself. The correctness of this diagnosis was demonstrated by the elimination of the iso-Mach line kinks when the $(\theta+t)_B$ distribution was smoothed out by the modified choice of boundary curves already discussed.

4.2. *The entropy correction*

The curvature of the bow shock wave causes an entropy gradient across the flow downstream, each streamline having an entropy value which is constant but different from those of its neighbours. Accordingly, in order to evaluate the second term in equation (3), it was necessary to identify the streamline upstream of the bow wave which corresponded to the point under computation. This was achieved by calculating the mass flow between the first approximation to the point and the boundary. Thus for H (figure 3), the mass flow across FH was calculated, where F was already corrected for entropy (and hence the mass flow between F and the boundary was known). Thus, the mass flow between the boundary and H was obtained, thereby locating the H-streamline upstream of the bow wave. From this ordinate, the corresponding bow wave slope was derived and hence the entropy increase. This in turn yielded the entropy differences $d\sigma$ between H and F, and between H and G, which were required for insertion in equation (3). The flow and position parameters for H were then recalculated with this entropy correction included. Fortunately, the correction was not large enough to necessitate any iterative repetition of the procedure. (No correction was applied for entropy changes produced by the recompression. This is not likely to lead to any appreciable error since, in the region computed, much of the recompression takes place through a fan or weak shock.) This system was used in computing the whole flow field, apart from the region very close to the sonic line which required special treatment as will be seen in § 4.3 below.

4.3. *The final step to the sonic line*

The usual system of characteristics computations as outlined in 4.1 above may be shown to assume that the Mach line segments are circular arcs. This assumption is fully justified in general for small steps, but in the neighbourhood of the sonic line the Mach lines curve strongly, and have been shown by Holt (1949) to behave like semi-cubical parabolae. This holds only for small $\nu = \frac{1}{2}\pi - \mu$, and was here taken to be true for $M \leqslant 1{\cdot}02$, corresponding to $\nu = 0{\cdot}2$ radian. Accordingly, a method was used whereby ϕ, ψ (figure 3) were averaged along a semicubical parabola rather than the usual circular arc. Thus if the semicubical parabola is $y^{*3} = cx^{*2}$, and the chord is $y^* = x^* \tan\eta$ (see figure 5), then it may be shown that $\tan\eta = \frac{3}{2}\tan\beta$. This has utilized an origin on the sonic line with the x-axis in the local flow direction. Translation of the origin to that of the characteristics network will not affect the purely angular relationship between η and β, but the angles to be averaged must be related to a new reference direction before the equation is used. This new reference direction, θ_s, will be the flow direction at the intersection of the sonic line and the relevant Mach line. Since the entropy term is negligible for this last step to the sonic line (see below), and since $t = 0$ on the sonic line, it

follows that θ_s is identical with the value of $\theta \pm t$ on the plus or minus Mach line. In place of the old ϕ, ψ (Mach line inclinations to free stream direction), we use ϕ^*, ψ^*, where for a plus Mach line, $\phi^* = \phi - \theta_{s+} = \theta - \mu - \theta_{s+} = -(\mu + t)$; and for a minus Mach line, $\psi^* = \psi - \theta_{s-} = \theta + \mu - \theta_{s-} = \mu + t$. Here, for any point, $\theta_{s+} = \theta + t$ (along the plus Mach line) and $\theta_{s-} = \theta - t$ (along the minus Mach line). Then, on a plus Mach line, $\eta = \phi^{*H}_F = \tan^{-1}(\frac{3}{2}\tan\phi^*)$ and, on a minus Mach line, $\eta = \psi^{*H}_G = \tan^{-1}(\frac{3}{2}\tan\psi^*)$, where the affices $\frac{H}{F}$, $\frac{H}{G}$ refer to average quantities between the points. Then $\phi^H_F = \phi^{*H}_F + \theta_{s+}$ and $\psi^H_G = \psi^{*H}_G + \theta_{s-}$. These latter values, ϕ^H_F, ψ^H_G (averages along the semicubical parabolae) were then used to determine x_H, y_H, as before.

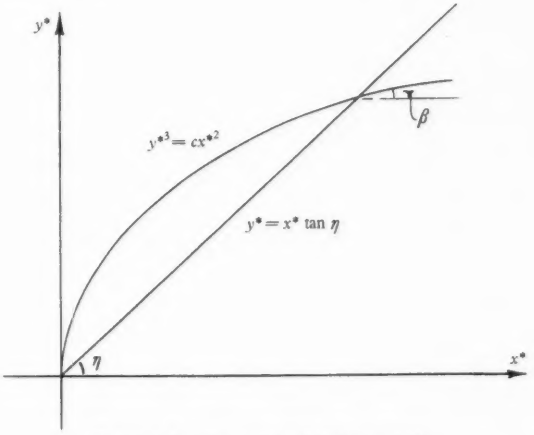

FIGURE 5. The semicubical parabola.

As will now be seen, it was not possible to correct this final step for entropy variations, but it will be shown that the correction would be negligible. The effect of the entropy correction is to increase the Mach number of the first approximation. Thus, in order to attain a specified Mach number M, it is necessary, when calculating the first approximation, to overshoot M to a lower value, which is then raised to the required value M by the correction. This is clearly impossible for $M = 1$, since the characteristics become imaginary for $M < 1$. However, this inability to correct for entropy is of no consequence, since the correction would be negligible for two reasons: (i) the step from $M = 1{\cdot}02$ to $M = 1{\cdot}00$ is geometrically very small, so that $d\sigma$ would be negligible; (ii) in this region, $\mu \to 90°$, hence $\sin 2\mu \to 0$. Accordingly, the correction term $d\sigma \sin 2\mu$ will be extremely small and its omission of no importance.

4.4. *Summary of the computations*

The use of the techniques described above, in §§ 4.1, 4.2 and 4.3, made possible the computation of almost all the supersonic flow field downstream of the sonic line and bow wave. Where necessary, due to rapid variation of the parameters, the mesh size was reduced in order to maintain the accuracy. The network was extended outwards until it intersected the bow wave.

Only about one-third of the sonic line proved to be calculable, since at C (see figure 6), about 0·85 plate thickness from the surface, the line curved strongly upstream. Outboard of this point, computations ceased to be possible upstream of the minus Mach line CA, leaving an indeterminate supersonic zone CAS, enclosed by the outermost portion of the sonic line, part of the bow wave, and the minus Mach line. Whilst conditions are fully known along this minus Mach line, these data are not sufficient to enable the mesh to be extended farther upstream since data along a plus Mach line also would be required.

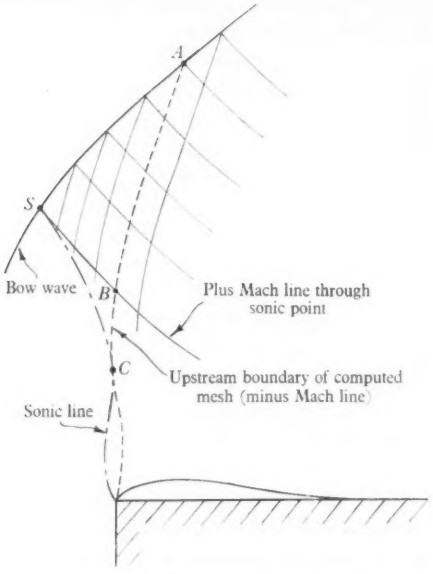

FIGURE 6. The indeterminate region.

Consideration has been given to the possibility of computing this zone by using base points on the bow wave outboard of the sonic point. This would not permit computation of the whole zone, but only that portion ABS which lies downstream of the plus Mach line through the sonic point. The undetermined portion of the sonic line, CS, would thus remain indeterminate by this method. It might, however, then be possible to use conditions along the present bounding minus Mach line, CA, and along the sonic point plus Mach line, SB, together. Whilst such a procedure seems feasible in principle, it would be inaccurate for the following reasons: (i) the present network and the bow wave are not in exact agreement at their intersection, A; (ii) the inevitable slight errors in t at the bow wave base points would be serious since in this region t is itself very small ($M \simeq 1$), but $\partial\mu/\partial t$ very large.

Under these circumstances, the scheme has not been pursued further.

The computed flow parameters at the network points have been used to draw in iso-Mach lines and streamlines by interpolation in μ and mass flow respectively. The network of Mach lines is shown in figures 7 and 8 and the resultant streamlines and iso-Mach lines in figure 9. These results will be discussed in § 5 below.

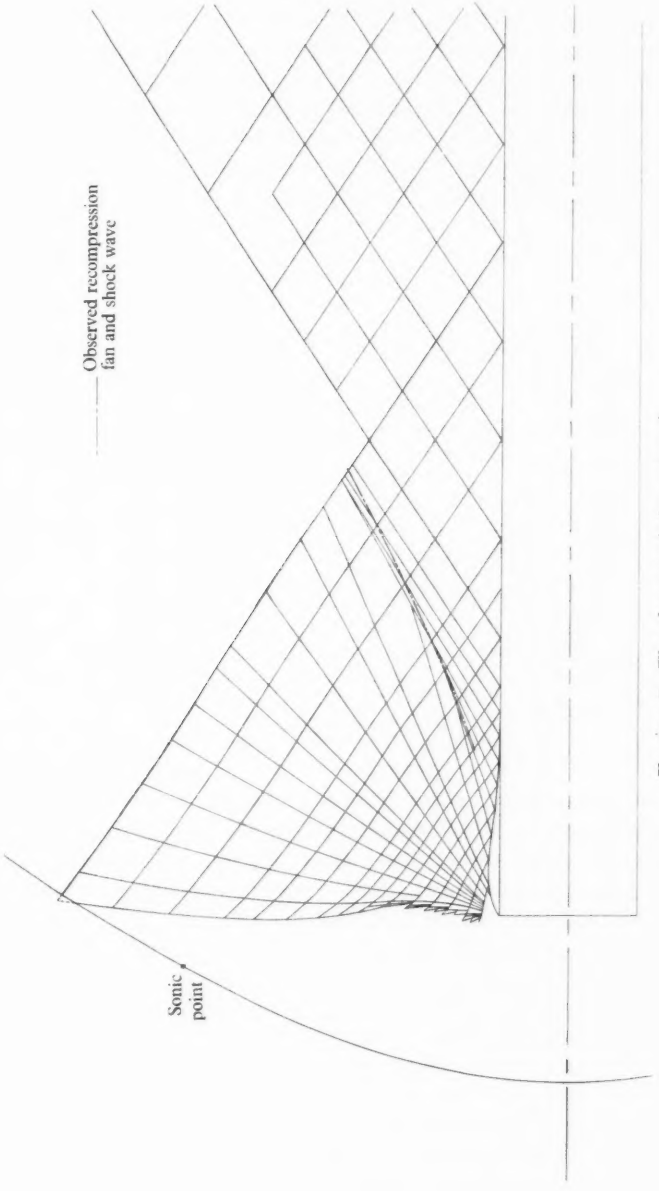

FIGURE 7. The characteristics network.

5. The computed flow field

5.1. *Conditions at the network-bow wave intersection*

It was of interest, when the characteristics network intersected the bow wave, to compare the network values of the flow parameters with those calculated from the shock wave equations at the relevant point. This is done in figure 10, where Mach number and flow direction downstream of a curved shock wave at $M = 1{\cdot}96$ are plotted against each other. Conditions at the intersection of the mesh and the bow wave, as predicted by the characteristics, are plotted as a single point for comparison.

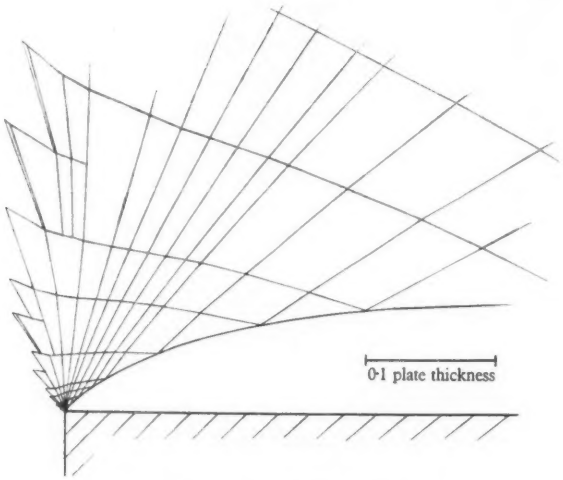

FIGURE 8. The nose region enlarged.

There are a number of sources from which the small discrepancy may arise: e.g. (i) errors in basic data, and incompatibility of curves fitted to boundary and bow wave; (ii) cumulative errors inevitable in any step-by-step method involving the use of mean quantities; (iii) neglect of the entropy change across the recompression shock may also have contributed.

Under these circumstances, the agreement is regarded as highly satisfactory, possibly due to the mutual cancellation of some errors.

It should be noted that the bow wave does not emerge from the computations as did the recompression shock wave. The bow wave results, as a normal shock wave, from the presence of a blunt-nosed body in the supersonic free stream. It thus enters the domain of the present calculations already determined, and is merely weakened by the incident expansion wavelets. As a result, the computation of the network did not in any way indicate the existence or location of the bow wave. Thus the mesh would have been extended farther outwards (into what is actually the free stream) had not photographic evidence of the bow wave location been available.

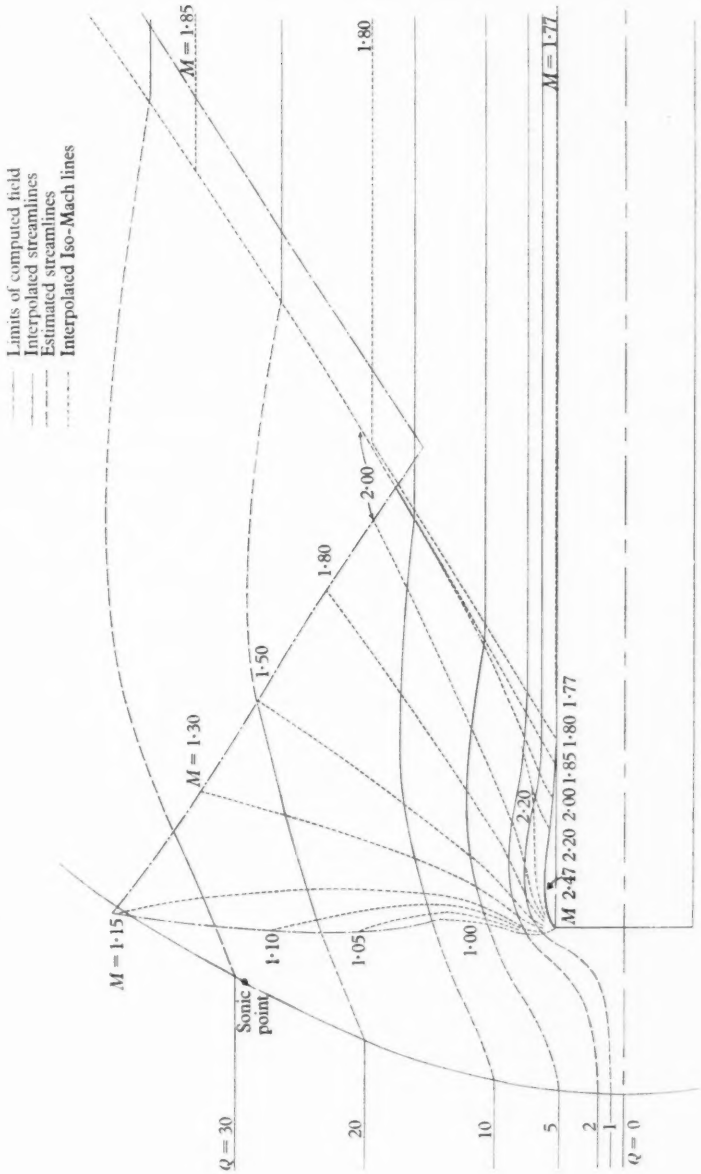

FIGURE 9. The streamlines and iso-Mach lines.

5.2. *The characteristics network (figures 7 and 8)*

The expansion Mach lines from the fan at the leading edge curve upstream and are reflected by the sonic line and bow wave back on to the surface as compression wavelets. Those which strike the sonic line form a cusp at that point, since the two Mach line families coincide at $M = 1{\cdot}00$. After a further reflexion from the surface, this time as compression waves, the Mach lines coalesce to form the recompression fan and shock wave, which agree well with the observed wave.

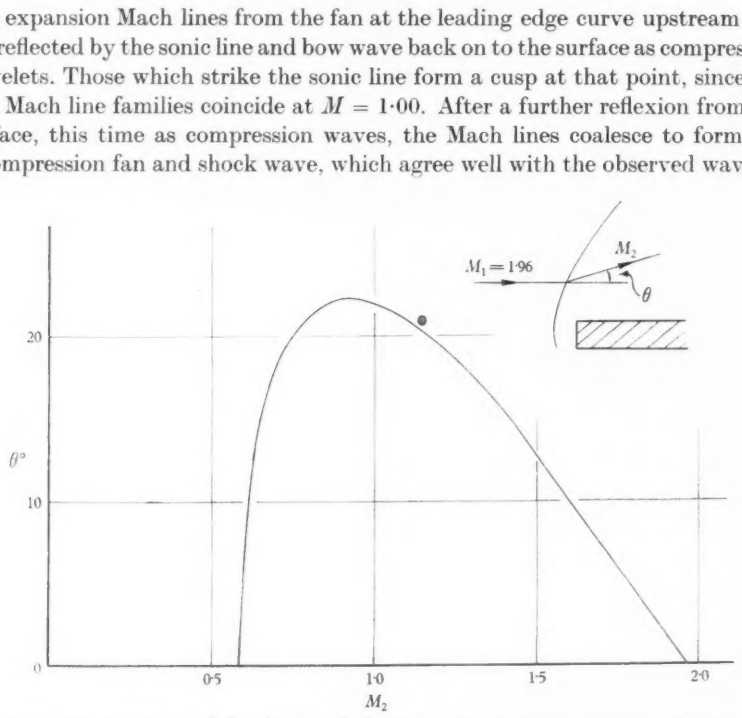

FIGURE 10. Accuracy of the characteristics network. ⊙ denotes computed values.

The leading expansion waves from the corner cause the sonic line to bulge upstream, and illustrate the manner in which it runs perpendicularly into the front face of the plate. The subsequent downstream bulge of the sonic line, followed by a further upstream bend, leads to the indeterminate region of supersonic flow ACS (see figure 6). In the first approximation, the sonic line would have become straight at C, approximately one plate thickness outboard of the surface, and would subsequently have coincided with a minus Mach line. The effect of the entropy correction has been to curve the sonic line upstream and the minus Mach line downstream, thereby producing between them the narrow triangular region, ACS, devoid of information along plus Mach lines. Accordingly, this triangular portion of the flow field cannot be computed by the present method. A possible alternative line of attack was considered in § 4.4 above, but was rejected for the reasons stated there.

Downstream of the recompression, the flow is parallel to the plate surface, but traversal of the curved bow wave has produced a gradient, normal to the surface, in entropy and hence in Mach number. The Mach lines in this region are slightly curved as a result.

5.3. *The streamlines and iso-Mach lines* (*figure* 9)

The streamlines have the expected shape; the subsonic portions have been drawn in qualitatively, but with the correct initial direction behind the bow wave. The entropy gradient referred to above leads to a gradient in mass flux. As a result, streamtubes of equal width in the free stream are no longer so downstream of the recompression. The displacement effect of the plate on the streamlines falls off with perpendicular distance from the plate.

The expansion fan from the leading edge accelerates the flow from $M = 1$ to $M = 2{\cdot}47$. The latter Mach number, the highest attained throughout the flow field, corresponds to the constant pressure portion of the separation bubble from the leading edge to just beyond the point of maximum height. This part of the bubble profile is thus the iso-Mach line of $M = 2{\cdot}47$.

The iso-Mach lines may be divided into two types:

(i) $M > M_1$ (where M_1 is free stream Mach number). These form closed curves; commencing in the expansion fan, they curve outwards and downstream, form a cusp in the recompression shock, and then descend again to the surface via the recompression fan. They thus enclose embedded regions of Mach number greater than their own, e.g. $M = 2{\cdot}0, 2{\cdot}2$ in figure 8. The case of $M = 2{\cdot}47$ discussed above is the limiting case of this type, in which the embedded region has collapsed on to the bubble profile.

(ii) $M < M_1$. These also commence in the leading edge fan, curve downstream, and then upstream again. They thus intersect the bow wave and not the recompression shock. For $M \geqslant 1{\cdot}77$, they possess another branch which rises from the concave portion of the bubble surface, through the recompression fan, and then turns downstream, parallel to the surface and coinciding with a streamline, e.g. $M = 1{\cdot}80$. $M = 1{\cdot}77$ is the limiting case of this type, being the constant Mach number along the plate surface downstream of the recompression region.

The iso-Mach line of $M = 2{\cdot}47$ has the same shape as the bubble profile since it coincides with that profile. It will also be noted that the remainder of the iso-Mach lines from the leading edge have this shape, which appears to be transmitted up the plus Mach lines. The similarity was heightened when the entropy correction was omitted, since the iso-Mach lines eventually became straight, corresponding to the flat surface downstream of the bubble reattachment point. The entropy correction subsequently produced the gentle upstream curvature in this region.

The shape of the outer portion of the sonic line, not calculable by the present technique, may be inferred from that of the $M = 1{\cdot}15$ iso-Mach line. In view of the slight discrepancy noted between the bow wave and the characteristics mesh, it is unlikely that the computed sonic line would pass through the bow wave sonic point marked. It would probably intersect the bow wave some distance inboard of this point.

The pattern of iso-Mach lines forms an interesting comparison and contrast with figure 11 of the paper by Roy (1957) which is reproduced here as figure 11. This figure, obtained from an interferogram, shows the streamlines and iso-Mach lines in the flow past a plate with a rounded leading edge. The Mach number was identical with that of the present work, namely 1·96. It is therefore instructive

to compare the two patterns, one taken from experimental observation, the other also derived from experimental data, but after lengthy step-by-step computations.

The different leading edge configuration has a considerable effect, of course, in that the rounded leading edge eliminates the separation bubble and subsequent recompression. Far downstream of the leading edge, however, agreement would be expected, and the streamlines and iso-Mach lines in this region do compare well, e.g. $M = 1{\cdot}80$. The absence of the bubble removes the distortion from the inboard ends of the leading edge iso-Mach lines, which therefore curve smoothly outwards to the bow wave. Again, since there is no bubble to accelerate the flow beyond the free stream Mach number, there is no embedded pocket of such flow, and a recompression shock wave is unnecessary.

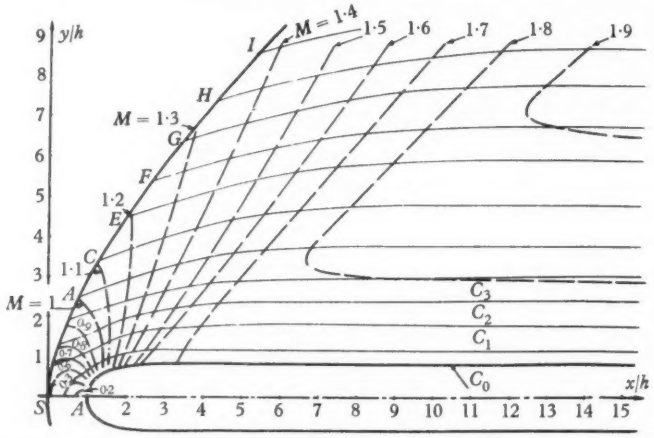

FIGURE 11. Flow past a plate with a rounded leading edge; reproduced from Roy (1957).

6. Conclusions

Commencing from the experimental observations of the flow direction and Mach number along the surface of the square-nosed flat plate with separation bubble at $M = 1{\cdot}96$, the external supersonic flow field has been computed by the method of characteristics. It has proved feasible to work upstream and outwards from the surface, as far as the sonic line and bow wave. The entropy gradient due to the curved bow wave has been incorporated in the calculations, and a special technique has been used for the region close to the sonic line. A small portion of the flow field, including the outer end of the sonic line has proved to be indeterminate by this method.

The values of the flow parameters at the mesh points have been used to plot streamlines and iso-Mach lines by interpolation. The agreement between the flow parameters predicted by the characteristics and by the shock wave equations at the network–bow wave intersection was found to be excellent. The iso-Mach line pattern has afforded an interesting comparison with results obtained in France by interferometry for a differently shaped leading edge at the same Mach number.

The author is particularly indebted to Dr N. H. Johannesen and to Prof. P. R. Owen for suggestions and advice during the course of the work, and to the Department of Scientific and Industrial Research for a maintenance grant. Thanks are due to M. Maurice Roy, Directeur-Général de l'O.N.E.R.A., for permission to reproduce figure 11.

REFERENCES

Bardsley, O. & Mair, W. A. 1951 *Phil. Mag.* **42**, 29.

Herbert, P. J. & Older, S. J. 1946 *Roy. Aircr. Estab., Tech. Note* no. C.W. 1.

Holder, D. W. & Chinneck, A. 1954 *Aero. Quart.* **4**, 317.

Holt, M. 1949 *Quart. J. Mech. Appl. Math.* **2**, 246.

Meyer, R. E. 1948 *Quart. J. Mech. Appl. Math.* **1**, 196.

Roy, M. 1957 *O.N.E.R.A.*, Publ. no. 90. (Further details are given in *La Rech. Aero.* no. 60, 1957.)

Rapid calculations for boundary-layer transfer using wedge solutions and asymptotic expansions

By H. J. MERK
Koninklijke/Shell-Laboratorium, Amsterdam, Holland

(Received 28 July 1958)

Exact transfer calculations for boundary layers with longitudinal pressure gradients are very complicated, but in the literature several approximate methods are known for the rapid calculation of both the wall friction and the heat transfer. A 'wedge method' propounded by Meksyn turns out to be one of the most rapid methods, being no less accurate than other approximate methods. A way of refining this method is proposed.

This paper also shows that asymptotic expansions provide convenient relations which are capable of expressing the Nusselt number explicitly in terms of the Prandtl number.

It is shown that, together with the asymptotic expansions, Meksyn's method permits rapid calculation of local heat transfer numbers. Some examples of application are given for elliptical cylinders and spheres for several values of the Prandtl number.

1. Introduction

This paper is concerned with the transfer of heat and mass from a body placed in a stream. Provided the Reynolds number of the flow lies within the approximate range from 10^2 to 10^5, we may state:

Assumption I. The transfer phenomena in the vicinity of a body submerged in a streaming fluid may be described by the laminar boundary-layer theory.

Furthermore we introduce:

Assumption II. There are no external volume forces in the streaming fluid.

This excludes free convection, so that we are only concerned with forced convection phenomena. Thus we include:

Assumption III. The main flow outside the boundary layer is irrotational.

This means that the intensity of the turbulence in the main flow has to be very low and that this flow may be calculated by means of the potential theory.

Restricting ourselves to the calculation of friction and heat transfer in unitary systems, we are only concerned with two boundary layers, viz. the dynamic boundary layer in which the transfer of momentum occurs, and the thermal boundary layer in which the transfer of heat occurs. It is well known that the boundary-layer theory can only be applied if the thickness δ of the dynamic boundary layer is small enough. If this condition is satisfied, we may ask whether or not the thickness δ_T of the thermal boundary layer is small enough to permit the application of the boundary-layer approximations to the calculation of the heat transfer.

It is known that $\delta_T < \delta$ for $\chi < \nu$, χ being the thermal diffusivity of the fluid and ν its kinematic viscosity. Introducing the Prandtl number $\sigma = \nu/\chi$, we conclude that for $\sigma > 1$, when δ is small enough, δ_T is small *a fortiori*. Hence, assumption I is legitimate if the thickness of the dynamic boundary layer is small enough.

For $\sigma < 1$, the thickness of the thermal boundary layer is greater than that of the dynamic boundary layer, so that in this range of the Prandtl number it may not suffice to assume that the thickness of the dynamic boundary layer is small enough. The limit $\sigma \to 0$ must especially be considered with care. This limit may be relevant if the kinematic viscosity is small (but finite) and the thermal diffusivity is very large. In this case the boundary-layer concept is not applicable to the calculation of the heat transfer, although it is applicable to the calculation of the friction. On the other hand, it is possible that at the limit $\sigma \to 0$ the kinematic viscosity approaches zero at small (but finite) values of the thermal diffusivity. This means that for $\sigma = 0$ we are concerned with heat transfer in a thermal boundary layer in a potential flow around the body considered. This problem has been investigated with great elegance by Boussinesq (1903, 1905) (see also Drew 1931), who introduced the concept of the thermal boundary layer before Prandtl (1904) proposed an analogous concept for the transfer of momentum. As a corollary of assumption I, we have thus to conclude that for $\sigma \to 0$ the boundary-layer theory of the heat transfer changes into Boussinesq's theory.

Although the boundary-layer concept simplifies the calculations considerably, the solution of the boundary-layer equations is generally still troublesome. The exact solution for boundary layers with an arbitrary longitudinal pressure gradient consists essentially in constructing power series in terms of the distance from the forward stagnation point of the body. The exact calculations by means of series expansion are cumbersome, because the convergency of the series is mostly bad. It is, therefore, generally necessary to perform the exact calculations numerically if the distance from the forward stagnation point is too large for the series expansion to be applied (e.g. see Prandtl 1938; Görtler 1939; Frössling 1940). In order to avoid the lengthy exact calculations, several approximate methods have been developed.

One of the best-known approximate methods is that of von Kármán (1921) and K. Pohlhausen (1921). Generally, this method is still troublesome and its accuracy is disappointing. Hence, we shall consider another group of approximate methods, called here the 'wedge methods', because these methods are based upon the well-known solutions of the boundary-layer equations for wedge-shaped profiles. The first wedge method was propounded by Falkner & Skan (1930, 1931). This method has been modified by Eckert (1942), Schuh (1949, 1954), Eckert & Livingood (1953), Kotschin & Loizjanski (see Kotschin, Kibel & Rose 1955), and by Smith (1956). All these wedge methods bear the same characteristic features: they are rapid and based upon some arbitrary hypothesis of physical nature, which has to be introduced in order to find the wedge element 'equivalent' to the element of the profile considered. The wedge methods of the authors named above differ only in the hypothesis used. Their fundamental disadvantage is that it is not clear how the calculations are to be improved if more accurate results are desired.

Meksyn (1947, 1948) has developed a method of calculation for the dynamic boundary layer, which may also be considered as a wedge method. This method consists essentially of a transformation of the boundary-layer equations and a mathematical simplification of the transformed equations. A great advantage of Meksyn's method is that no physical hypothesis is needed; the simplifications introduced are of a mathematical nature. As a result, it is possible to refine the calculations in a straightforward way. Furthermore, Meksyn's method has the following three advantages: (1) For wedge-shaped profiles (and hence in the vicinity of the forward stagnation point) the method yields exact results. (2) It may be expected that for arbitrary profiles successive refinements of the method converge towards the exact solution. (3) The method provides probably one of the most rapid calculations hitherto propounded in the literature.

It is quite easy to extend Meksyn's method to the calculation of heat transfer. In his original papers Meksyn applied complicated transformations allowing for the extension of the equations to lower values of the Reynolds number. If we are concerned with the pure boundary-layer equations only, it is possible to obtain Meksyn's final equations in a simple way. This will be shown in the next section.

In the present paper we have restricted ourselves to the most simple boundary-layer problems by the introduction of the following two assumptions:

Assumption IV. All physical quantities (viscosity, thermal conductivity, heat capacity) of the fluid are constant throughout the boundary layer.

Assumption V. The Mach number of the flow is low. The latter assumption means that in the thermal energy equations the dissipation and pressure terms may be neglected, while furthermore the density of the fluid may be considered as a constant.

It has to be stressed that the last two assumptions are not essential for the application of Meksyn's method.

2. Fundamental equations

Let us consider steady two-dimensional or rotationally symmetrical boundary-layer flows. For these cases we may introduce the coordinates (x, y), x being the distance from the forward stagnation point measured along the circumference of the two-dimensional profile or median line of the rotationally symmetrical body, and y being the normal distance from the wall of the body. For rotationally symmetrical bodies we also introduce r, the distance from a surface element of the body to the axis of symmetry. Denoting the components of the velocity parallel to the x- and y-axis by u and v respectively and making use of assumption IV, the equations of the dynamic boundary layer are

$$\left(u\frac{\partial}{\partial x}+v\frac{\partial}{\partial y}\right)u=-\frac{1}{\rho}\frac{\partial p}{\partial x}+\nu\frac{\partial^2 u}{\partial y^2}, \tag{1}$$

$$\frac{\partial p}{\partial y}=O(1), \tag{2}$$

$$\frac{\partial(ru)}{\partial x}+\frac{\partial(rv)}{\partial y}=0. \tag{3}$$

(Note that equation (2) holds for curved surfaces; for flat surfaces we may put $\partial p/\partial y = 0$.) These are the boundary-layer equations for rotationally symmetrical bodies. For a two-dimensional boundary layer, equations (1) and (2) retain the same forms, but in the continuity equation (3) r has to be dropped. Hence, the two-dimensional boundary-layer equations are formally obtained from (1), (2) and (3) by putting r equal to a constant. From (1) and the well-known fact that at the end of the boundary layer $\partial u/\partial y$ and $\partial^2 u/\partial y^2$ are very small, we obtain

$$\frac{\partial p}{\partial x} \doteq \frac{dp_e}{dx} = -\rho u_e \frac{du_e}{dx}, \tag{4}$$

where subscript e denotes the conditions at the end of the boundary layer. The boundary conditions are

$$u = v = 0 \text{ for } y = 0, \quad \text{and} \quad u \to u_e \text{ for } y \to \infty. \tag{5}$$

For the calculation of the heat transfer, we also need the thermal energy equation. Denoting the temperature by T and making use of the assumptions IV and V, the boundary-layer approximation to the thermal energy equation becomes

$$\left(u\frac{\partial}{\partial x} + v\frac{\partial}{\partial y}\right) T = \chi \frac{\partial^2 T}{\partial y^2}, \tag{6}$$

with the boundary conditions

$$T = T_w \text{ for } y = 0, \quad \text{and} \quad T \to T_e \text{ for } y \to \infty, \tag{7}$$

where the subscript w denotes the conditions at the wall.

In order to satisfy (3), a stream function ψ is introduced, such that

$$u = \frac{L}{r}\frac{\partial \psi}{\partial y}, \quad v = -\frac{L}{r}\frac{\partial \psi}{\partial x}, \tag{8}$$

L being a reference length of the body considered. For $r = L$, (8) defines the stream function of a two-dimensional flow.

The x and y coordinates will now be transformed by writing

$$\xi = \int_0^x \frac{u_e(x)}{V}\frac{r^2}{L^2}\frac{dx}{L}, \quad \eta = \left(\frac{R}{2\xi}\right)^{\frac{1}{2}} \frac{u_e}{V}\frac{r}{L}\frac{y}{L}, \tag{9}$$

where V is the velocity of the oncoming flow, and $R = VL/\nu$. The stream function $\psi(x, y)$ will be written

$$\psi(x, y) = VL(2\xi/R)^{\frac{1}{2}} f(\xi, \eta). \tag{10}$$

Equations (9) and (10) represent the essential parts of Meksyn's transformations; and it is easily recognized that (9) also contains the transformation used by Mangler (1948) for rotationally symmetrical boundary layers. From (8), (9) and (10) we obtain

$$u = u_e \frac{\partial f}{\partial \eta}, \tag{11a}$$

$$v = -\frac{r}{L}\frac{u_e}{(2\xi R)^{\frac{1}{2}}}\left\{f + 2\xi\frac{\partial f}{\partial \xi} + (\Lambda - 1)\,\eta\frac{\partial f}{\partial \eta}\right\}. \tag{11b}$$

Here Λ is the 'wedge variable' defined by

$$\Lambda = \frac{2\xi}{u_e}\frac{du_e}{d\xi} = 2\left(\frac{L}{r}\frac{V}{u_e}\right)^2\left\{\int_0^x \frac{r^2}{L^2}\frac{u_e}{V}\frac{dx}{L}\right\}\frac{du_e/V}{dx/L}. \tag{12}$$

We remark that for pure wedge flow, $r = L$ and $u_e = cx^m$. It then follows from (12) that $\Lambda = 2m/(m+1) = \text{const}$. From (9) and (11) we derive

$$u\frac{\partial}{\partial x} + v\frac{\partial}{\partial y} = \frac{r^2}{2L^3\xi}\frac{u_e^2}{V}\left\{2\xi\left(\frac{\partial f}{\partial \eta}\frac{\partial}{\partial \xi} - \frac{\partial f}{\partial \xi}\frac{\partial}{\partial \eta}\right) - f\frac{\partial}{\partial \eta}\right\}. \tag{13}$$

Making use of (4), (9), (11a), (12) and (13), the transformation of (1) is now easily obtained:

$$f''' + ff'' + \Lambda(1 - f'^2) = 2\xi\frac{\partial(f', f)}{\partial(\xi, \eta)}, \tag{14}$$

while the boundary conditions (5) become

$$\left.\begin{aligned} f + 2\xi\frac{\partial f}{\partial \xi} = 0, \quad \text{and} \quad f' = 0 \text{ for } \eta = 0, \\ f' = 1 \text{ for } \eta \to \infty. \end{aligned}\right\} \tag{15}$$

In (14) and (15) the accents refer to differentiation with respect to η, while on the right-hand side of (14) the Jacobian has been introduced as a convenient notation.

In order to transform (6), we introduce

$$T(x, y) = T_w + (T_e - T_w)\,\vartheta(\xi, \eta). \tag{16}$$

On the assumption that T_w and T_e do not depend on x, the thermal energy equation and its boundary conditions become

$$\vartheta'' + \sigma f\vartheta' = 2\xi\sigma\frac{\partial(\vartheta, f)}{\partial(\xi, \eta)}, \tag{17}$$

with $$\vartheta = 0 \text{ for } \eta = 0, \quad \text{and} \quad \vartheta = 1 \text{ for } \eta \to \infty. \tag{18}$$

Herewith the transformations are completed, and we have now to solve the equations (14) and (17) with the boundary conditions (15) and (18) respectively. For that purpose we remark that in the boundary layer r depends only on x; moreover, the dependence of u_e on x can be calculated from the potential theory or derived from experiments. Hence, ξ depends only on x, and for a given body we may consider x and u_e as known functions of ξ. As a result Λ is a known function of ξ. Inverting this function we may also say that for a given body, ξ is a function of Λ. The solution of (14) may thus be written as follows:

$$f(\xi, \eta) = f_0(\Lambda, \eta) + 2\xi\frac{d\Lambda}{d\xi}f_1(\Lambda, \eta) + \ldots. \tag{19}$$

Substituting (19) in (14) and (15), we get

$$\left.\begin{aligned} f_0''' + f_0 f_0'' + \Lambda(1 - f_0'^2) = 0, \\ f_0 = f_0' = 0 \text{ for } \eta = 0, \quad \text{and} \quad f_0' = 1 \text{ for } \eta \to \infty, \end{aligned}\right\} \tag{20}$$

$$\left.\begin{aligned} f_1''' + f_0 f_1'' - 2\Lambda f_0' f_1' + f_0'' f_1 = \frac{\partial(f_0', f_0)}{\partial(\Lambda, \eta)}, \\ f_1 = -\frac{\partial f_0}{\partial \Lambda}, \quad f_1' = 0 \text{ for } \eta = 0, \quad \text{and} \quad f_1' = 0 \text{ for } \eta \to \infty, \end{aligned}\right\} \tag{21}$$

and so on. The local friction coefficient is calculated from

$$c_f = \frac{\mu(\partial u/\partial y)_{y=0}}{\frac{1}{2}\rho V^2},$$

or, after transformation,

$$c_f R^{\frac{1}{2}} = 2\frac{r}{L}\frac{(u_e/V)^2}{(2\xi)^{\frac{1}{2}}}\left(A_0 + 2\xi\frac{d\Lambda}{d\xi}A_1 + \ldots\right), \tag{22}$$

where

$$A_k \equiv A_k(\Lambda) = f_k''(\Lambda, 0) \quad (k = 0, 1, 2\ldots). \tag{23}$$

In order to solve (17), we put

$$\vartheta(\xi, \eta) = \vartheta_0(\Lambda, \eta) + 2\xi\frac{d\Lambda}{d\xi}\vartheta_1(\Lambda, \eta) + \ldots. \tag{24}$$

Substituting (24) in (17) and (18), we then obtain

$$\left.\begin{aligned} \vartheta_0'' + \sigma f_0 \vartheta_0' = 0, \\ \vartheta_0 = 0 \text{ for } \eta = 0, \quad \text{and} \quad \vartheta_0 = 1 \text{ for } \eta \to \infty, \end{aligned}\right\} \tag{25}$$

$$\left.\begin{aligned} \vartheta_1'' + \sigma f_0 \vartheta_1' = -\sigma f_1 \vartheta_0' + \frac{\partial(\vartheta_0, f_0)}{\partial(\Lambda, \eta)}, \\ \vartheta_1 = 0 \text{ for } \eta = 0, \quad \text{and} \quad \vartheta_1 = 0 \text{ for } \eta \to \infty, \end{aligned}\right\} \tag{26}$$

and so on. The local Nusselt number is defined by

$$N = -\frac{(\partial T/\partial y)_{y=0}}{L(T_w - T_e)} = \frac{1}{L}\left(\frac{\partial\vartheta}{\partial y}\right)_{y=0},$$

or, after transformation,

$$\frac{N}{R^{\frac{1}{2}}} = \frac{r}{L}\frac{u_e/V}{(2\xi)^{\frac{1}{2}}}\left(E_0 + 2\xi\frac{d\Lambda}{d\xi}E_1 + \ldots\right), \tag{27}$$

where

$$E_k \equiv E_k(\Lambda) = \vartheta_k'(\Lambda, 0) \quad (k = 0, 1, 2\ldots). \tag{28}$$

The transformations (9) and (10), and the expansions (19) and (24), are closely related to those being proposed by Görtler (1957). The latter author, however, expands the wedge variable Λ in terms of ξ. If this is done, Meksyn's original approximation method cannot be applied, so that Λ is retained here as an independent variable replacing the variable ξ. This is the principal difference between Meksyn's and Görtler's methods. According to Görtler, Meksyn's treatment involves the calculation of the potential flow around the body considered before attacking the boundary-layer problem. However, it is easily shown that the transformations (9) and (10) may be derived from those given by Meksyn if the equipotentials and streamlines around the given body are expressed in terms of the velocity of the potential flow around that body. We are therefore of the opinion that Meksyn's method is of great value for rapid boundary-layer calculations for any given $u_e(x)$.

The calculation of the local friction coefficient and the local Nusselt number may now proceed as follows. For a given body, r and u_e are known functions of x, so that for each value of x the quantities ξ, Λ, $d\Lambda/d\xi$, etc., can be calculated. Hence, for each value of x, the corresponding values of A_k and E_k can be determined from tables or diagrams representing A_k and E_k as functions of Λ and σ.

Thereupon, the local friction coefficient and the local Nusselt number are rapidly calculated from (22) and (27) respectively. As soon as A_k and E_k are known, this calculation can proceed very rapidly. A_0 has been calculated by Hartree (1937), while E_0 has been calculated by Eckert (1942) for $\sigma = 0{\cdot}7$, $0{\cdot}8$, 1, 5 and 10. As far as we know, A_k and E_k for $k \geqslant 1$ have not been calculated as yet. However, for the application of a pure wedge method we need only A_0 and E_0, since for wedge-shaped profiles (for which Λ = constant) only the first terms at the right-hand sides of (19), (22), (24) and (27) are retained, while all other terms vanish. As a result, application of a pure wedge method to arbitrary two-dimensional profiles or rotationally symmetrical bodies means that only the first terms at the right-hand sides of (22) and (27) have to be retained (this approximation will be called Meksyn's wedge method). Since A_1 and E_1 are finite, this procedure is legitimate if ξ and/or $d\Lambda/d\xi$ are small. Generally speaking, this is the case in the vicinity of the forward stagnation point. At some distance from the forward stagnation point the second terms in (22) and (27) also become important. However, comparing the results obtained by Meksyn's wedge method with those obtained by the wedge methods mentioned in § 1, it appears that the accuracy of Meksyn's wedge method is of the same order of magnitude as that of the others. This demonstrates the rapid convergence of the series (22) and (27). It may be expected that even in the vicinity of the separation point of the boundary layer the series (22) and (27) yield satisfactory results if only two terms are retained.

Finally, we remark that the same method may be used if the assumptions IV and V are rejected. For gases it is, for example, convenient to apply first Stewartson's (1950) transformation (see also Cohen & Reshotko 1955) to the boundary-layer equations, whereupon 'wedge coordinates' analogous to those defined by (9) may be introduced. It is also possible to account for variations in the temperature of the wall. We have made analogous calculations for unsteady two-dimensional boundary layers. For unsteady rotationally symmetrical boundary layers the method fails, because then it is no longer possible to apply Mangler's transformation.

Using Meksyn's wedge method, we have also performed mass transfer calculations accounting for a velocity normal to the wall of the body. All these modifications of Meksyn's wedge method are not treated in this paper, because we intend to discuss only the principles of this method and not all its possible extensions.

3. Asymptotic expansion of the Nusselt number for a flat plate

We shall now discuss how the Nusselt number may be represented explicitly as a function of the Prandtl number. For that purpose we consider first the most simple case, viz. that of the flat plate without a longitudinal pressure gradient. In that case we have $r = L$, $u_e = V$, $\Lambda = 0$, $f = f_0$ and $\vartheta = \vartheta_0$. Hence, (27) becomes

$$\frac{N}{R^{\frac{1}{2}}} = \left(\frac{L}{2x}\right)^{\frac{1}{2}} E.$$

Averaging the Nusselt number over the length L of the plate, we get

$$\frac{\overline{N}}{R^{\frac{1}{2}}} = \frac{1}{L}\int_0^L \frac{N}{R^{\frac{1}{2}}}\,dx = 2^{\frac{1}{2}}E. \tag{29}$$

In the same manner the average value of the friction coefficient is obtained from (22), yielding

$$\bar{c}_f R^{\frac{1}{2}} = 2^{\frac{3}{2}} A. \tag{30}$$

In order to calculate E, we derive from (25), for $\vartheta = \vartheta_0$ and $f = f_0$,

$$\frac{1}{E} = \int_0^\infty \exp(-\sigma F)\, d\eta, \tag{31}$$

where

$$F \equiv F(\eta) = \int_0^\eta f(\eta)\, d\eta. \tag{32}$$

Formula (31) has been worked out by several authors. First of all we mention the exact calculations performed by E. Pohlhausen (1921). Other authors remarked that for large values of the Prandtl number the thickness δ_T is only a small fraction of the thickness δ, so that for the calculation of E the velocity profile in the thermal boundary layer may be linearized, that is, in (31) the function F may be represented by $\frac{1}{2}A\eta^2$. This procedure has already been applied by Falkner & Skan (1930, 1931), while the approximate calculations made by Piercy & Preston (1936) are in fact based upon the same principle. Lighthill (1950) developed an elegant method of calculating the heat transfer in laminar boundary layers, which is also based upon linearized velocity profiles. Tifford (1951), remarking that Lighthill's results are only valid for high values of the Prandtl number, modified Lighthill's formulae in order to obtain results valid for $\sigma \doteqdot 1$.

Frössling (1940) and Schuh (1949, 1954) also discussed the limit $\sigma \to \infty$, while Davies & Bourne (1956) developed a method where the velocity profile is represented by $c\eta^n$, n being determined in such a way that the results for $\sigma \doteqdot 1$ agree as closely as possible with the exact solution. Finally we may mention a paper by Morgan & Warner (1956) containing a survey of applications of heat transfer calculations in the limit $\sigma \to \infty$.

In the papers mentioned above, the formulae for the Nusselt number represent the first term of an asymptotic expansion for high values of the Prandtl number. In order to obtain formulae for lower values of σ, the expansion has to be extended. This may be done in several ways. An obvious way is to substitute $\tau = F$ in (31) and to consider τ as a new integration variable. In that way (31) becomes

$$\frac{1}{E(\sigma)} = \int_0^\infty e^{-\sigma\tau} \frac{d\eta}{d\tau}\, d\tau. \tag{33}$$

This formula shows that $1/E(\sigma)$ may be considered as the Laplace transform of $d\eta/d\tau$. Hence, the asymptotic expansion of $1/E(\sigma)$ may be obtained by means of Abel's well-known asymptotic theorem (see, for instance, Doetsch 1943). In order to apply this theorem we have to expand $F(\eta)$ in a power series. Putting $\Lambda = 0$, the expansion of $f = f_0$ is easily derived from (20). This expression has already been derived by Blasius (1908) and reads on as follows:

$$\tau \equiv F = A\frac{\eta^3}{3!} - A^2\frac{\eta^6}{6!} + 11A^3\frac{\eta^9}{9!} - 375A^4\frac{\eta^{12}}{12!} + O(\eta^{15}), \tag{34}$$

where O is the well-known Bachmann–Landau symbol. Inversion of (34) yields

$$\eta = \left(\frac{6\tau}{A}\right)^{\frac{1}{3}} \left\{1 + \frac{1}{60}\tau - \frac{1}{1{,}260}\tau^2 + \frac{23}{891{,}000}\tau^3 + O(\tau^4)\right\}. \tag{35}$$

Substituting (35) in (33), we obtain

$$\frac{1}{E(\sigma)} = \frac{1}{3}\left(\frac{6}{A}\right)^{\frac{1}{3}} \int_0^\infty e^{-\sigma\tau}\tau^{-\frac{2}{3}}\left(1+\frac{1}{15}\tau-\frac{1}{180}\tau^2+\frac{23}{89{,}100}\tau^3+O(\tau^4)\right)d\tau.$$

On term-by-term integration of the right-hand side of the last equation, an asymptotic expansion is obtained. Since the reciprocal of an asymptotic expansion is again an asymptotic expansion, a simple calculation brings forth the following result:

$$E(\sigma) = \frac{(A\sigma/6)^{\frac{1}{3}}}{\Gamma(\frac{4}{3})}\left(1-\frac{1}{45}\sigma^{-1}+\frac{2}{675}\sigma^{-2}-\frac{1{,}168}{3{,}007{,}125}\sigma^{-3}+O(\sigma^{-4})\right), \tag{36}$$

	$\overline{N}/R^{\frac{1}{3}}$					
	Asymptotic expansion (37)					
σ	1 term	2 terms	3 terms	4 terms	Exact	Tifford
0·1	—	—	—	0·2846	0·2762	0·294
0·5	0·5377	0·5138	0·5202	0·5185	0·5182	0·520
0·6	0·5714	0·5502	0·5549	0·5539	0·5537	0·554
0·7	0·6015	0·5824	0·5860	0·5853	0·5853	0·585
0·8	0·6289	0·6114	0·6143	0·6138	0·6138	0·614
0·9	0·6541	0·6380	0·6403	0·6400	0·6400	0·640
1·0	0·6775	0·6624	0·6644	0·6641	0·6641	0·664
1·1	0·6994	0·6853	0·6870	0·6868	0·6868	0·687
7	1·2959	1·2918	1·2919	1·2919	1·2919	1·32
10	1·4595	1·4563	1·4563	1·4563	1·4563	1·50
15	1·6708	1·6683	1·6683	1·6683	1·6682	1·73

TABLE 1

where Γ denotes the gamma-function. The coefficient A has been calculated by Blasius (1908) and by Töpfer (1912). According to the latter author we have $A = 0{\cdot}33206\sqrt{2} = 0{\cdot}46960$, while $\Gamma(\frac{4}{3}) = 0{\cdot}89298$. Substituting (36) in (29) and making use of the given values of A and $\Gamma(\frac{4}{3})$, we obtain

$$\frac{\overline{N}}{R^{\frac{1}{3}}} = 0{\cdot}6775\sigma^{\frac{1}{3}}\left(1-\frac{1}{45}\sigma^{-1}+\frac{2}{675}\sigma^{-2}-\frac{1{,}168}{3{,}007{,}125}\sigma^{-3}+O(\sigma^{-4})\right). \tag{37}$$

The Nusselt number calculated by means of (37) may be compared with the exact calculations made by E. Pohlhausen (1921). For that purpose we have extended Pohlhausen's calculations in order to obtain results in four figures (Pohlhausen gives only three figures), while we have also performed calculations for $\sigma = 0{\cdot}5$ and $0{\cdot}1$. The results are shown in table 1, where values calculated by means of Tifford's (1951) formula are also included. For a flat plate Tifford's formula reads

$$\frac{\overline{N}}{R^{\frac{1}{3}}} = 0{\cdot}664\sigma^{0{\cdot}35}. \tag{38}$$

Table 1 shows that Tifford's formula yields satisfactory results if $\sigma \doteqdot 1$; for very high and low values of the Prandtl number formula (38) fails. Furthermore,

it appears that for $\sigma \geqslant 0{\cdot}5$ our expansion (37) leads to surprisingly good results even to the fourth decimal place. Even for $\sigma = 0{\cdot}1$, this expansion may be used if its convergency is improved by means of Euler's transformation (for $\sigma \geqslant 0{\cdot}5$, Euler's transformation does not improve the convergency), since the value calculated by (37) is then only about 3 % too high.

Table 1 indicates how many terms of the expansion have to be retained. For $\sigma \geqslant 1$, two terms of the expansion are sufficient if the desired accuracy is not higher than 0·3 %. For $\sigma \geqslant 10$, one term is sufficient.

For $\sigma = 1$, we have $\vartheta = f'$, so that apparently the expansion (37) may also be used to calculate A. This has already been proposed by Meksyn (1950, 1955, 1956), who worked out this method to calculate the friction coefficients and separation points of boundary layers with longitudinal pressure gradient. As far as we know this author did not derive expansions of type (37) showing the dependence of the Nusselt number on the Prandtl number.

4. Asymptotic expansion of E_0 for arbitrary values of the wedge variable

We shall now show that by the asymptotic method one can also easily calculate the transfer coefficients for $\Lambda \neq 0$, i.e. for boundary layers with longitudinal pressure gradient. For that purpose we calculate E_0 from (25). Again we have

$$\frac{1}{E_0} = \int_0^\infty \exp(-\sigma F_0)\, d\eta, \tag{39}$$

F_0 being given by

$$F_0(\eta) = \int_0^\eta f_0(\eta)\, d\eta. \tag{40}$$

From (20) we derive

$$f_0 = A_0 \frac{\eta^2}{2!} - \Lambda \frac{\eta^3}{3!} + A_0^2(2\Lambda - 1)\frac{\eta^5}{5!} + O(\eta^6),$$

where A_0 is defined by (23). From the last expansion we obtain

$$\tau \equiv F_0 = A_0 \frac{\eta^3}{3!} - \Lambda \frac{\eta^4}{4!} + A_0^2(2\Lambda - 1)\frac{\eta^6}{6!} + O(\eta^7),$$

or, after inversion,

$$\eta = \left(\frac{6}{A_0}\right)^{\frac{1}{3}} \tau^{\frac{1}{3}} \left\{1 + \frac{\Lambda}{72}\left(\frac{6}{A_0}\right)^{\frac{4}{3}} \tau^{\frac{1}{3}} + \frac{\Lambda^2}{1728}\left(\frac{6}{A_0}\right)^{\frac{8}{3}} \tau^{\frac{2}{3}} + \left(\frac{35}{864}\frac{\Lambda^3}{A_0^4} - \frac{2\Lambda - 1}{60}\right)\tau + O(\tau^{\frac{4}{3}})\right\}. \tag{41}$$

Substituting (41) in (39), we may use the same method as in § 3. The result of the calculations is given by

$$\frac{1}{E_0} = \tfrac{1}{3}\Gamma(\tfrac{1}{3})\left(\frac{6}{A_0\sigma}\right)^{\frac{1}{3}} \left\{1 + \frac{\Lambda}{36}\frac{\Gamma(\frac{2}{3})}{\Gamma(\frac{1}{3})}\left(\frac{6}{A_0}\right)^{\frac{4}{3}} \sigma^{-\frac{1}{3}} + \frac{\Lambda^2}{576}\frac{\Gamma(1)}{\Gamma(\frac{1}{3})}\left(\frac{6}{A_0}\right)^{\frac{8}{3}} \sigma^{-\frac{2}{3}} + \frac{1}{3}\left(\frac{35}{216}\frac{\Lambda^3}{A_0^4} - \frac{2\Lambda - 1}{15}\right)\sigma^{-1} + O(\sigma^{-\frac{4}{3}})\right\}.$$

From this expansion it follows (with $\Gamma(\frac{1}{3}) = 2{\cdot}6789$ and $\Gamma(\frac{2}{3}) = 1{\cdot}3541$) that

$$E_0 = 0{\cdot}6163(A_0\sigma)^{\frac{1}{3}}\left\{1 - 0{\cdot}1531\Lambda A_0^{-\frac{4}{3}}\sigma^{-\frac{1}{3}} - 0{\cdot}0536\Lambda^2 A_0^{-\frac{8}{3}}\sigma^{-\frac{2}{3}} + \left(\frac{2\Lambda - 1}{45} - 0{\cdot}03402\Lambda^3 A_0^{-4}\right)\sigma^{-1} + O(\sigma^{-\frac{4}{3}})\right\}. \quad (42)$$

The quantity A_0 has been calculated by Hartree (1937) and in figure 1 is represented as a function of Λ for $-0{\cdot}1988 \leqslant \Lambda \leqslant 1$. In order to show that the

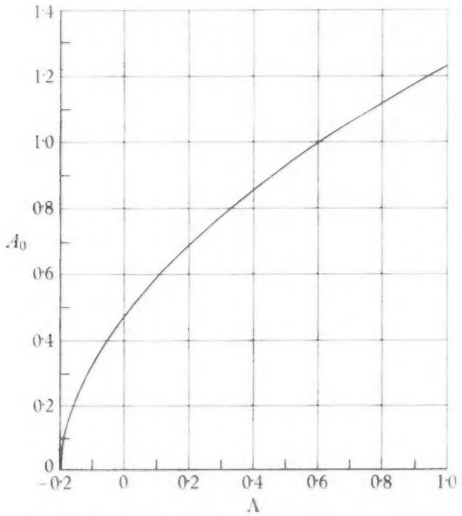

FIGURE 1. A_0 as a function of the wedge variable Λ, according to Hartree (1937).

	E_0 for $\sigma = 1$	
Λ	Eckert	Expansion (42)
1·0	0·5704	0·5689 (−0·3 %)
0·5	0·5390	0·5370 (−0·4 %)
0·0	0·4696	0·4684 (−0·3 %)
−0·14	0·4160	0·4196 (+0·9 %)

TABLE 2

expansion (42) may be used for finite values of the Prandtl numbers, we compare the values calculated from (42) with those calculated exactly by Eckert (1942). Table 2 shows that expansion (42) leads to satisfactory results for $\sigma = 1$. For $\sigma \geqslant 0{\cdot}7$, the expansion is even more accurate than the interpolation formula proposed by Eckert (1942). Furthermore, table 2 shows that the accuracy of the expansion decreases as Λ decreases. This is due to the fact that A_0 approaches zero if Λ approaches $-0{\cdot}1988$. For $A_0 = 0$, the expansion (42) is meaningless and

has to be replaced by another expansion. Putting $A_0 = 0$ ($\Lambda = -0{\cdot}1988$), we derive from (20)

$$f_0 = -\Lambda\frac{\eta^3}{3!} - 2\Lambda^2(2-3\Lambda)\frac{\eta^7}{7!} - 16\Lambda^3(2-3\Lambda)(8-7\Lambda)\frac{\eta^{11}}{11!} + O(\eta^{15}).$$

Applying the same technique as before, we find

$$\eta = \left(\frac{24}{-\Lambda}\right)^{\frac{1}{3}}\tau^{\frac{1}{3}}\left[1 + \frac{1}{140}(2-3\Lambda)\tau + \left\{\frac{13}{39{,}200}(2-3\Lambda)^2 - \frac{2(2-3\Lambda)(8-7\Lambda)}{17{,}325}\right\}\tau^2 + O(\tau^3)\right]. \quad (43)$$

Substituting (43) in (39) and putting $\Lambda = -0{\cdot}1988$, we obtain

$$E_0 = 0{\cdot}3328\sigma^{\frac{1}{3}}\{1 - 0{\cdot}02318\sigma^{-1} + 0{\cdot}00001345\sigma^{-2} + O(\sigma^{-3})\}. \quad (44)$$

For $\sigma = 0{\cdot}7$ this expansion yields $E_0 = 0{\cdot}2943$, while according to the exact calculations made by Brown & Donoughe (1951) we should have $E_0 = 0{\cdot}2939$. Since in both cases the fourth figure is not reliable, the agreement is satisfactory.

Λ ...	1·6	1·0	0·5	0·2	0	−0·14	−0·1988
η^*	0·5439	0·6479	0·8044	0·9839	1·2167	1·5967	2·3587

TABLE 3

It is also possible to derive expansions valid for very low values of the Prandtl number. In this case the thickness of the dynamic boundary layer is only a small fraction of the thickness of the thermal boundary layer. This means that in (39) f_0 may now be approximated by the asymptotic expansion in terms of η. Since $f_0' = 1$ for $\eta \to \infty$, we may write

$$f_0 \sim \eta - \eta^*, \quad (45)$$

where η^* may be interpreted as a reduced displacement thickness defined by

$$\eta^* = \lim_{\eta\to\infty}\int_0^\eta (1-f_0')\,d\eta = \lim_{\eta\to\infty}\{\eta - f_0(\eta)\}.$$

Substituting (45) in (39), we obtain

$$E_0 = (2\sigma/\pi)^{\frac{1}{2}}\frac{\exp(-\frac{1}{2}\eta^{*2}\sigma)}{1+\operatorname{erf}\{\eta^*(\frac{1}{2}\sigma)^{\frac{1}{2}}\}}, \quad (46)$$

where

$$\operatorname{erf}(z) = \frac{2}{\sqrt{\pi}}\int_0^z e^{-y^2}\,dy.$$

For low values of the Prandtl number, the right-hand side of (46) may be expanded further. The result is

$$E_0 = (2\sigma/\pi)^{\frac{1}{2}}[1 - \eta^*(2\sigma/\pi)^{\frac{1}{2}} + \ldots]. \quad (47)$$

Values for η^* have been provided by Eckert (1942), and are given in table 3.

The interpretation of (47) is obvious: the first term at the right-hand side of (47) represents the heat transfer in a potential flow and agrees with the formulae derived by Boussinesq (1903, 1905). This interpretation is in accordance with the considerations in § 1. The second term in (47) represents a first-order correction accounting for small viscosity effects. For flat plates, formula (47) has been discussed by Sparrow & Gregg (1957). These authors show that (at least for flat plates) (47) yields satisfactory results for values of the Prandtl number smaller than about 0·03.

Finally, in figure 2, E_0 is represented as a function of Λ for some values of the Prandtl number.

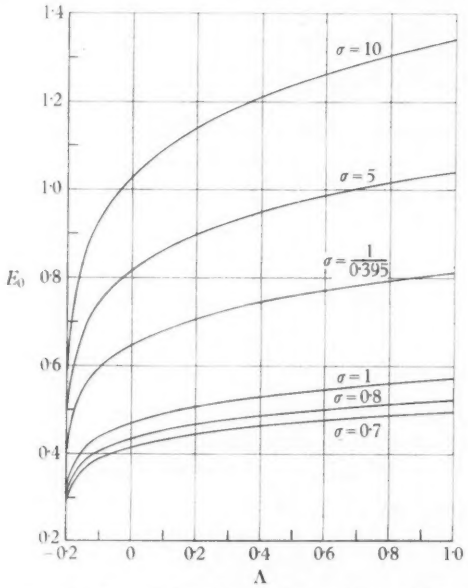

FIGURE 2. E_0 as a function of the wedge variable Λ, for some values of the Prandtl number.

5. Application to the calculation of the local heat transfer

Meksyn (1947, 1948) has already given some applications to the calculation of the local friction coefficient, so that we shall confine ourselves to the calculation of the local heat transfer. Let us first consider some two-dimensional profiles, viz. elliptical cylinders. The elliptical profile is determined by the ratio a/b of its semi-axes, a being parallel to the oncoming flow (see figure 3). The case $a/b = 1$ represents the circular cylinder, and $a/b = \infty$ the flat plate parallel to the direction of the oncoming flow. Furthermore, we shall consider the cases $a/b = 2$ and 4. The reference length L will be defined by $L = 2a$.

In order to calculate the wedge variable we have to know u_e as a function of x. For elliptical cylinders the potential theory yields

$$\left(\frac{u_e}{V}\right)^2 = \left(1+\frac{a}{b}\right)^2 \frac{1-\cos 2\phi}{1+(a/b)^2+\{1-(a/b)^2\}\cos 2\phi}, \tag{48}$$

where ϕ is the angular coordinate (see figure 3). Since we have taken for our two-dimensional profiles $r = L$, we obtain from (12) and (48)

$$\Lambda = \frac{4}{1+(a/b)^2+\{1-(a/b)^2\}\cos 2\phi}\,\frac{\cos\phi}{1+\cos\phi}. \tag{49}$$

Formula (48) is the more reliable the more slender the elliptical profiles. For broad profiles the wake behind the cylinder has an important influence on u_e, and

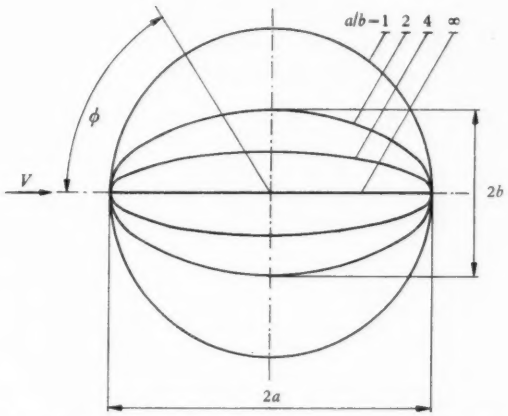

FIGURE 3. Sketch of the elliptical profiles considered in the text.

this influence is not accounted for in (48). Hence, for circular cylinders it is advisable to derive u_e from experiments instead of from (48). For that purpose u_e is written as

$$u_e/V = u_1(x/L) - u_3(x/L)^3 - u_5(x/L)^5,$$

where L is now equal to the diameter of the cylinder. According to Hiemenz (1911) we have

$$u_1 = 3{\cdot}631, \quad u_3 = 2{\cdot}171, \quad u_5 = 1{\cdot}514$$

for $R = 18{,}500$, while according to the measurements made by Schmidt & Wenner (1941) we have

$$u_1 = 3{\cdot}631, \quad u_3 = 3{\cdot}275, \quad u_5 = 0{\cdot}168$$

for $R = 170{,}000$.

In figure 4 the curves of the wedge variable are given. For $a/b = 1$, three curves are given, which are all calculated from (12) for $r = L$. The calculation of the solid curve is based upon u_e according to the potential theory, that of the dashed curve upon u_e according to the measurements made by Schmidt & Wenner (1941), and that of the dash-dotted curve upon u_e according to the measurements made by Hiemenz (1911).

Figure 4 shows that in the vicinity of the forward stagnation point $d\Lambda/dx \doteqdot 0$, while moreover ξ is small. Hence, in this region Meksyn's wedge method is near to the mark. If a/b increases, this region decreases, but at the same time the slope of the (Λ, x)-curves at median values of x/L becomes smaller, indicating that at median values of x/L Meksyn's wedge method is fairly accurate. This is to be

expected, since slender profiles behave approximately like flat plates and for these Meksyn's wedge method is exact.

At the vicinity of the separation point of the boundary layer, which according to Hartree (1937) is determined by $\Lambda = -0{\cdot}1988$, the slope of the (Λ, x)-curves is large, so that in this region the method is no longer reliable. This may also be demonstrated by means of the calculated position of the separation point. Denoting the separation point by suffix s, we obtain from the wedge method $\phi_s = 95{\cdot}2°$ for a circular cylinder (u_e according to the potential theory), while the series expansion of Blasius leads to $\phi_s = 110°$. If u_e is represented by the measurements made by Schmidt & Wenner, we then find $\phi_s = 72{\cdot}4°$, while the experimental value is given by $\phi_s \doteq 80°$. For the elliptical cylinder with $a/b = 2$ and u_e

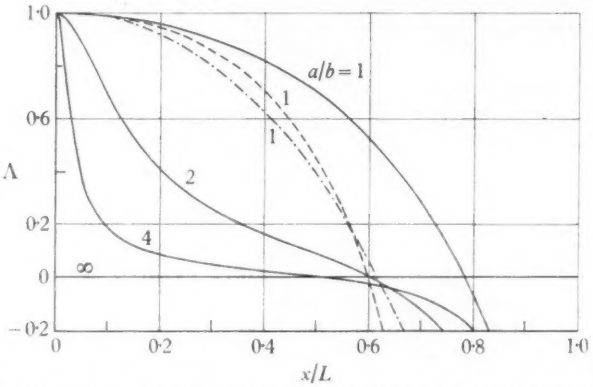

FIGURE 4. Wedge variable for elliptical profiles; solid curves according to the potential theory, dashed curve according to Schmidt & Wenner (1941), dash-dotted curve according to Hiemenz (1911).

according to the potential theory, we get from Meksyn's wedge method $\phi_s = 105{\cdot}8°$, from Eckert's wedge method $\phi_s = 115°$, and from the integral method of Pohlhausen $\phi_s = 120{\cdot}8°$. Apparently the separation points calculated from Meksyn's zero-order approximation are too low.

In figure 5 the local Nusselt numbers are given for the circular cylinder for $\sigma = 0{\cdot}7$, 1, 5 and 10. The calculations are based upon the velocity distribution measured by Schmidt & Wenner. For $\sigma = 0{\cdot}7$ the calculations may be compared with those of Eckert (1942) and Frössling (1940). In figure 5 the dashed curve is calculated by Eckert and the dash-dotted curve by Frössling. For $\phi < 50°$ the agreement is satisfactory, but for higher values of ϕ discrepancies exist. Frössling's calculations are based upon series expansions in terms of x/L containing only three terms, so that Frössling's curve is no longer reliable for $\phi > 50°$. Hence, it is not possible to decide whether Eckert's or our curve is to be preferred. In figure 6 the local Nusselt numbers calculated from Meksyn's wedge method are compared with those measured by Schmidt & Wenner. The three calculated curves correspond to those given in figure 4 for $a/b = 1$. The curve calculated by means of the velocity distribution measured by Schmidt & Wenner is satisfactory, though the theoretical value at the forward stagnation point is too low (it has to be borne in

mind that at this point the theoretical value is exact). The curve calculated by Eckert (not given in figure 6) gives a worse fit to the experimental curves, since Eckert's curve is too flat in the vicinity of the separation point. As far as we know, no calculations have as yet been performed for values of σ other than 0·7, so that we cannot compare our calculations with others for $\sigma = 1$, 5 and 10.

In figure 7 the local Nusselt number is given for the elliptical profile with $a/b = 2$. The dashed curve is calculated by Eckert. At the separation point this curve is again higher than ours.

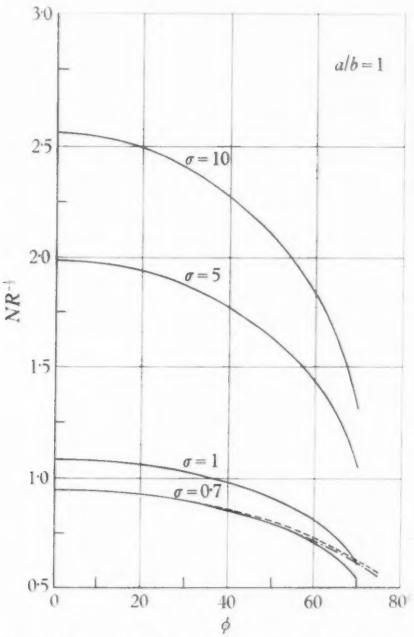

FIGURE 5. The local Nusselt number for circular cylinders; solid curves are calculated according to Meksyn's method, dashed curve according to Eckert (1942), dash-dotted curve according to Frössling (1940).

In figure 8 the calculations are represented for elliptical profiles with $a/b = 4$. In this case the difference between Eckert's calculations and ours is negligible.

For $\sigma > 10$ the calculations may be performed by means of the first term of the expansion (42), so that

$$E_0(\Lambda, \sigma) = 0{\cdot}6163\{A_0(\Lambda)\,\sigma\}^{\frac{1}{3}}. \tag{50}$$

At the separation point we obtain from (44)

$$E_0(-0{\cdot}1988, \sigma) = 0{\cdot}3328\sigma^{\frac{1}{3}}. \tag{51}$$

Hence, if the quantity $N/(R^{\frac{1}{2}}\sigma^{\frac{1}{3}})$ is plotted against x, then in the limiting case $\sigma \to \infty$ the curves approach zero as x approaches the separation point, though the local heat transfer at this point is not zero. The results of the calculations are shown in figure 9. Together with figures 5, 7 and 8, figure 9 shows the behaviour of the local heat transfer of elliptical cylinders for $\sigma \geqslant 0{\cdot}7$.

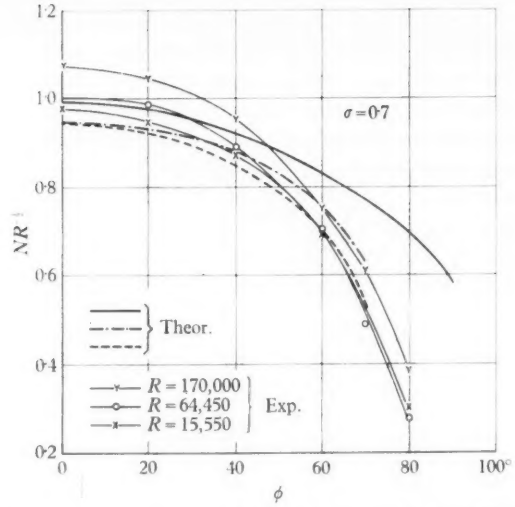

FIGURE 6. Comparison between calculated and measured local Nusselt numbers for circular cylinders at $\sigma = 0{\cdot}7$.

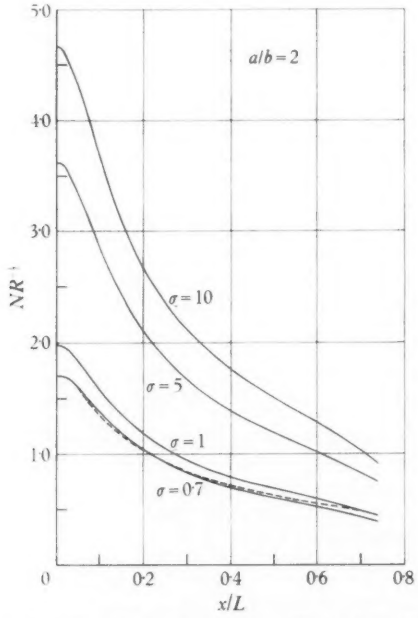

FIGURE 7. The local Nusselt number for an elliptical profile with $a/b = 2$; the dashed curve is calculated by Eckert (1942).

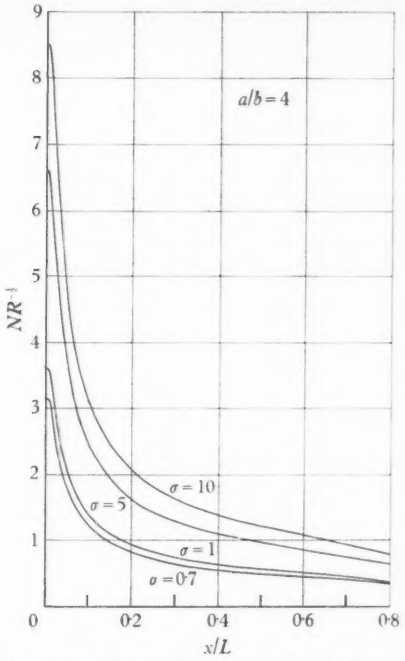

FIGURE 8. The local Nusselt number for an elliptical profile with $a/b = 4$.

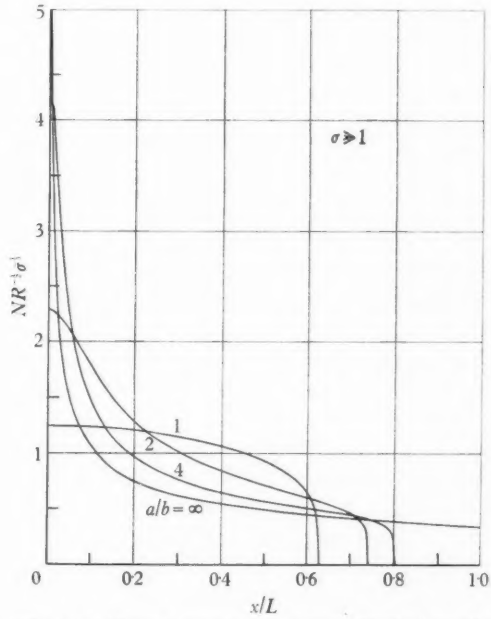

FIGURE 9. The local Nusselt number for some elliptical profiles at $\sigma \gg 1$.

Finally, we shall discuss the application to spheres. Putting L equal to the diameter of the sphere, we have

$$r/L = \tfrac{1}{2}\sin\phi = \tfrac{1}{2}\sin(2x/L). \tag{52}$$

The velocity u_e may be derived from the measurements made by Fage for $R = 157{,}200$. Frössling (1940) represented these measurements by

$$u_e/V = 3(x/L) - 3{\cdot}4966(x/L)^3 + 4{\cdot}7391(x/L)^5 - 5{\cdot}1481(x/L)^7. \tag{53}$$

From (52) and (53) the wedge variable can be calculated, whereupon the local Nusselt number is easily computed by means of Meksyn's wedge method. The

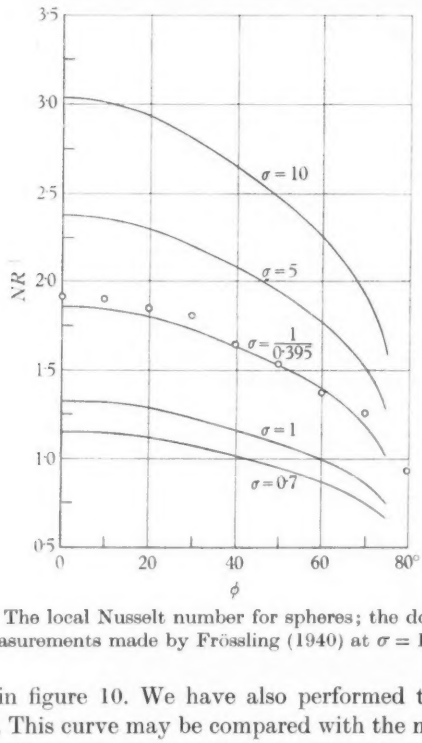

FIGURE 10. The local Nusselt number for spheres; the dots represent the measurements made by Frössling (1940) at $\sigma = 1/0{\cdot}395$.

results are shown in figure 10. We have also performed the calculations for $\sigma = 1/0{\cdot}395 = 2{\cdot}56$. This curve may be compared with the measurements made by Frössling (1938). The agreement between experiment and theory is surprisingly good, but may be accidental, because the measurements were performed at $R = 1060$ while the calculations are based upon the velocity distribution of Fage measured at $R = 157{,}200$.

Figure 11 represents the local Nusselt number for $\sigma \gg 1$ (say $\sigma > 10$). Comparing this curve with the corresponding curve for the circular cylinder, it appears that under equal conditions the local heat flux of spheres is higher than that of circular cylinders. This may be explained physically by the spatial divergence of the streamlines in the boundary layer of the sphere, which is lacking in the boundary layer of the circular cylinder. Under equal conditions this effect makes the boundary layer of the sphere thinner than that of the circular cylinder.

This paper is a part of a doctoral thesis presented at the Technological University at Delft. The author is indebted to Prof. Dr J. A. Prins of the Technological University for helpful discussions and suggestions.

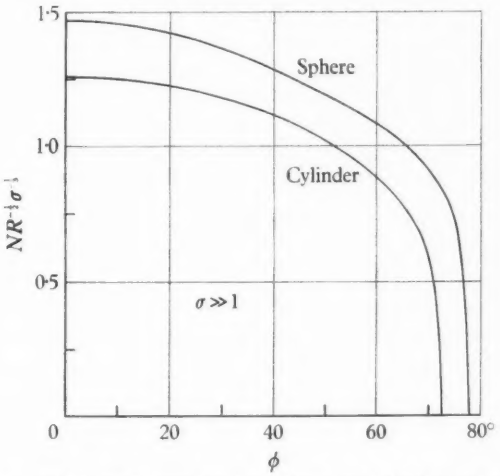

FIGURE 11. The local Nusselt number for spheres and circular cylinders at $\sigma \gg 1$.

REFERENCES

BLASIUS, H. 1908 *Z. Math. Phys.* **56**, 1; also *Nat. Adv. Comm. Aero., Wash., Tech. Mem.* no. 1256.

BOUSSINESQ, J. 1903 *Théorie Analytique de la Chaleur*, vol. II. Paris: Gauthier-Villars.

BOUSSINESQ, J. 1905 *J. Math. Pures Appl.* **1**, 285.

BROWN, W. B. & DONOUGHE, P. L. 1951 *Nat. Adv. Comm. Aero., Wash., Tech. Note*, no. 2479.

COHEN, C. B. & RESHOTKO, E. 1955 *Nat. Adv. Comm. Aero., Wash., Tech. Note*, no. 3326.

DAVIES, D. B. & BOURNE, D. E. 1956 *Quart. J. Mech. Appl. Math.* **9**, 457.

DOETSCH, G. 1943 *Theorie und Anwendung der Laplace-Transformation.* New York: Dover.

DREW, T. B. 1931 *Trans. Amer. Inst. Chem. Engrs*, **26**, 6.

ECKERT, E. 1942 V.D.I.-Forschungsheft **416**.

ECKERT, E. & LIVINGOOD, J. N. B. 1953 *Nat. Adv. Comm. Aero., Wash., Rep.* no. 1118.

FALKNER, V. M. & SKAN, S. W. 1930 *Aero. Res. Coun. Lond., Rep. & Mem.* no. 1314: also *Phil. Mag.* (7), **12**, 865 (1931).

FRÖSSLING, N. 1938 *Beitr. Geophys.* **52**, 170.

FRÖSSLING, N. 1940 *Lunds Univ. Arsskr., N.F. Avd.* 2, **36**, no. 4.

GÖRTLER, H. 1939 *Z. angew. Math. Mech.* **19**, 129.

GÖRTLER, H. 1957 *J. Math. Mech.* **6**, 1.

HARTREE, D. R. 1937 *Proc. Camb. Phil. Soc.* **33**, 223.

HIEMENZ, K. 1911 Dissertation, Göttingen; also *Dinglers Polytech. J.* **326**, 32 (1911).

KÁRMÁN, Th. VON 1921 *Z. angew. Math. Mech.* **1**, 233; also *Nat. Adv. Comm. Aero., Wash., Tech. Mem.* no. 1092.

KOTSCHIN, N. J., KIBEL, I. A. & ROSE, N. W. 1955 *Theoretische Hydromechanik II, Akad. Verlag, Berlin*, p. 399.

LIGHTHILL, M. J. 1950 *Proc. Roy. Soc.* A, **202**, 359.

MANGLER, W. 1948 *Z. angew. Math. Mech.* **28**, 97.

MEKSYN, D. 1947 *Proc. Roy. Soc.* A, **192**, 545, 567.
MEKSYN, D. 1948 *Proc. Roy. Soc.* A, **194**, 218.
MEKSYN, D. 1950 *Proc. Roy. Soc.* A, **201**, 268, 279.
MEKSYN, D. 1955 *Proc. Roy. Soc.* A, **231**, 274.
MEKSYN, D. 1956 *Proc. Roy. Soc.* A, **237**, 543.
MORGAN, G. W. & WARNER, W. H. 1956 *J. Aero. Sci.* **23**, 937.
PIERCY, N. A. V. & PRESTON, J. H. 1936 *Phil. Mag.* **21**, 995.
POHLHAUSEN, E. 1921 *Z. angew. Math. Mech.* **1**, 115.
POHLHAUSEN, K. 1921 *Z. angew. Math. Mech.* **1**, 252.
PRANDTL, L. 1904 *Proc. 3rd Int. Math. Congr., Heidelberg*, p. 484.
PRANDTL, L. 1938 *Z. angew. Math. Mech.* **18**, 77; also *Nat. Adv. Comm. Aero., Wash., Tech. Mem.* no. 959.
SCHMIDT, E. & WENNER, K. 1941 *Forsch. Ing.-Wes.* **12**, 65.
SCHUH, H. 1949 Temperaturgrenzschichten. *Göttinger Monographien*, B, **6**.
SCHUH, H. 1954 *Forsch. Ing.-Wes.* **20**, 37.
SMITH, A. M. O. 1956 *J. Aero. Sci.* **23**, 901.
SPARROW, E. M. & GREGG, J. L. 1957 *J. Aero. Sci.* **24**, 852.
STEWARTSON, K. 1950 *Proc. Roy. Soc.* A, **200**, 84.
TIFFORD, A. N. 1951 *J. Aero. Sci.* **18**, 283.
TÖPFER, C. 1912 *Z. Math. Phys.* **60**, 397.

On the drag of a flat plate at zero incidence in almost-free-molecule flow

By V. C. LIU

University of Michigan Research Institute, Ann Arbor

(Received 11 August 1958)

A physical theory is proposed for the skin friction on a flat plate at zero incidence in the transition flow regime, i.e. in the flow of a moderately rarefied gas. The ratio of the molecular mean free path to the characteristic size of the plate is assumed of order unity or larger. A general formula for the perturbation to the well-known friction of the free-molecule theory is given. This perturbation is attributed to the intermolecular collisions which are neglected on the basis of the free-molecule hypothesis. The expected rate of collisions are calculated for rigid spheres, using the classical kinetic theory.

Although this is intended as an approximate theory, the theoretical results check surprisingly well with the limited experimental data that are available. The present theory shows that the ratio of the Reynolds number to the Mach number squared is the governing parameter for determining the intermolecular collision effect on skin friction in the transition flow regime.

1. Introduction

The treatment of rarefied gas dynamics has been greatly simplified by the use of the free-molecule hypothesis when the molecular mean free path λ is many times greater than the characteristic dimension L of the particular flow field. In this hypothesis it is assumed that the gas dynamic effects of collisions between the molecules incident on and reflected from a surface element are negligible compared to those between the incident molecules and the surface element. This basic postulate allows the molecular motion of the incident stream to be treated as having the Maxwellian (equilibrium) distribution. Gas dynamic problems of this nature are amenable to solution provided the mechanism of molecular reflexions at the solid surface is known.

Similarly, treatment of gas dynamic problems in the slip flow regime, where the ratio λ/L is much less than unity, has been moderately successful, at least in a few specific cases (Schaaf 1956).

On the other hand, the least rewarding efforts have been in the study of flow phenomena in the transition regime, where λ is of the same order as L. Mathematically, the classical approaches to such rarefied gas problems always start with the Maxwell–Boltzmann equation for the molecular distribution function. The general technique (Jaffé 1930; Keller 1948; Wang Chang & Uhlenbeck 1954) is based on a perturbation expansion of the Maxwell–Boltzmann equation in

powers of L/λ. The calculations are in general formidable and few results of direct aerodynamic interest are available.

Unfortunately, experimental investigations in the transition flow regime have also been fraught with difficulties. From the astronautical point of view, the flow conditions existing in the transition regime correspond approximately to the case of ballistic missile flight at an altitude of about 100 km.

It appears that for the purpose of elucidating the physical mechanism of the phenomena, one might use a physical approach entailing a slight relaxation of the conditions imposed by the free-molecule hypothesis. The proposed principle of treating this 'almost-free-molecule flow' starts with the following assumptions: (1) The rate of collisions between the molecules incident on and reflected from a surface element is small compared to that between the incident molecules and the surface element in question. (2) The probability of a reflected molecule colliding twice with the incident molecules before it is deflected away is negligible compared to the probability of its colliding only once. The single-collision* effects are calculated on the basis of Maxwellian distribution for the molecular velocities. In other words, the theory of the almost-free-molecule flow is essentially a higher order iteration of the corresponding free-molecule analysis. The intermolecular collisions are calculated for rigid spheres based on the classical kinetic theory. (3) The molecules are reflected diffusely from the surface without preferred direction.

As in other mean-free-path methods of treating kinetic problems, the almost-free-molecule calculation is expected to indicate quickly the order of magnitude of certain gas dynamic quantities in question and their functional dependence upon molecular variables. It should be kept in mind, however, that this approximate theory, like many other elementary theories of complicated phenomena, can by no means be regarded as a complete equivalent of an exact theory such as the yet-to-be-obtained solution to the Maxwell–Boltzmann equation for the case of a transition flow along a plate. Nevertheless, the results predicted by the theory for both the drag of a flat plate at zero incidence and the Pitot pressure (Liu 1957) in the transition flow regime were found to show remarkable consistency with the limited measurements available.

2. Flat plate in a free-molecule flow

Consider a flat plate situated in a free stream of infinite extent with mean velocity V_1. If the intermolecular collisions occurring near the plate are negligible, we may use the Maxwellian distribution for the velocities of the impinging molecules relative to an observer moving with the stream. Assuming that the plate is in the y, z-plane such that the direction of flow makes an angle α with the y-axis and is perpendicular to the z-axis, we have the distribution function (Jeans 1925)

$$f = (\beta^3/\pi^{\frac{3}{2}}) \exp\{-\beta^2[(u - V_1 \sin\alpha)^2 + (v + V_1 \cos\alpha)^2 + w^2]\}, \tag{2.1}$$

where $\beta = (2RT_1)^{-\frac{1}{2}}$ denotes the reciprocal of the most probable velocity of the molecules relative to the mean motion of the gas; T_1, the free-stream temperature; and R, the gas constant.

* Heineman (1948) earlier used a similar idea in treating the drag on a flat blunt body in very-high-speed flow.

The number of molecules, N_i, that are incident on a unit area per unit time is given by

$$N_i = \int_{-\infty}^{\infty}\int_{-\infty}^{\infty}\int_{0}^{\infty} n_1 u f \, du\, dv\, dw, \tag{2.2}$$

where n_1 denotes the number density of molecules in the free stream. Equation (2.2), on integration, becomes

$$N_i = n_1\left(\frac{RT_1}{2\pi}\right)^{\frac{1}{2}}\{\exp(-S_1^2\sin^2\alpha)+\sqrt{\pi}\,S_1\sin\alpha[1+\operatorname{erf}(S_1\sin\alpha)]\}, \tag{2.3}$$

where $S_1 = V_1/(2RT_1)^{\frac{1}{2}}$, and subscript 1 denotes the free-stream condition.

To calculate the shearing stress, τ_i, due to the impact of the incident molecules on the plate, we have

$$\tau_i = \int_{-\infty}^{\infty}\int_{-\infty}^{\infty}\int_{0}^{\infty} n_1 m u v f \, du\, dv\, dw. \tag{2.4}$$

where m denotes the molecular mass. For the special case where $\alpha = 0$, $\tau_i/\frac{1}{2}\rho_1 V_1^2 = 1/\sqrt{\pi}\,S_1$ (Patterson 1956), where ρ_1 denotes the free-stream density.

If the molecules are reflected diffusely from the plate, $\tau_r = 0$ (where τ_r denotes the shearing stress due to the reflected molecules), since no preferred direction exists. Thus, under the free-molecule hypothesis, the drag coefficient of a flat plate, C_{DF}, becomes

$$C_{DF} = 2\tau_i/\tfrac{1}{2}\rho_1 V_1^2 = 2/\sqrt{\pi}\,S_1. \tag{2.5}$$

3. Rate of intermolecular collisions and loss of shearing stress

It is obvious that loss of shearing stress on the plate can result when the incident molecules are prevented from reaching the plate by intermolecular collisions. On the other hand, the molecules emerging from such collisions may still strike the plate and thereby contribute additional shearing stress. From this it follows that in an almost-free-molecule flow the net loss of shearing stress (relative to its 'free-molecule' value) due to the intermolecular collisions is equal to the difference between these two aforementioned contributions.

To calculate the potential contribution to shearing stress by the incident molecules about to collide with the diffusely reflected molecules, we first need to know the rate of such intermolecular collisions for each incident molecule. Let c_i denote the absolute velocity of a molecule incident upon a plate, n_0 and $\bar{c}_0$ denote, respectively, the number density and the mean velocities of molecules re-emitted randomly from the plate. If $\bar{C}_r$ represents the mean relative velocities of collisions between the incident molecule, with velocity c_i, and the diffused molecules, with a mean velocity $\bar{c}_0$, we have the expected collision rate (Kennard 1938)

$$E_0 = \pi\sigma^2 n_0 \bar{C}_r, \tag{3.1}$$

where $\pi\sigma^2$ denotes the collision cross-section of the equivalent rigid spheres. Since

$$\bar{C}_r = \int_{\theta_i}^{\theta_i+\frac{1}{2}\pi} \tfrac{1}{2} C_r \sin\theta \, d\theta, \tag{3.2}$$

where $\theta = \theta_i + \theta_0$ (see figure 1), and

$$C_r^2 = c_i^2 + \bar{c}_0^2 + 2\bar{c}_0 c_i \cos\theta, \tag{3.3}$$

we have from (3.1)

$$E_0 = -\frac{\pi\sigma^2 n_0}{6\bar{c}_0 c_i}(c_i+\bar{c}_0)^3 \left\{\left[1 - \frac{2\bar{c}_0 c_i}{(c_i+\bar{c}_0)^2}(1+\sin\theta_i)\right]^{\frac{3}{2}} - \left[1 - \frac{2\bar{c}_0 c_i}{(c_i+\bar{c}_0)^2}(1-\cos\theta_i)\right]^{\frac{3}{2}}\right\}. \tag{3.4}$$

Note that the term $2(\bar{c}_0/c_i)/(1+\bar{c}_0/c_i)^2$ is always small compared to unity. We can obtain a fair approximation by retaining the first-order terms only in the power series expansion of E_0 in equation (3.4). The approximate rate of collisions at the plate becomes

$$E_0 = \tfrac{1}{2}\pi\sigma^2 n_0 (c_i+\bar{c}_0)(\sin\theta_i + \cos\theta_i). \tag{3.5}$$

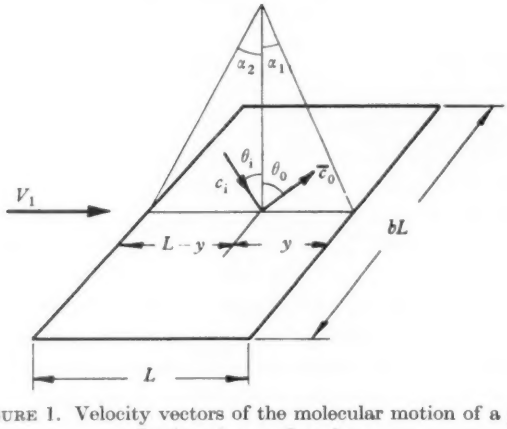

FIGURE 1. Velocity vectors of the molecular motion of a gas flowing along a flat plate.

At distance x from the plate, the collision rate is reduced by the following factors: (1) the molecular scattering effect, $\exp(-x/\lambda_1)$; (2) the bilateral free expansion of the reflected molecules, $bL^2/(x+L)(x+bL)$, where b denotes the aspect ratio of the span to the chord of the plate (see figure 1). Therefore, the likelihood of collisions by an incident molecule between distances x and $x+dx$ becomes

$$E\,dt = E\frac{dx}{u} = \frac{\frac{1}{2}bL^2\pi\sigma^2 n_0}{(x+L)(x+bL)} e^{-x/\lambda_1}(c_i+\bar{c}_0)(\sin\theta_i+\cos\theta_i)\frac{dx}{u}. \tag{3.6}$$

If all the collided molecules are deflected away from the plate, we can calculate the potential loss of shearing stress with the use of equations (2.4) and (3.6). To avoid mathematical complexity, we can get a fair approximation by using the mean incident velocity [equation (2.3)] at a given angle θ_i without directly taking into account the random distribution of the molecular velocities. To carry the approximation further, we consider only those intermolecular collisions that occur in the semi-infinite region based on the plate.

If there were no collisions, the tangential momentum integral of the incident molecules that would have hit the plate can be written as

$$\tau_{11} = \frac{b}{2}\pi\sigma^2 n\rho_1 V_1^2 L \int_0^\infty \frac{(c_i/V_1)(\bar{c}_0+c_i/V_1)}{(x+L)(x+bL)} e^{-x/\lambda_1} \int_0^L \int_{\alpha_1}^{-\alpha_2} \sin\theta_i(\sin\theta_i+\cos\theta_i)\, d\theta_i\, dy\, dx, \tag{3.7}$$

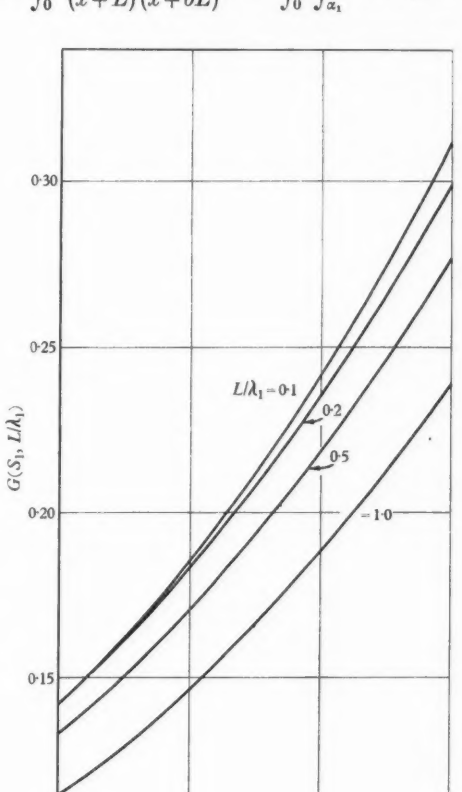

FIGURE 2. G-function for a plate of infinite span ($b = \infty$).

where $\alpha_1 = \tan^{-1}(y/x)$, $\alpha_2 = \tan^{-1}[(L-y)/x]$, and c_i is taken to be the mean velocity

$$\bar{c}_i = \left(\frac{RT_1}{2\pi}\right)^{\frac{1}{2}} \{\exp(-S_1^2\sin^2\theta_i) + \sqrt{\pi}\, S_1 \sin\theta_i[1+\operatorname{erf}(S_1\sin\theta_i)]\}. \tag{3.8}$$

For the case where the speed ratio S_1 is smaller than unity, we may approximate $\bar{c}_i$ given in equation (3.8) by the power series

$$\bar{c}_i = \left(\frac{RT_1}{2\pi}\right)^{\frac{1}{2}} [1+\sqrt{\pi}\, S_1 \sin\theta_i - 3S_1^2\sin^2\theta_i + \ldots]. \tag{3.9}$$

With the approximate expression for $\bar{c}_i$, as given in equation (3.9), the multiple integrations of equation (3.7) can be performed. Thus,

$$\tau_{11} = -\tfrac{1}{2}\pi\sigma^2 n_0 \rho_1 V_1^2 (L/S_1^2)\, G, \tag{3.10}$$

where G is a function of S_1, b and L/λ_1 (see figures 2 and 3).

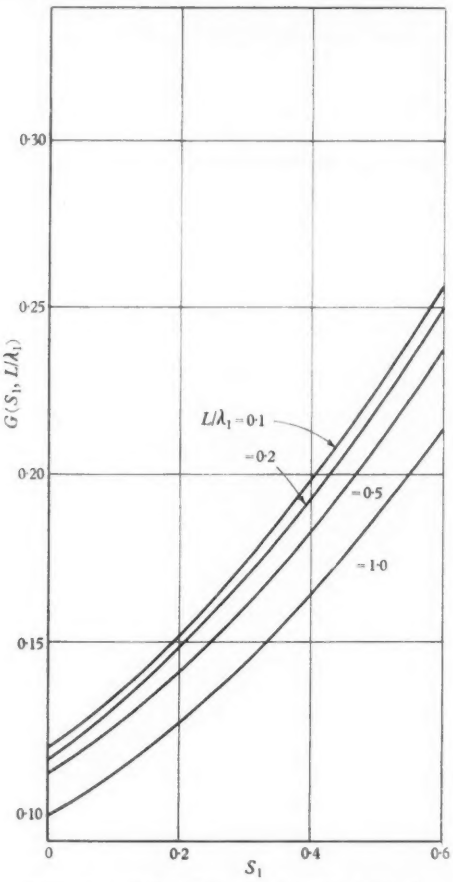

FIGURE 3. G-function for a square plate ($b = 1$).

(i) For the case $b = \infty$,

$$\begin{aligned} G(S_1, L/\lambda_1) = {} & \frac{5}{4\pi}\int_0^\infty \frac{e^{-(L/\lambda_1)t}}{1+t}\left[\cot^{-1}t - t\log\frac{1+t^2}{t^2}\right]dt + \frac{S_1}{\sqrt{\pi}}\int_0^\infty \frac{e^{-(L/\lambda_1)t}}{1+t} \\ & \times\left[(1+t^2)^{\frac{1}{2}} + \frac{t^2}{(1+t^2)^{\frac{1}{2}}} - 2t\right]dt - \frac{1}{8}\left(\frac{1}{2}+\frac{3}{\pi}\right)S_1^2\int_0^\infty \frac{e^{-(L/\lambda_1)t}}{1+t} \\ & \times\left[4t\log\frac{1+t^2}{t^2} - 3\cot^{-1}t - \frac{t}{1+t^2}\right]dt + \frac{S_1^3}{5\sqrt{\pi}}\int_0^\infty \frac{e^{-(L/\lambda_1)t}}{1+t} \\ & \times\left[(1+t^2)^{\frac{1}{2}} + 2\frac{t^2}{(1+t^2)^{\frac{1}{2}}} - \frac{1}{3}\frac{t^4}{(1+t^2)^{\frac{3}{2}}} - \frac{8}{3}t\right]dt. \end{aligned} \tag{3.11}$$

(ii) For the case $b = 1$,

$$G(S_1, L/\lambda_1) = \frac{5}{4\pi}\int_0^\infty \frac{e^{-(L/\lambda_1)t}}{(1+t)^2}\left[\cot^{-1}t - t\log\frac{1+t^2}{t^2}\right]dt + \frac{S_1}{\sqrt{\pi}}\int_0^\infty \frac{e^{-(L/\lambda_1)t}}{(1+t)^2}$$
$$\times\left[(1+t^2)^{\frac{1}{2}} + \frac{t^2}{(1+t^2)^{\frac{1}{2}}} - 2t\right]dt - \frac{1}{8}\left(\frac{1}{2}+\frac{3}{\pi}\right)S_1^2\int_0^\infty \frac{e^{-(L/\lambda_1)t}}{(1+t)^2}$$
$$\times\left[4t\log\frac{1+t^2}{t^2} - 3\cot^{-1}t - \frac{t}{1+t^2}\right]dt + \frac{S_1^3}{5\sqrt{\pi}}\int_0^\infty \frac{e^{-(L/\lambda_1)t}}{(1+t)^2}$$
$$\times\left[(1+t^2)^{\frac{1}{2}} + 2\frac{t^2}{(1+t^2)^{\frac{1}{2}}} - \frac{1}{3}\frac{t^4}{(1+t^2)^{\frac{3}{2}}} - \tfrac{8}{3}t\right]dt. \qquad (3.12)$$

4. Contribution to the shearing stress by the scattered molecules

A specific difficulty of the present problem is the determination of the shearing stress, τ_{10}, on the plate due to the impact of the molecules emerging from the intermolecular collisions. Before entering into this determination, we wish to emphasize that these evaluations are mere approximations.

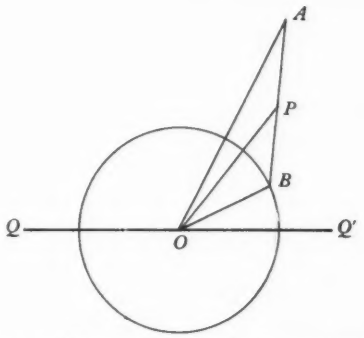

FIGURE 4. Velocity vector diagram of molecular encounters between an incident molecule and the molecules reflected from a plate.

We begin with a theorem of Maxwell (Jeans 1925). If two molecules collide with such velocities that their centre of gravity is stationary before collision and, therefore, also after collision, then all directions are equally probable for the velocity of either molecule following collision. From this it follows that, if two molecules collide in any way, the expected velocity of either is exactly equal to the velocity of the centre of gravity of the colliding pair.

Consider an incident molecule A with velocity c_i which is represented by OA in figure 4. Let $\bar{c}_0$, represented by OB, be the velocity of a reflected molecule B from the plate. Their relative velocity is therefore represented by AB; the velocity of the centre of gravity, by OP, where P is the mid-point of AB. The expected velocity of A, emerging from collision with B, is represented by OP.

In the present analysis of skin friction, we are concerned primarily, though not exclusively, with the component of OP along the plate QQ' since the tangential momentum transfer to the plate is of particular interest. By reason of symmetry in molecular distributions above and below the plate, we can determine the

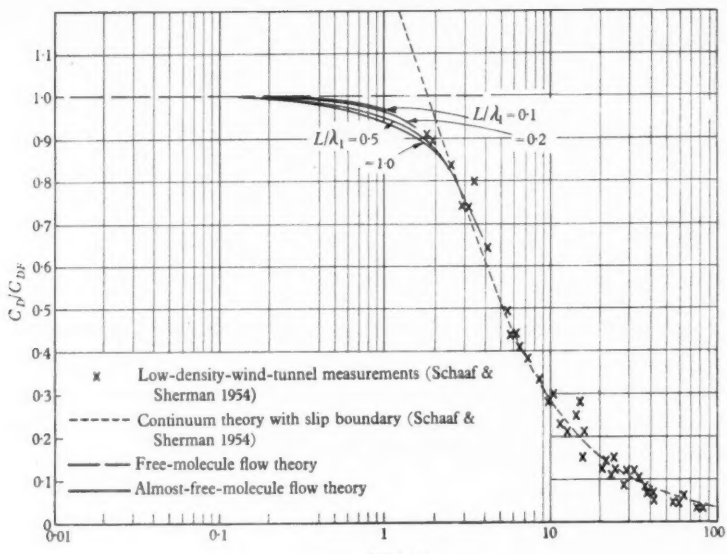

FIGURE 5. Comparison of theoretical and measured values of C_D/C_{DF} ($b = \infty$ is assumed in the almost-free-molecule-flow analysis).

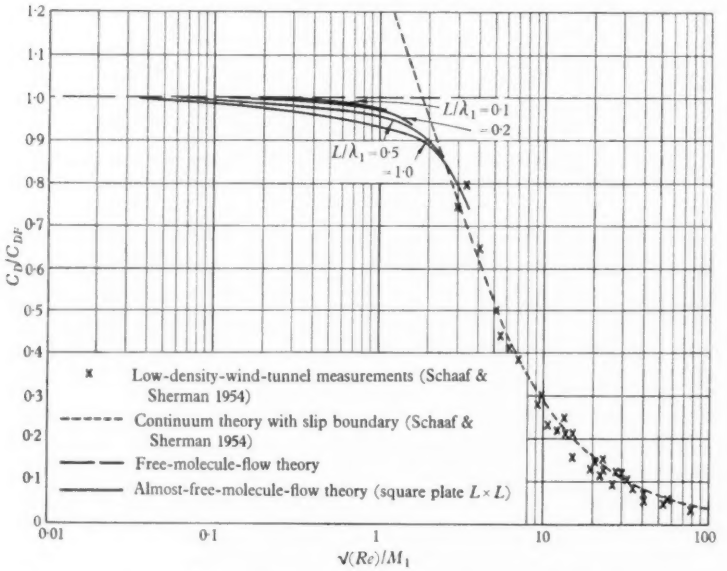

FIGURE 6. Comparison of theoretical and measured values of C_D/C_{DF} ($b = 1$ is assumed in the almost-free-molecule-flow analysis).

expectation of the final velocity of A by averaging the components of the velocity OP over all possible directions for OB. Now the similarity can be established between the analysis herein for the expected final velocity of A and the classical calculation for the *persistence of molecular velocities* in the kinetic theory of gases (Jeans 1925). After the collision with another randomly moving molecule of equal size, the velocity of a given molecule will, on the average, still retain a component in the direction of its original motion. This characteristic is called the persistence of velocities after collision. It has been shown by Jeans (1925) approximately, and by Chapman & Cowling (1952) exactly, that the mean persistence, for identical molecules in collisions, is equal to 0·406 times the original velocity.

Provided that the above-mentioned hypothesis is valid, the mean expected velocity of the centre of gravity of molecules A and B will be equal to $0{\cdot}406c_i$ in the direction OA. From this it follows that the additional shearing stress, τ_{10}, to the plate due to the impact of the molecules (both A and B) emerging from the intermolecular collisions will amount to approximately 81·2 % of τ_{11} (see equation 3.10).

5. The drag coefficient of a flat plate

Given the intermolecular collision effect on skin friction of a surface as worked out in §§ 3 and 4, the drag coefficient, C_D, of a flat plate at zero incidence in an almost-free-molecule flow follows from (2.5). Thus

$$C_D = (2/\sqrt{\pi}\, S_1) - 0{\cdot}376\pi\sigma^2 n_0 (L/S_1^2)\, G. \tag{5.1}$$

Dividing equation (5.1) by C_{DF} leads to

$$C_D/C_{DF} = 1 - 0{\cdot}188\pi^{\frac{3}{2}}\sigma^2 n_0 (L/S_1^2)\, G. \tag{5.2}$$

In the case when $T_0 = T_1$ and, therefore, $n_0 = n_1$, and since

$$\sqrt{2}\,\pi\sigma^2 n_1 = 1/\lambda, \quad S_1 = (\gamma/2)^{\frac{1}{2}} M_1 \quad \text{and} \quad L/\lambda_1 = 0{\cdot}499(8/\pi\gamma)^{\frac{1}{2}}\, Re/M_1,$$

where M_1 and Re denotes the free-stream Mach number and Reynolds number respectively, we have

$$C_D/C_{DF} = 1 - 0{\cdot}188(Re/M_1^2)\, G. \tag{5.3}$$

The comparison of C_D/C_{DF} computed from equation (5.3), for a two-dimensional plate ($b = \infty$) and a square plate ($b = 1$) at various values of S_1 and L/λ_1, with those obtained from measurements in a low-density wind tunnel (Schaaf & Sherman 1954) are shown in figures 5 and 6, respectively.

6. Conclusions

Considering the number of serious simplifications made in the formulation process, we cannot expect the theory to predict results with greater accuracy than the right order of magnitude. The surprisingly close agreement between the theory and the limited measurements that are available should be taken with guarded optimism until a wider variety of experimental results is available.

The present theory does show that Re/M^2 is the governing parameter for the determination of the intermolecular collision effect on skin friction of a shear flow

in the transition regime. It is of interest to compare the present result on intermolecular collision effect with that on Pitot pressure in an almost-free molecule flow (Liu 1957). In the case of Pitot pressure, Re/M_1 instead of Re/M_1^2 becomes the corresponding governing parameter. This exhibits the difference in physical mechanisms between the shear flow effect (skin friction) and the impact flow effect (Pitot pressure) in the transition regime.

The research reported in this paper has been supported by the Meteorological Branch of the U.S. Army Signal Corps under Contract No. DA-36-039-SC-64659 with The University of Michigan. The author wishes to record his indebtedness to Prof. Sydney Chapman for his reading of the manuscript and his stimulating discussions of this work; and to Mr Howard Jew for assistance in the numerical computations.

REFERENCES

Chapman, S. & Cowling, T. G. 1952 *Mathematical Theory of Non-Uniform Gases.* Cambridge University Press.

Heineman, M. 1948 *Commun. Appl. Math.* **1**, 259.

Jaffé, G. 1930 *Ann. Physik*, **6**, 195.

Jeans, J. H. 1925 *Dynamical Theory of Gases.* Cambridge University Press.

Keller, J. B. 1948 *Commun. Appl. Math.* **1**, 275.

Kennard, E. H. 1938 *Kinetic Theory of Gases.* New York: McGraw-Hill.

Liu, V. C. 1957 *On Pitot Pressure in an Almost-Free-Molecule Flow—a physical Theory of Flow of the Rarefied Gases.* High Altitude Engineering Laboratory Research Paper no. 18, The University of Michigan, Ann Arbor; also *J. Aero. Sci.* **25**, 1958, 779.

Patterson, G. N. 1956 *Molecular Flow of Gases.* New York: Wiley.

Schaaf, S. A. 1956 *Appl. Mech. Rev.* **9**, 413.

Schaff, S. A. & Sherman, F. S. 1954 *J. Aero. Sci.* **21**, 85.

Wang Chang, C. S. & Uhlenbeck, G. E. 1954 *The Couette Flow between two Parallel Plates as a Function of the Knudsen Number.* The University of Michigan Engineering Research Institute, Project 1999.

REVIEWS

Statistical Theory of Irreversible Processes. By R. EISENSCHITZ. Oxford: Clarendon Press, 1958. 84 pp. 8*s*. 6*d*.

There is probably no physical generalization more firmly established than the Second Law of Thermodynamics. Indeed, the thermodynamic theory of equilibrium and its statistical basis are so well understood that there seems little room for further fundamental advance in this subject. Such, however, is far from true of the theory of passage towards equilibrium: here even the fundamental principles are still under dispute, and are the subject of much discussion at the present time.

It is generally agreed that a non-equilibrium situation, like a state of equilibrium, should be described by a probability distribution over phase space (or in quantum mechanics by the corresponding density operator). In equilibrium theory this distribution is obtained by maximizing the entropy, which is a well-defined integral of the distribution function. In non-equilibrium theory, however, this procedure will not work owing to the reversibility of the microscopic equations of motion; if the same integral is maximized at a certain instant, the resulting distribution function yields in general no instantaneous change in the macroscopic observables whose values are used to specify the non-equilibrium situation; indeed the entropy itself remains constant throughout time because of Liouville's theorem.

This difficulty was by-passed by Boltzmann in arriving at his famous equation for the time-development of the properties of a perfect gas in disequilibrium. The essence of Boltzmann's theory was to ignore the prior correlation of the velocities of two colliding molecules, so that the history of an individual molecule could be regarded as a stochastic time sequence. With this assumption Boltzmann was able to prove his famous H-Theorem, according to which the entropy per particle increases steadily with time. For strongly interacting systems, however, any statistical definition of the entropy must include particle correlation terms, if it is to agree with the thermodynamically measured entropy; thus Boltzmann's equation cannot be directly applied.

Historically, the next successful theory of an irreversible phenomenon was the Einstein theory of Brownian diffusion. A Brownian particle is supposed to be subject not only to viscous drag but also to a rapidly fluctuating force with a very short correlation time. In this way irreversible behaviour is obtained, but at the expense of introducing a somewhat artificial theoretical distinction between two effects which are actually of the same physical origin.

The most powerful result yet obtained in the theory of disequilibrium is undoubtedly that of Onsager, and has been justly described as the Fourth Law of Thermodynamics. By very general arguments, appealing only to microscopic reversibility and to the linear character of many dissipative phenomena, Onsager was able to show that in systems where two dissipative processes interact (such as diffusion and thermal conduction) there is a symmetry between

the mutual effects of the two processes. Onsager's Law is of great generality and has been verified experimentally with the utmost precision in many different situations. It is, indeed, the most important single statement in the modern subject of non-equilibrium thermodynamics.

It is against this background that current work must be viewed. In non-equilibrium thermodynamics the entropy is calculated by integrating an entropy density, which in turn is estimated by assuming equilibrium conditions to prevail in each small element of the system. It is clear, therefore, that it is not the entropy but the entropy density which should be given a proper statistical definition, and Boltzmann's theory implicitly does this. But it might be asked whether one cannot, as Boltzmann did, obtain a satisfactory statistical theory which makes no explicit reference to the entropy. This is the line of thought which has been pursued most diligently by recent workers, and various procedures have been proposed. It is well recognized, for example, that although the distribution in phase space of a closed system develops reversibly, nevertheless, if this distribution is 'coarse-grained'—that is to say averaged over cells of small but finite phase volume—then the entropy calculated from the coarse-grained distribution increases steadily with the time, and from a macroscopic point of view the system shows irreversible behaviour. In practice the coarse-graining procedure is necessarily drastic; one must average over the co-ordinates and the momenta of all the particles except a very few so as to obtain an equation of motion in a reasonably small number of variables. Unfortunately, it then becomes very difficult to make any quantitative statement about the time-development of the few-particle distribution functions, so that although irreversible behaviour is ensured, the transport coefficients are still inaccessible to calculation.

A different but related procedure has been developed by Kirkwood and his collaborators. Kirkwood postulates the existence of a small finite time, short compared with the macroscopic relaxation time, but long enough for the average force on a molecule due to its neighbours to be effectively randomized. He then obtains equations for the transport coefficients of a liquid in terms of the autocorrelation integrals of the intermolecular forces and the problem is then reduced to evaluating these integrals. Though Kirkwood's formalism seems to be essentially correct its exploitation demands laborious analysis and has not yet proved very fruitful in the interpretation of experimental data.

Dr Eisenschitz's little book does not, unfortunately, do justice to its subject. The chapters appear to be arranged in an almost random order: the last (Chapter IX) is an elementary exposition of probability theory; Boltzmann's H-Theorem appears at the end of Chapter VII, which is concerned with statistical quantum mechanics; the theory of Brownian movement and of stochastic processes generally does not appear until Chapter VIII, and at the end of this chapter there is a superficial mention of Onsager's theorem, with no reference to its method of derivation. Equilibrium statistical mechanics is dealt with summarily in Chapter II, which occupies exactly four pages and concludes with the remarkable statement: 'These examples should be sufficient to show the achievements and limitations of the classical theory of equilibrium.' The

meat of the book ought to be in Chapter III, entitled 'Irreversibility', but on page 11, after promising to show that a coarse-grained distribution develops irreversibly, the author introduces without warning the time-smoothing device, which has no logical connexion with the coarse-graining procedure. In this of all chapters the author should have attempted to make clear the necessary and sufficient conditions for irreversible behaviour, but he provides no indication as to what sort of phenomena ought to be irreversible, or why, and makes no comment on the question whether irreversibility can occur in a system containing a finite number of particles. In view of the author's scientific reputation, the book is a serious disappointment to anyone who wishes to understand clearly what has been achieved and what are the outstanding problems in this field.

H. C. Longuet-Higgins

An Introduction to Fluid Dynamics. By G. Temple. Oxford: Clarendon Press, 1958. 195 pp. 25*s*.

The chapter headings in this short book are: 1. Introduction; 2. The properties of the perfect fluid; 3. Bernoulli's theorem; 4. Irrotational flow; 5. The velocity potential; 6. The complex potential and velocity in plane parallel flow; 7. 'Point' sources, doublets, and vortices in plane parallel flow; 8. Equivalent layers of sources, doublets and vortices; 9. Simple fields of flow obtained by superposition; 10. The forces on a body in a uniform stream; 11. Simple fields of flow obtained by conformal mapping; 12. Discontinuous flow; 13. The design of wing profiles; 14. Point sources and doublets in axi-symmetric flow; 15. Slender-body theory.

In the preface the author states: 'The object of this book is to provide an introduction to Fluid Dynamics, primarily for students reading for Honours in Mathematics and Theoretical Physics. There is an undoubted need for such a work, for although we have the comprehensive treatises of Lamb and of Milne-Thomson, there is no elementary account of the basic principles of modern Fluid Dynamics. The works of Basset and Ramsey still repay consultation, but the emphasis in Fluid Dynamics is no longer on analytical solutions of ingenious problems but on the development of the physical significance of the fundamental principles.

'Our main purpose therefore is to introduce Fluid Dynamics as a branch of dynamics and to concentrate on the fundamental dynamical principles and their immediate applications to the types of fluid flow which are actually observed or produced, especially to the "disturbance" flow produced by the motion of a solid body through a fluid....

'This book, however, is limited to the theoretical aspect of Fluid Dynamics, and is, moreover, restricted to the theory of the perfect fluid....'

Accordingly, readers will expect an account of the scope and physical limitations of the frictionless perfect-fluid model, a difficult and interesting subject which the author would be well qualified to treat. The perfect fluid was discredited early in the history of hydrodynamics when it was found to lead to D'Alembert's paradox, that bluff bodies in steady motion through a perfect

fluid experience no drag. Since then, however, the perfect fluid has been shown to be applicable in many important situations (not including the steady motion of a bluff body), in particular in the theory of aerofoils and slender bodies, and of water and sound waves. To explain the reasons for this success must involve some discussion of such topics as viscosity, boundary layers, flow separation, hydrodynamic stability, etc., which in the older books were relegated to the later chapters, but without which no real understanding of the subject is possible.

Such an explanation is not to be found in Prof. Temple's book. Viscosity and the Reynolds number are each mentioned once (on p. 20), the boundary layer a few times, and no comparison with experiments is given at any point. A student without previous knowledge of fluid dynamics would necessarily get a very erroneous idea of its problems and methods from this book. For instance, when the potential flow past a circular cylinder is discussed on p. 118, should not a warning be given that the results may not be applied to steady flow, but that they may be applied to the initial stage of flow accelerated from rest and also to oscillations of small amplitude? The emphasis throughout this book is not really more physical than in the older books mentioned by Prof. Temple. It seems a pity that we are not given a full discussion of any one problem, say the flow past a circular cylinder or the Thwaites flap mentioned in chapter 9, including all that is known experimentally, with diagrams and photographs.

Although the neglect of the non-mathematical aspects severely limits the utility of this book as a first introduction, the discussion of the mathematics of potential flow is in many places original and elegant and will appeal to the reader with some previous knowledge, and some common difficulties are clearly explained in the book.

In chapter 1 it is emphasized that Newton's laws must be applied to a mass of fluid consisting always of the same particles. In §4.7 Kelvin's circulation theorem is proved in the Lagrangian description of motion, whereby obscurities commonly found in the proof of this theorem are avoided. Chapter 8 is devoted to the representation of two-dimensional flows by sources and dipoles (Green's theorem) and also by sources and vortices. The treatment, based on complex integration is very neat; I have not seen it before. The discontinuous flow past a plate is calculated more simply than in the standard texts, by Helmholtz's original method. Many of the problems and examples are well chosen and interesting and often taken from recent research work. It is made clear, at any rate, that the subject is not now a merely academic exercise. However, the ideal well-balanced introduction to fluid dynamics still remains to be written.

F. URSELL

Mathematical Theory of Compressible Fluid Flow. By RICHARD VON MISES, completed by HILDA GEIRINGER and G. S. S. LUDFORD. New York: Academic Press Inc., 1958. 514 pp. $15.00.

Ten years and more ago, the publication of any book on the theory of compressible fluid flow was an event of great importance to all workers in the field, and whatever the merits and demerits of the work, it was almost bound to have

some value. But in the past decade the situation has changed completely; an almost embarrassing number of books on this subject has appeared, and any new works must now exhibit special qualities of originality or exposition if they are to be successful. It is pleasant to be able to record that these qualities are evident in the case of this book by von Mises. This is the third volume in the Series of Monographs on Applied Mathematics and Mechanics prepared under the auspices of the Applied Physics Laboratory, The Johns Hopkins University, and is a worthy companion to its distinguished predecessors in the series. According to the preface, the first half of the book was completed by von Mises before his untimely death in 1953, and the second half was written by Hilda Geiringer (Mrs R. von Mises) and G. S. S. Ludford using von Mises's papers and lecture notes for guidance. So well has the addition been made that much more than a casual examination of the text is required to detect the change of authorship.

The book is divided into five chapters, the first two of which deal with the general theory of compressible flow. The equations of motion are derived by what might be described as classical methods, except that the usual equations of state and energy are replaced by an original feature of the author's in the form of a *specifying equation*, which is a general relation between the pressure, density, and velocity, their derivatives, and the space co-ordinates and time. Energy relations and the influence of viscosity and heat conduction in a fluid are then considered, and the first chapter concludes with a discussion of the acoustical equations. The second chapter contains derivations and discussions, often in considerable and valuable detail, of some consequences of the general equations. The theory of characteristics is introduced here; the treatment given is almost entirely mathematical (rather than physical), but is very detailed, particularly for the case of two variables, and the present reviewer found it most illuminating on a number of points.

The next chapter is concerned with one-dimensional flow, and starts with an article on steady flow with viscosity and heat conduction present, followed by articles on non-steady flow of an ideal fluid, and simple waves. Shocks are then introduced and are given a long discussion on the basis of an ideal gas with constant specific heats, with due attention to the non-isentropic flow behind curved shocks.

Chapter IV contains an account of the theory of plane steady potential flow, with emphasis on the supersonic case and the method of characteristics. The hodograph equations are derived and discussed, both for the velocity potential and stream function and for their Legendre transforms. Then the exact solutions for radial, vortex, and spiral flows are examined, and limiting lines are given a brief mention. Articles on the Chaplygin–Kármán–Tsien approximation and simple waves are followed by extensive discussions of limit and branch lines, and Chaplygin's hodograph method.

The last chapter deals with integration theory and shocks. Hodograph theory is developed still further, following the method of Lighthill and Cherry, and there is a useful account of Bergman's integral transformation method. Further aspects of shock theory and non-isentropic flows are given, and the

chapter ends with a particularly interesting article on the current theoretical ideas and difficulties associated with the transonic flow problem.

The work ends with nearly forty pages of Notes and Addenda, which are collected footnotes on the main text. These notes are extraordinarily informative, and the reviewer found most of them quite fascinating, particularly for the amount of historical matter which is contained in them. It appears from the preface that these notes were placed together at the back of the volume, instead of on the actual pages to which they refer, in accord with 'von Mises's practice of keeping text free from distraction'; however, on the assumption that they are meant to be read in conjunction with the appropriate matter of the text, the continual necessity for reference to the end of the book is far more distracting.

The whole work is essentially mathematical in concept, as would be expected from such an eminent mathematician as von Mises, and personally the reviewer found the presentation and content very much to his taste. But there are other points of view on this matter, and undoubtedly there are many who would prefer a closer contact with the physical ideas behind the theory than is to be found here. As it is, the book provides a mine of information on its subject which should be invaluable to students and research workers in the field of theoretical mechanics, and engineers with mathematical leanings will also find much which will be of profit to them. It must be remarked that the book is not easy reading, in the sense that much more than a casual study is required in many places in order to extract the full value of the text; of course, this is almost inevitable in a work of any depth.

The reviewer found himself at variance with the author over the derivation of the equations of motion. The reviewer holds the opinion that the integral forms of these equations are more fundamental than their differential forms, since the former cover more general types of flow than the latter, including discontinuous motions, and the differential forms can be deduced from the integral forms once suitable conditions have been imposed on the derivatives of the dependent variables. Thus, in a fully deductive mathematical treatment, it would seem to be more appropriate to take the integral equations as a starting point. Also there are difficulties in the application of Newton's Laws of Motion which are not mentioned by the author.

The preface states that 'The present book contains no extensive discussion of the approximation theories.... It was the author's intention to discuss these in the second part of his work....' The death of the author before this second part could be written is a great loss, for it is certain that von Mises would have had much of interest to write on this topic, as on those subjects which he has covered so well in the present book.

G. N. Ward

N

O

P

A

Now in its second year

THE PHYSICS OF FLUIDS

EDITOR, F. N. FRENKIEL,

Applied Physics Lab., Johns Hopkins University, Silver Spring, Md.

ASSOCIATE EDITORS

Walker Bleakney	Jesse W. Beams	Carl Eckart
J. M. Burgers	S. Chandrasekhar	J. E. Mayer
Joseph Kaplan	Hugh L. Dryden	G. N. Patterson
John G. Kirkwood	Raymond J. Emrich	Lyman Spitzer, Jr.
Galen B. Schubauer	Arnold M. Kuethe	G. E. Uhlenbeck
Peter Wegener	Edward Teller	James A. Van Allen

Original contributions covering kinetic theory, statistical mechanics, structure and general physics of gases, liquids and other fluids and including:

- Magneto-Fluid Dynamics
- Ionized Fluid and Plasma Physics
- Shock and Detonation Wave Phenomena
- Dynamics of Compressible Fluids
- Boundary Layer and Turbulence Phenomena
- Liquid State Physics and Superfluidity
- Hypersonic Physics
- Rarefied Gas Phenomena
- Upper Atmosphere Phenomena
- Physical Aeronomy
- Transport Phenomena
- Hydrodynamics

As well as certain basic aspects of physics of fluids bordering geophysics, astrophysics, biophysics and other fields of science.

ISSUED BI-MONTHLY— SUBSCRIPTIONS: $10.00 DOMESTIC, $11.00 FOREIGN

Subscription orders and inquiries should be sent to the Publisher:

American Institute of Physics, 335 East 45 Street, New York 17, N.Y.

JOURNAL OF FLUID MECHANICS

Volume 5, Part 3 April 1959

CONTENTS

Experimental studies of supercavitating flow about simple two-dimensional bodies in a jet
by EDWARD SILBERMAN *page* 337

Steady flow through non-uniform gauzes of arbitrary shape
by J. W. ELDER 355

A new approach to problems of shock dynamics. Part 2. Three-dimensional problems
by G. B. WHITHAM 369

The propagation of small disturbances in hydromagnetics
by G. S. S. LUDFORD 387

Cellular convection with finite amplitude in a rotating fluid
by G. VERONIS 401

Ring vortices generated electromagnetically
by CHIA-SHUN YIH 436

The supersonic flow past a leading edge separation bubble
by A. W. SHARP 445

Rapid calculations for boundary-layer transfer using wedge solutions and asymptotic expansions
by H. J. MERK 460

On the drag of a flat plate at zero incidence in almost-free-molecule flow
by V. C. LIU 481

REVIEWS

Statistical Theory of Irreversible Processes 491

An Introduction to Fluid Dynamics 493

Mathematical Theory of Compressible Fluid Flow 494

Printed in Great Britain at the University Press, Cambridge
(Brooke Crutchley, University Printer)